Imperial College London

CHARACTERISATION OF ENCAPSULATED EMBRYONIC STEM CELLS USING SILAC-BASED PROTEOMICS

By Sarah Alsobaie

A THESIS SUBMITTED IN PARTIAL FULFILLMENT OF THE REQUIREMENTS FOR THE DEGREE OF DOCTOR OF PHILOSOPHY AND DIPLOMA OF IMPERIAL COLLEGE LONDON

DEPARTMENT OF CHEMISTRY
FACULTY OF NATURAL SCIENCES
IMPERIAL COLLEGE LONDON

2015

Abstract:
The embryonic stem cells have two hallmarks characters, the ability to reproduce self-renewal and generate other cell lineages. Despite the excessive advance in stem cell research, their clinical applications delay owing lack of an optimal culture condition *in vitro*. Combining biometrical scaffold with stem cells provides a promising way to cellular delivery and tissue transplant. *In vitro* 3D culture offers both a model to understand self-renewal and stem cell behaviour *in vivo* as a route to industrial production. We have used a variety of analytical tools including proteomics and quantitative RT-PCR to compare 3D (both static & dynamic) with 2D cultures. We further show that 3D dynamic culture increases expression of the master gene regulators (Oct4, Nanog and Sox2). Consistent with this Rex1, an inner-cell mass (ICM) associated marker, is over-expressed in 3D dynamic culture whereas Fgf5, an epiblast transition marker is down-regulated. Using SILAC-based proteomics to compare 2D vs. 3D dynamic culture, we show that encapsulated stem cell are characterized by glycolytic pathways down-regulation and increased mitochondrial respiratory proteins. Additionally, ECM proteins expression (laminin, fibronectin, heparan sulfate (HS) proteoglycans, agrin, and nidogen-2) were up-regulated. Cells shortly after encapsulation in 3D constructs (both static &dynamic) showed high oxygen uptake rates compared to 2D culture. After 9 days of encapsulation glucose uptake increased in both static & dynamic 3D cultures and was combined with a pronounced increase in cell density and up-regulation of hypoxia induce-factors (HIf-1α and Hif-2α). This shift in metabolism toward anaerobic glycolysis is associated with high expression of hexokinas2 (Hk2) and increased lactate production. Despite extensive cell proliferation at day 18, where cell numbers reached up to 80k/ bead, cells in dynamic culture switched back from anaerobic to aerobic metabolism. This alteration in energy consumption was not associated with nutrient depletion since both glucose and glutamate were not depleted in the culture medium. By monitoring the oxygen consumption, hypoxia-induced factors expression as well as Oct4 levels at different time points, we demonstrate that the stem cells self-renewal status in 3D condition is regulated despite the metabolism transitions. We postulate that the 3D culture environment provides the niche required sensing and responding to external and internal stimuli different from recognised *in vitro* embryonic stem cell behaviour.

DECLARATION

This thesis contains personal work carried out by the author. It has not been submitted and/or accepted in any form for any degree or diploma in any university. To the best of my knowledge and belief, it does not contain work by any other person, unless otherwise acknowledged.

ACKNOWLEDGEMENTS

I would like to express my special appreciation and thanks to my advisor Professor Tony Cass, you have been a tremendous mentor for me. I'd also like to thank my co-supervisor, Sakis Mantalaris and his group member for accepting me in their research team. I dedicate this thesis to my previous supervisor Judit Nagy who is no longer with us. Also, I'd like to thanks my colleagues in Tony Cass group, Sanjiv, Muthu, Tao, Ben, Dan, Hazeeq and very special thanks to my best friends and supporters Jaya and Nawal in good and bad times. Special thanks to the great gift in my life, my sister Tamador. Thank you for supporting me for everything, and especially I can't thank you enough for encouraging me throughout this experience. All my beloved large family members including my father, Mohammed, Abdulaziz, Abdulrahman, Ibrahim, Saad, Nesreen, Saud, and Fayz, for letting me through all the difficulties. I have experienced your guidance day by day. You are the one who let me finish my degree. Finally, words can not express how grateful I am to my mother Heila Alhammad, for all of the sacrifices that you've made on my behalf. Your prayer for me is what has sustained me thus far.

CONFERENCE PROCEEDINGS

1. 12th annual meeting of International Society for Stem Cell Research (ISSCR) from 18 to 21 June 2014(poster presentation).
2. Imperial postgraduate symposium 2010 (poster presentation).
3. Imperial postgraduate symposium 2011 (Talk).
4. BSPR-EBI Meeting 2011 (Poster presentation).
5. SymBioSE Basal 2011 (Poster presentation).
6. Worl Stm Cell Summit 2015 (Poster Presentation).

Contents

LIST OF FIGURES

LIST OF TABLES

CHAPTER 1: Literature Review

1. Introduction

1.1. Stem Cells

1.1.1. Stem Cells and Self-renewal

Stem cells are generally defined by two principal characteristics, namely: (i) *self-renewal*, the maintenance of an undifferentiated state following cell division, and (ii) *potency,* the capacity to differentiate into specialised sub-types. Stem cells are considered to be the key to understanding development and disease, possessing important prospects for regenerative medicine, and can be exploited as platforms for drug discovery and toxicology programmes (Ronaghi et al., 2010).

The origin of a stem cell defines its potency and associated use. Cells produced by the first few divisions of the fertilised egg are considered totipotent and can differentiate into embryonic and extraembryonic cell types (Fig.1, i). Embryonic stem cells (ESC) originate in the inner cell mass (ICM) of an embryo's blastocyst. Following implantation in the uterus, the ICM divides into the hypoblast and epiblast, the former creating the yolk sac and the latter deriving the three primary germ layers (Fig.1 ii & iii): ectoderm, endoderm, and mesoderm. ESC are thus by definition pluripotent; able to expand into the majority of cellular lines within the body, but not having the capability of producing the extra-embryonic tissues, which originate in the trophoblast that surrounds the ICM (Rippon and Bishop, 2004).

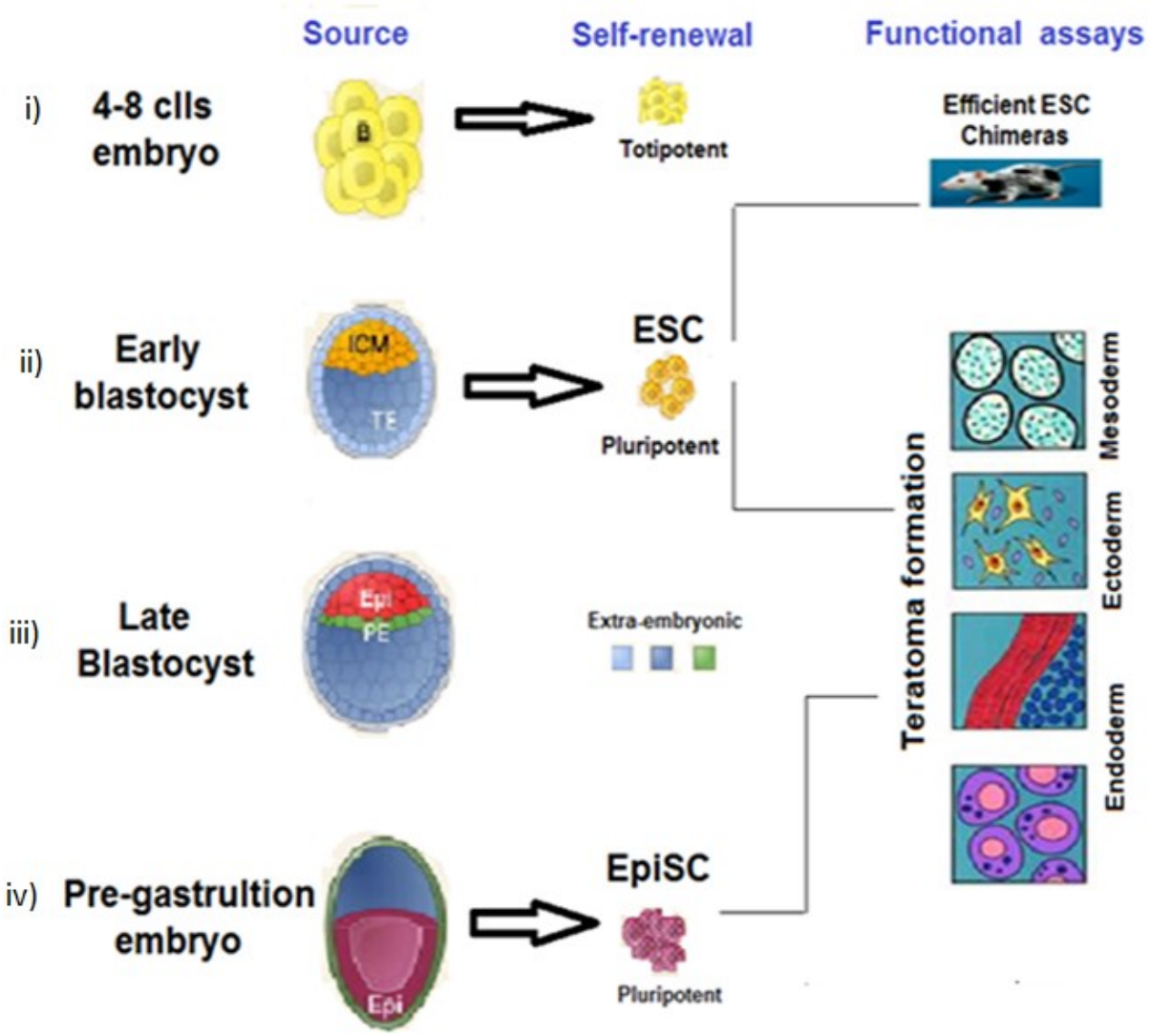

Figure 1 Embryonic and epiblast stem cells characteristics

i) Cells derived from the 4 - 8 cell embryo are totipotent; able to create all embryonic and extraembryonic tissue.

ii) ESC are pluripotent stem cells derived from the inner cell mass of a blastocyst, an early-stage pre-implantation embryo.

iv) EpiSCs are derived from the post-implantation, pre-gastrulation embryo. Both EpiSC and mESC and hESC can form teratomas, however, only mESC can form chimeric mice.

Murine ESC (mESC) were first isolated from the ICM in 1981 (Evans and Kaufman, 1981), (Martin, 1981). A number of assays, both *in vitro* and *in vivo* have been developed for establishing ESC functionality.

ESC have the capability to differentiate into derivatives of the three primary germ layers. *In vitro*, pluripotency is verified by means of an embryoid body (EB) formation assay, where culture in the absence of leukaemia inhibitory factor (LIF) results in three-dimensional aggregates termed EBs. EBs can be assessed for the expression of markers defining the three primary germ layers as markers of differentiation ability. Chimera formation (i.e. a single organism composed of genetically distinct cells) after blastocyst injection or morula aggregation is the principal functional assay of the developmental potential of mESC (Mintz and Illmensee, 1975). The teratoma assay represents an additional functional assay to demonstrate pluripotency. A standard mESC line will have the capacity to generate large tumours that contain all three germ layers (i.e. teratomas) when grafted to severe combined immunodeficient (SCID) mice (Bradley et al., 1984), (Nagy et al., 1993).

Murine experiments were followed up by derivation of ES cells from humans (hESC) with great potential for therapy (Thomson, 1998). Similar to mESC, hESC were able to reproduce indefinitely and produce cells from all three germ layers. Pluripotency could be examined *in vitro* and *in vivo* with the aid of EB and teratoma assays respectively. However, ethical concerns limit the use of chimera and tetraploid complementation assays.

Comparisons of mouse and human ESC lines have shown numerous significant differences between the cell types, both in response to external growth factors and inherent cell surface marker expression. Characterisation of stem cell colonies is usually accomplished as a result of the assessment of intracellular and/or cell surface markers. Both, mESC and hESC commonly express the nuclear markers octamer-binding transcription factor (Oct) 3/4 and

Nanog (Andrews et al., 2005). Additionally, mESC can further be assessed for expression of the stage-specific embryonic antigen marker–1 (SSEA-1) and the lack of either SSEA-3 or -4. Contradictory to these findings, in hESC SSEA-3 or -4 expression is characteristic of undifferentiated cells and in SSEA-1 characteristic of differentiation. Others are perceived when investigating the culture conditions for mESC and hESC.

mESC are recognized as being rapidly proliferate with short cell cycle times of 11-16 hours (Orford and Scadden, 2008). This is attributed to the persistent presence of cyclin E-CDK2 during the course of the cell cycle that permits the conversion from the M to the late G phase. mESC can divide in an unlimited fashion for numerous passages whilst retaining pluripotency at the same time as preserving genomic stability (Smith, 2001).

1.1.2 Epiblast stem cells

The differences in growth factors needed to promote pluripotency mouse and human ESC *in vitro* culture were thought to be species-specific (Pera et al., 2000). Subsequently, the finding of a discrete colony of pluripotent stem cells isolated from the post-implantation/pre-gastrulation stage of mice blastocysts revealed the existence and confirmation of more than one pluripotent cell type (Brons et al., 2007),(Tesar et al., 2007). Epiblast stem cells (EpiSC) are pluripotent but primed to differentiate into certain lineages. In contrast to mESC, mEpiSC cannot exist as single cells but only in colonies (Nichols and Smith, 2009). Functionally, EpiSC as well as mESC and hESC can form teratomas, however, only mESC and hESC can form chimeric mice (Fig. 1, iv).

The lack of ability of EpiSC to give rise to chimeras provides a definite confirmation that different pluripotent cellular states are present, based on germline developmental capacity, dividing the ‘naive’ and ‘primed’ pluripotent cell types. Fundamentally, pluripotent stem cells

in ‘naive’ and ‘primed’ states are labelled as mESC and EpiSC respectively. mESC are primitive and demonstrate 2 activated X chromosomes (XaXa), while one of the X chromosomes is turned off upon transformation into EpiSC (XaXi). This differentiation can consequently be reserved by the insertion of Klf4 to revert mESC flip back to ‘naive’ state (Guo et al., 2009). Moreover, research suggests developmental preferences of EpiSC with respect to certain lineages. For instance, the presence of the Brachyury (as a mesendodermal marker) is adversely associated with EpiSC potential to return to the ‘naive’ pluripotent state (Bernemann et al., 2011).

In the mouse, the naive and primed states can be stabilized ex vivo, represented by embryonic stem cells (mESC) and epiblast stem cells (EpiSC), respectively. Culture conditions for the two types of cells differ, reflecting the use of different signalling pathways to maintain pluripotency and self-renewal (Fig. 2). mESC maintenance is dependent on LIF and BMP4, or combined inhibition of Gsk3 and the MAP kinase pathway (Fig. 2A) (Yang and Weinberg, 2008). EpiSC maintenance requires both Activin and FGF2 (Fig. 2B) (Brons et al. 2007; Greber et al. 2010). In humans, ESC have been derived from blastocysts and, until recently, were regarded as the human equivalent of mESC. However, based on multiple characteristics such as flat morphology, dependence on growth factors, or X-chromosome inactivation, hESC (and human induced pluripotent stem cell [iPSC]) are closer to mouse EpiSC than to mESC and, as such, more likely correspond to the primed rather than the naïve state of pluripotency (Tesar et al. 2007; Stadtfeld and Hochedlinger 2010).

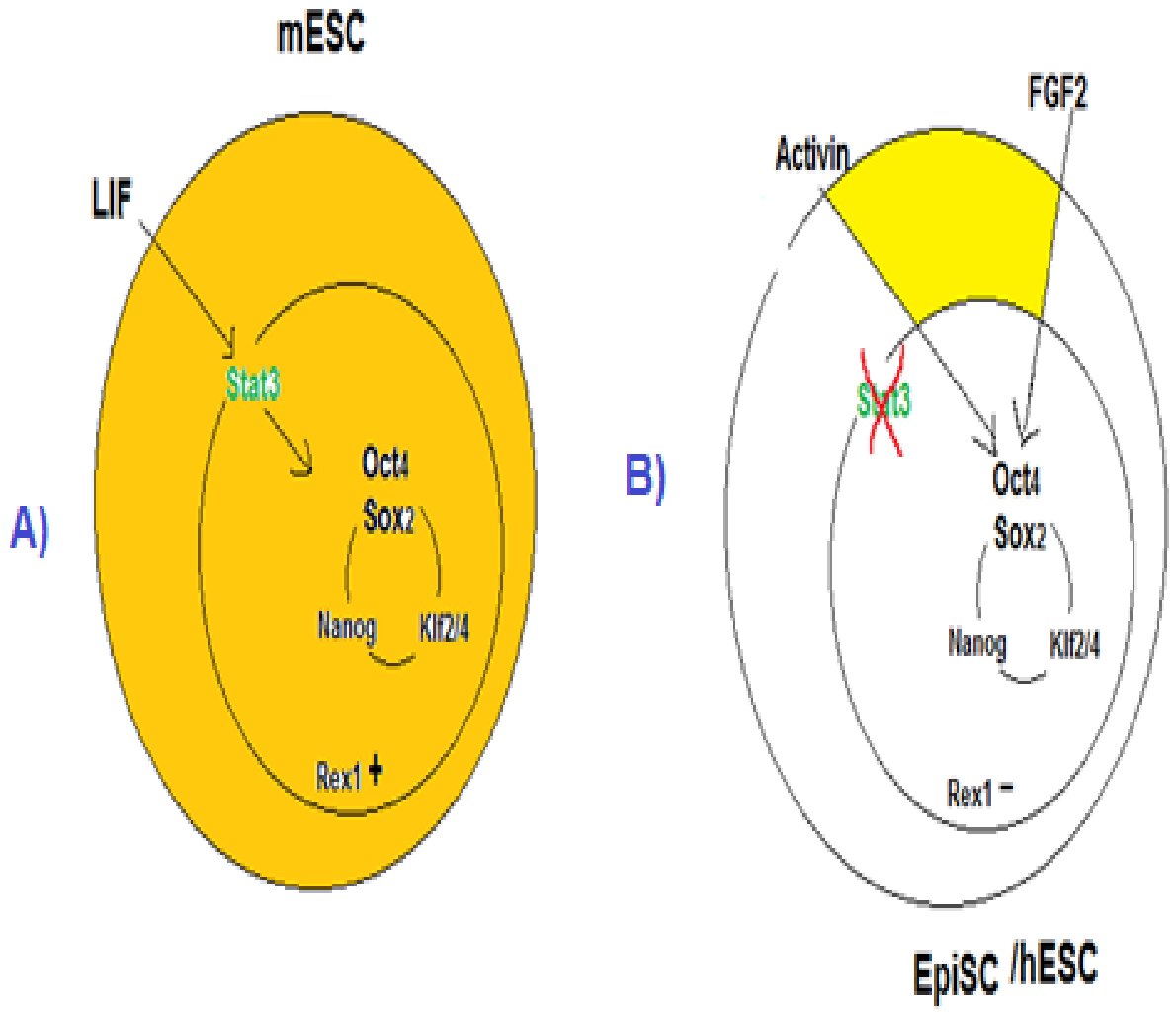

Figure 2 Essential growth factor to sustain pluripotency *in vitro*

Culture conditions for mES cells differ from EpiSC or hES cells. mESC rely on LIF/STAT3 signalling to maintain pluripotency (A), while both EpiSC and hESC depend on FGF2/Activin growth factors (B).

Even though, there are differences in the functionality of mESC and hESC the cellular markers of pluripotency are the same in humans and mice. This includes the presence of the nuclear transcription factor Oct3/4 (POU domain, class 5, transcription factor 1-POU5F1) that is essential for pluripotency of the stem cells. Removal of Oct3/4 in mouse embryos led to the deficiency of an inner cell mass materialization indicative of its capacity for forming pluripotent cells (Nichols et al., 1998). Similarly, the Sox2 transcription factor is associated with maintaining pluripotency via Oct-Sox enhancers that regulate the expression of pluripotent stem cell-specific genes, such as Nanog, Oct3/4 and Sox2 itself. Interestingly, forced expression of Oct3/4 rescues the pluripotency of Sox2-null ESC (Masui et al., 2007). Also, Nanog knockout models of mice gave rise to mESCs that were capable of self-renewal but differentiated more rapidly (Chambers et al., 2007). Consequently, the interaction of Oct3/4, Nanog, and Sox2 were established as perform a basic role in sustaining pluripotency in ESC of humans (Boyer et al., 2005) and mice (Loh et al., 2006).

Biologists have employed many tools to identify the gene expression profile that is cardinal in the regulation of the pluripotent state. Comparative studies that examined the specific gene expression patterns in several pluripotent cells, or their differentiated progeny, identified specific growth and transcription factors that are cardinal for the maintenance of the pluripotency of the stem cells such as Oct 3/4, Nanog, and Sox2 (Bhattacharya et al., 2004), (Richards et al., 2004), (Mitsui et al., 2003). In a proof-of-principle experiment, Takahashi & Yamanaka selected 24 genes that had been associated with maintenance of pluripotency in ESC and transduced them into MEF. Subsequent to the creation of ESC-like colonies, each gene was removed from the transduction process to assess its significance.

Finally, the following four factors were found sufficient to induce reprogramming: Oct3-4, Sox2, c-Myc and Klf4 REF. The resulting cells, termed induced pluripotent stem cells (iPSC) exhibited ESC-like characteristics in the sense of morphology, proliferation and teratoma formation (Takahashi and Yamanaka, 2006).

1.2. Stem Cell Culture

1.2.1. mESC culture medium

Maintenance of the stem cells in an undifferentiated state without chromosomal aberrations is still a challenging task for stem cell scientists. ESC require extrinsic growth factors to maintain their pluripotency in culture. Early work in mESC culture employed a feeder coating of mouse embryonic fibroblasts (MEF) as cradle signalling for the maintenance of pluripotency (Fig. 3A) (Finch and Ephrussi, 1967), (Martin and Evans, 1975). Although MEFs were initially used for both mESC and hESC culture, the growth factors that maintain pluripotency in these two ESC types are fundamentally different. For instance, it was discovered that LIF, an interleukin-6 cytokine produced by MEF, inhibited differentiation in mESC by activating the JAK/STAT3 pathway (Mintz and Illmensee, 1975), (Evans and Kaufman, 1981) (Smith et al., 1988). Human LIF, while serving the same biological role, is unable to maintain the pluripotent state of hESC (Daheron et al., 2004). Typically, mESC pluripotency can be maintained by activating the LIF/STAT3 and BMP pathways, while hESC require TGF-β/Nodal and FGF/MEK activation (Fig. 4)(Guofeng Han et al., 2013).

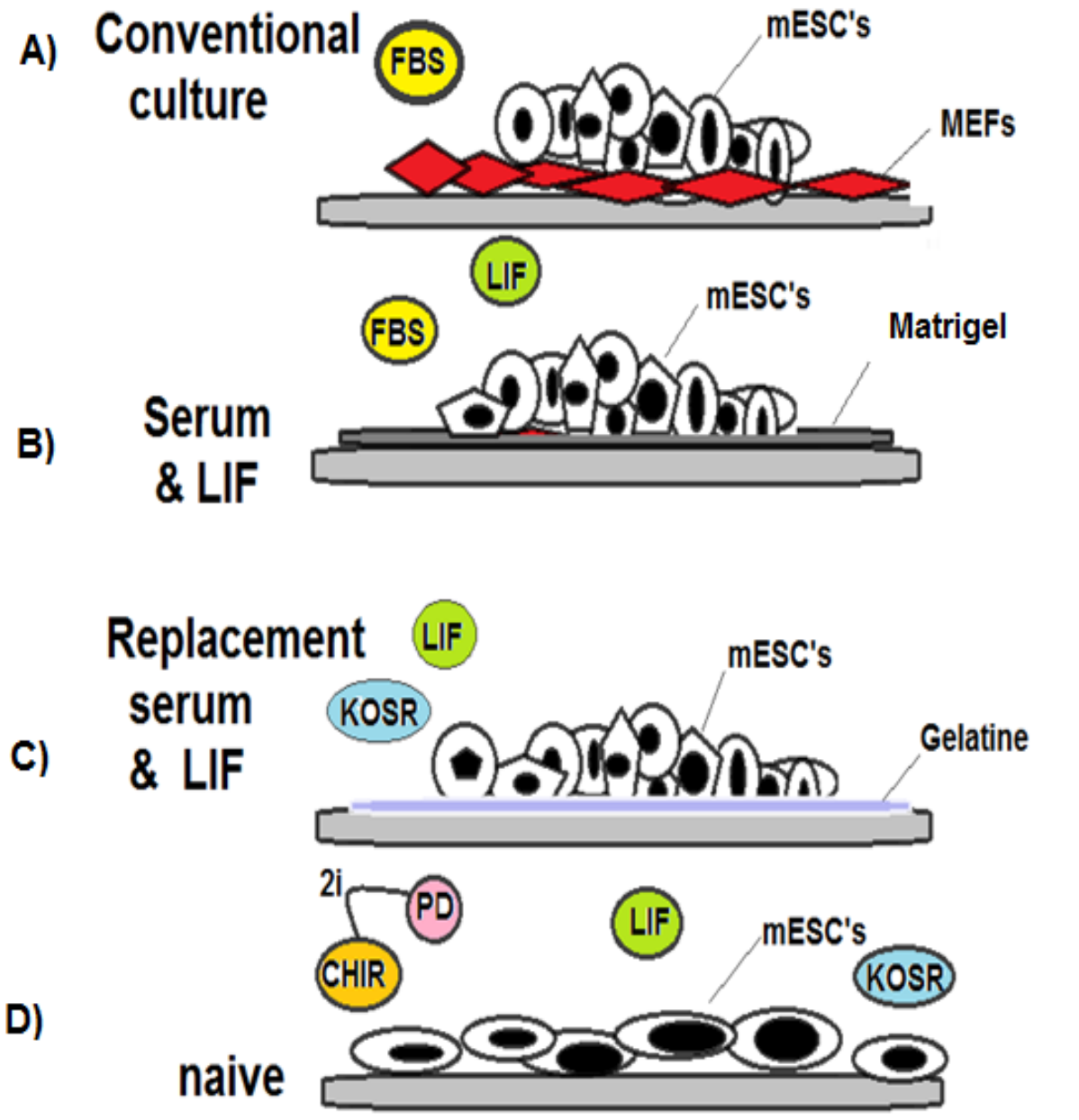

Figure 3 *In vitro* culture of mESC toward defined pluripotent niche

The conventional mESC culture protocol *in vitro* (A), compared to more recent approaches that aim to better define culture conditions using LIF (B), KOSR (C) and 2i medium (D).

Given the disadvantages arising from the need for culture with feeder layers (contamination, costs, poorly-defined environment) a number of approaches have been developed to substitute the MEF (Ratcliffe et al., 2011). mESC could be cultured on a gelatin matrix with the addition of LIF and bone morphogenetic protein (BMP) (Fig. 3B) (Bertolotti et al. (2009), (Williams et al., 1988).

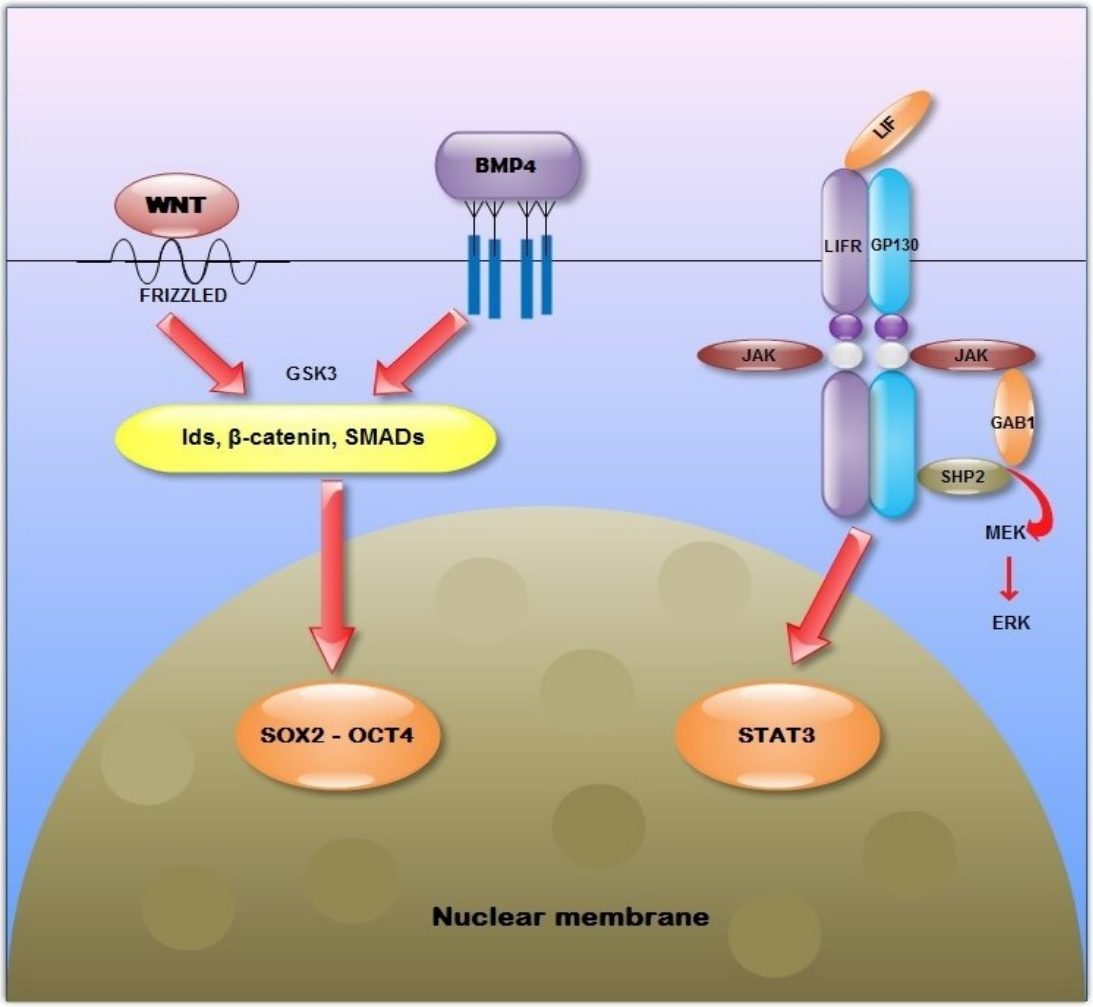

Figure 4 Mouse Embryonic Stem Cell Self-Renewal Signalling Pathway

External growth factors such as LIF bind to GP130/LIFR triggering JAK, which in turn leads to STAT3 phosphorylation. BMP4 sustains ESC self-renewal by inhibition of both extracellular receptor kinase (ERK) and p38 mitogen-activated protein kinase (MAPK) signalling.

Foetal bovine serum (FBS) represents the blood fraction remaining after the natural coagulation of blood, followed by centrifugation to remove any remaining red blood cells. FBS was used from early ESC cultures, as it contains nutrients, water carrier proteins, growth factors, hormones and attachment factors (Fig. 3B). However, FBS is not defined and can vary from batch to batch. In addition, serum contains growth factors that can promote spontaneous differentiation of mESC (Nagy et al., 1993). Defined serum, called knockout replacement serum (KOSR), provides an alternative to FBS to grow stem cells (Fig. 3C) (Klimanskaya et al., 2006). Similarly to FBS, however, KOSR can vary from batch to batch (Klimanskaya et al., 2007). Using bFGF and LIF, in a defined medium can be sufficient to avoid feeder or FBS, this medium is known as ESN2. However, mESC in ESN2 must be grown as suspension culture (Andrews et al., 2005),(Xu et al., 2002). Using ERK/MAPK and GSK3 inhibitors (2i medium) is sufficient to retain pluripotency, however mESC cultured in 2i (Fig. 3D, & Fig.5) media still respond to LIF, which enhances cloning efficiency and proliferation rates (Nichols et al., 2009).

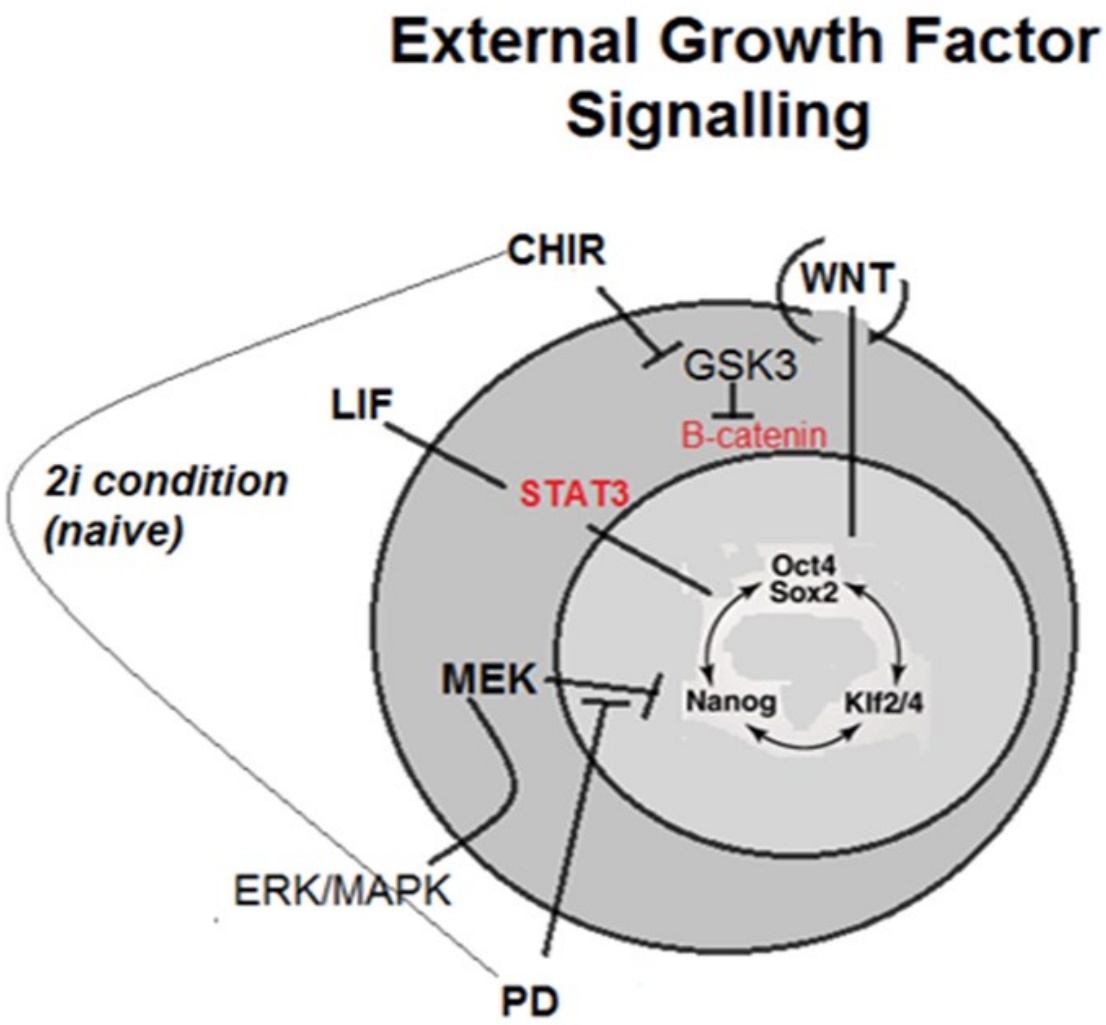

Figure 5 External growth factor signalling in ESC culture

There are different growth factor and chemical inhibitors use to maintain mESCs self-renewal *in vitro* such as CHIR that inhibit GSK3 signalling pathway or PD inhibitor which supress MEK pathway.

1.2.2. mESC culture matrix components

The use of individual single peptides or ECM proteins underestimates the complexity of the stem cell niche *in vivo*. The stem cell niche represents a dynamic space with constant interaction between external and internal environments during stem cell maturation and transition. For example, ECM protein degradation and turnover are in dynamic progression to facilitate ESC migration and differentiation. Thus, replicating the cell-cell interactions, transmembrane proteins, ECM, soluble factors and mechanical stimuli of the niche represents a difficult task (Joddar and Ito, 2013).

Native niche ECM found in the basement membrane (BM) is composed of several proteins, such as: Laminin (LN), Nidogen, collagen, fibronectin (FN) and perlecan (Gunwar et al., 1998, Kohfeldt et al., 1998). The distribution of BM components aids tissue specification and regulation of cellular behaviour (Noonan and Hassell, 1993). *In-situ* RT-PCR has shown that the three germ layers of the embryo produce these proteins (Gersdorff et al., 2005).

The interaction between different ECM matrix proteins is essential for scaffold organisation and their assembly role in cell fate decisions (Singh and Schwarzbauer, 2012). The composition of ECM is complicated thus difficult to modulate due to inherent ECM network complexity. Geoffrey et al show that mESC produce FN in order to adhere to gelatine and to retain self-renewal (Hunt et al., 2012). The maintenance of mESC *ex vivo* requires the presence of a feeder layer, which provides ESC with matrix rich in FN for attachment.

FN and LN are multi-domain ECM glycoproteins with various binding sites, such as proteoglycan, collagen and integrins. Their interaction in the ECM network enhances cell

adhesion and has a significant impact in cell development and differentiation. FN1 has been linked to a number of signalling pathways essential for mESCs self-renewal and proliferation. For example, FN1 phosphorylates Akt and activate PI3K/Akt signalling and group oncogene such as C-Myc, associated with self-renewal (Park et al., 2011). Subsequently, it promotes cell survival and proliferation through the activation of Rho-GTPase and caveolin-1 signalling. Furthermore, Kenneth et al showed a correlation between STAT3 activation and ES cells adherent to FN1 compared to non-adherent cells (Shain et al., 2009). FN-deficient embryos are unable to develop into the mesoderm linage (George et al., 1993) while LN-null embryos have epiblast differentiation defects (Li et al., 2002). Culturing mESC in FN- and LN-coated surface leads to a decrease in AP activity, Nanog and SSEA1, and an increase in FGF5 a marker for primitive ectoderm (Hayashi et al., 2007). There is an increase in FN and LN expression during primitive endoderm development. This may justify their essential roles in ESC differentiation (Li et al., 2003, Pimton et al., 2011).

LN is one of the main BM structures present in the ICM, the origin of ESC. LN contributes to cellular migration, proliferation and differentiation unlike other ECM proteins strictly involved in structural support. LN is a glycoprotein made up of α- β- and γ-chains. A total of 15 different combinations have been identified *in vivo*. These different LN subunits are strongly associated with tissue specifications and functions. LN subunit alpha-1 (LAMA1) is found in early development of certain epithelium tissues and triggers differentiation toward primitive ectoderm (Li et al., 2004). In contrast, LN subunit alpha-5 (LAMA5) is found restrictively in the ICM of embryos and adult BM. Stem cells grown in LAMA5 coated matrices are able to retain pluripotency for 170 days in the absence of LIF whereas cells on LAMA1-coated surfaces fail to maintain self-renewal and proliferation (Hunt et al., 2012). It has been suggested that deletion of the Lamc1 protein result in cells that fail to process primitive endoderm cells and post-implantation development (Smyth et al., 1999).

Perlecan, otherwise known as heparan sulphate proteoglycan core protein (Hspg2), is a BM-specific protein encoded by the Hspg2 gene. Perlecan is a negatively charged membrane bound protein that serves as extracellular protein (Pries et al., 2000) and is involved in metabolism, cell defence, wound healing and intracellular signalling (Bernfield et al., 1999). The specific role of Hspg2 in ECM is to bind and mediate fibroblast growth factor (FGF) signalling. For instance, the interaction between Hspg2 and FGF4 plays an active role in the early developmental stage and FGF2 at the late developmental stage. Similarly, Daniel et al found that ESC deficient in Hspg2 retained their undifferentiated status and failed to commit to any cell linage after LIF withdrawal. This may be due to the disruption of essential FGF2 signalling that inhibits Nanog and promotes ESC lineage commitment (Kraushaar et al., 2010). In addition, Hspg2 can function as mechanosensor mediating cell differentiation in response to shear stress (Bernfield et al., 1999) (Nikmanesh et al., 2012). Hspg2 can also interact with F-actin bundles and contribute to cell contraction and stabilisation. Lanner et al found that Hspg2 knockouts induced self-renewal by up-regulating Nanog expression and reducing embryonic cell heterogeneity by decreasing the phosphorylation of ERK1/2 (Lanner et al., 2010). In contrast, Sasaki et al postulated that presence of Hspg2 is essential for embryonic development and maintenance of self-renewal owing to its role in regulating a number of signalling pathways such as LIF/STAT3 and Wnt/β-catenin (Sasaki et al., 2008). This is because of the present of Hspg2 in the early, two-cell stage, and embryo (French et al., 1999, Carson et al., 1993). Furthermore, Hspg2-deficient mice are unable to survive beyond day ten (Costell et al., 1999). In contrast, Forsberg suggest that Hspg2-deficent ESCs are able to differentiate to most mesoderm lineage cells apart from adipocytes (Forsberg et al., 1999). Consistent with Sasaki et al demonstrated that ESCs deficient in Hspg2 spontaneously differentiated to extra embryonic endoderm (Sasaki et al., 2008) whereas Johnson et al reported the lack of Hspg2 leads to a neural lineage differentiation. The different impacts of reducing Hspg2 function

relate to differences in knockout targets. Such variation may be linked with the direct inhibition of N-sulfation or by indirect silencing of genes that encode the enzyme responsible for Hspg2 post-translational modification (PTM) (Tamm et al., 2012). Hence the blocking of enzyme synthesis may be inefficient owing to the presence of several enzymes in the Golgi apparatus that may contribute to the PTM of Hspg2.

Collagen XVIII, also named endostatin, is one of three known proteoglycan family, deposited in BM alongside with Agrin and Perlecan. Collagen XVIII serves as a peripheral membrane protein or secreted ECM protein and is known to possess negatively charged polysaccharide side chains. At early stages of embryo implantation (day 5) collagen XVIII is expressed and in the maturation stage, it is localised specifically in endoderm and epithelium tissue (Gersdorff et al., 2005). Collagen XVIII and collagen IV exist at the same level and abundance as collagen IV in the BM. Nevertheless, collagen-deficient mice survive after day 9, a possible indication that collagen is less essential in early development. Agrin is a member of proteoglycan family localized in the ECM of the synaptic cleft of neural and neuromuscular junctions and plays a vital role in cytoskeleton reformation, protein signalling activation and interaction with cytoskeleton protein such as Rac and PAK (Jogi et al., 2002).

Nidogen (NID), a member of the BM glycoprotein family contains three global domains with a potential role in connecting and assembling BM proteins. It cross-links both LN and collagen, which are the two main BM components. Two distinct Nidogen proteins NID2 and NID1 are known. NID2-null mice show no significant change in basement membrane organisation (Clapham, 2007). However, mice deficient both in NID1 and NID2 have disrupted BM organisation and matrix assembly (Hausmann et al., 2013). NID2 mRNA expression level in embryos is higher than in adults, whereas at protein level NID2 shows a lower level in adult tissue compared with NID1. Nevertheless, cells preferably bind and interact with NID2 rather than NID1 (Shoshan-Barmatz et al., 2006) .

The amount of ECM proteins in the stem cells niche contributes to cell fate determination in similar manner to Oct4/Sox2/Nanog, where a balanced concentration ratio is required to retain pluripotency. In this respect, change in the relative amounts of ECM components may results in ES cells differentiation (Niwa et al., 2000).

With the above information, using single or multiple ECM proteins can successfully control stem cell fate. For example using FN and LN to direct neural cell lineage commitment, or collagen to promote osteogenic differentiation (Hosseinkhani et al., 2008, Goetz et al., 2006).

1.2.2. mESC culture matrix architecture`

As mentioned above, the modification of the culture environment has a significant impact on the pluripotent state. Despite the considerable advances in mESC culture, the majority of protocols use a two-dimensional (2D) monolayer mode on a plastic (e.g. polystyrene) surface. The 2D culture method does not model the natural three-dimensional (3D) environment of cells. Cells adhered to an artificial surface are in contact with other cells only at their periphery, limiting inter-cellular contact and communication. Additionally, the lack of oxygen and nutrient gradients is non-physiological (Keung et al., 2011a) (Lund et al., 2009). Furthermore, in 2D culture models, cells are in contact with a horizontal plane on their basal side and with culture medium exposed on their apical side, which is different from *in vivo* stem cell niches that are 3D microenvironments. The use of glass and plastic substrates represents another weakness in 2D culture as it lacks the extracellular matrix (ECM) elements, biomechanical properties and growth factors of the natural environment (Lutolf et al., 2009). The stem cell niche consists of webs of ECM proteins and polysaccharides that encase the proliferating stem cells (Lutolf et al., 2009). For example, in the pre-implantation stages, the mouse embryo (i.e.

in vivo niche of PSCs) has a support of collagen IV and FN that also convey signals by means of cell-surface receptors (Kraehenbuehl et al., 2011).

A number of studies have examined the effects in cell culture in 2D and 3D environments. Migration rates of cells such as fibroblasts are affected by adhesion to the 2D substrate, while appropriate cell differentiation is observed in 3D matrices. Pampaloni et al cultured Mardin-Darby canine kidney (MDCK) cells on 2-D uncoated plastic, 2-D collagen-coated plastic and in 3-D collagen gel using proteomics to examine differentially regulated proteins. 3D substrate culture led to the formation of elementary kidney sub-organ structures and polarisation in both apical and basolateral surfaces. In sharp constant, MDCK cells on 2D monolayers had partial polarisation. These changes were in line with proteomics showing differential expression of antioxidant proteins, actin-binding proteins and glycolytic enzymes (Pampaloni et al., 2010). Thus 2D cultures may not entirely reflect the activities of cancer cells *in vivo*, emphasizing the limitation of 2D cultures as in vitro models for progression of malignant disease.

Mesenchymal stem cell (MSCs) destiny was also shown to be dependent on matrix stiffness ranging from soft, (1 kPa), intermediate (10 kPa) to stiff (100 kPa) (Engler et al., 2006). The decisive influences of the microenvironment was later exhibited in ESC as gene expression analysis emphasized many dissimilarities associated with ECM, cell growth, proliferation and differentiation in 3D vs. 2D cultured mESC (Liu et al., 2006). The impact of substrate stiffness and mechanosensing were further illustrated on mESC in culture utilising the variable rigidity of polydimethylsiloxane (PDMS) substrates.

The escalation in substrate rigidity resulted in an increased expression of genes involved with development of the primordial streak and growing mesendoderm. Furthermore, a shift towards osteogenicity (Evans et al., 2009) was also observed on stiffer substrates (Evans et al., 2009). Kraehenbuehl et al and Lutolf et al have suggested the potential impact of the rigidity

of bioengineered materials on either the differentiated or undifferentiated expansion of PSCs. (Kraehenbuehl et al., 2011, Lutolf et al., 2009).

In an intriguing study by Wang et al, mESC were cultured on substrate stiffness of either 0.6 kPa (similar to the cell) or by introducing small cyclic stresses of 17.5 Pa at frequency of 0.3 Hz through magnetic bead directed distribution of the cells. The tractive forces bought about alterations in cellular shape directed pluripotent cells towards differentiation. Chowdhury et al showed that differentiated mESC cultured under the influences of comparable cyclic stresses of 17.5 Pa were less effective for cell spreading (Chowdhury et al., 2010f). Research utilising polyacrylamide gel based substrates with variable stiffness confirmed that soft gels (0.6 kPa) were able to retain the expression of Oct3/4 in mESC during the 5 day period of culture without LIF, while in rigid culture dishes cells differentiated spontaneously in the presence of LIF. Due to the scarcity of PSC culture consuming “non-TCP” substrates, there is scope for utilization and development of biomaterials that can facilitate or mimic physiologically similar microenvironments.

Biomaterial science concerns the production of materials that can be seeded with cells.

General characteristics that a biomaterial must fulfill include:

(i) Biocompatibility,

(ii) Biodegradation in an appropriate timeframe that permits sufficient cellular growth while not producing harmful degradation products.

(iii) Mechanical properties that coincide with cell growth (i.e. a significant amount of 3D support in the early stages without obstructing cellular ECM production in the later stages).

More specific biomaterial attributes relate to the aim of recreating the non-mechanical attributes of the ECM. These properties include mediation of cell adhesion (e.g. via integrins), as well pro-survival -proliferation signals (e.g. via cytokines attached to the ECM). It has also been increasingly recognized, as shown by the studies above, that biomaterials are involved in mechano-chemical transduction.

Materials thus far have been traditionally divided in two categories, namely: (i) naturally derived materials (e.g. collagen) and (ii) synthetic materials (e.g. polystyrene). Material obtained from biological origins has a distinct advantage of ready availability and ability to aid biological signalling while requiring extensive testing in order to avoid inter-batch variability. On the other hand, synthetic polymers can be created to meet specific biomechanical properties, rate of degradation and porosity (Kraehenbuehl et al., 2011). As already mentioned, the ECM carries out secondary roles beyond its mechanical properties. Synthetic scaffold materials can be modified to include properties such as cell adhesion and proliferation. Cell adhesion to scaffolds is dependent on the presentation of small peptide adhesion domains that bind to integrin receptors. Peptide sequences that have been added on synthetic materials to improve adhesion include Arg-Gly-Asp (RGD), Tyr-Ile- Gly-Ser-Arg (YIGSR) and Arg-Glu-Asp-Val (REDV).

Together, these results suggest that culturing PSCs on conventional tissue culture plastic may result in phenotypical alterations to their normal *in vivo* state, and the use of appropriate biomaterials may help with enhancing the stem cell culture conditions.

1.3. Alginate hydrogels

Hydrogels are frequently exploited for generating novel scaffolds in tissue engineering research. Hydrogels are porous substances that can house living cells, extending a microenvironment where cells can further proliferate and release growth factors and metabolic waste products. Amongst several other hydrogels, such as fibrin, gelatin and hyaluronic acid, alginate is widely used in tissue engineering due to its particular biocompatibility and non-irritant properties. The cues faced by a cell are extremely different between soft substrate or plastic surface (2D) and a typical 3D ECM. The 3D culture provides cells with cell-cell and cell-matrix interaction. Also it overcomes the stiffness of plastic culture flask (Fig. 6). Furthermore, cells grown in alginate hydrogels are protected against immune regulation.

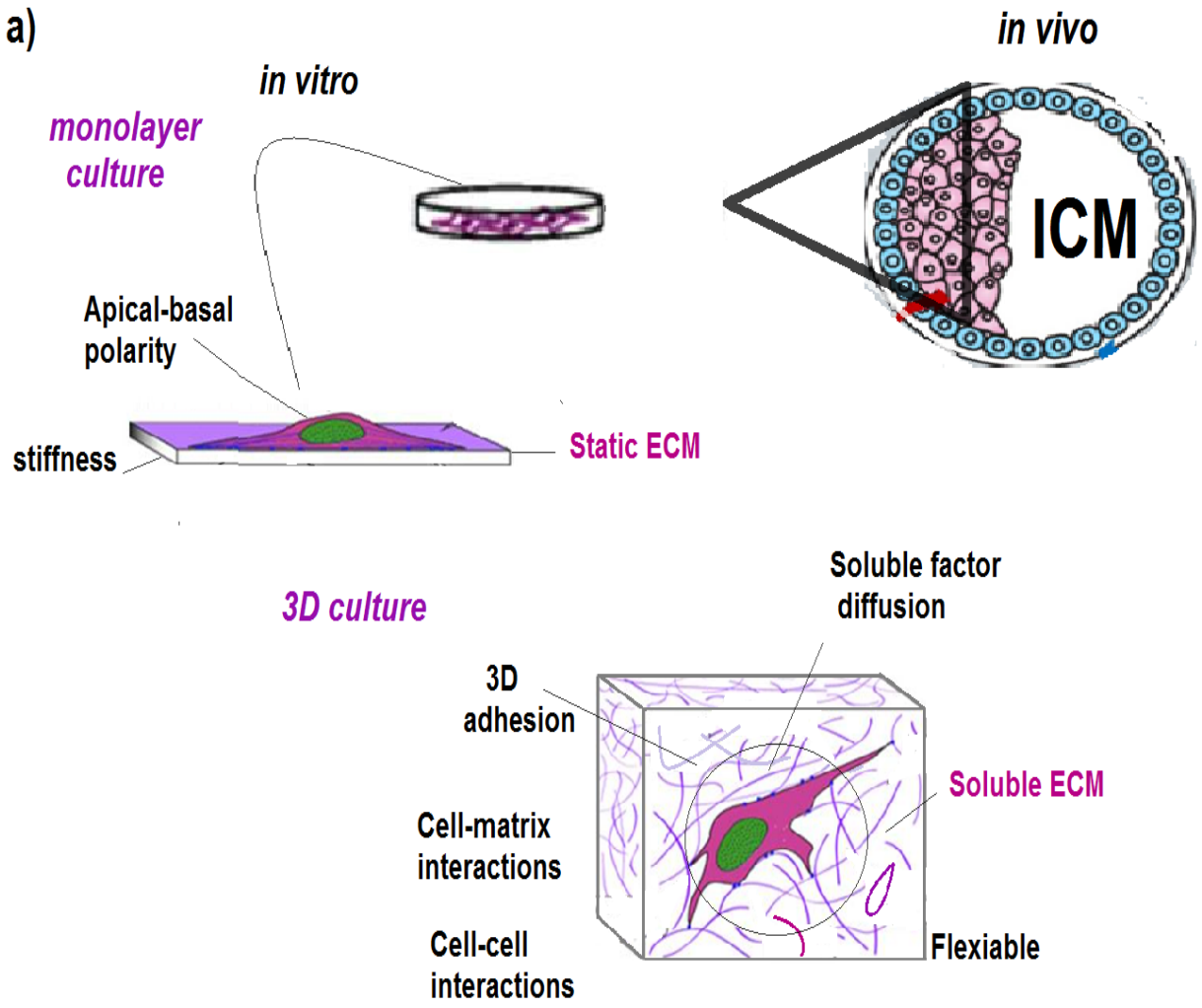

Figure 6 2D vs. 3D stem cell culture

The ability of *in vitro* 3D culture to resemble the *in vivo* environment in terms of topographical, mechanical, adhesive and soluble cues obtain enhanced condition for stem cells. This figure is adapted from (Baker and Chen, 2012)

Water-soluble alginate is a polysaccharide composed of two types of glycan: guluronic acid and mannuronic acid. The guluronic acid content provides strength to the hydrogels (Wikström, 2013). Furthermore, association of alginate with divalent cations such as Ca^{+2} make

the gel firmer and more durable (Fig. 7) (Wikström, 2013); (Lee et al., 2012). At higher concentrations, Ca^{+2} results in more porous gels that can contribute to increased distension and outflow. This can influence the immunological isolation of the cells captured in the gel. Disadvantages of alginate-based hydrogels include the fact that they are not biodegradable *in vivo* and the level of manual dexterity needed in handling them, as they are very soft (Kuo et al., 2012).

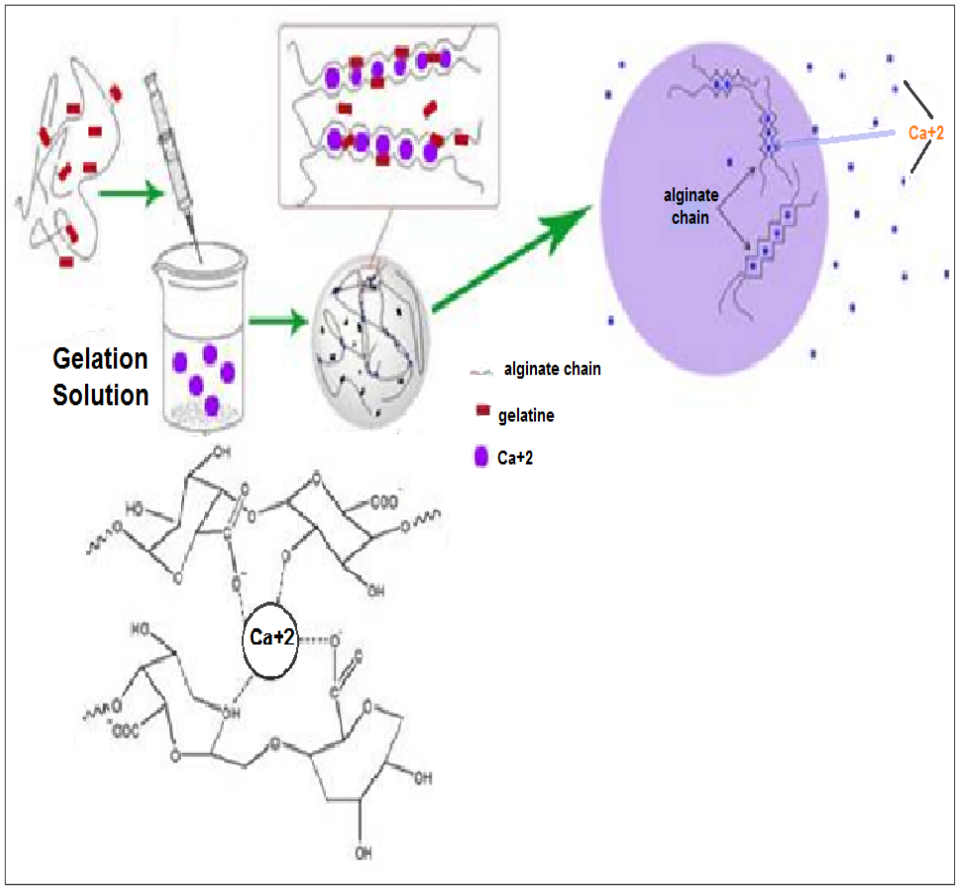

Figure 7 Alginate acid encapsulation using calcium chloride

The process of encapsulating alginate chains using calcium ions. Adapted from (María Chávarri, 2012)

In recent times, the use of alginates in biomedical fields has played an important role in terms of tissue engineering or drug delivery. However, alginates lack adhesive properties due

to their hydrophilic nature and the negatively charged groups on the chains (Therese Andersen and Christensen, 2012). In spite of their poor adhesive properties, alginates are attractive biomaterials owing to their ease of fabrication using different coating surfaces or mechanical manipulations. The manipulation of variables such as mechanical stress has been shown to have a significant influence in stem cell fate determination (Fisher et al., 2009) by providing mechanical cues. For instances, MSCs grown at different substrate stiffness such as soft, mild or rigid can differentiate either to neuron, myoblast or osteoblast respectively (Engler et al., 2006). Likewise, modifying the alginate surface by small molecule such as chemically modified PEG doped with phosphate groups enhances bone mineralisation of MSCs. (Benoit et al., 2008).

1.4. Dynamic bioreactors

Static culture is typically dependent on the passive diffusion of the soluble factors in culture media (Placzek et al., 2009). Randers-Eichhorn et al examined O_2 levels in the gas and liquid phases of murine hybridoma culture. They found that O_2 transfer through the liquid under standard laboratory conditions was greater than that predicted by passive diffusion due to microscale mixing. However, over time O_2 at the bottom of the flasks reached zero (Randers-Eichhorn et al., 1996). This suggests that use of static vessels in culturing PSCs is not adequate, particularly in a 3D cultured system of rapidly growing cells. Nonetheless, low mass transport of nutrient and oxygen can facilitate heterogeneous cultures that may further induces cell differentiation or gain of an anomalous karyotype (Azarin and Palecek, 2010). Consequently, a substitute for management of cells at an industrial scale is by means of dynamic environments that can overcome the limitations of conventional culture.

Numerous bioreactor designs have been presented for industrial PSC culture where the primary focus is on improving mass transport and reducing culture heterogeneities. The stirred suspension and rotating wall vessel (RWV) bioreactor configurations are the most widely used. In addition RWV bioreactors vessels have been successfully exploited for embryoid body formation; *in vitro* cultured PSC cells in 3D environment in hydrogels or as aggregates. Stirred suspension bioreactors are normally operated at 30-60 rpm, leading to a high amount of shear stress in the freely suspended PSCs ((Rodrigues et al., 2011), (Placzek et al., 2009)). Alternatively, RWV bioreactors that have high aspect ratio vessel (HARV) or slow turning lateral vessel (STLV) geometries result in PSC suspensions with minimal shear stress and free fall culture conditions ((Placzek et al., 2009), (Hwang et al., 2009)).

Kinney et al also examined the potential effects of different hydrodynamic and other bioreactor conditions on stem cell cultures (Kinney et al., 2011). Bioreactor hydrodynamics affect industrial scale culture of PSCs due to alteration in spheroid size, homogeneity of nutrient supply, kinetics of aggregation, and yield of spheroids. Due to these aforementioned factors PSCs cultures have shown variable rates of expansion, viability, and metabolic activity (Kinney et al., 2011). Additionally, the effect of shear stress due to rotation of culture vessels has been shown to differentiate hESC lines in to the IMR 90 phenotype when rotated at 100-120 rpm. However, further research suggests, even after reduction in shear stress this did not affect spontaneous differentiation and it was later suggested that an altered distribution of soluble factors due to forceful movement of the culture vessel was affecting hPSC differentiation (Leung et al., 2011).

Additionally, global expression analysis by Roy et al further suggested that mESC differentiated along the hematopoietic lineage when cultured on polymeric scaffolding (Roy et al. 2011). Dynamic culture of stem cells also increased ECM production, cellular adhesion, and elevation in gene transcription when compared with a 3D static system. In addition, BMP-4

expression occurred exclusively in dynamic cultures, which further strengthens the above findings. All these results support the idea that the hydrodynamics of spinner flask cultures dynamically stimulate a microenvironment that induces a hematopoietic lineage differentiation (Liu et al., 2006). Additional investigation of mESC in bioreactors with distinctive hydrodynamic properties demonstrated an increase in Sca-1+ cells (markers of hematopoietic stem cells) suggestive of presence of stem and progenitor cell types while c-Kit+ endothelial cells were produced in rotator flask cultures consistent with the hypothesis that the hydrodynamics of a culture is capable of manipulating PSC fate (Fridley et al., 2010).

1.5. Proteomics

1.5.1. Genomic vs. Proteomic Characterisation of mESC

While analysis of the genome and transcriptome examine DNA and RNA expression respectively, they fail to elucidate the dynamics of cellular proteins such as quantity, stability, cellular localization, post-translational modifications (PTMs), and their communications (Stanton and Bakre, 2007). To complement the transcriptomics studies it is desirable to also perform a proteomics analysis. This is particularly pertinent as there is little association of transcriptional profiles with stem cells differentiation (Anderson and Seilhamer, 1997, Wei et al., 2005) (Unwin and Whetton, 2006, Cloonan et al., 2008). These investigations inferred that differential mRNA expression in stem cell progeny does not necessarily mirror the protein expression. Analysis of the proteome also allows the possibility to study the post translational modification of proteins (Unwin and Whetton, 2007);(Brill et al., 2009); (Smith and Workman, 2009); (Guo et al., 2012, Williamson and Whetton, 2011). The term “Proteome” was coined by Marc Wilkins in 1994 where PROTE comes from word protein and OME from genomes

(Yu et al., 2007). Proteome is defined as an analysis of complete set of proteins in a cell, tissue, or organism (Baharvand et al., 2007a). Of the several questions to be answered in cell biology, proteomics has been used to study the self-renewal and differentiation of stem cells (Van Hoof et al., 2006); (Liu et al., 2010). Additionally, PTMs that regulate cellular destiny outcomes, either by means of phosphorylation or ubiquitination are of critical importance (Baharvand et al., 2007b).

Technological developments in protein fractionation and mass spectrometry (MS), have significantly improved the ability to investigate and abstract biological evidence from intricate cellular experiments. Identification of mESC proteomes has been made by utilising two-dimensional-sodium dodecyl sulphate-polyacrylamide gel electrophoresis (2D-SDS-PAGE) approaches coupled with MS for protein identification (Gundry et al., 2010, Baharvand et al., 2008). Nevertheless the identification of low abundance proteins is still a limiting factor. An alternative non-gel approach that could help would be Multidimensional Protein Identification Technology (MUDPIT), however, that would only provide qualitative data. Therefore the focus has been directed towards more quantitative proteomic methodologies (O'Brien et al., 2010, Graumann et al., 2008a).

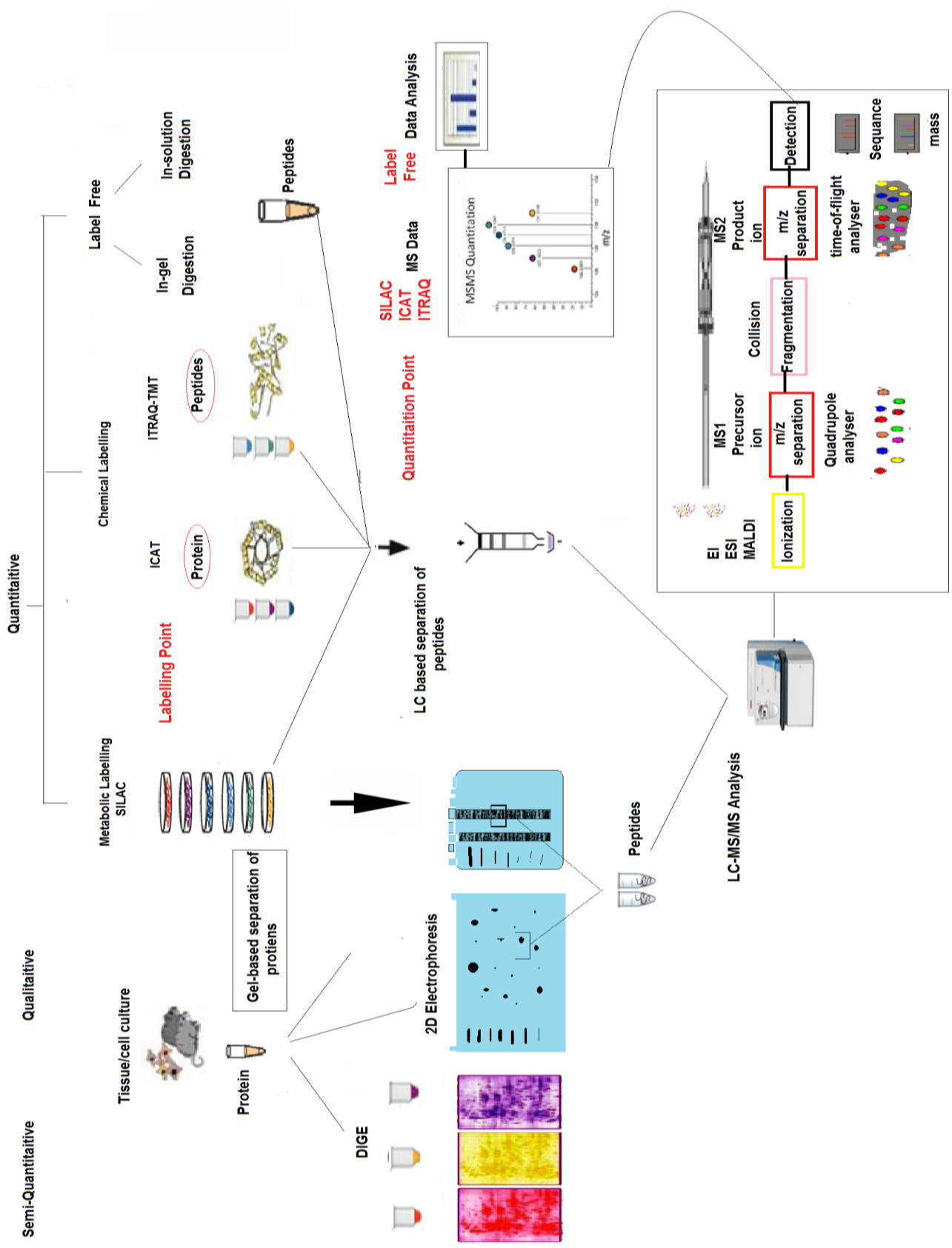

Figure 8 Proteomics workflows Comparison of quantitative, qualitative or semi-quantitative proteomics workflow

In the gel based strategy, gel bands (from 1D gel) or protein spots (from 2D gel) are obtained. This is followed by trypsin digestion and MS analysis of peptides. In contrast, in-solution digested (ISD) MS based strategy, the proteins are not fractioned using gel but partially separated followed by LC/LC-MS/MS for peptide separation and sequencing. Labelling points in each workflow exist whereby (Fig. 8, red circle) samples are isotopically labelled for LC-MS analysis except in label-free quantification. In label-free quantification, samples are individually analysed and data compared using multiple approaches involving spectral counting and peak intensity. In contrast, metabolic labelling is associated with pre-isotopic labelling of proteins. Following that, prior to quantitative analysis samples are combined and processed simultaneously. Protein extracts in both isotopic and isobaric tags before labelling. However, isobaric tags LC-MS/MS analysis produce spectra of peptide fragment ion obtained in MS1 and the cleaved tag spectra produced in MS2. The MS2 spectra identify peptide and use to relative quantitation. Heavy peptide standard curves are used to speculate quantities of un-labelled samples for absolute quantitation. Metabolic labelling workflow has reduced experimental bias due to prior labelling of protein in vivo. On the other hand, label-free workflows increase this risk due to individually analysed samples.

There is an inverse relationship between protein quantified and identified in the sample. Sample complexity is a critical factor in peptide quantitation, as identification and quantification rates are inversely proportional to sample complexity (Fig. 9a). Methods such as affinity purification are often performed to remove high-abundance proteins and reduce sample complexity. In-line liquid chromatography (LC) is also a common pre-MS fractionation process to chemically separate peptides to further reduce sample complexity. Cells can also be grown in different stable isotope labelling amino acids (SILAC) media then obtained, combined and digested for LC-MS/MS analysis (Fig. 9b). Data are analysed using the Max-Quant software, both protein identification and relative quantification obtained from the MS/MS spectra. The ratios of the SILAC pairs are used for relative quantification.

Quantitative analyses have also been carried for direct evaluation of the phosphoproteome to understand mESC self-renewal and differentiation (Li et al., 2011). Findings from research of Li et al advocated the dynamic status of the proteome in mESC. Together both genomic and proteomic research data that have been obtained on mESC up till now have uncovered and indicated role of several intracellular signalling pathways now consider to be fundamental to pluripotency.

1.5.2. Mass Spectrometry of Proteins and Peptides

A standard MS peptide analysis proceeds in multiple phases. Firstly, it is by measuring the mass-to-charge ratios of unfractionated peptides. Following selection of specific peptides on the basis of comparative abundance in the first mass analyser (e.g. Quadruple 1) disintegration takes place in a collision cell (Quadruple 2). The mass-to-charge ratio (m/z), of each disintegrated ion is exposed to a second mass analyser to collect the time of flight, Linear Ion

Trap, Orbitrap, and Ion Cyclotron Resonance cell. This procedure is known as tandem MS, or MS/MS.

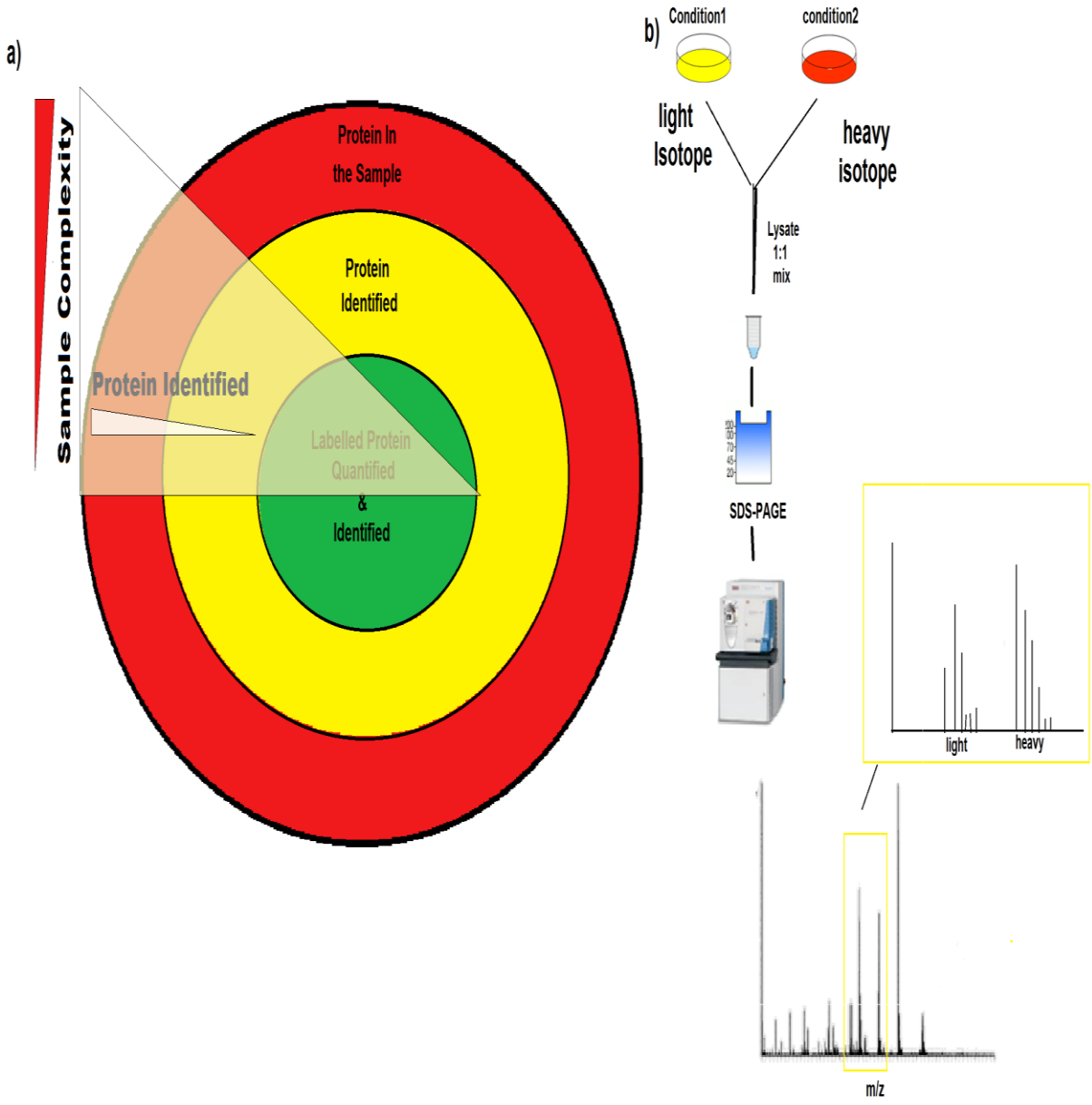

Figure 9 Workflow of the stable isotope labelling amino acids (SILAC) media Relationship between protein identification and sample complexity (A), and the workflow of the SILAC

Comprehensive examination of the product ion masses in the MS/MS spectrum delivers knowledge about the peptide sequence chosen for fragmentation and, by extrapolation, identification of the protein to which it correlates. Earlier types of MS instrumentation were not capable of performing these assays. Ionization was achieved through electron impact or chemical ionization and will result in increased in-source fragmentation of biomolecules. Therefore, advances in soft ionization techniques, for example matrix-assisted laser desorption ionization (MALDI) and electrospray ionization (ESI) transformed protein analysis (Fenn et al., 1989), (Whitehouse et al., 1985). MALDI and ESI are so called 'soft techniques' due to little in-source fragmentation occurring of the ionized protein species and this facilitates the quantification of mass of the complete biomolecule or protein. Additionally, ESI and MALDI may be easily coupled with MS. The most widely exploited hybrid instrument for proteomic experiments is a mass analyser that measures of time of flight (TOF) (Chernushevich et al., 2001), (Roepstorff, 2000), quadruple (Q), ion trap (LIT) (Yost and Boyd, 1990), Fourier transform ion cyclotron resonance (FT-ICR) (Peterman et al., 2005), and Orbitrap (Gizzi et al., 2005). Every one of these above mentioned analysers have advantages and disadvantages.

1.5.3. Proteomic Analysis of Complex Mixtures

Developments in instrument scan speed mean that, MS analysers can identify a limited number of ions in any given time. To sort the elements of a sample chromatographic separation has been applied prior to MS initially by partition with a reversed phase (RP) column that separates on the basis of hydrophobicity. To further simplify samples a secondary separation method is often utilised following the RP using either strong cation exchange (SCX) or 1D-SDS-PAGE (Bendall et al., 2009), (Fang et al., 2010). One discrete benefit of ESI is its compatibility with several on-line separation techniques that can be directly coupled to the MS analysis.

1.5.4. Peptide Identification from Mass Spectra

The MS principle relates to ionisation of chemical compounds to generate charged molecules or molecule fragments. Amino acids can then be identified by calculating the mass-to-charge ratios (Domon and Aebersold, 2006). One of the most widely employed fragmentation techniques in MS is collision-induced dissociation (CID) (Hayes and Gross, 1990), (Morris et al., 1996). In CID, peptide ions are accelerated into a collision course with inert gas molecules such as helium, nitrogen or argon. As well as CID, electron capture detection (ECD) and electron transfer dissociation (ETD) have been used in the current generation of mass spectrometers (Appella and Anderson, 2007), (Zubarev et al., 2000). This advance in instrumentation facilitates the generation of spectra through two complementary fragmentation techniques (Swaney et al., 2008).

Following fragmentation peptides were characterised either with the aid of the appropriate software or with standard search engines to compare the detected or observed and speculative or theoretical peptide spectra creating, an *in silico* assimilate of a sequenced databank (Forner et al., 2007). Search engines achieve peptide matches created on a range of metrics proposed to produce a score demonstrative of the quality of match amongst the detected and theoretical spectrum (Forner et al., 2007), (Johnson et al., 2005). Recent developments in software allow searching of peptide spectra in a databank of formerly obtained MS/MS experimental spectra (Lam et al., 2008). These *in silico* lead to both better sensitivity and speed. However, restrictions exist due to the subject matter of the spectrum databanks. Further substitution of the earlier methods involves *de novo* approaches that utilise electronic means to sequence the peptides straight from the MS/MS spectrum (Xu and Ma, 2006). In such *de novo* approaches information about the fragmentation methods used in the MS and fundamental search considerations that is provided by the researcher allows peptide chain reconstruction (Dancik et al., 1999), (Xu and Ma, 2006). *De novo* methods of sequencing possess a lot of promise due

to the potential for identification of formerly unidentified peptide sequences and PTMs. In spite of this, operating an amalgamation of several search engines has been effective in accomplishing optimal analysis (Boutilier et al., 2005), (Jones et al., 2009).

1.5.6. Quantitative Proteomics and SILAC

With the technological advancement in proteomics, MS, and bioinformatics a very long list of protein candidates is generated that often challenges the biologist for delineating the specific biologic importance of particular proteins (Ahn et al., 2010). Therefore a quantitative approach can be exploited to abstract the most biologically relevant information from a vast proteomic data set. Quantitative proteomics is widely used to obtain biologically meaningful data when investigating cellular signalling during differentiation (Figure 6a). MS is semi-quantitative therefore quantitative labelling is often used. However, with recent advances in technology label free approaches are also becoming popular ((Mueller et al., 2008), (Domon and Aebersold, 2010)).

In MS-based proteomics, quantitative approaches usually employ stable isotopes for production of 'heavy' and 'light' samples that maintain their chemical stability and can be distinguished and evaluated by MS assessment. Quantitative labelling can be applied either at protein or peptide level, before performing the MS analysis. For peptide level labelling it is generally primary amines that are marked for comprehensive sample analysis. Additionally, isobaric and tandem mass tags (TMT) for comparative and total quantification could only be achieved after protein digestion (Ross et al., 2004). Dimethyl labelling methodologies for peptide labelling have also been utilised effectively with minimal reagent consumption. Whereas chemical labelling approaches like ICAT have confirmed their applications, using metabolic labelling such as SILAC (Figure 9b) is preferable for cell culture (Ahn et al., 2010).

Alternatively, metabolic insertion of isotopically labelled amino acids to tag peptides of interest is widely used. Of several isotopic labelling approaches, stable isotope labelling of amino acids in cell culture (SILAC) permits metabolic incorporation of ^{13}C and ^{15}N in amino acids into the cellular proteome (Fig. 9b) (Mann, 2006), (Ong et al., 2002). Supplementary techniques founded on the principle of metabolic assimilation of ^{15}N have been commonly used (Krijgsveld et al., 2003). These approaches depend on the addition of isotopically marked amino acids, which are integrated into recently, produced proteins (Larance et al., 2011). There are number of advantages in using the comprehensive SILAC approach. These include minimisation of the variability introduced due to separate sample handling prior to SILAC; labelled samples (heavy and light) are pooled and processed together. The heavy amino acid has been shown to have no effect on cellular metabolism or phenotypic switch particularly in stem cells (Graumann et al., 2008a). Additionally, complete amino acid incorporation can only be achieved after 5 passages.

However, there are three major artefacts that could be introduced in the SILAC ratio calculation. These errors involved incomplete corporation of the isotopes, metabolic arginine to proline conversion, or errors introduced by mixing unequal amounts of protein in the two-samples (Park et al., 2012). For instance, incomplete incorporation of heavy isotope can lead to the presence of additional light peptides whereas arginine to proline conversion leads to reduction of ions of the peptides in the heavy isotope labelled samples. It has been suggested that proline to arginine conversion can be reduced to a minimum if the culture is supplied with excess proline (Lossner et al., 2011). However, using 15% of KORS in ES cells cultures provides cells with 800mg/L of proline (Bendall et al., 2008). Coincidentally, KORS contains no free arginine or lysine making it compatible with SILAC application (Bendall et al., 2008). Hence, extended culture of the ES cells in the SILAC media (minimum of 14 days) results in maximum labelling of Arg and Lys residues (96%)(Bendall et al., 2008).

In all the above stated metabolic methodologies, diversely labelled samples are blended in definitive proportions, and the comparative abundance of proteins can be related quantitatively on the basis of the respective intensities of the peptide in their mass spectrum. Therefore, isotopically labelled amino acids by means of any aforementioned methods allows observation and investigation of the minuscule alteration in cellular phases over time.

1.6. Aims and hypothesis:

Pluripotent stem cell culture typically involves feeder layers, non-defined and variable culture media, 2D culture plates that are typically made of plastic. PSC *in vivo* exist within a physiological environment that is completely different both in terms of structure and components. There is strong aim for a more physiological microenvironment optimising cell-to-cell, cell-to-ECM contact, mechanical and chemical stimuli. Appropriate 3D culture provides important 'niche' components and plays a role in determining stem cell fate. 3D culture represents a step of intermediate complexity between *in vivo* niche and *in vitro* 2D cultures. However, comprehensive characterisations of the effects of 3D culture conditions *in vitro* and their suitability as imitation of the *in vivo* environment are still not clear. Even the regulatory mechanisms underlying the self-renewal ability of SCs under standard protocols are poorly defined. Understanding pluripotency and differentiation mechanisms in the 3-D cultures might allow us to manipulate the fate of stem cells for production and therapeutic purposes.

Hydrogels, an example of materials used to form 3D structures, have been used as culture substrates to create more suitable microenvironments for SC culture (e.g. mESC encapsulation within alginate beads (Hwang et al., 2009). One of the main advantages of alginates it is their ability to maintain the cells in culture for prolonged periods of time without passaging or the use of feeder cells. However, using 3D cultures potentially leads to diffusion barriers that may

limit transport rates. The use of bioreactors that employ rotary or stirring may enhance transport rates (Hwang et al., 2009, Placzek et al., 2009, Rodrigues et al., 2011). The improvements in mass transport in bioreactors improve the reproducibility of process conditions as well as homogeneity of the cell population, compared with static cultures (Placzek et al., 2009). In addition, using bioreactors aids scale up of cell production.

Previous work using alginate beads found they could enable pluripotency maintenance for up to 250 days without cell passaging (Siti-Ismail et al., 2008). Additional work also showed the improved capacity of perfusion bioreactors to sustain a naïve mESC population over batch culture as a result of a decrease in metabolic stress through washing out waste metabolites with fresh medium (Yeo et al., 2013). However, studies directed at the large-scale analysis of cells in this micro-environment to determine the effects of 3D culture on the undifferentiated expansion of ESC's, needs to be undertaken.

The aim of this work is to investigate the effect of 3D culture using alginate beads and bioreactors on ESC self-renewal, potency and differentiation. The mechanisms pertaining to control of self-renewal will also be investigated using proteomics. Critical to these studies will be the development of efficient methods for the extraction and analysis of proteins. Comprehensive protein analysis will be performed in ESC culture in 2D, 3D static and 3D dynamic (i.e. bioreactor) conditions.

1.6.1. The work-flow used in this research is as follows:

- Investigate the effect of 3D culture on cell viability, proliferation, and gene expression both at short exposure and prolonged adaptation.

- Development of efficient methods for the extraction of proteins from the 3-D environment.
- Employ protein identification methods that use SILAC to facilitate the comparative analysis of mESC in 2D, 3D static and 3D dynamic conditions.
- Interpretation of the behaviour of mESC in different culture environments in the light of the differential protein expression data.
- Functional validation of the identified proteins at short (3 days) and long (18 days) culture time.

CHAPTER 2: Material and methods

2.1. The mESCs Culture

2.1.1. Preparation of cell maintenance media for culture of mouse embryonic stem cells (mESCs)

Dulbecco's Modified Eagles Media (DMEM) without sodium pyruvate was supplemented with 10% (v/v) foetal bovine serum (FBS; Gibco) or 15% knockout replacement serum, 100 units ml^{-1} penicillin, 100 µg ml^{-1} streptomycin, 2 mM L-glutamine (all supplied by Gibco, Invitrogen, UK), 0.1 mM β-Mercaptoethanol (Sigma-Aldrich, Poole, UK) and 1000 U ml^{-1} of Leukemia Inhibitory Factor (LIF; Millipore, U.K. Limited, UK).

2.1.2. *In vitro* culture of mouse embryonic stem cells (mESC) culture

A commercially supplied mES cell lines (Catalogue No: CRL-1821) were obtained from American Type Culture Collection – ATCC). Cells were routinely cultured in tissue culture flask coated with 0.1% gelatin (Sigma-Aldrich, UK) in humidified cell culture incubators (Nuaire, Nu – 5510E, Triple Red Ltd.) at 37°C and 5% CO_2. The cultures were substituted with fresh media daily, and passaged every 3 days at a seeding density of (2–4) $\times 10^4$ cells/cm^2. Prior to sub-culture, culture media was aspirated and washed with 1X PBS (without calcium and magnesium) (Gibco) followed by addition of 0.05% (v/v) trypsin-ethylene diamine tetraacetic acid (Trypsin-EDTA; Gibco) solution at 37^0C and 5% CO_2 for 5 minutes. Cell suspensions were then re-suspended gently using a Gilson pipette for 1 minute to ensure completely dissociation and single cell suspension. Complete cell culture media was added to stop the dissociation reaction and washed with 1× PBS (phosphate buffered saline). Cell suspension

was then centrifuged at 360 g and cell supernatant was removed. Fresh cell culture media was added and cell pellet was suspended gently to ensure a single cell suspension.

2.1.3. Alginate beads encapsulation

To aim for a 3 dimensional culture, the cells are cultured as explained in section above 2.1.2. followed by an isolation of cell pellet. Cell pellet was then re-suspended in 1.1% (w/v) alginic acid (Sigma, UK) and 0.1% (v/v) porcine gelatin (Sigma, UK) solution (both were dissolved in PBS, adjusted for pH 7.4 and filtered through a 0.2 mm filter) using a Model P-1 (Amersham Biosciences, UK). This cell suspension was then dripped with an aid of 25-gauge needle into sterile alginate gelatin solution consisting of 100 mM $CaCl_2$ (Sigma, UK), 10 mM HEPES (Sigma, UK), and 0.01% (v/v) Tween (Sigma, UK) at pH 7.4 with constant gentle stirring. Roughly, 25,000 cells were encapsulated in every alginate hydrogel batch solution. The hydrogels were maintained in $CaCl_2$ solution with gentle stirring for 6–10 min followed by washing in excess of PBS. Cells were then replenished daily with the 2D cell culture media at 37°C in a 5% CO_2 humidified incubator for 4 days.

2.1.4. Rotating wall vessel high aspect ratio vessel (HARV) bioreactor culture

HARV bioreactor vessels (Cellon S.A (Bascharage, Luxembourg) with a volume of 50 ml were employed as a “well-mixed” fed batch cultures. These vessels have a large radius-to-depth ratio offering high aspect ratio for gaseous exchange surface area to vessel depth by means of gas permeable membrane. Three single vessels were accompanied to a rotator base regulated by a peripheral control unit. These vessels were controlled between 18–22 RPM to maintain the 3D alginate beads in suspension form. The rotary wall mobility ensures a steady state of freefall, diminishing three-dimensional homogeneities at low degrees of shear stress

[0.5–2 dyn.cm-^{2} (Placzek et al., 2009)]. Around 500 beads (from 4 ml alginate/single mESC solution) were seeded with 50 ml of media to fill up the vessel.

2.2. Viability and Cell Proliferation

2.2.1. DNA quantification

DNA quantification is contemplated as a reliable technique for indirect estimation of mESC (Ng et al., 2005). Thus, a similar protocol as Randle et al was employed with minor adjustments (Randle et al., 2007). The mESCs were depolymerized and washed from the alginate bead cultures followed by the culture (as mentioned in section 2.6.5.) ahead of snap freezing and storage at -80ºC. Subsequently, cell pellets were digested by proteinase K (Sigma-Aldrich, Poole, UK) and centrifuged at 600 RCF. The digested cell supernatant was then mixed with PicoGreen® reagent (Invitrogen, Paisley, UK) and assessed at an excitation/emission wavelength of 365 nm /460 nm using a MFX micro-titer plate fluorometer (Dynex Technologies, West Sussex, UK).

2.2.2. Live/dead staining

Viability analysis of mESCs in 3D hydrogel cultures was performed with an aid of in situ LIVE/DEAD viability staining (Invitrogen, UK). This kit utilizes a fluorescence dye, calcein AM [3', 6'-Di (O-acetyl)-2', 7'-bis [N, N-bisn (carboxymethyl) aminomethyl] fluorescein, tetraacetoxymethyl ester] to identify live cells, which is metabolized by cellular esterases to produce a green fluorescence within in the cytoplasm. While, another dye ethidium homodimer-1 (EthD-1) binds to nucleic acid of the cells and produce a red fluorescence that is indicative of the compromised integrity of cell membrane. In advance of staining, mESCs

beads were accumulated and washed twice using 1X PBS. A working solution of 4 mM EthD-1 and 2 mM calcein AM solution was supplemented to the beads followed by incubation for 30 minutes with gentle rocking in while protecting from light. Subsequent to the staining, the beads were washed thoroughly (3×) in excess of PBS to avoid nonspecific staining and visualized within the next half an hour on a BX51 fluorescence microscope (Olympus) and assessed using analysis^D software (Olympus).

2.2.3. Cell Proliferation Assay (MTS Assay)

The viability potential of mESCs in different culture media was analysed indirectly through assessment of metabolic activity in a time dependent fashion by using a Cell Titre 96 Aqueous One Solution Reagent MTS [3-(4, 5-dimethylthiazol-2-yl)-5-(3-carboxymethoxyphenyl)-2-(4-sulfophenyl)-2H tetrazolium] assay (Promega, UK) as per manufacturer's guidelines. The experiment was performed in 24-well tissue culture polystyrene plates (VWR International Ltd.) coated with 0.1% gelatin (Sigma). 24-well plates were seeded with $3x10^4$ cells/cm^2 and cultured and incubated in each primary differentiation culture media for a time course of 1, 2, 3, 4, and 5 days. The cells or beads were incubated with MTS solution for 3 hours at the end of each incubation period. 100 mL of the cell culture supernatant was isolated from samples and transferred into a separate 96-well plate and read at 490 nm wavelength using an enzyme-linked immunosorbent assay (ELISA) reader (ELx808, BIO-TEK, USA).

2.3. Media analysis

Nutrient and metabolite concentrations were investigated in 1 ml of cell culture supernatants using the Bioprofile 400 Analyzer (Nova Biomedical, Flintshire, UK) at different time point's

throughout the cultures. During the media sampling every 24 hours of the 3D cultures, the change in media was normalized to fresh media collected at the same time.

2.4. Polymerase Chain Reaction (PCR)

2.4.1. RNA extraction

Cell pellets were stored at -80^{0}C and subjected to mature mRNA (> 200 nucleotides) extraction utilizing the Resay kit (Qiagen, West Sussex, UK), according to the manufacturers protocol. Harvested cells were subjected to disruption in RLT buffer added with 1% β-Mercaptoethanol and homogenized using a Qi shredder spin column, at the (1400 RPM) centrifugation 2 minutes. Further, equal amount of Ethanol was added to the cell lysates to aid the precipitation of RNA to the RNeasy membrane column. The membrane column was washed twice with RW1 buffer followed by washing with RPE buffer and removal of ethanol. Also, contamination of the DNA was removed with the aid of the DNase elution of RNA was carried out in a 1.5 ml collection tube using RNase-free water. RNA quantification was accomplished on a UV spectrometer and the A260 / A280 ratio of > 1.70 was selected as a threshold to ensure purity of RNA sample. The RNA samples were then modified to achieve a working concentration of 10 µg/ml for eventual two-step polymerase chain reaction (PCR). This addition did not result in more than 2% volume change therefore seemed insignificant.

2.4.2. Polymerase chain reaction (PCR) amplification

1µg RNA in a final volume of 20µl was reverse-transcribed into cDNA using the Thermo script reverse transcription-polymerase chain reaction (RT-PCR) system (Invitrogen Ltd., Paisley UK). Oligo (dt) 20 was then utilised for prime RT reactions that facilitated the corresponding cDNA to be amplified in PCR with different sites of gene specific primers. RNA template and primer was denatured by incubating at 65^{0}C for 5 minutes followed by positioning on ice during the addition of master mix. Master Mix was composed of 4µl of 5 X cDNA

synthesis buffers (250 mM Tris acetate pH 8.4, 375 mM potassium acetate, 40 mM magnesium acetate, stabilizer), 1 µl of 0.1 M dithiothreitol (DTT; a reducing agent for the RT), 40U RNase Out (an RNase inhibitor), 1 µl RNase free water, 2 µl of 10 mM dNTP mix and 15U/ µl Thermo Script RT. The reaction mixtures were then transferred into a thermal 96 cycler (Perkin Elmer Gene Amp PCR System 2400; AB Applied Biosystems, Warrington, UK) and incubated at 50^0C for 30 min afterwards 85ºC for 5 min. cDNA samples were stored at -20°C prior to use. Each reaction confined of 50 µl mix. In the 50 µl PCR reaction mix, the final concentration of $MgCl_2$ and dNTP (Promega, UK) were 3 mM and 10 mM, respectively. Eppendorf Thermal Cycler (Eppendorf AG, Hamburg, Germany) was used for the DNA amplification. DNA denaturation and the commencement of Taq DNA Polymerase (Fermentas, Life Sciences, UK) was conducted at 94ºC for 10 min, subsequent to 40 cycles of template denaturation at 94ºC (5 seconds) and primer annealing at 56ºC and primer extension at 72ºC (30sec). Total RNA was obtained employing the RNeasy Mini Kit (QIAGEN) as per manufacturer's guidelines. Also, First-Strand cDNA was produced with random hexamers as primers, using Super-Script First-Strand Synthesis System according to the manufacturer's procedure (Promega). Each sample was progressed with SYBR Green supermix (BIOLINE) in triplicates. PCR conditions comprised of an initial denaturation step of 2 minutes at 95°C, subsequent to the 40 cycles of PCR consisting of 15 seconds at 95°C and finally 20 seconds at 60°C. Average of triplicate Ct values of gene of interest (GOI) and b-actin were then divided to normalise the obtained data. Fold change of GOI transcript levels between sample A and sample B = 2– Δ ΔCt, where Δ Ct = Ct (GOI) – Ct (GAPDH) and Δ Ct = Δ Ct (A) Δ Ct (B).

Table 1: Primer Sequence List

Oligo sequence (5' to 3')	Oligo name
GGGTCATGGCTAACGTGC	F:Twist
CAGCTTGCCATCTTGGAGTC	R:Twist
ATGATCGCCTGCTTATTCACG	F:HK2
CGCCTAGAAATCTCCAGAAGGG	R:HK2
CTCTAATGTCCTCCCTTGTTGCC	F:Brachury
TGCAGATTGTCTTTGGCTACTTTG	R:Brachury
GTGACGTTGACATCCGTAAAGA	F:β-actin
GCCGGACTCATCGTACTCC	R:β-actin
CTCCAACGGGCATCTTCATTAT	F:N-cadherin
CAAGTGAAACCGGGCTATCAG	R:N-cadherin
AGAGTCAGATCGCTCAGATCC	F:nestin
GCAGAGTCCTGTATGTAGCCAC	R:nestin
GATGACGGCGACATGGTTTAC	F:HIF-1α
CTCACTGGGCCATTTCTGTGT	R:HIF-1α
TGGTCAAGAAACATTTCAACGCC	F:slug
GGTGAGGATCTCTGGTTTTGGTA	R:slug
CAAGAGCTTGTCAGAATCAGG	F:N-cadherin
CATTTGGATCATCCGCATC	R:N-cadherin
TGGAGCCCGAATACAGGAAGA	F:Hspg2
AGATCCGTCCGCATTCCCT	R:Hspg2
GCTCAGCAAATCGTGCAGC	F:Fn1
CCATAGCAGGTACAAACCAGG	R:Fn1
CAGTTCCGAGGTCTACACCTT	F:Cdh1
TGAATCGGGAGTCTTCCGAAAA	R:Cdh1
TGCCTTTCTTTACCGACGAGT	F:FGF4
GCGTAGGATTCGTAGGCGTT	R:FGF4
GAACATGTGTAAGCTGCGG	F:Oct4
CAGACTCCACCTCACACG	R:Oct4
GCTCCTGCACACAGAAGAAA	F:Rex1
GTCTTAGCTGCTTCCTTCTTGA	R:Rex1
TCTTCCTGGTCCCCACAGTTT	F:Nanog
GCAAGAATAGTTCTCGGGATGAA	R:Nanog
AATATTTGCTGTGTCTCAGG	F:FGF5
TAAATTTGGCACTTGCATGG	R:FGF5
TTGATACCTGAGACCGGGAAG	F:BMP4
ACATCTGTAGAAGTGTCGCCTC	R:BMP4
CACACGCTGCCTTGTGTCT	F:Snai1
GGTCAGCAAAAGCACGGTT	R:Snai1
GCGGAGTGGAAACTTTTGTCC	F:Sox2
CGGGAAGCGTGTACTTATCCTT	R:Sox2

2.4.3. Agarose gel electrophoresis

PCR products were seceded on 2% (w/v) agarose gel [made up in 1X TAE buffer (Tris Acetate EDTA; Sigma Aldrich, UK)] containing 0.4 M Tris acetate, 10 mM EDTA (ethylene diamine tetra acetic acid), pH 8 and pictured by ethidium bromide fluorescence (Sigma Aldrich, UK) method. Size of products estimated by means of 50bp and 100bp ladders (Fermentas, Life Sciences, UK). Further, digital images of ethidium bromide-stained gels were attained using the Bio-Rad (Hemel Hempstead, UK) Fluor-S Multi imager system.

2.5. Fixed samples immunocytochemistry

Cells at undifferentiated phases were confirmed by immunostaining for pluripotency marker POU5F1/Oct4 (octamer-binding transcription factor 4) and SSEA-1 (stage-specific embryonic antigen 1) correspondingly. Cells were fixed with 4% paraformaldehyde (Sigma) for 10 min and washed in excess of PBS. Fixed cells were incubated with 0.2% Triton X-100 to aid permeability (Sigma) then blocked with 10% (v/v) goat serum (Sigma) to avoid nonspecific binding. The primary antibodies, rabbit anti-Oct4 [(diluted 1:80 in bovine serum albumin (BSA) / azide solution; Santa Cruz Biotechnology, UK)], were incubated on an overnight at 4°C followed by washing with PBS. Fluorescein isothiocyanate (FITC)-conjugated rabbit anti-goat immunoglobulin G (IgG) secondary antibody either from Jackson Immunoresearch Laboratory, USA or Santa Cruz Biotechnology antibodies were added at RT for 1 hour at a dilution of 10^4. Cell nucleus were also counterstained with DAPI (4', 6-diamidino-2-phenylindole; Sigma) and observed under epifluorescence on a BX-60 microscope (Olympus, Japan). Images were seized using a Zeiss Axiocam digital camera and were analysed using KS-300 software (Imaging Associates, Thame, UK).

Table 2: List of Antibodies for Immunocytochemistry Staining

Antigen	Primary	Secondary	Blocking Serum
Oct-4	1:80 Rabbit polyclonal (Santa Cruz Biotech)	1:80 goat anti-rabbit FITC (Santa Cruz Biotech)	3% Normal goat serum (Santa Cruz Biotech)
SSEA-1	1:200 Mouse monoclonal (Santa Cruz Biotech)	1:200 Goat anti-mouse Texas red (Santa Cruz Biotech)	3% Normal goat serum (Santa Cruz Biotech)

2.6. Proteomics

2.6.1. One Dimensional protein separation

15-20 µg protein were amalgamated with 3 µl of NuPAGE LDS sample buffer (4X), 1 µl of NuPAGE reducing agent (10X) and deionised water up to 20 µl. Samples were subsequently boiled at 70^0C for 10 minutes on a heat block preceding to execute SDS poly acrylamide gel electrophoresis.

2.6.2. Two Dimensional gel electrophoresis

2-D gel electrophoresis was executed with 11-cm IPG strips with a nonlinear gradient of pH ranging from 3–11 followed by overnight passive rehydration with 200 µl of rehydration solution [2 M thiourea, 7 M urea, 4% (w/v) CHAPS, 1% (w/v) ASB14, 0.3% (w/v) DTT, 0.5% (v/v) IPG buffer pH 3–10 NL)]. Protein samples were loaded exercising a cup-loading application and determined as follows: (1) 500 V, 1 s, gradient; (2) 500 V, 4 h, step and hold; (3) 1,000 V, 1 h, gradient; (4)1,000 V, 1 h, step and hold; (5) 3,500 V, 4 h, step and hold; (6)

8,000 V, 5 h, step and hold for a total of 70 kVh. Before commencement of second dimension separation, the focused strips were equilibrated for 15 minute in the equilibration buffer [50 mM Tris-HCl pH 8.8, 6 M urea, 30% (v/v) glycerin, 2% (w/v) SDS, 20 mM DTT, 0.01% bromophenol blue; Sigma]. Subsequently, equilibrated strips were overlaid on to the Bis-Tris 4–12% (w/v) polyacrylamide gel (Bio-Rad, UK) and run at 40 V for 10 min then at 150 V for 50 min until the bromophenol blue dye reached to the bottom of the gels. Protein distribution was confirmed by staining the gels with a colloid coomassie blue (Instant Blue, Expedeon).

2.6.3. Sypro-ruby stain

Sypro-ruby stain was performed for identification of protein. Gels were fixed overnight in 50% methanol and 10% acetic acid followed by staining with Sypro Ruby staining (SYPRO® RUBY Gel Satin, Invitrogen). Gels were de-stained in 10% methanol and 7% acetic acid for 30 min on the shaker at RT.

2.6.4. Difference gel electrophoresis (DIGE)

The pH of the samples were adjusted to pH 8.5 followed by labelling with Cy-dyes (CyDye DIGE Fluor, minimal labelling kit, 25−8010−65; GE Healthcare, UK) as per manufacturer's guidelines. 50 µg of protein from each batch of mESCs culture in 2 dimension flask and mESCs encapsulated in alginate hydrogel protein samples were labelled with 400 *p*mol of Cy3 or Cy5 dyes correspondingly in a mutual manner. The internal standards were pooled from the aliquots of all the samples were labelled with Cy2. This labelling reaction was performed on ice for 30 minute and extinguished by the addition of 10 *n*mol of lysine. Subsequently, an equal volume of 2X sample buffer (2% w/v DTT, 2% v/v IPG buffer pH 3−10 NL) was further added to each

sample. Samples labelled with Cy2, Cy3 and Cy5 were pooled and harnessed by rehydrating overnight with 18 cm strip.

Table 3: DIGE Experimental Design

Culture Type	Brief Description	Experimental Group
2D	Protein extract labelled with Cy3(Red)	Extract from cells grow in flat plastic culture flasks
3D(static)	Protein extract labelled withCy5(green)	Extract from cells encapsulated in alginate hydrogel beads grown in static culture
2D+3D(static)	Internal Standard label with Cy2(yellow)	Equal mixture of proteins from the 2D and 3D(static) cultures

2.6.5. Alginate dissociation buffer

Media was removed and 500 beads were suspended in 30 ml buffer containing 15 mM Tris-HCl (pH 7.5), 60 mM KCl, 15 mM NaCl, 5 mM $MgCl_2$, and 250 mM sucrose. That result in to the floating of the beads. 10 ml of 200 mM citrate was supplemented to the buffer with through mixing for approximately 15 minutes or till beads starts dissolving. This mixture was then centrifuged for 10 min at 600 G and washed twice with PBS, This obtained cell pellet was then snap froze in liquid nitrogen and stored at - 80 for further analysis.

2.6.6. Stable isotope labelling with amino acids in cell culture (SILAC) labelling of the cells

Mouse embryonic stem cells were cultured in Dulbecco/Vogt modified Eagle's minimal essential media [(DMEM); Thermo Fisher 88207)] supplemented with 15% knockout replacement serum (Invitrogen 10828-028) and 5% penicillin streptomycin antibiotics (Invitrogen 15140-122), 5% glutmax (Invitrogen 3505-038) and 5% MEM non-essential amino acids solution (Invitrogen 11140-050) for SILAC labelling. Isotopes of either light (Arg0,

Sigma, A5006; Lys0, Sigma, L5501) or heavy (Arg10, Cambridge Isotope Laboratories, CNLM-539; Lys8, Cambridge Isotope Laboratories CNLM-291) arginine and lysine were added in to achieve a concentration of 28 µg/ml for arginine and 49 µg/ml. For lysine (Arg0/Lys0: arginine and lysine with normal "light" carbon (12C) and nitrogen (14N); Arg10/Lys8: arginine and lysine derivatives with "heavy" carbons (13C) and nitrogen (15N).

Table 4: SILAC experiment design *(adaptive phase for 5 passages in mESCs 2D cultures)*

<table>
<tr><th colspan="6">Adaptive Phase</th></tr>
<tr><th>Culture Type</th><th colspan="2">SILAC label</th><th>Adaption</th><th>Experimental group</th><th>Group Abbreviation</th></tr>
<tr><td rowspan="3">2D</td><td colspan="2">Heavy Lys8/Arg10</td><td rowspan="3">Cells adapted 2D culture coated with 1.1% gelatin in Heavy SILAC labelled for 5 passages</td><td>3 days in 2D 1.1% gelatin coated flask</td><td>2D</td></tr>
<tr><td>0.798 mM L-Lysine 2HCl ($^{13}C_6$, $^{15}N_2$) CNLM-291</td><td>0.398 mM L-Arginine HCl ($^{13}C_6$, $^{15}N_4$) CNLM-539</td><td>Cell encapsulated in alginate hydrogel static culture</td><td>3Ds</td></tr>
<tr><td>Cells encapsulated in alginate HARV bioreactor</td><td>3Dd</td></tr>
<tr><td rowspan="3">2D</td><td colspan="2">Light Lys0/Arg0</td><td rowspan="3">Cells adapted 2D culture coated with 1.1% gelatin Light SILAC labelled for 5 passages</td><td>3 days in 2D 1.1% gelatin coated flask</td><td>2D</td></tr>
<tr><td>0.798 mM L-Lysine (Sigma, L5501)</td><td>0.398mM L-Arginine (Sigma, A5006)</td><td>Cell encapsulated in alginate hydrogel static culture</td><td>3Ds</td></tr>
<tr><td>Cells encapsulated in alginate HARV bioreactor</td><td>3Dd</td></tr>
</table>

Cells were established for full integration of the labels after five passages. Cell dissociation buffer (Invitrogen 13151-014) was applied for to avoid trace contamination of any amino acid. The cell culture media in either 2D or 3D was replaced every day with fresh media containing LIF (Table 4 and 5).

Table 5: SILAC experiment design (experimental phase)

<table>
<tr><th colspan="5">Experimental phase</th></tr>
<tr><th>LC/MSMS protein identification</th><th>Group symbol</th><th>Experimental group</th><th colspan="2">Brief Description</th></tr>
<tr><td rowspan="2">First LC/MSMS group separated in 1D gel and 5 gel slice digested</td><td rowspan="2">2D/3Ds</td><td rowspan="2">Equal mixture of SILAC labelled cells 2D(heavy):3Ds(Light)</td><td colspan="2">15% KOSR+1000units/ml LIF+SILAC media</td></tr>
<tr><td>2D grow for 3 days on SILAC heavy labelled Arg10 and Lys8 in 1.1% coated gelatine culture flask</td><td>3D (Static) grow for 3 days in unlabelled SILAC Arg0 and Ly0 Media</td></tr>
<tr><td rowspan="2">Second LC/MSMS group separated in 1D gel and 5 gel slice digested</td><td rowspan="2">3Ds/3Dd</td><td rowspan="2">Equal mixture of SILAC labelled cells 3D Static (heavy):3D dynamic (Light)</td><td colspan="2">15% KOSR+1000units/ml LIF+SILAC media</td></tr>
<tr><td>3D (Static) grow for 3 days in SILAC heavy labelled Arg10 and Lys8 media</td><td>3D (Dynamic) grow for 3 days in HARV bioreactor in SILAC unlabelled Arg0 and Ly0 media</td></tr>
<tr><td rowspan="2">Third LC/MSMS group separated in 1D gel and 5 gel slice digested</td><td rowspan="2">3Ds/2D</td><td rowspan="2">Equal mixture of SILAC labelled cells 3Dd (heavy):2D (Light)</td><td colspan="2">15% KOSR+1000units/ml LIF+SILAC media</td></tr>
<tr><td>3D (Dynamic) grow for 3 days in HARV bioreactor in SILAC heavy labelled Arg10 and Lys8 media</td><td>2D grow in 1.1% alginate coated flask in SILAC unlabelled Arg0 and Ly0 media</td></tr>
</table>

2.6.7. Protein Extraction

Embryonic Stem cells were mixed with equal amount of heavy and light arginine and lysine derivatives to achieve a cell pellet of roughly 2 million cells. Cell pellets were then re-suspended in cold RIPA lysis buffer (Sigma, R0278) followed by sonication at 20% amplitude for 3 second each for 1.5 min with 5 second interval and incubated on ice for 10 min. The lysates were then centrifuged for removal of debris. Protein quantification was then performed using BCA protein assay kit (Thermo Fisher). 25mg of protein of each sample were then subjected to 4–12% NuPage Novex Bis-Tris gel (Invitrogen, NP0321) in three separate lanes. Gels were stained using the colloidal coomassie blue staining (Invitrogen, LC6025) as per the manufacturer's guidelines. The gels were sliced into 5 slices containing roughly the same protein amount followed by in-gel digestion was executed.

2.6.8. BCA protein assay

Pierce TM BCA protein Assay was performed as pre-manufacturer instructions.

2.6.9. Western blot

Cell lysis was performed and incubated on ice for 30 min followed by centrifugation at 16000 g for 10 min at 4°C. The supernatant was isolated, and the colorimetric protein quantification was performed with BCA assay kit. 10 µg of protein were subjected to 10% SDS PAGE followed by electrophoretic transfer on to a polyvinylidene difluoride (PVDF) membrane. PVDF membranes were then probed with UCP2 Antibody (C-20; Santa Cruz) antibody at a dilution of 1:1000. A mouse anti goat IgG secondary antibody (Santa Cruz) conjugated with horseradish peroxidase (HRP) were used as dilution of 1:5000. The differential

expression of protein was visualized with using an electrochemiluminescence (ECL) detection system (Pierce, Rockford, IL, USA) (Table 6).

Table 6: Western Blot Antibodies

Primary Antibody	Secondary Antibody	Blocking Serum
UCP2 antibody, goat polyclonal IgG 1:1000 (C-20 Santa Cruz)	Mouse anti-goat IgG-HRP 1:5000(SC-2354)	5% Milk
Akt antibody, rabbit monoclonal 1:1000 (CellSignalling)	Goat anti-rabbit IgG-HRP 1:5000	5% Milk

2.7. Mass Spectrometry

The protein identification by mass spectrometry was performed by Dr. Benjamin Thomas and Dr. Svenja Hester, in the Central Proteomics Facility (CPF), Dunn School of Pathology, University of Oxford.

2.7.1. Trypsin digestion

Solutions required: Solution B: 0.04 g ammonium bicarbonate (ammonium hydrogen carbonate) in 10 mL Milli-Q grade water and 10 mL HPLC grade acetonitrile. 25 mM ammonium bicarbonate: 0.04 g in 20 mL Milli-Q grade water. 10 mM DTT: 0.031 g in 20 mL of 25 mM ammonium bicarbonate solution. 55 mM Iodoacetamide: 0.2 g in 20 mL of 25 mM ammonium bicarbonate solution. Promega Sequencing Grade Modified Trypsin (catalogue number: V5111) was reconstituted in 1 vial trypsin to 100 µL Promega re-suspension buffer. 5 µL aliquots were stored at -200C for further use that was activated by supplementing with 95 µL of 25 mM ammonium bicarbonate. Extraction buffer was composed of 10 mL of Milli-Q grade water, 10 mL of acetonitrile and 20 µl of formic acid.

Gel were cut with a clean scalpel on a clean surface and added into a tube with 1mm dice. Bands were washed with 100 µl of solution B two times for 30 minutes and supernatant was discarded. Gels were washed repeatedly until the blue colour disappeared. Afterwards, gels were washed in 100 µL of 100% acetonitrile for 10 minutes that will lead to the dehydration of gel pieces turning white. These dehydrated gels were then dried either in Speed Vac or at bench top for 10 minutes (all acetonitrile should have evaporated). 100 µL of 10 mM DTT was for 30 minutes at 37^0C and supernatant was discarded followed by washing twice with 25 mM ammonium bicarbonate solution, and then in acetonitrile. Gels were then incubated in dark with 100 µL of 55 mM Iodoacetamide for 60 minutes and supernatant were discarded followed by two times washing with 100 µL of solution B for 10 minutes. Gels were washed again in 100 µL of 100% acetonitrile until turned white and dried either in Speed Vac or bench top for 10 minutes. 20 µL of added to each tube and digested over-night at 37^0C. 1 µL of formic acid was added to inhibit the digestion with subsequent removal of peptides and transferred in to a clean tube. Each gel piece was incubated with 50 uL of extraction buffer and incubated for 30 minutes. Finally, all the supernatants were removed and pooled for further analysis.

2.7.2. Mass Spec Method –Q Exactive – 50cm EASY-spray

Samples were investigated on an Ultimate 3000 RSLCnano HPLC (Dionex, Camberley, UK) system connected to a Q Exactive Orbitrap mass spectrometer (Thermo Electron, Hemel Hempstead, UK). Samples were determined on EASY-Spray column with a 50 cm X 75 micrometre diameter (Thermo, Hemel Hempstead) paired to a µ-Guard column of 1 mm long and with 300 micrometre inner diameter saturated with C18 PepMap phase (Thermo, Hemel Hempstead). Peptides were inserted in the guard column while maintaining the flow rate of 10 µl min-1 and desalted for on the trap for 300 seconds. Subsequently, trap was substituted in-line with the analytical column and the peptides were resolved for 120 minute at a gradient

flow-rate of 300nL min-1. Mass spectrometry was performed in a "Top 10" data dependent acquiring mode. Precursor scans were executed in the Orbitrap with resolving power of 60,000 at m/z 200 followed by the identification of ten most intense precursor ions with an aid of quadruple which were then fragmented by HCD at a 30% of normalised collision energy 3 m/z were set as a threshold for quadruple isolation. Ions at Charge state of ≥+1 were excluded from selection for fragmentation analyses. Dynamic exclusion was permitted for 40s.

2.7.3. Computational Interpretation of Peptide Mass Spectra

Spectra were searched against the protein sequence and decoy databases described above using S MASCOT (Proteome Discoverer 1.3, Thermo Scientific). Fully tryptic peptides with up to 2 missed cleavages were considered. Mass tolerance filters of 5 ppm (MS1) and 0.5 Da (MS2) were applied. Static cysteine modifications of either carbamidomethylation (IAM-alkylation, +57.0215 Da) or ethanolyl (IE-alkylation, +44.0262 Da) were included on the basis of which modifying reagent was used. Oxidation of methionine (+15.9949 Da) was allowed as a dynamic modification. PSMs were filtered using Percolator (implemented in Proteome Discoverer) to control false discovery rates (FDR) to <1% as determined using a reverse sequence decoy database. Based on our experimental design, three-separated MS files were generated from each group of comparison. First MS files contained protein SILAC ratio of 2D cells labelled with heavy isotopes to 3D static labelled with lights arginine and lysine. The second MS files provided proteins identification ration of 3D dynamic (heavy) to 2D culture (light) and the final data set belongs to SILAC ratio difference between 3D static (light Arg, Lys) compared to 3D dynamic(heavy Arg, Lys). Filtering the data based on the number of observed peptides provided a list of 1986 proteins that passed the detection threshold. This conservative setting with a minimum of three unique peptides per protein was used for identification. Further, annotation of proteins from the cellular components Gene Ontology

category was done using the ProteinCentre website (ProteinCenter software available from Thermo SCIENTIFIC).

2.7.4. Annotation

The combined set of hits from the 2D vs 3D methods was used to perform functional enrichment analysis in DAVID (Database for functional annotation analysis; www.david.abcc.ncifcrf.gov last updated 17/08/2014),

2.8. Transmission electron microscopy (TEM)

Either cell suspensions or beads were subjected to washing in buffer containing 0.1 M phosphate and 0.1 M sucrose and cleansed twice in PBS. Samples were then fixed in 3% (v/v) glutaraldehyde in cacodylate buffer at pH 7.2 for half an hour. Further, cell samples were subjected to fixation in 1% (v/v) of osmium tetroxide made up in 0.1M cacodylate buffer and removed to 50% (v/v) ethanol. Cell samples were then centrifuged and the subsequent cell pellets were sheathed in molten agar. These agar blocks were then dehydrated and insinuated with Araldite epoxy resin (Taab Laboratories Ltd, Reading, UK) and implanted in moulds. The resin was then polymerized at 60oC for one day. Sectioning of polymerised resin either as semi-thin (1µm) or ultra-thin (60-80 nm) were implemented with a Reichert-Jung Ultracut E ultra-microtome (Leica Microsystems Nussloch GmbH Wetzlar, Germany). These semi-thin sections of selected areas of interest were visualised on light microscope, and stained with toluidine blue [0.8% (v/v) Agar Scientific, Stansted, UK] in borax91 (0.8% (w/v)) with pyronin Y [0.16% (w/v)]. While, the ultra-thin sections were stained in uranyl acetate made in ethanol (50% (v/v)), and then in Reynold's lead citrate. Philips CM10 transmission electron microscope (Amsterdam, The Netherlands) was used for the visualization of ultrathin sections.

2.9. Seahorse

Cells were plated in cell culture grade plastics and switched to non-buffered DMEM supplemented with metabolic substrates such as glucose, glutamine and fatty acids. Respiration was then measured with under basal control conditions and after the addition of oligomycin (ATP synthase inhibitor), FCCP for assessment of maximal respiratory capacity, and subsequently in Rotenone / Antimycin A (abates mitochondrial respiration completely). These experiments were conducted using a XF cell Mito stress test kit (XF24 Extracellular Flux Analyzer Seahorse Bioscience).

2.9.1. Mitochondrial respiration assay

XF24 extracellular flux analyser (Seahorse Bioscience) were utilised for oxygen consumption rates (OCR) and extracellular acidifications rates (ECAR). Cells were briefly plated into XF24 cell culture microplate. Depending on cell titration experiments cells were sustained for 4 hours. OCR plates were stabilised in the absence of CO_2 prior to the experiment for 1 h in non-buffered XF assay media added with glucose (25 mM), glutaMAX (2 mM), 1X nonessential amino acids, sodium pyruvate (1 mM), and FBS (1%). ECAR plates were stabilised in non-buffered DMEM added with NaCl (143 mM), phenol red (3 mg/l), and L-glutamine (2 mM). Glycolytic activities were cross-examined by consecutive addition of 10 mM glucose , 0.5 µg/ml oligomycin, and 100 mM 2-deoxy-D-glucose for estimation of basal glycolytic rate, glycolytic capacity (in the presence of oligomycin), and glycolytic reserve. Glycolytic reserve was calculated by subtracting the basal rate by glycolytic capacity. Mitochondrial activities were probed thorough subsequent addition of 0.5 µg ml-1 oligomycin, 1 µM of carbonyl cyanide 4-(trifluoromethoxy) phenylhydrazone (FCCP), and 0.5 µM of

rotenone for estimation of rates of basal respiration, oxidative capacity (respiration in presence of FCCP), and oxidative reserve (i.e. oxidative capacity subtracted with basal respiration).

2.10. Statistical analysis

Quantitative analysis measured in triplicate and error bars on graphs is standard deviation (SD) of the mean. The comparison between groups was made using analysis of variance (ANOVA). The significant level is $p<0.05$.

CHAPTER 3: Effect of 3D Culture on Gene Expression

3. Introduction

Most of our understanding of biological stem cell processes has been largely obtained from monolayer cultures on (2D) plates with >1 GPa elastic modulus polystyrene. Cells *in vivo* exist embedded in a complex environment that involves ECM, mechanical cues, combinations of growth factors and cytokines. The plastic surface of tissue culture lacks the structural, mechanical and biochemical cues that provide ESCs with some resemblance of their in vivo environment (Keung et al., 2011b). Using various natural or synthetic biomaterials, or encapsulating 3D constructs, not only help avoid extrinsic factors supplement, it may mimic as well an environment similar to that in vivo ((Chowdhury et al., 2010a) (Randle et al., 2007); (Hwang et al., 2009).

What a 3D substrate provides to cells that distinguishes it from 2D sitting always simplified as a matter of dimensional difference, ignoring crucial factors such as diffusion. For instance, MDCK cells, which phosphorylate ERK by hepatocyte growth factor (HGF), respond differentially to soluble HGF in a micro-scale gel compared with mm-scale gel confirming sensitivity of cells to diffusion rate or concentration gradients (Baker and Chen, 2012). Mass transport is a limiting factor for 3D culture in a static condition. This limitation is reduced when encapsulated cells are seeded into a dynamic bioreactor with a 'well mixed' motion ((Randle et al., 2007) (Hwang et al., 2009). For instance, a rotary wall vessel (RWV) bioreactor provides alginate hydrogel with a constant fall motion. This bioreactor is an example of a dynamic motion culture that aids mass transfer with minimal shear stress. Using a high aspect ratio vessel (HARV) increases passive diffusion transport by 100 times in comparison with RWV, and it improves cell densities to approximately three million cells/ml, due to an absence of shear stress and improved passive mass transport (Randle *et al.*, 2007).

Previously in our group, a 3D culture-enabled expansion of ESCs for 200 days in the absence of feeder cells and without sub-passaging. In addition, it was shown that hydrogel beads encapsulated murine embryonic stem cells (mESCs) grown in a dynamic bioreactor-enhanced LIF/STAT3 signaling by up-regulating LIF receptor expression (LIFR), which promotes proliferation and self-renewal, compared with a similar configuration in a static culture (Yeo *et al.*, 2013). In this chapter, we will discuss the effects of 3D culture either static or dynamic on mESC self-renewal, proliferation, viability and metabolic parameters with or without serum conditions.

3.1. Aim

The aim of this chapter is to assess the effects of 3D mESCs culture on cell viability, proliferation, metabolic profiles, self-renewal, differentiation and morphology.

3.1.1. Objectives

1. Optimise a suitable 3D environment to maintain mESCs.

2. Assess the effects of different feeding regimes, serum or no serum, on cell proliferation and metabolic profiles

3. Determine the effects of 3D static/dynamic condition on the growth kinetics, pluripotency level, and metabolic parameters.

3.1.2. Experimental methods

The mESCs were transferred from adherent 2D cells to alginate beads and the effect of 3D culture on self-renewal was compared to 2D culture (Fig. 10). The mESCs in 3D hydrogel were maintained either using a dynamic bioreactor or in static culture up to 18 days. The medium was collected every 24 hours in order to analyse metabolic parameters. In addition, the number of viable cells was indirectly estimated at different time points based on pre-measured relative cell number using standard curves for both MTS(colorimetric assay) and DNA quantification assays (fluorescence units). (For standard curve please refer to appendix figure number 48 and 49).

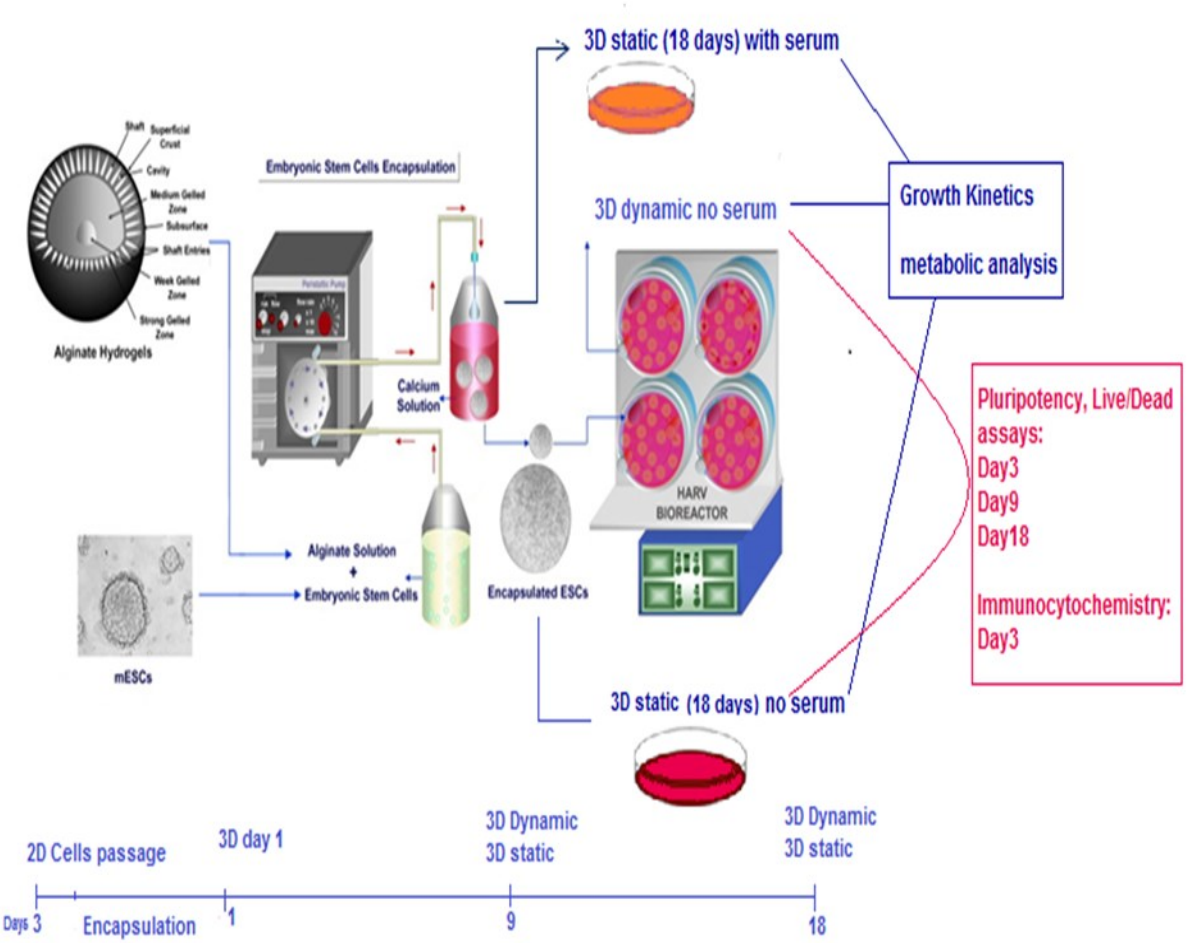

Figure 10 Summery of Experimental plan for Comparison of Serum, Serum Free (Both Static and Dynamic)

Culture period time is 3 days for 2D culture, 18 days for 3D static (both with serum and without serum) and dynamic (without serum). Sample collected at Day 3 for ICC, Q-PCR, and light microscopic micrograph to compared 2D culture with 3D static and dynamic without serum. In addition, Q-PCR comparison between 3D static and dynamic culture was done at day 9 and 18. Daily sample obtained for metabolic analysis (glucose, lactate, glutamate, ammonia) for 3D static (with or without serum) and dynamic culture. Growth kinetics comparison between 3D static with and without serum was made at day 5, 7, and 11 respectively.

3.2. Results

3.2.1. Examining the effect of absence of serum on cell viability

In order to assess the effect of presence/absence of serum on mESCs behaviour, the cells were encapsulated in 3D hydrogel and maintained in a static culture in media with FBS (Foetal bovine serum) or without using knockout replacement serum (KOSR). The growth kinetics were shown to be similar between serum containing and not containing 3D static cultures until day 7, where declining kinetics observed in serum culture compared with the ability to maintain maximal cell numbers reach to 40,000 per bead in serum-free by day 11 (Fig. 11, i , iii & iii).

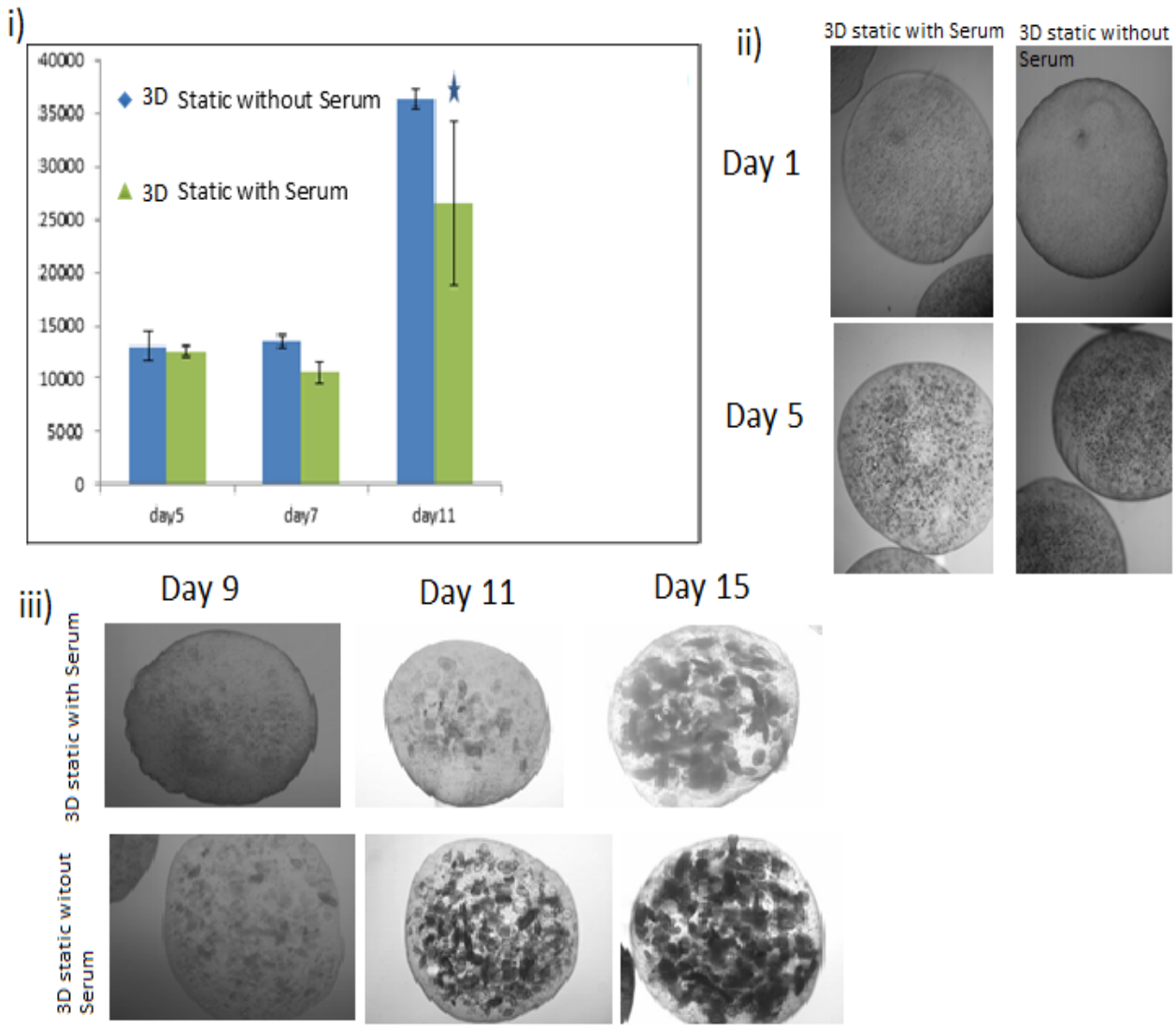

Figure 11 Growth kinetics comparison of static without serum (blue), static with serum (blue) is made at different days of the culture

i) Growth Kinetics using DNA quantification.

ii) Micrographic images of both cultures from day 1 to 5 (static with or without serum).

iii) Illustrate difference in cell viability and growth improvement in particulate from day 9 to 11.

Analysing the accumulated metabolites in the culture medium may reveal factors that were likely to cause these differences in cell proliferation between 3D static with or without serum. The metabolic parameters of the culture media were analysed every 24 hours to assess the effect of the absence of serum on cell viability (Fig. 13).

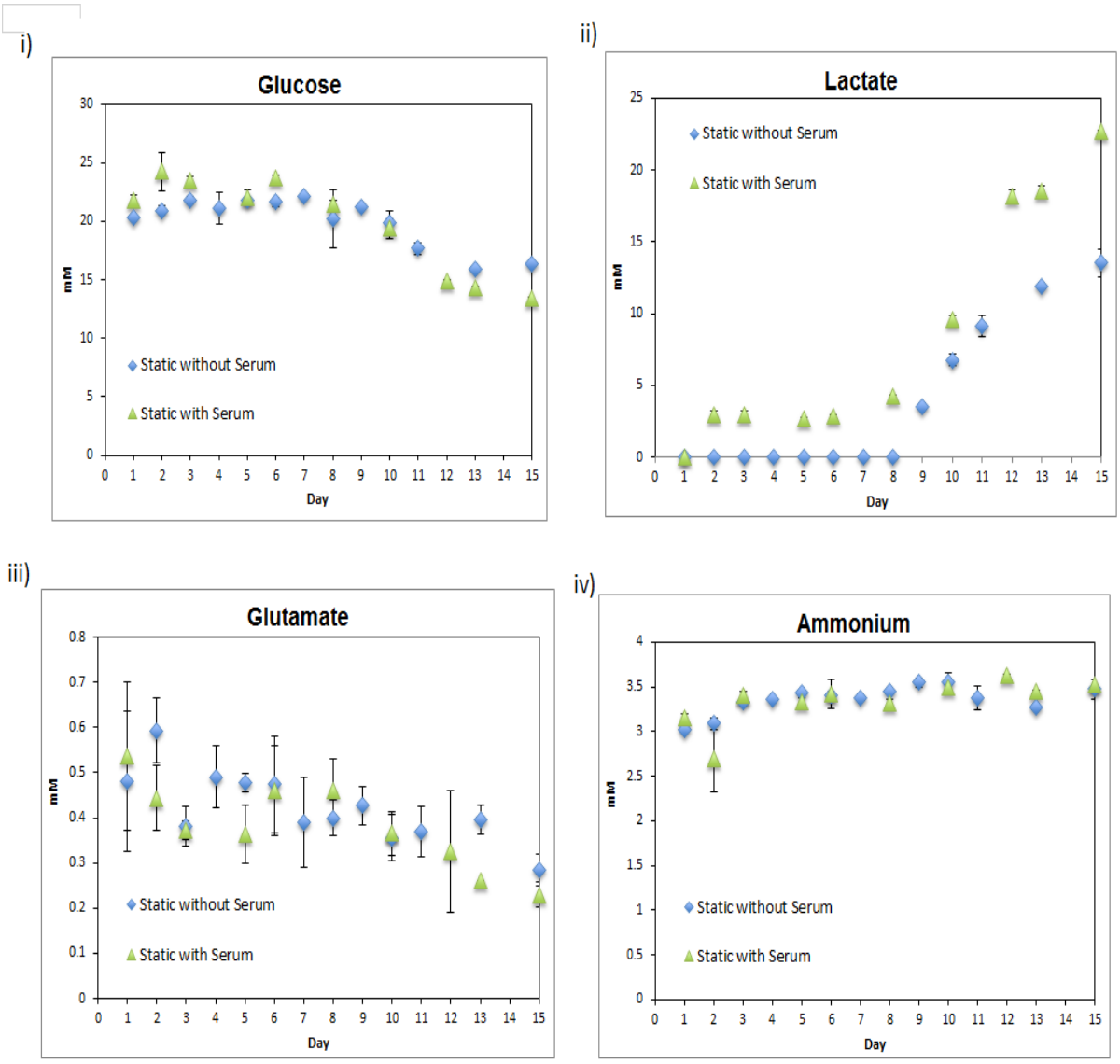

Figure 12 3D static with and without Serum Metabolic Profile

Analysis of i) glucose, ii) lactate, iii) glutamate, and iv) ammonia. The values are means ± SD for N=3 (*p<0.01).

The glucose (main nutrient) in serum or serum free media was supplied at 25 mM in DMEM whereas glutamine was 5 mM concentration. The glucose and glutamine consumption showed no significant difference between the two sets (Fig. 12, i, iii). The glucose metabolism product is primarily lactate whereas glutamate consumption produces ammonia. The ammonia concentration showed no difference between the serum and the serum free media (Fig. 12, iv). The level of ammonia did not reach 4 mM until day 11 in both cultures where 6 mM is reported to be toxic for mESCs (Chaudhry et al., 2009).

In contrast, lactate was observed in high accumulations in 3D static cultures in the presence of serum compared with serum-free medium (Fig. 12, ii). The lactate level was significantly higher, reaching to 25 mM in 3D static culture in the presence of serum at day 15 compared to cells maintained in the absence of serum.

It is established that a lactate level above 16 mM leads to a decrease in mESCs growth of more than three-fold (Ouyang et al., 2007). Unlike ammonia, which showed no differences between the two sets, the lactate accumulation can likely be destructive to proliferation in serum culture. Hence, reducing the glucose supplement by half leads to an increase in cell viability by 40 % due to a reduction in lactate accumulation (Chen et al., 2010).

3.2.2. Effect of an immediate transfer of encapsulated cells to a HARV bioreactor on cell proliferation /viability

Proliferation, viability and metabolic parameters were measured at different time points to compare cells growing on 3D dynamic to cells in 3D static condition. Cell viability was measured using MTS assay, where viable cells convert tetrazolium salts to a formazan in metabolically active cells. After four hours, the first MTS measurements showed about double the number of cells in both condition from the initial seeding densities until after 24 hours of

encapsulation when the viability declined to the level of the initial seeding in dynamic culture (Fig.13, i).

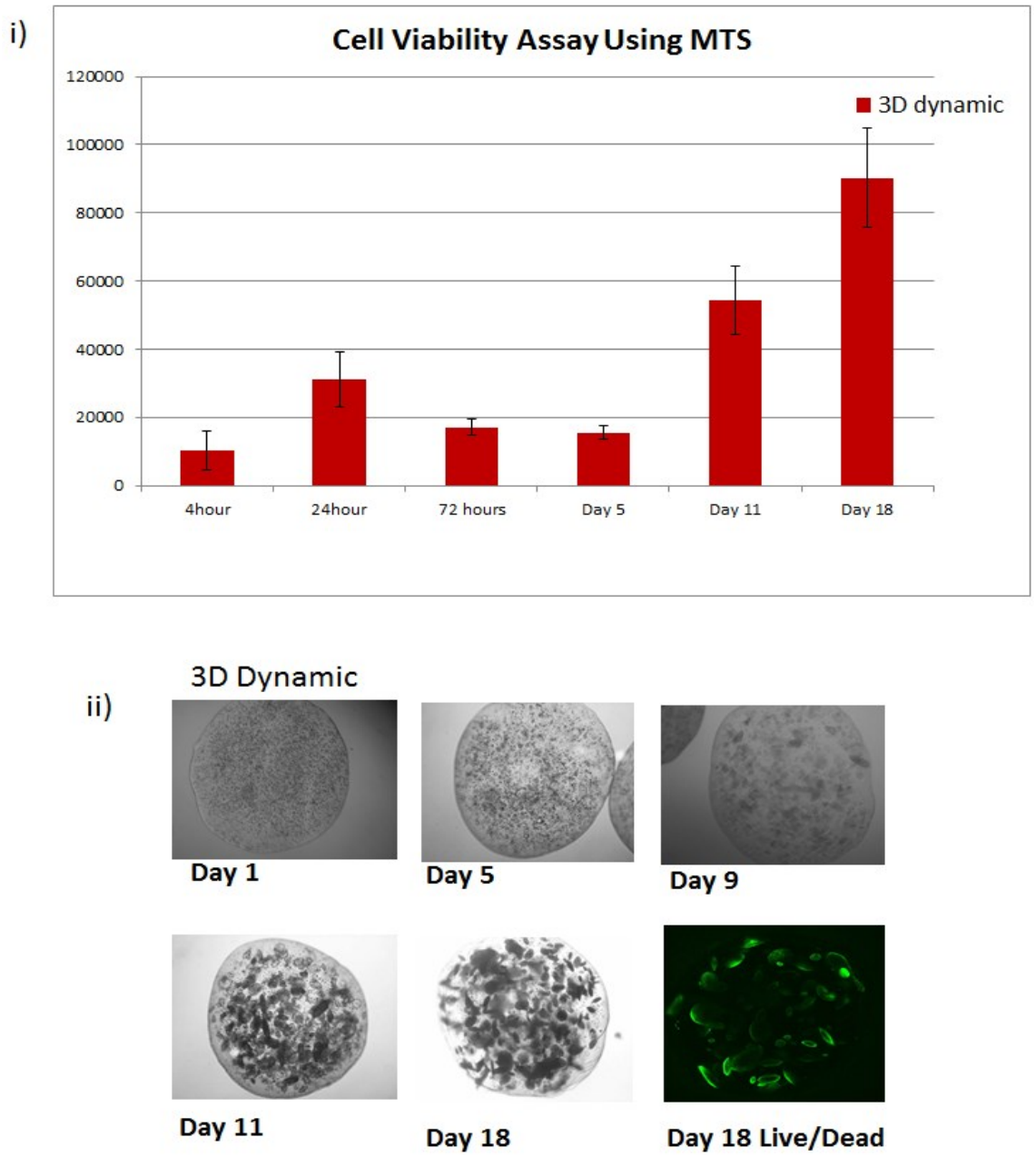

Figure 13 Cells viability of mESCs grown in 3D dynamic culture

i) Cells viability measure using MTS assay at different time point. The values are means ± SD for N=3 (*p<0.01).

ii) Micrograph of beads at different time point and the last image showed confocal graph of beads at day 18 where green color detect cell viability using Live/Dead assay.

The mESCs were rapidly divided in averages of four to five hours (Wang *et al.*, 2011). In addition, the frequency of cell division can be size-dependent, as rounded small cells enter the cell cycle frequently (Tzur *et al.*, 2009). The micrograph shows encapsulated cells are small and rounded in structure compared to dish-adherent cells (Fig. 13, ii). This may contribute to the increment of cell division and proliferation. However after 72 hours, cell viability decreased in both 3D static and dynamic (Fig. 14, i). Our growth curves' kinetics share a similar pattern with the number of alginate-encapsulated SC studies that show an immediate drop in cell growth followed by viability recovery (Bertolotti et al., 2009, Wang et al., 2009d, Chayosumrit et al., 2010, Penolazzi et al., 2010). This decline in cell viability suggests the immediate response of SCs to changes in the surrounding environments is by triggering cell death.

Combining live/dead assays and confocal microscopy enabled the acquisition of in-depth images of cell viability in the different layers of the beads: top, middle and bottom. The cells in the middle of the alginate beads showed a higher prevalence of cell death. This may be associated with the decrease in the cells' oxygenation. Recently, O_2 measurements of the scaffold core have reached to 0% or 3% when fresh media were supplied to the cells. However, the oxygen level was almost zero at day 7. In addition, hepatocytes maintained in alginate beads showed signs of necrosis at the middle of the scaffolds, compared to viable cells near the surface (Yu *et al.*, 2014). Similar to this, the live/dead assays showed higher cell death in the middle of hydrogel compared to cells on the outside, where viability is higher. The decrease in oxygenation in 3D constructs was associated mostly with static culture. However, even in dynamic cultures with enhanced mass transfer, cell viability was low. Similarly, the number of cells using DNA quantification assays increased significantly from Day 3 of the culture (Fig.14, i), suggesting an adaptive response to changes in the surrounding environments.

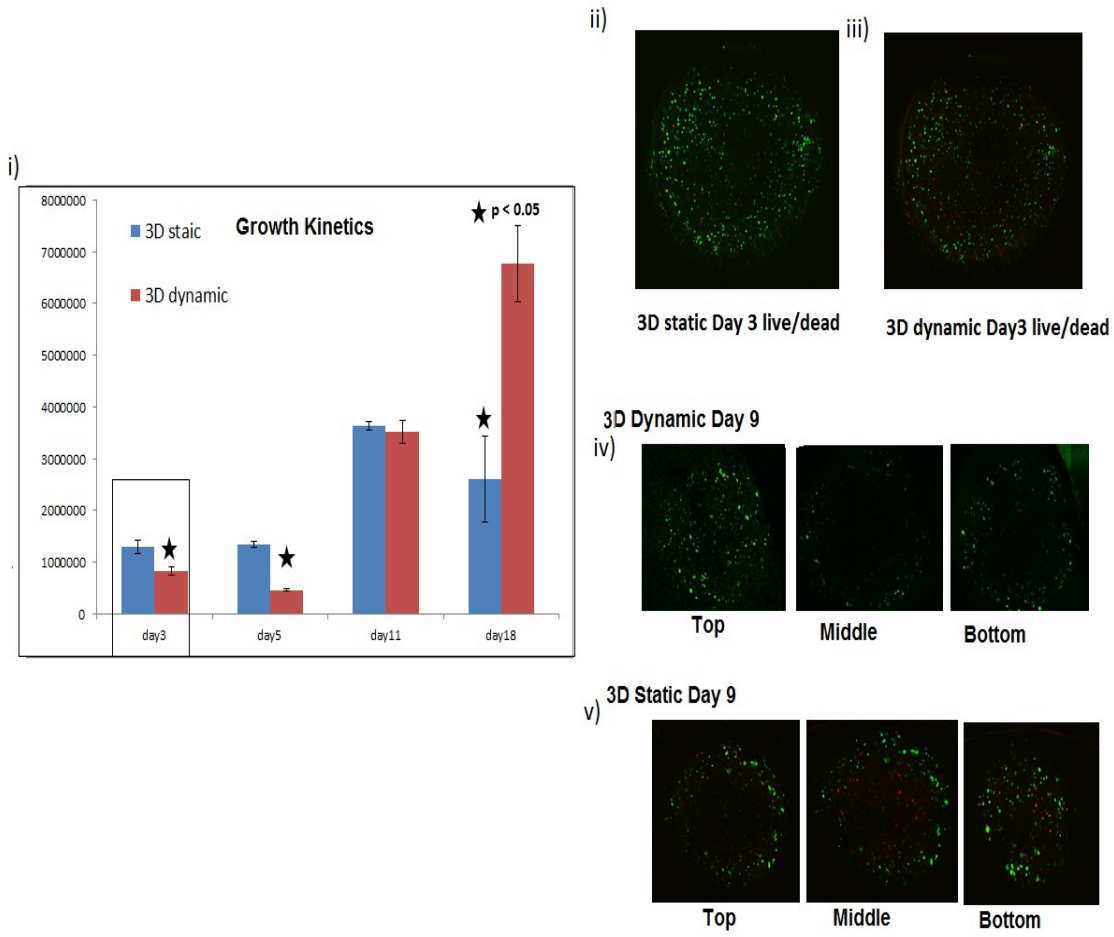

Figure 14 Growth Kinetics and Cell Viability of 3D without Serum Dynamic and Static

i) Growth kinetics, ii) live/dead assay at day 3 both static and dynamic were number of dead cells (red) increased similar like growth kinetics .In iv and v) showed viability at top, middle and bottom of the beads at day 9 for both culture.

Metabolic analysis of glucose, lactate, glutamate, ammonium, growth kinetics and live/dead assays at day 3, both static and dynamic, showed the number of dead cells (red) increase similarly like growth kinetics (Fig. 14, ii-iii). In 3D dynamic and static, viability was shown at the top, middle and bottom of the beads at day 9 for both cultures. (See Fig. 14, iv-v for a micrographic of dynamic and static culture).

The growth kinetics was also assisted using glucose consumption and lactate production measurements. Neither glucose nor glutamine was totally exhausted from the maintenance medium throughout the culture period because daily feeding was provided (Fig. 15 i-iii-iv). Lactate accumulated above 15 mM at Day 15, whereas at earlier times the lactate was almost undetectable, and this may be due to the low sensitivity of instruments used for this assay (Fig. 15, ii). However, accumulation of lactate as 16 mM has a significant effect on mESC self-renewal and expansion (Ouyang et al., 2007). In spite of Ouyang and colleagues' result, their culture media was replenished every three days, exposing the mESCs to continuous lactate-inhibitory effects, whereas in this study the media was changed daily.

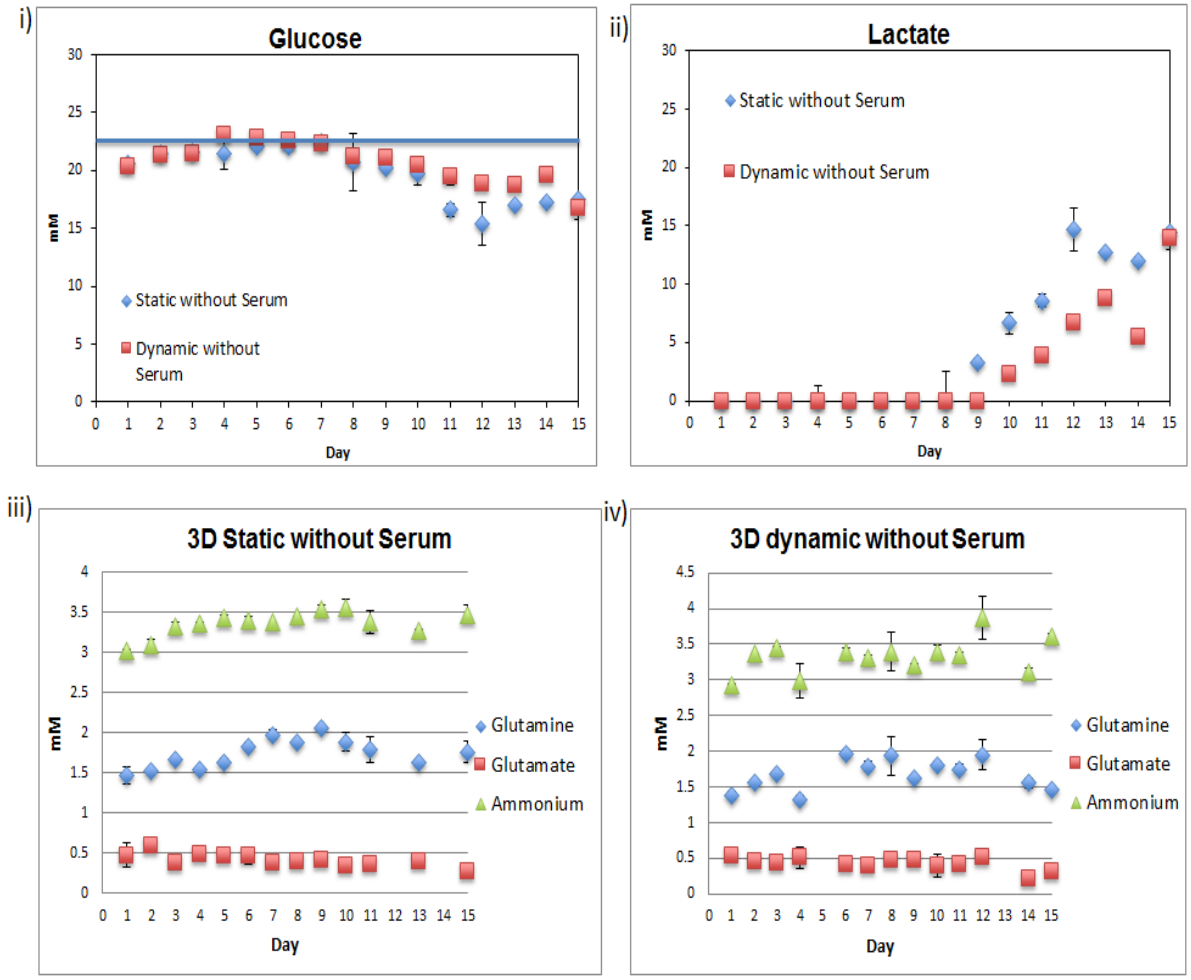

Figure 15 Metabolic profile of 3D static and dynamic culture

Analysis of i) glucose, ii) lactate, iii) glutamate, and iv) ammonia. The values are means ± SD for N=3 (*p<0.01).

3.2.3. Self-renewal or differentiation?

The use of immunocytochemistry (ICC) confirmed the presence of Oct-4 (nuclear) and SSEA1 (cell surface-marker) positive colonies in the three cultures (Fig. 16, b-d). However, ICC is a qualitative assay and both markers used may be associated as well with early differentiation, such as primed stem cells and PGCs, which both possess SSEA1^{+}/Oct-4^{+}

colonies (Ouyang et al., 2007). Therefore, relative quantification of gene expression was done to assess the differences between different cultures. As shown in Fig. 16a, the *Oct-4*, *Nanog* and *c-Myc* expressions were significantly down-regulated on 3D static culture compared with 2D or 3D dynamic respectively. Consequently, *FGF4* and *UTF1*, which are downstream targets for Oct-4, showed an increase in expression on 3D dynamic culture. Consistency with that *Rex1*, associated with ICM (*Zfp42*), was expressed to a higher extent in 3D dynamic cultures. The *Rex1* down-regulation is an early marker of ESCs differentiation. *Rex1* deletion contributes to impaired embryo phenotypes (Chen *et al.*, 2010) and the addition of *Rex1* to reprogramming cocktails has significantly improved the efficiency of induced pluripotent cells (Wang *et al.*, 2011).

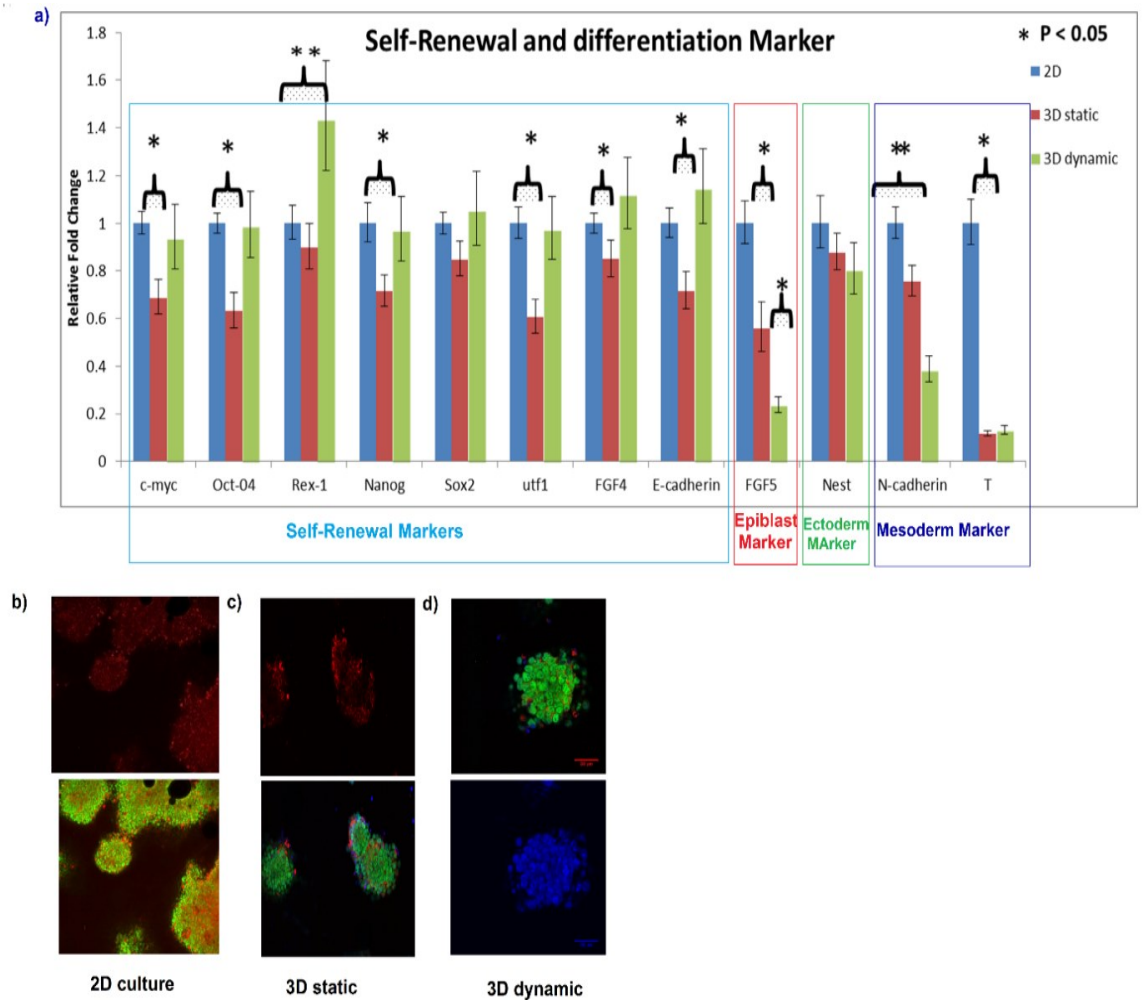

Figure 16 Day 3 mRNA Expression of Differentiation and Pluripotency Markers of 3D (both static and dynamic) versus 2Dcultures

a) Relative gene expression analysis of pluripotency associated genes (c-Myc, Oct4, Rex1, Nanog, Sox2, Utf1, FGF4, E-cadherin) and lineage early differentiation markers(FGF5, Nestin, N-cadherin, T (Brachyury)) for dynamic and static cultures. Relative gene expression for both 3D static and dynamic culture is normalized against 2D cultures and β-actin gene expression. Values are means ± SD, N=3 (*: $p<0.05$)

b) Immunocytochemistry of Oct4 (green), SSEA1 (red), and nucleus (blue) for b) 2D culture, c) 3D static, and d) 3D dynamic.

In contrast to dynamic culture, gene profiles of 3D static culture suggest a decrease in self-renewal. Yet, there was no pronounced differentiation towards either mesoderm (Brachyury) or ectoderm linages (Nestin). However, *FGF5*, an early-stage differentiation marker, showed a distinct down-regulation on 3D dynamic culture compared to either 2D or 3D static culture. FGF5 can also be considered an epiblast marker, and its expression indicates transition of ESCs from naive to primed state (Yu *et al.*, 2014) (Vallier *et al.*, 2009). *FGF5* in 3D dynamic culture was correlated with high *Rex1* expression. This may suggest a capability of dynamic culture in retaining the naive state of ESCs. In contrast, Toh and Voldman showed that dynamic bioreactors enhance *FGF5* expression, compared with self-renewing static culture (Toh and Voldman, 2011). This variation may be due to lower shear stress in the HARV bioreactor we used in this study compared to that used in their work.

Other self-renewal markers, which showed differences in expression between modes of culture, were *BMP4* and *Nodal*. Both *BMP4* and Nodal ligands cooperate to support self-renewal in ESCs, while BMP4 and Nodal activation on epiblast stem cells (EpiSC) induce cell differentiation (Vallier et al., 2009, Galvin et al., 2010). However, a lower-level of BMP4 expression in dynamic culture (Fig.17, c) had no distinct role with the up-regulation of pluripotency markers, owing to *BMP4*'s role in promoting lineage commitment rather than self-renewal (Fei et al., 2010, Zhang et al., 2010).

In contrast, Nodal responsible for neuroectodermal inhibition was highly expressed in 3D dynamic culture. However, if the activation of Nodal induces Smad2/3 activation, as a downstream target, ESCs will transit to EpiSCs (Greber et al., 2010). Both *Smad2* and *Smad3* have shown no significant change in the three culture modes (Fig. 17, c).

Consistent with pluripotency gene profile, differentiation markers such as Brachyury (*T*), a mesoderm early differentiation marker, showed significant up-regulation in 2D culture, whereas there was no pronounced expression of the early neuroectodermal gene Nestin in all three culture modes. Consequently, *Sox2*, a self-renewal and early neuroectodermal progenitor marker, showed no difference between the three culture conditions.

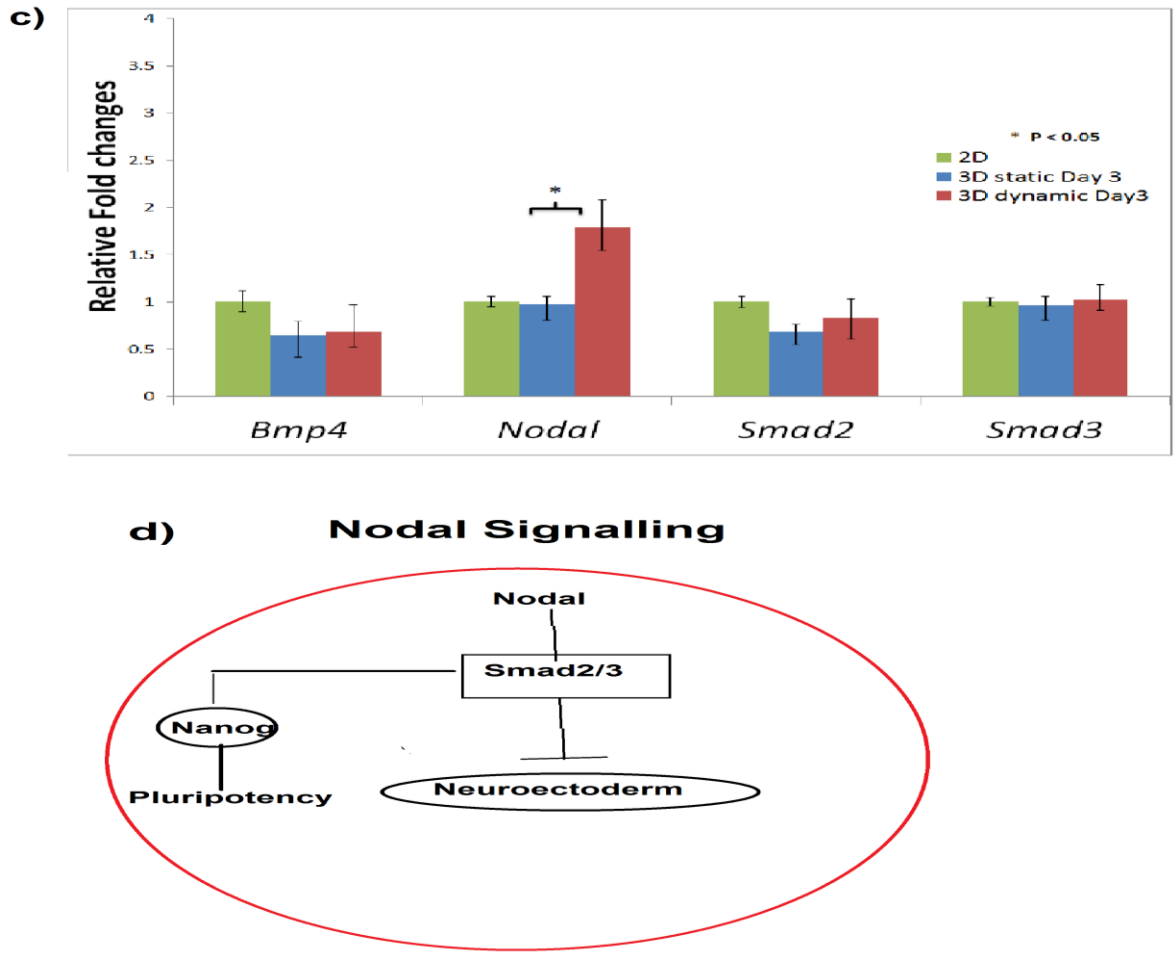

Figure 17 TGFβ signalling of mESCs and mRNA Expression

c) Relative gene expression of Bmp4, Nodal, and Smad2/3. Data of 3D static and dynamic culture were normalised to 2D and β-actin expression. Values are means ± SD, N=3 (*: $p<0.05$).

d) Schematic illustrate Nodal regulation of mESCs fate.

3.2.4. The epithelial mesenchymal transition

Changes in cell morphology from epithelial-flattened adherent cells to more mesenchymal phenotypes with rounded shapes are associated with 3D constructs and cancer spheroid formation (Chu et al., 2009, Kuo et al., 2012, Kolind et al., 2012). This effect is known as the epithelial mesenchymal transition (EMT), and their plasticity is defined as the ability to switch to reverse mesenchymal epithelial transition (MET). EMT occurs in early development, and also in cancer metastasis, and is characterised by the loss of epithelial phenotype, E-cadherin suppression, increasing the expression of the mesenchymal markers *Snail, Twist, Slug* and N-cadherin (Zhang *et al.*, 2010).

Alteration in cellular morphology may be introduced due to the transfer of cells from 2D plastic plates to 3D soft matrices (Fig. 18, c). Monitoring EMT gene expression markers showed no significant change in *Twist* and *Slug* (*Snai2*) markers in both 3D cultures (dynamic and static) at day 3 of encapsulation (Fig. 18, a). Slug (S*nai2*) expression varies in metastasis or in normal EMT cell physiology during development (Chu *et al.*, 2009). Conversely, the up-regulation of *Twist* in 2D culture can be linked as well to mesoderm development in relation to highly expressed Brachyury (Kolind *et al.*, 2012).

In addition, *Snail* (Snai1) showed high expression in 3D dynamic culture without a repressive effect on E-cadherin (*Cdh1*) or the stimulation of N-cadherin (*Cdh2*). The up-regulation of *Cdh1* and down-regulation of Cdh2 mRNA expression suggested a distinct role of Snail in this context (Fig. 18, b). Therefore, *Snai*l's high expression in 3D dynamic culture may enhance cell survival later on the culture period owing to *Snail*'s role in programmed cell death resistance (Zhou *et al.,* 2014).

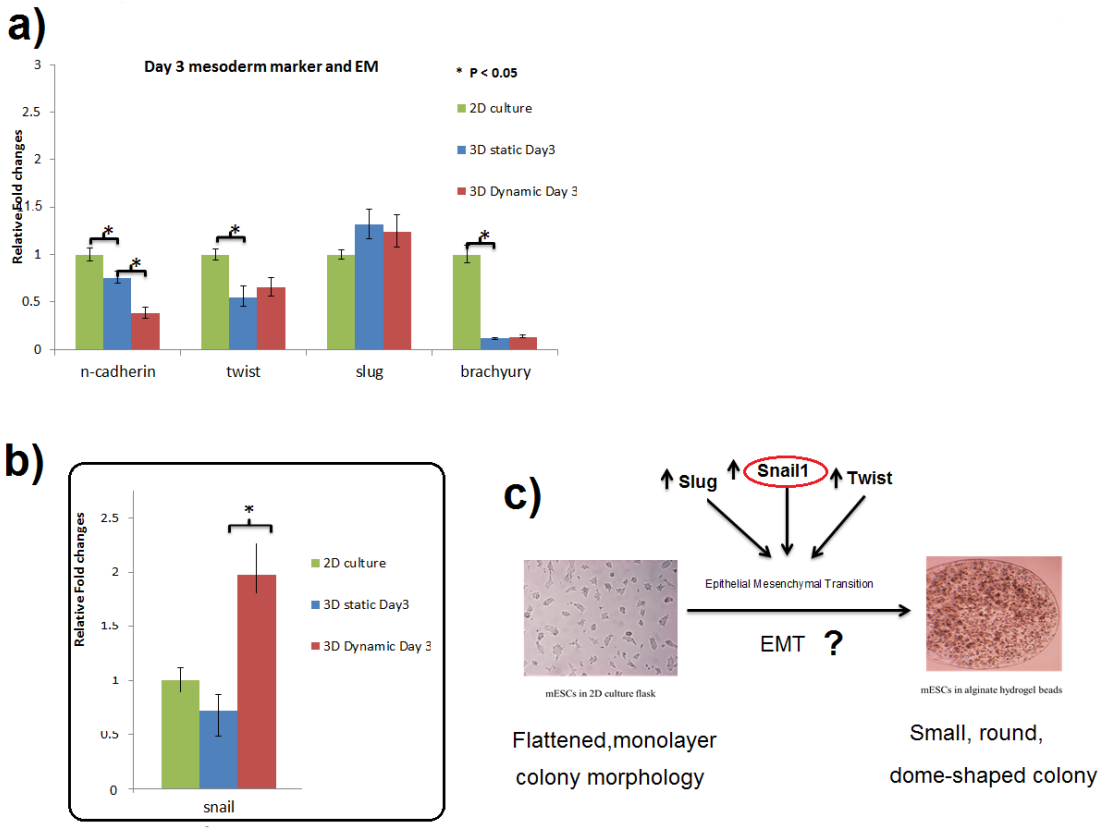

Figure 18 Epithelial-Mesenchymal Transition Progression from Monolayer to 3D Constructs

a) Relative gene expression of mesoderm markers (n-cadherin, twist, slug (snai2) and Brachyury) normalised to 2D culture and β-actin expression.

b) Snail expression showed 2 fold increases in dynamic culture.

c) Schematic illustrate change in cell morphology during transferring mESCs from adherent monolayer culture (2D) to encapsulated alginate beads.

Consistent with this observation, the *Snail* expression at day 9 showed up-regulation in both 3D static (1.5-fold) and dynamic culture (1-fold) in correlation with increases in cell proliferation (Fig. 19, b). Both *Cdh2* and *Cdh1* (direct *Snai1* target) were up-regulated in 3D static culture at Day 9 (Fig. 19, a). In contrast, in 3D dynamic culture, Cdh2 was down-regulated while Cdh1 was up-regulated two-fold (Fig. 19, a). *Cdh1* plays an essential role in ESCs self-renewal and their survival (Chowdhury et al., 2010a). The cells in dynamic condition

favour *Cdh1* and this may be due to its role in cell-ECM interactions and mechanosensors (Moledina et al., 2012a).

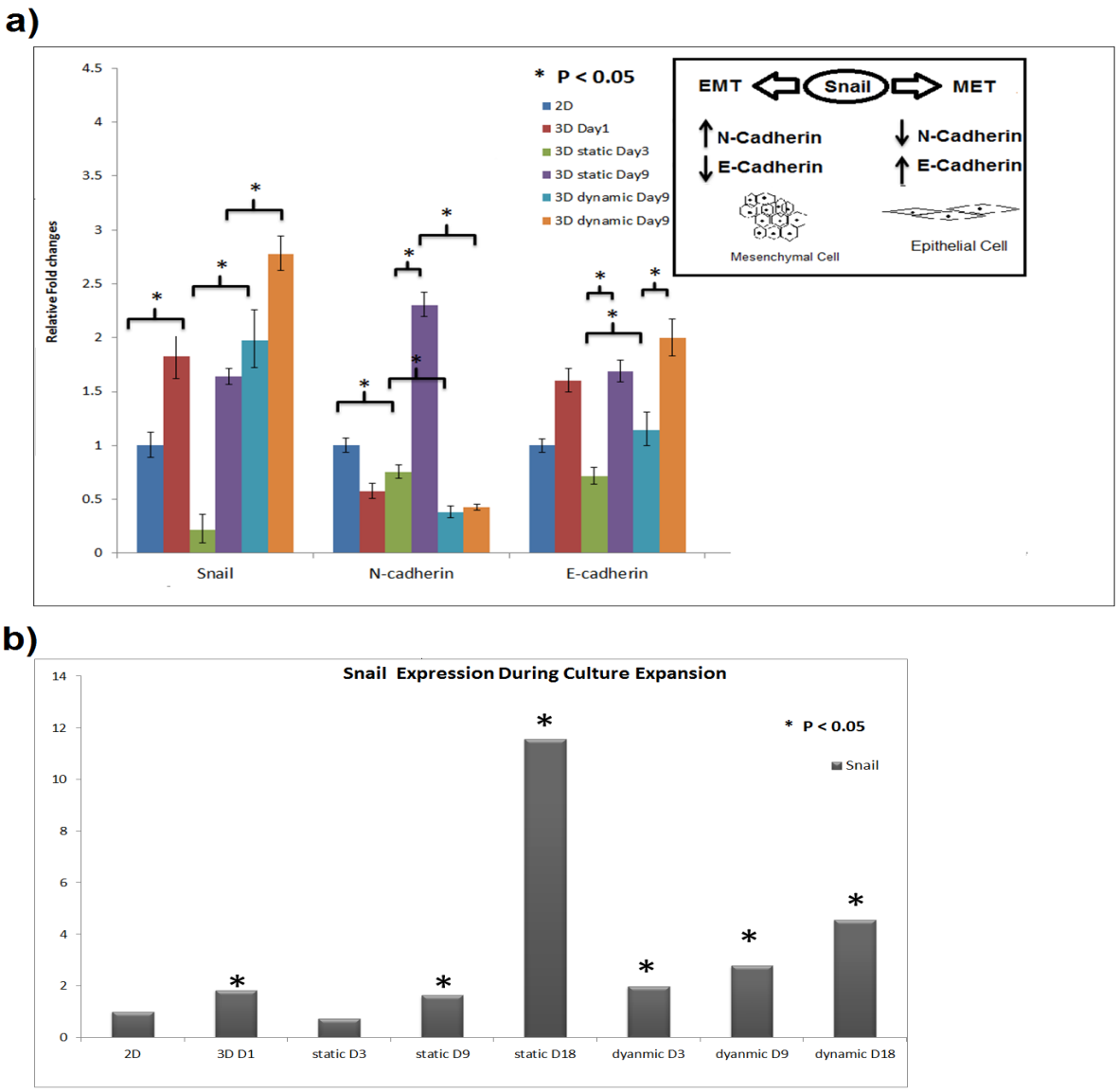

Figure 19 Snail Reciprocal Regulation of N-cadherin and E-cadherin

a) Loss of E-cadherin and up-regulation of N-cadherin expression is significance for EMT process. EMT regulate by Snail. Relative gene expression of Snail, N-cadherin, and E-cadherin at day 1, and 3 and 9 of both static and dynamic culture normalised against 2D culture and β-actin expression.

b) Steady increase of Snail expression from first day of encapsulation throughout the culture period for both 3D static and dynamic cultures.

At an adherent junction, *Cdh*1 is found to promote interaction between apical and basal cytoskeleton (Chowdhury et al., 2010a). The E-cadherin can also direct cells' morphology towards fluid flow (durotaxis), or 'directed cell movement via mechanical cues' (Chang et al., 2010b).

Snail shows a steady increase in expression in 3D dynamic culture and this may be associated with the increase in cell number. However, *Snail* shows a more-than-ten-fold increase in 3D static culture at Day 18. Recently (Fig. 19, b), *Snail* has been suggested to promote *Oct-4* expression, and its silencing leads to down-regulation of the self-renewal marker (Zhou *et al.*, 2014). This finding may contribute to the increment of *Oct-4* expression in both 3D cultures now discussed in Section 3.2.5.

3.2.5. The effect of prolonged adaption on Oct-4 expression

The expression of *Oct-4* was monitored at different points of cell adaption in 3D culture. Interestingly, the *Oct-4* expression at different days (Day 3, Day 9 and Day 18) and culture modes (static or dynamic) was significantly changed (Fig. 20). As early as three days in 3D culture, the cells in 3D static culture had reduced *Oct-4* expression, whereas 3D dynamic cultures showed *Oct-4* up-regulation in comparison to 2D cultures. At long adaption times (18 days), the expression of Oct-4 was four-fold higher in dynamic compared to 3D static culture. There was steady increase on Oct-4 expression during the culture period in both 3D conditions suggesting enhancement of self-renewal.

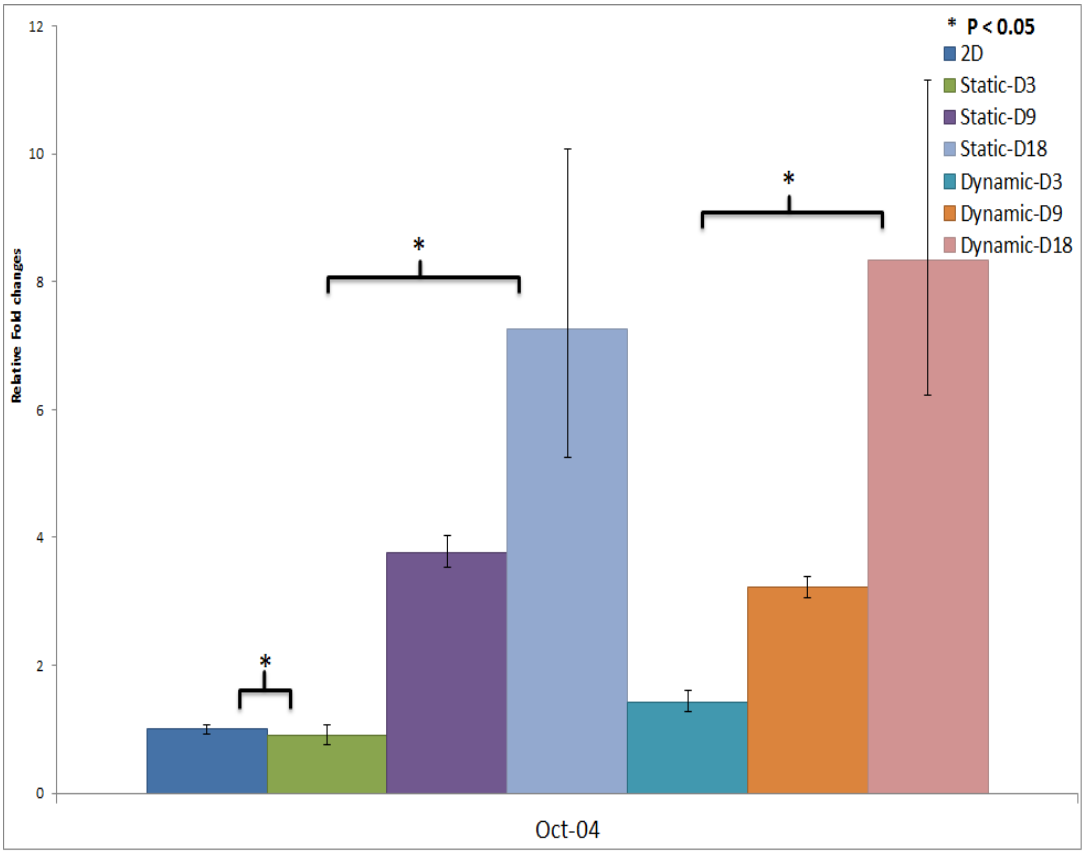

Figure 20 Prolonged 3D Culture Adaption Effect on Oct-4 Expression

Relative gene expression of Oct-4 at prolonged adaption of 3D static and dynamic culture normalised against 2D culture and β-actin expression. Values are means ± SD, N=3 (*: $p<0.05$).

3.3. Discussion

The interactions of stem cells with their environment in terms of external stimuli that are determinates for cell fate are little understood. The metabolic parameter measurement reveals that both glucose and glutamine were not depleted from the culture, while lactate and ammonia were in concentrations that affect mESCs viability in serum contained medium . For instance, lactate accumulation beyond 16 mM can have an inhibitory effect on both cell proliferation and pluripotency (Ouyang et al., 2007). Similarly, the correlation between lactate accumulation and self-renewal exit has been established by previous work in our group. Yeo *et al.* (2013) have shown that encapsulated mESCs in static conditions are unable to expand as viable or pluripotent cells. These findings suggest that accumulation of lactate above 25 mM induces cell differentiation in alginate-encapsulated mESCs (Yeo *et al.*, 2013). In contrast, our results show the capability of alginate beads in the absence of serum in both dynamic and static condition to expand pluripotent and viable stem cells. This could be due to avoiding serum in our encapsulated mESCs. By using replacement serum (KORS), lactate accumulation effectively reduces to 14 mM compared with 25 mM in serum-based 3D culture. Furthermore, KORS in our work enables self-renewal given to high Oct-4 expression and enhanced cells viability. This may involve a difference in growth factor ingredients as serum with LIF is found to promote spontaneous mESCs differentiation.

However, during the early days of culture, *Rex1*, a sensitive marker for pluripotency, was highly expressed in 3D dynamic, compared to 2D or 3D static cultures. This data suggests enhancement of self-renewal in dynamic culture. *Rex1* recognises as highly specific inner cell mass (blastocyst stage). Positively expressed, *Rex1* is highly associated with self-renewal of mESCs, and its knockouts result in loss of pluripotency (Son et al., 2013). In addition to Rex1, other self-renewal markers, such as *Nanog* and *Oct-4*, are up-regulated, whereas an early

differentiation marker, *FGF5*, was down-regulated. *Oct-4* is a master transcriptional regulator for the maintenance of naive pluripotency and has an essential role in embryonic development. The expression of *Oct-4* is detected in the early stages of embryo development, including oocytes, blastomeres, inner cell mass (ICM) and also during post-implantation of the epiblast stage and in germ cells. The *Oct-4* knockout is lethal for pre-implantation in mouse embryos due to the failure of pluripotent ICM formation. Moreover, inhibition of *Oct-4* leads to the loss of ESC self-renewal as well as its overexpression (Wilson *et al.*, 2014).

Interestingly, *Oct-4* expression was found to be at integrin-mediated focal adhesions. Therefore, growing mESCs on rigid surfaces inhibits *Oct-4* expression despite the presence of LIF (Moledina et al., 2012b). In contrast, using soft substrates withstands self-renewal for more than five days without LIF supplements (Chowdhury et al., 2010a). However, arguing that the hydrogel soft substrate contributes to self-renewal can be disputed by the failure of 3D static culture to promote *Oct-4* expression in a similar manner to dynamic sitting. Therefore, the presence of hydrodynamic flow could be the enhancer. Recently, *Oct-4* expression has been reported to be enhanced two-fold by fluid flow in a microchip independent of shear stress. Thus, up-regulation of pluripotency master genes may be due to the presence of the freefall environment in the HARV bioreactor. Simulated microgravity is found to be sufficient to sustain mESCs pluripotency in the absence of LIF (Kawahara *et al.*, 2009). This is further supported by a recently published paper that showed that 3D dynamic encapsulation helps fibroblast reprogramming and the acquisition of 'stemness' without transcription factors transition (Han *et al.*, 2013).

After extending encapsulated cells growing on 3D cultures without passaging, the *Oct*-4 high expression was still sustained, despite an increase in cell density. The Oct-4 expression is found to be regulated by Rho/ROCK (Rho-associated kinase) signalling that promotes self-

renewal in a cell-density dependent manner. Limiting the Rho/ROCK pathway by reducing cell-cell interaction (contact inhibition ROCK1 and ROCK2) enhances sensitivity to LIF signalling at low cell density (Chang et al., 2010a). In contrast to this finding, high cell density in static and dynamic 3D cultures promotes higher Oct-4 expression, compared to the early days of the culture where cell density is low. This may be due to differences in cell growth dimensions and morphology. In conventional monolayer culture, the cells are grown in the horizontal plane, not in a vertical dimension. Thus, LIF diffuses freely in the monolayer of cells and may rapidly equilibrate, whereas the presence of 3D substrate and deposition of ECM slows down diffusion. Using a dynamic bioreactor was found to enhance LIF delivery to the cells and overcome the inheritance problem of cell density (Moledina et al., 2012b). Similarly, measurement of LIF receptor expression shows up-regulation in dynamic culture that enhances LIF/STAT3 phosphorylation activity to promote self-renewal.

In conclusion, the 3D system combined alginate beads and HARV bioreactor enabled the expansion of viable pluripotent mESCs using serum-free media. Investigating signalling pathways that underlie self-renewal enhancement in next chapters will expand our view in in-vitro pluripotency.

CHAPTER4: Different Proteomics Approaches to Extract &Identify Proteins from 3D cultures

4. Introduction

The plastic surface of tissue culture lacks the structural, mechanical and biochemical cues that provide ESC with some resemblance to their *in vivo* environment (Lund et al., 2009). The use of natural or synthetic 3D constructs may mimic an environment similar to that *in vivo* ((Chowdhury et al., 2010a), (Randle et al., 2007), (Hwang et al., 2009)).

However, switching culture conditions from 2D to 3D has been associated with dramatic molecular alterations. There has been a lack of proteomics studies focusing on molecular changes arising from the transition of adherent ESC to suspension culture (Konze et al., 2014). Conversely, often studies examining the mechanisms of 2D versus 3D culture rely on gene expression analyses either using transcription profile or arrays (Boutilier et al., 2005, Bradley et al., 1984). The instability of mRNA, differential translational rates of expressed genes, and protein degradation limit transcription profiling. Additionally, expression of some proteins and their respective mRNA level has been poorly correlated. Undeniably, proteomic analysis can obtain coverage of various translated proteins and provide critical information about the post-translational modifications and protein localisation. Thus, detailed characterisation with techniques such as 2D gel electrophoresis is required to identify the signals that led to these molecular changes. Proteomics remain as a crucial technique to reveal and gain insight in developmental biology (Patterson and Aebersold, 2003).

4.1. Overall Aim

In this chapter I will focus on the optimisation of protocols for extraction and solubilisation of proteins from alginate hydrogel beads utilising different approaches. These comprise precipitation, desalting, 1D and 2-D gel electrophoresis and mass spectrometry (MS).

4.1.1. Specific Objectives

1. Comparison of different extraction protocol.
2. Determination of the most efficient 3D culture sample preparation workflows based on protein yields and purity.

4.2. Results

4.2.1. In situ extraction

4.2.1.1. 16-BAC PAGE electrophoresis

The cationic detergent 16-benzyldimethyl-n-hexadacylammonium chloride (16-BAC) solubilises and positively charges proteins (Hartinger et al., 1996). Based on this assumption protein complexes should enter the gel towards the cathode whereas polysaccharides will migrate to the opposite direction separating it from negatively charged alginate. Cells without beads were used as negative control whereas non-capsulated cells were used as positive control. Cells with alginate were extracted using 16-BAC extraction buffer. The solution was completely homogenised using sonication avoiding the heating due to the presence of urea in the extraction buffer. Homogenised samples along with positive controls and alginate alone run in the gel towards cathode. The negative control containing no cells was not stained for protein or glycoprotein demonstrating failure of either alginate or gelatine to migrate into the

gel (Fig. 21, i). The positive control cells without alginate showed well separated protein bands along the gel suggesting that there were no technical issues in the procedure (Fig. 21, ii). Despite the diffusion of protein from the cells with beads in the gel, protein was caught up in the stacking layer and could not travel further down (Fig. 21, iii). This may be due to protein aggregation and crosslinking leading to sizeable polymers. Furthermore, addition of DTT did not improve the protein migration in the gel. This might be either due to altered pH or due to gel overloading. In addition, determination of relative protein concentration was hindered by high salt contamination in the sample. Difficulties in estimation of the protein concentration and protein mobility problems led to discontinuation of this approach (Ralf J. Braun, 2009).

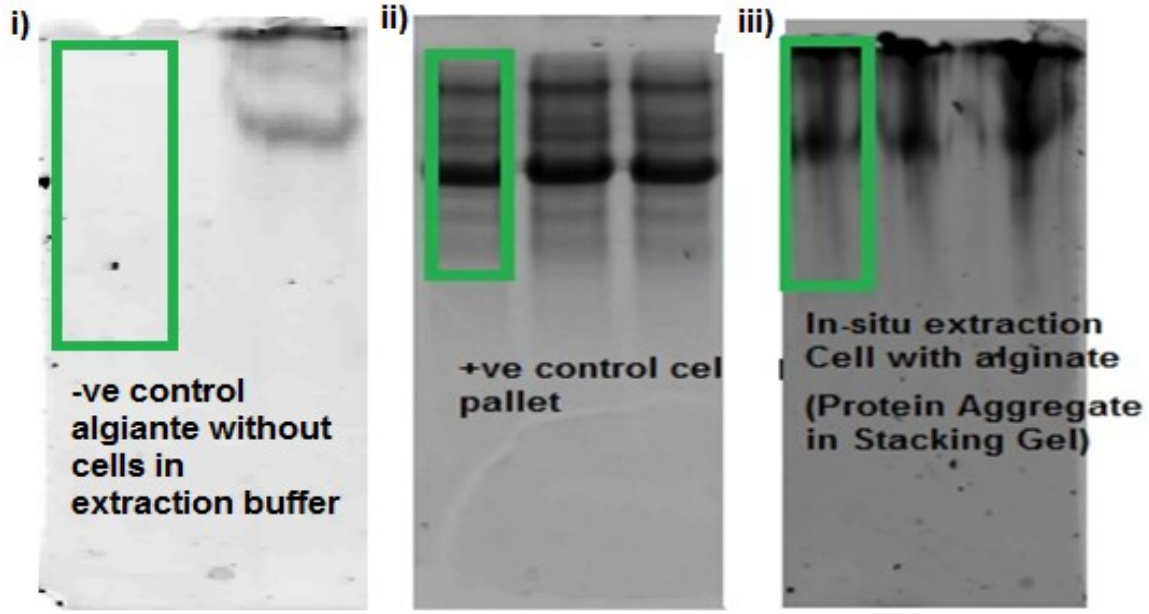

Figure 21 In Situ Extraction 16-BAC/SDS-PAGE

mESCs encapsulated in alginate beads dissolved in 16-BAC extraction buffer and loaded in 16-BAC/first dimensional gel. (i) Cell-free alginate was loaded as negative control for the run whereas positive control (cell pellet obtained from 2D culture) can be seen in (ii). In (iii) *in situ* extraction of proteins from encapsulated cells using 16-BAC gels was demonstrated; it was obvious that proteins failed to migrate to resolving gel suggesting protein aggregation in stack gel.

4.2.1.1. RNeasy Plant extraction kit:

In order to overcome the aforementioned issues with extraction, a RNeasy plant mini kit from Qiagen was employed following a protocol from Wang et al (Wang et al., 2009a). Wang et al suggested that the cells grown in alginate beads can be treated as a plant cell rich in carbohydrate. Therefore, a more stringent cell lysis by powdering beads using liquid nitrogen and grinding in pestle and mortar was followed as per manufacturer guidelines. QIA shredder spin columns to filters were used for separating RNA from the lysate before washing with ethanol. The lysates containing protein and alginate were collected and were then separated by Sevag's solution (n-butanol /chloroform, 3:1). After frequent vortexing the aqueous phase was discarded and the interphase containing protein was carefully isolated in a separate tube (Fig. 22, A). Carbohydrates and proteins have a different polarity, which helped in proper phase separation. Subsequently, proteins were precipitated using acetone and then separated on a SDS-PAGE gel. However, the protein recovery was low as shown by staining with coomassie blue after precipitation. Proteins at both high and low molecular weight were absent (Fig. 22, B). In addition, RNA quality was also confirmed using denatured-formaldehyde agarose gel electrophoresis (Fig. 22, C). The gels were stained with ethidium bromide to increased sensitivity to detect S18 and S28 bands, the total RNA band was shown low purity of sample (Sharma et al., 2003), (Wang et al., 2008), (Wang et al., 2009a).

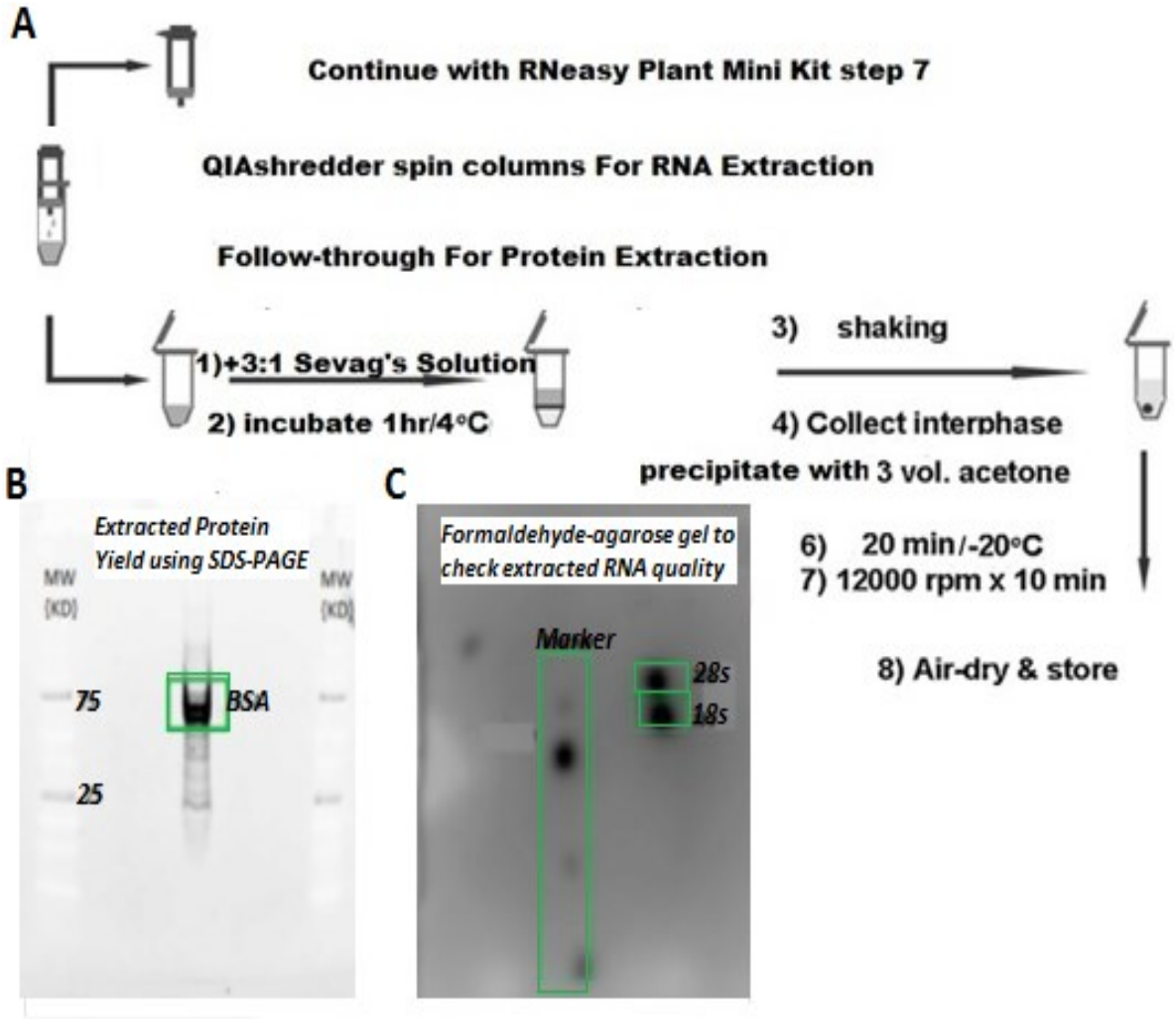

Figure 22 Alginate Beads Treatment like Plant Polysaccharide-Rich Wall

Low protein yield using RNeasy Plant extraction kit. (A)This diagram illustrated steps of proteins extraction follow the protocol published in (Wang et al., 2008),(Wang et al., 2009a). In (B) protein recovered after precipitation was stained with coomassie blue; proteins at both high and low molecular weight were absent. In contrast, in (C) FA gel shows positive 28S and 18S bands. Figure A modified from (Wang et al., 2008)

4.3.1.3. Mechanical disrupters

Encapsulated cell proteins were extracted using different mechanical disruption methods. Cell extracts were homogenised in urea buffer and then mechanically processed using a QIA-shredder, Ultrasonic Sonicator, or cell disrupter. Proteins yields were then compared using 4-12% SDS-PAGE, which suggested that there were no significant differences among different extraction procedures (Fig. 23, i). Protein extracts were then precipitated using different precipitation methods and re-suspended in 2-DE buffer.

However, 2DE gel showed no protein spots. The sample precipitated at the cup during the first dimension, although complete solubilisation had been achieved using a high amount of urea in the sample buffer (8mM). This precipitation may be due to high salt and extract impurities (Fig. 23, ii).

Therefore, buffer exchange and dialysis was preformed prior to 2DE gel buffer addition to remove detergent and divalent cations using CHAPS and mixed bed resin followed by desalting using a commercial clean up kit from GE healthcare. However, the proteins were precipitated at acidic pH during the second gel dimension and the protein diffusion suggested that protein degradation had occurred (Fig. 23, iii). In addition, the incompatibility of 2DE gel non-ionic detergent buffer and high salt contamination further reduced the solubility of protein.

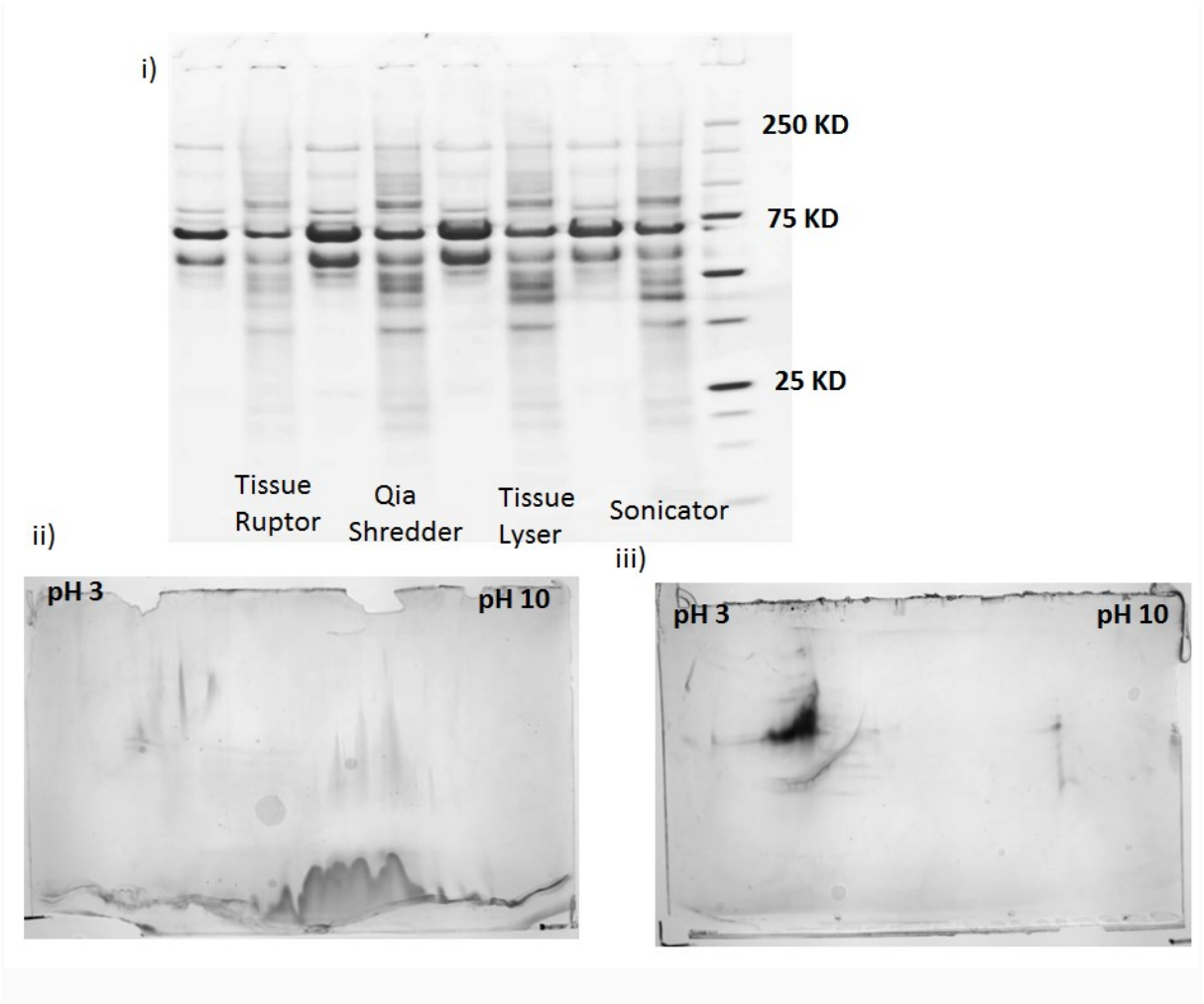

Figure 23 Gel-Based Optimisation of Alginate Beads Dissociation Protocol

i) Shows using different instruments to in situ protein extraction of 3D cultures. Sonication was method of choice.

ii) There were no protein spots in 2DE gels.

iii) Sample precipitate on the protein loading cup due to impurity of the sample. Protein aggregate at the acidic end of the IPG strip after using different precipitation to desalt the sample.

4.3.2. *Ex situ* extraction

In order to improve protein extraction from alginate beads a number of steps should be considered. For instance, using a consistent and short period of dissociation, and limiting the time between cell collection and addition of extraction buffer.

To develop an efficient protocol, high citrate concentrations were used to bind calcium (used in alginate beads gelation) in presence of a sucrose buffer (0.25 mM, pH 7). The sucrose acts as cushion to reduce the effect of osmotic pressure and protect the cell membrane. Immediately following alginate harvesting, the cell pellet was washed twice with PBS and protein was extracted using RIPA buffer combined with 3 minutes of sonication. The quality of protein yield was comparable to 2D control cells. This is implied by the presence of low molecular weight proteins bands, improvement of protein yields and reduced salt or alginate contamination (Fig. 24, a). In the 1D gel glycoprotein stain was used to check the removal of alginate from protein extract (Fig. 24, b). The cell pellet contained no glycoprotein, while the supernatant was positive. In concordance, the negative control including alginate without cells showed a similar positive stain. Extract from 3D culture run on 2DE gel to validate the efficiency of the developed protocol. The gel showed smears and low resolution due to the sensitivity of 2D gel to salt on the sample (Fig. 25, i). After using clean up-kit, there was significant improvement on the gel resolution (Fig. 25, ii).

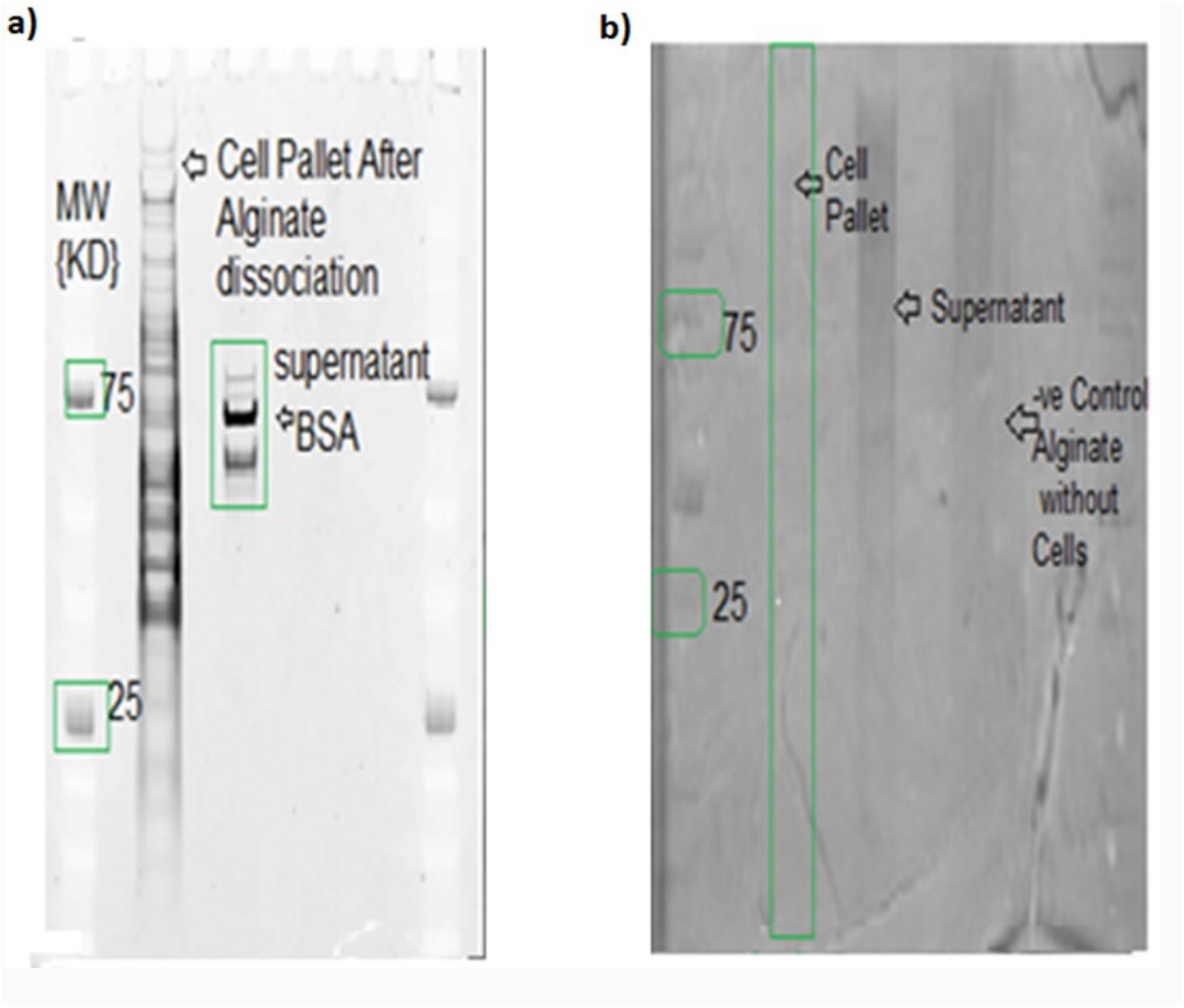

Figure 24 Developed Protocol to Dissociate Alginate Beads for Protein Extracts

a) Final protocol used to extract cells from alginate hydrogel (refer to methods and material chapter) contains sucrose and high concentrations of citrate.

b) It can be seen in the 1D gel, using glycoprotein stains to check the removal of alginate from protein extract. The cell pellet contained no glycoprotein, while the supernatant was positive. In concordance, the negative control including alginate without cells showed a similar positive stain

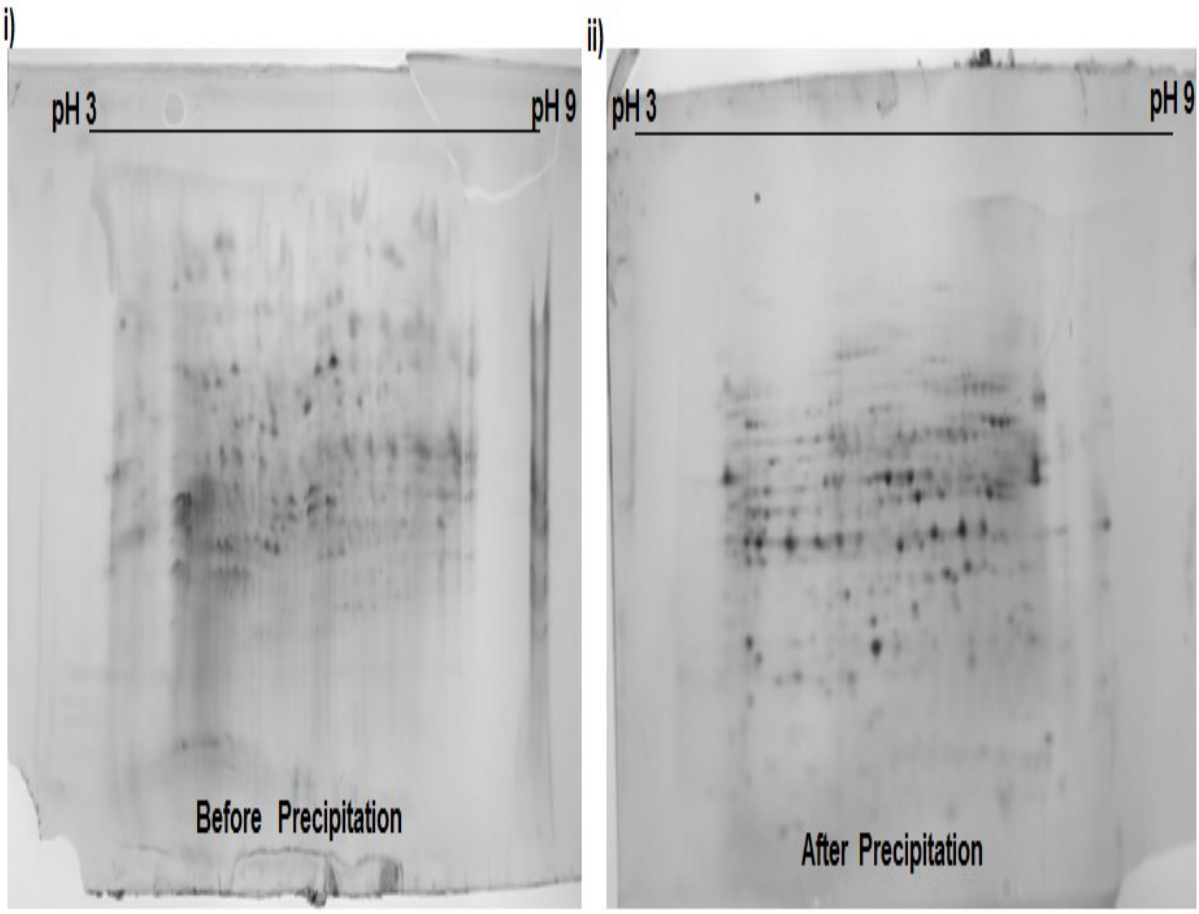

Figure 25 2DE gel of protein Extract before and after clean-up sample Using Developed Protocol

i) It is clear that beads dissociation improve proteins separation and migration in 2DE gel. However,

ii) First gel show smears that improved by using commercial available clean up kit as shown in the second gel.

4.3.2. Gel based proteomics

4.3.2.1. Comparative study of 2D versus 3D culture using 2-DE gel

Attempts to address the difference between 2D and 3D cell culture were performed by assisting different markers of pluripotency and early germ-layer. mESC were plated either in 2D culture (Fig. 26, A) or encapsulated in alginate beads (Fig. 26, B) for 3 days prior to analysis. RNA was extracted and RT-PCR was performed for a number of markers. Pluripotency markers Oct4 and Rex1 were both expressed in 2D and 3D culture. Oct4 was more strongly expressed in 3D compared with 2D. In contrast, the intensity of Rex1 was same in both 2D and 3D cultures. There was no expression for specific-linage marker AFP (endoderm-derived marker) and Nestin (ectoderm-derived marker), with the exception of slight expression of Brachyury (mesoderm-derived marker) (Fig. 26, C).

Establishing a protocol that yields high protein concentration with minimum degradation, has aided in preparing the 2-DE gel. In order to evaluate protein expression, extracts were processed with protocol mentioned on 4.3.2. 2DE electrophoresis of proteins extracted from cells cultured in 2D (Fig. 26, D) and 3D (Fig. 26, E) culture was successfully performed using the newly developed protocol. The gel showed clear differences between protein spots.

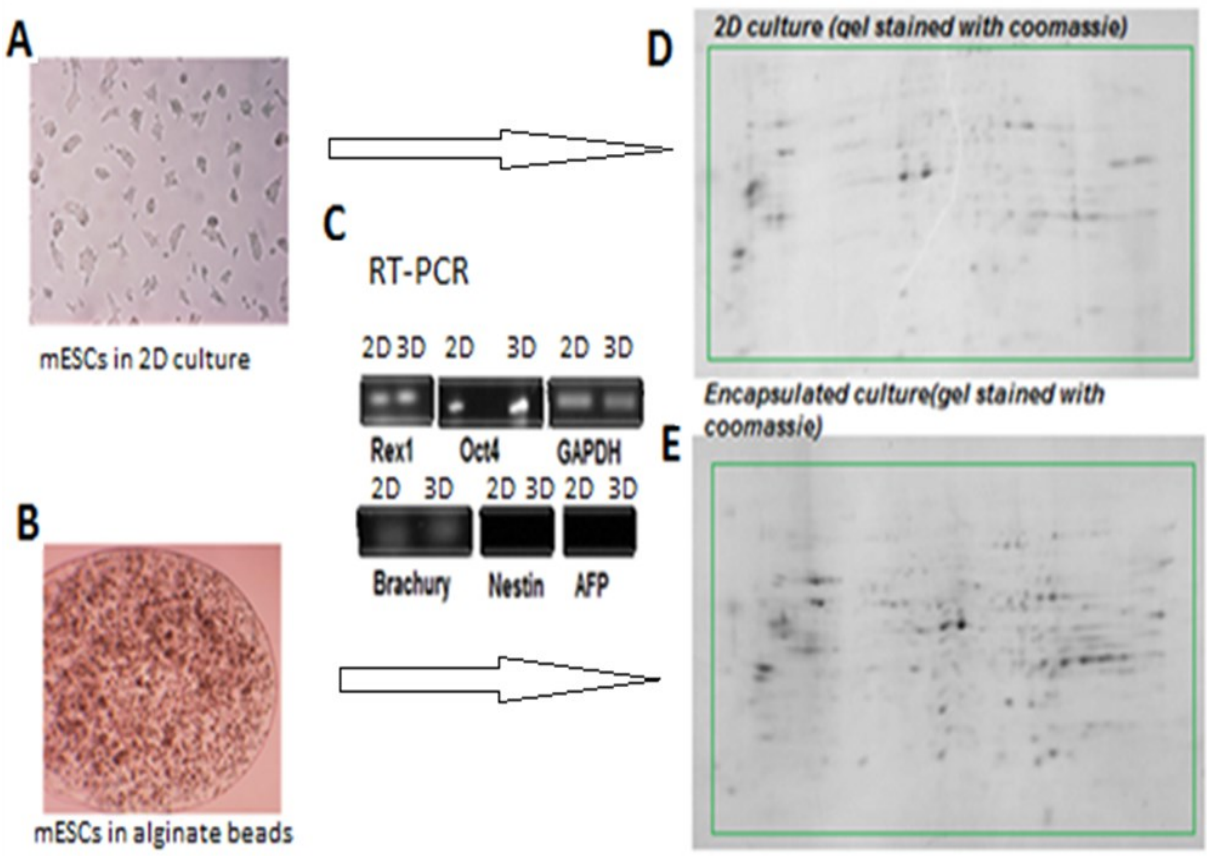

Figure 26 *Comparison of 3D culture versus 2D culture*

mESC were plated either in 2D culture (A) or encapsulated in alginate beads (B) for 3 days prior to analysis. RNA was extracted and RT-PCR was performed for a number of markers. In (C) gene expression was assessed for 2D and 3D conditions using RT-PCR. Oct4 and Rex1 were both pluripotency marker were expressed in 2D and 3D culture. Oct4 was more strongly expressed in 3D compared with 2D. In contrast, the intensity of Rex1 was same in both 2D and 3D cultures. There was no expression for specific-linage marker AFP (endoderm-derived marker) and Nestin (ectoderm-derived marker), with the exception of slight expression of Brachyury (mesoderm-derived marker). 2DE electrophoresis of proteins extracted from cells cultured in 2D (D) and 3D (E) culture was successfully performed using the newly developed protocol.

4.3.2.1. Semi-quantitative comparison between 2D and 3D cultures using DIGE

Using 2-DE gel electrophoresis illustrated the difference between two groups proteome. To validate that the results were not introduced due to technical issues, 2D-Differential In-Gel Electrophoresis (DIGE) technique was used to compare 2D versus 3D culture. 2D cells and 3D cells were lysed and labelled with Cy3 and Cy5, respectively. As internal standard, equal amount of 2D and 3D cell lysates were mixed and labelled with Cy2 (for experiment design please refer to Table 3 on chapter 2). In Fig. 27, green and red spots corresponded to protein that overexpressed on 2D and 3D cells. By contrast, yellow spots represented protein spots that were equally expressed in both conditions. DIGE has been widely used for semi-quantitative assessment of changes in proteins expression between two samples. Additionally, DIGE overcomes some of the limitations of 2-DE gels such as a poor quantitation and low reproducibility. This work was done in collaboration with DeltaDot Ltd.

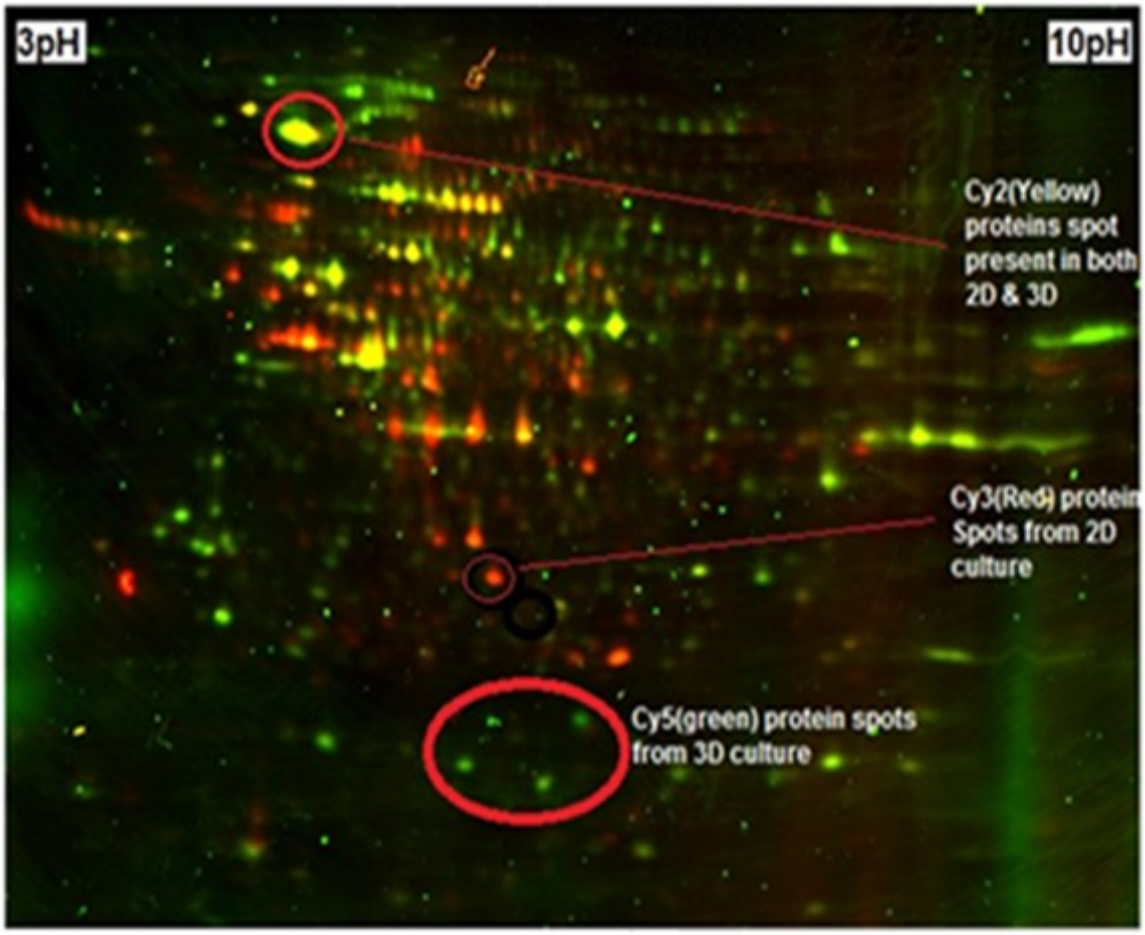

Figure 27 2D-Differential In-Gel Electrophoresis (DIGE) of 2D versus 3D Culture.
2DE-DIGE image for proteins extracted from 2D and 3D. The experiment was done using 18-cm strips 3-10 pH running on the tower gel system from GE healthcare**.**

4.3.2.2. The 2-DE gel lake of reproducibility

Extracts derived by dissociating cells encapsulated in alginate (two separate biological replicates) were spotted on the second dimension and stained by Sypro Ruby (Fig. 28, i-iv). Each 3D sample was represented by two technical replicates for each sample (Fig. 28, (i, ii replicates) and iii & iv (iii, iv replicates)) prepared on the 2-DE gels.

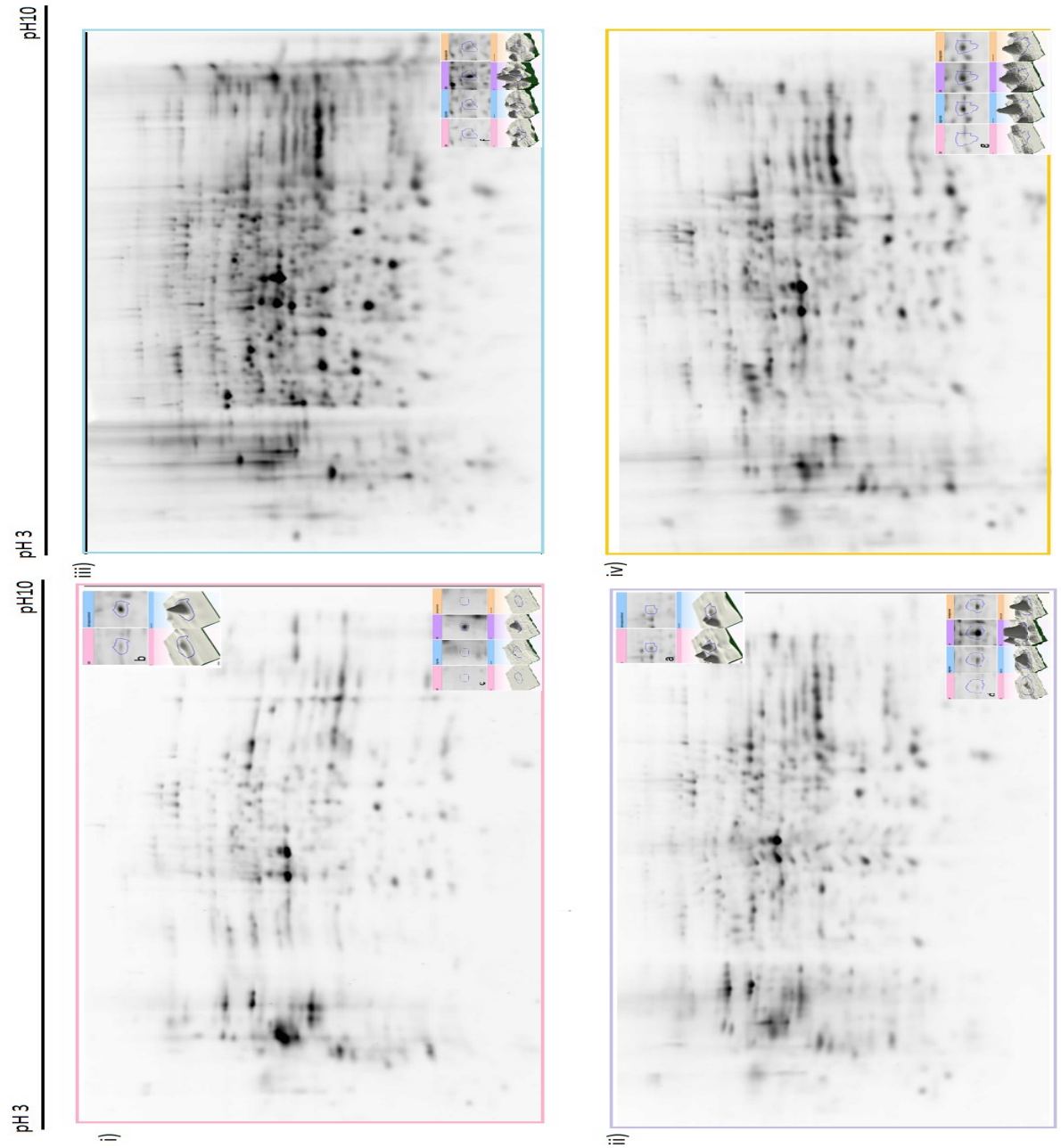

Figure 28 SameSpot Analysis of Four Gels Replicates from two Independent Experiments of Protein extracted from Alginate Encapsulated Cells

Proteins extracted for four gels from cells that were encapsulated in alginate beads i) & ii) are technical replicates for the first biological sample. Whereas iii) and iv) are the technical replicates for the second biological replicate. These gels were visualized by Sypro-Ruby. There were similarities and differences between the four gels. SameSpot analysis of the four gels or two technical replicates on the small box inside the gel figure represented the protein spots difference either in quantity or appearance despite similar protein load.

The purpose of this experiment was to evaluate the performance of the extraction protocol of alginate embedded cells and reproducibility of 2DE gels. The difference between the two biological and two technical replicate gels was estimated using SameSpot software from Totallab® (last updated 16.09.2014, http://www.totallab.com/products/samespots/overview/). The difference not only involved biological replicates but there was low reproducibility between the two technical gels. A number of images were picked to reflect the appearance, disappearance or changes in intensity of protein spots (Fig. 28 boxes inside the gels).

4.3. Discussion

This chapter addresses the use of different sample preparation workflows to reduce contamination and loss during protein extraction from encapsulated mESC. To identify the appropriate approach for protein extraction, *in-situ* extraction was compared to a control sample from monolayer cells. The reason behind attempting *in situ* extraction was to avoid protein loss and confirmation that might occur during alginate dissolution. A broad range of conventional extraction methods was evaluated, including 16 BAC-PAGE electrophoresis, RNeasy Plant extraction kit, different mechanical extractions, precipitation and desalting techniques. These resulted in inefficient protein recovery. Furthermore, the use of these techniques has led to protein degradation, with Coomassie staining revealing absence of lower weight proteins in the *in situ* extraction of alginate samples. The presence of high salt concentrations used to facilitate cross-linking of alginates, was incompatible with solubilisation buffers such as SDS.

Isolating the cells from the beads improved the protein yield and minimised exogenous contamination. Therefore, there was an absolute necessity to optimise the protocol to enable alginate dissociation to extract proteins. Using high citrate concentrations and sucrose reduces

metabolic change introduced to the cell during extraction by stabilising proteins and preventing aggregation. Additionally, the duration of exposure to dissociation buffer was shorten to avoid protein degradation. The efficiency of this protocol was confirmed by proteins yields, presence of low molecular weight proteins, and reduced contamination. Together, this approach was fruitful to overcome the obstacles of *in-situ* extraction.

Subsequently, a profile of protein comparison was made using 2-DE electrophoresis. However, heterogeneity found between the technical and biological replicates introduces critical variations in protein profiling preventing useful biological interpretation. This lacked in reproducibility between gels is due to confounding factors of 2-DE gel in sample preparation procedures, protein spot picking and identification may have masked the any biologically meaningful differences. Additionally, given that protein expression was expected to alter in 3D versus 2D culture, might involve deposition of extracellular matrix (ECM) and synthesis of cell membrane proteins. These proteins were however difficult to visualise using 2DE gel due to their high hydrophobicity. In addition, 2-DE gel possessed other shortcomings that confound identification of several classes of proteins including low abundance proteins, large or small proteins, and proteins with extreme isoelectric points. Although, conventional 2-DE based proteomics is a common method of choice for most proteomic experiments, it under represents hydrophobic and low molecular weight proteins. In addition, it has a lack of reproducibility due to the multiple steps involved in its workflow (Brewis and Brennan, 2010).

In addition, protein extraction from 3D constructs employs additional multistep sample preparation workflow. This is due to the presence of the alginate that could lead to contamination and loss of protein. In proteomics, sample preparation is a critical step due to the impact it can have on accuracy and sensitivity in the data obtained and its subsequent data analysis. However, the development of highly sensitive mass spectrometry presents an

alternative in comprehensive proteome identification approach especially when combined with SILAC which we will discuss in upcoming chapter.

CHAPTER 5: Effect Of 3D Culture on mESCs Global Proteome

5. Introduction

The stem cell niche microenvironment is a fundamental regulator of ESC behaviour. Besides cell-to-cell and cell-to-extracellular matrix (ECM) contact, the stem cell niche microenvironment alters cellular morphology, survival, apoptosis, proliferation, and differentiation (Tibbitt and Anseth, 2009). Cell culture methodologies that mimic the biochemical and architectural characteristics of the *in vivo* micro-environment will improve ESC culture.

Current three-dimensional (3D) culture methodologies have aimed to mimic ECM micro-architecture. Interestingly, ESC behaviour *in vivo* and under 3D culture conditions exhibit a strong overlap, since they better mimic the characteristics of the *in vivo* ESC environment. For example, the use of a 3D chitosan-alginate scaffold, allowed cellular proliferation and functionality for 21 days and also maintained pluripotency in an immunodeficient mouse model and teratoma formation. The use of encapsulated human ESCs (hESCs) in calcium alginate microcapsules allowed pluripotency and differentiation to mesendoderm, definitive endoderm, and primitive gut tube. Human ESCs encapsulated in 3D hyaluronic acid capsules maintained their undifferentiated state, preserved their normal karyotype, and maintained their full differentiation capacity as indicated by embryoid body formation (Azarin et al., 2012b).

A number of studies have examined ESC behaviour down to the transcriptome level, as well as the ESC chromatin state. However, such approaches ignore translational and post-translational modifications that affect both quantity and function (Mikkelsen et al., 2007). Mass spectrometry (MS) proteomics allows the systematic quantitative and qualitative exploration

the entire proteome, overcoming these issues. Extensive studies into the mouse ESC (mESCs) proteome have identified 1,790 and 1,775 peptides. Additionally peptide quantitation has only been performed using peptide counting but a quantitative study of all proteins expression is yet to be performed. The use of metabolic labelling methodologies such as Stable Isotope Labelling by Amino Acids in Cell Culture (SILAC) allows accurate quantitation. SILAC eliminates error-prone parallel steps present in protein purification protocols. While metabolic labelling methods have been used on transformed cell lines, labelling of ESCs, a cell type that is difficult to culture, has not yet been demonstrated (Graumann et al., 2008c).

In this chapter, we hypothesized that 3D culture conditions offer a distinct advantage to produce healthier mESCs than standard 2D culture. In order to gain further insight in the biological differences between 2D and 3D culture, we analysed and compared the protein expression profiles using SILAC of mESCs cultured in traditional 2D culture, 3D alginate beads in static and dynamic culture conditions. The identification of differential protein expression across these three distinct cell culture methodologies will aid in identifying the factors contributing to pluripotency.

6.1. Overall Aim

- Interpretation of the behaviour of mESCs in different culture environments in the light of the differential protein expression data.

- Use the data obtained from large-scale analysis, to determine the reason why 3D dynamic culture enhanced undifferentiated expansion of mESCs inferred to gene profiles at days 3 of culture.

6.2. Experiment design

Following the Bendall protocol, our cells were adapted for 5 passages in 2D culture to achieve the complete incorporation. SILAC maintained media depend on controlled amino acid content in order to accomplish maximum labelling product. Therefore, dialyzed FBS was replaced with the conventional serum to reduce amino acid availability in cell culture. Supplementation of SILAC media with 15% KOSR was extended for SILAC procedure to stem cells. Coincidently, using KOSR provides mESCs with 800 mg/ml of proline in addition to KOSR lack of arginine and lysine (Bendall et al., 2008).

Following labelling, MS based proteomics were used to identify proteins in complex mixture. Once the cells achieved 96 % efficient labelling (checked using MS), protein extracted from the similar cell number and pooled together. We had three groups, the mixture of 2D cells labelled with heavy mixed with 3D static labelled with light isotopes, 3D static (heavy) combined with the same cell number from 3D dynamic (labelled with light), and last cell mixture was 3D dynamic (heavy) with 2D (light). The three protein extracts was quantified and fractionated by 1-D gel electrophoresis and stained with Colloidal Coomassie Blue. To reduce complexity, samples were separated by 1D gel electrophoresis and fractioned prior to analysis. In gel digestion additionally aid protein purification and contaminant removal such as high salt contamination from Ca^{+2} encapsulated beads. Using gel to separate proteins helped in identification of membrane proteins while in solution digestion approach is method of choice for specifically soluble proteins (Gundry et al., 2009).

Next the gel cut into 5 slices and the slices subjected to in gel trypsin digestion (for experiment design and further information please refer to chapter 2, section 2.6.6. and Fig. 29). The digests are then analysed by tandem mass spectrometry and the ratio of intensities of the corresponding heavy and light peaks calculated using ProteomeDiscovere software.

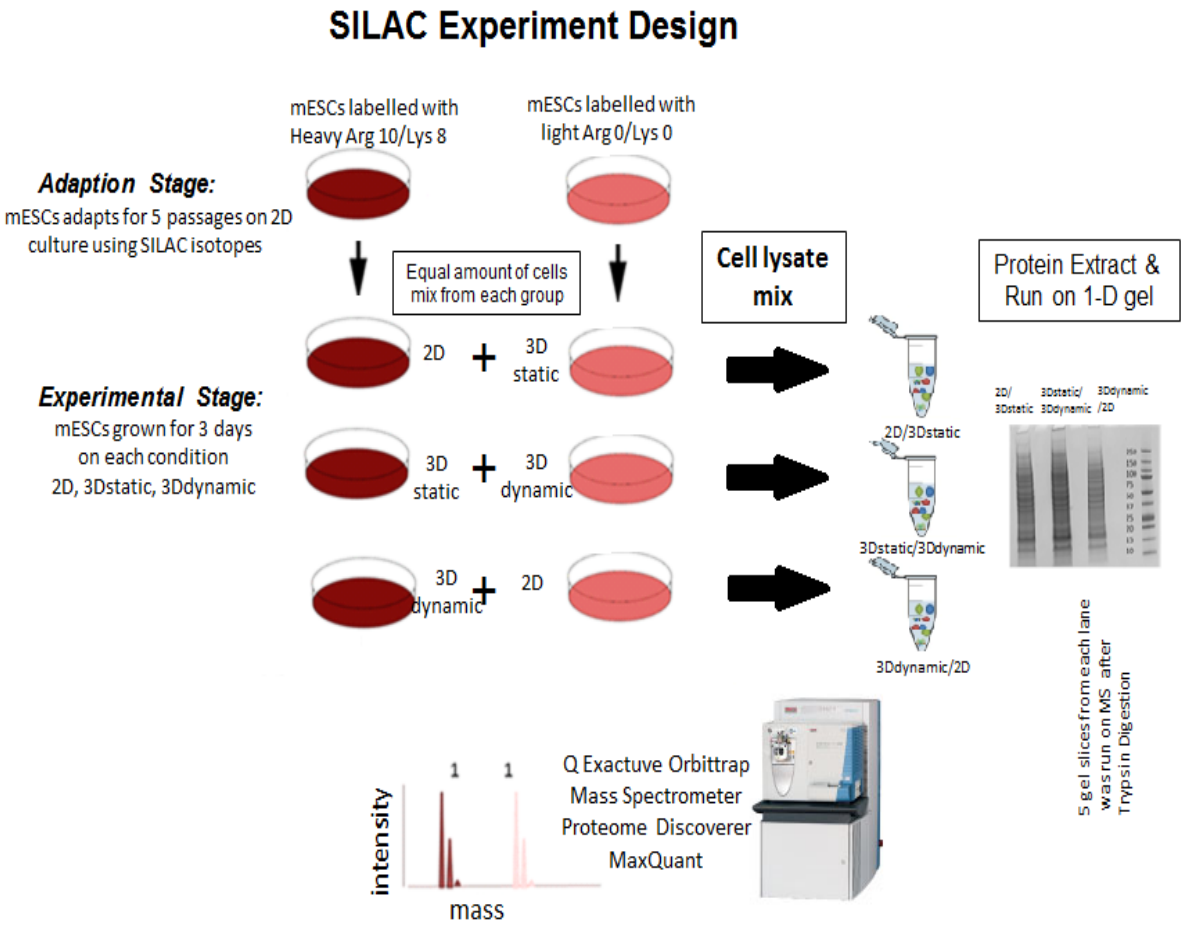

Figure 29 Diagram illustrated the SILAC experiment design

The mESCs were adapted in SILAC media both heavy and light arginine and lysine. After 5 passages cells transfer to either 3D static or 3D dynamic for three days. Mixture of cell pallets from each group obtained to give three proteins extracts samples. First sample is 2D (heavy) mixed with similar cell number from 3D static (light). Second sample resembles equal mixture of 3D static (heavy) and 3D dynamic (light) labelled cells. Third sample is equal cell number obtained from 3D dynamic (heavy) and 2D culture (light) isotope labelled. Equal protein concentration separate on 1D SDS/PAGE. Then 5 bands were subjected to LC-MSMS separation.

5.3. Results

5.3.1. In-depth proteomics approach using combination of SILAC and LC/MSMS

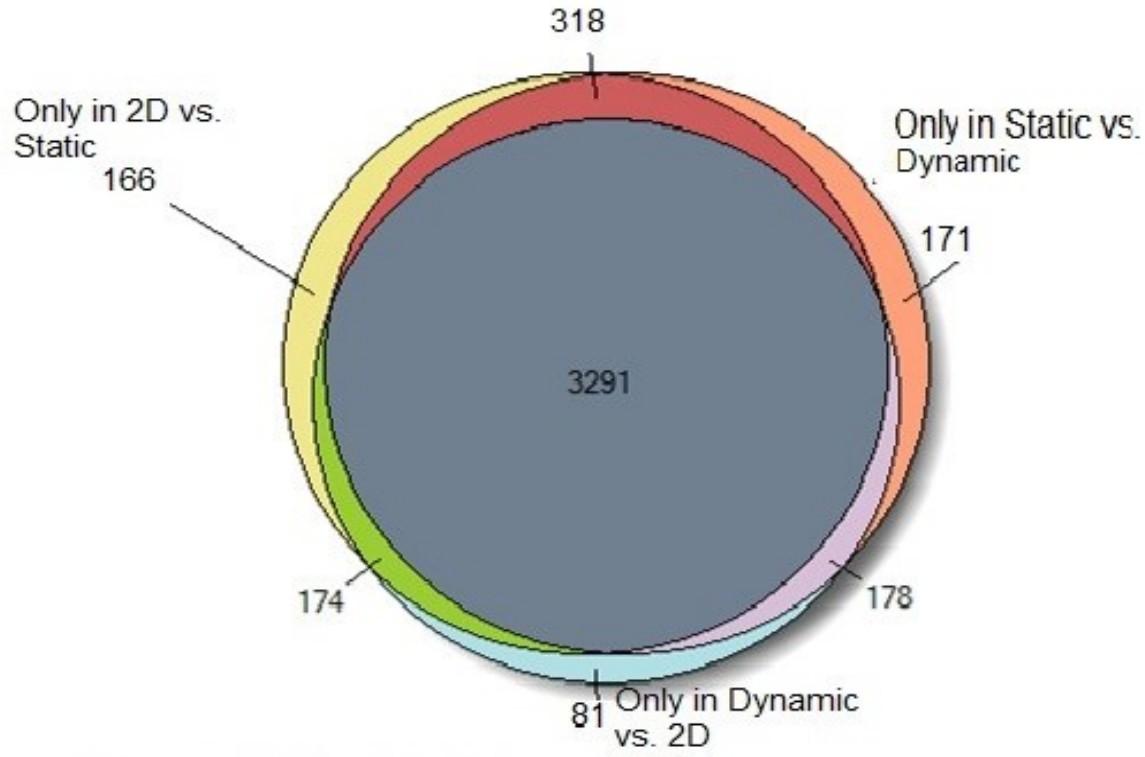

	Exclusive	Total	Description
	166	3949	2D vs. Static
	171	3958	3Ds vs. Dynamic
	81	3724	Dynamic vs.2D
	318	3609	2D vs. Static/ Static vs. Dvnamic
	178	3469	Static vs. Dvnamic/ Dynamic vs. 2D
	174	3465	2D vs. Static/ Dynamic vs. 2D
	3291	3291	Proteins present in all three groups
Sum	4379		

Figure 30 Venn Diagram of Number of Proteins Identified on Each Group

Proteins share between the three mass spectrometry files out of 4379 proteins, only 3291 proteins present in all groups 2D (heavy SILAC) vs. static (Light SILAC) or dynamic (heavy SILAC) vs. 2D (light SILAC).

ES cells cultured under 3D and 2D conditions display different biological characteristics. However, a global differential analysis between encapsulated mESCs and monolayer cultured cells at the protein level combined SILAC and MS has not yet been performed to our

knowledge. A total of 4379 high-confidence non-redundant proteins were identified using QExcutive mass spectrometry. Out of these proteins, only 3219 hits were identified on the three MS files (Fig. 30). We analysed the L/H ratio for all proteins, and 1968 proteins were quantified and shared between comparison groups. In order to consider a protein to be differentially expressed, we applied the conditions that at least three high-confidence (≥95%) unique peptides were identified, and that the peptides exhibited a fold change ≥2. Testing for multiple comparisons from the quantitative information eventually led to 527 differentially expressed proteins. Among them, compared with 2D models, a total of 120 proteins were up-regulated in 3D dynamic culture and 182 were down-regulated in 3D static models

Self-renewal proteins were identified, indicating sensitivity of our sub-fraction to detect low abundance transcriptional factors. Twenty proteins associated with self-renewal were identified with no significant difference between the three groups (Appendix Table. 7). For example, *Pou5f1 (Oct4), Sox2, CD9 and Dppa5a*, proteins known for their roles in self-renewal signalling networks were expressed at comparable levels on 2D/3D statics, 2D/3D dynamics and 3D statics/3D dynamics cultures. We analysed the list of all observed proteins through Gene Ontology enrichment analysis using DAVID website to enable interpretation of the enriched functional categories as indicative of cellular status (Fig. 31 and Fig. 32).

Over 233 genes relating to glycolysis and transmembrane proteins were significantly enriched. We also found mitochondrial proteins categories significantly enriched. Expression of extracellular matrix (ECM) proteins and cell surface membrane proteins increased in both 3D cultures vs 2D culture (Appendix Table. 20). Consistent with this, 41 vacuole proteins were also increased in both 3D cultures which have a role in protein secretion. Furthermore, mitochondrial proteins were elevated in both 3D cultures, suggesting a need to cope with possible higher energy demands in encapsulated cells to secret ECM. Dynamic culture showed a decrease in 45 out of 126 ER proteins identified and 66 out of 830 nucleus proteins.

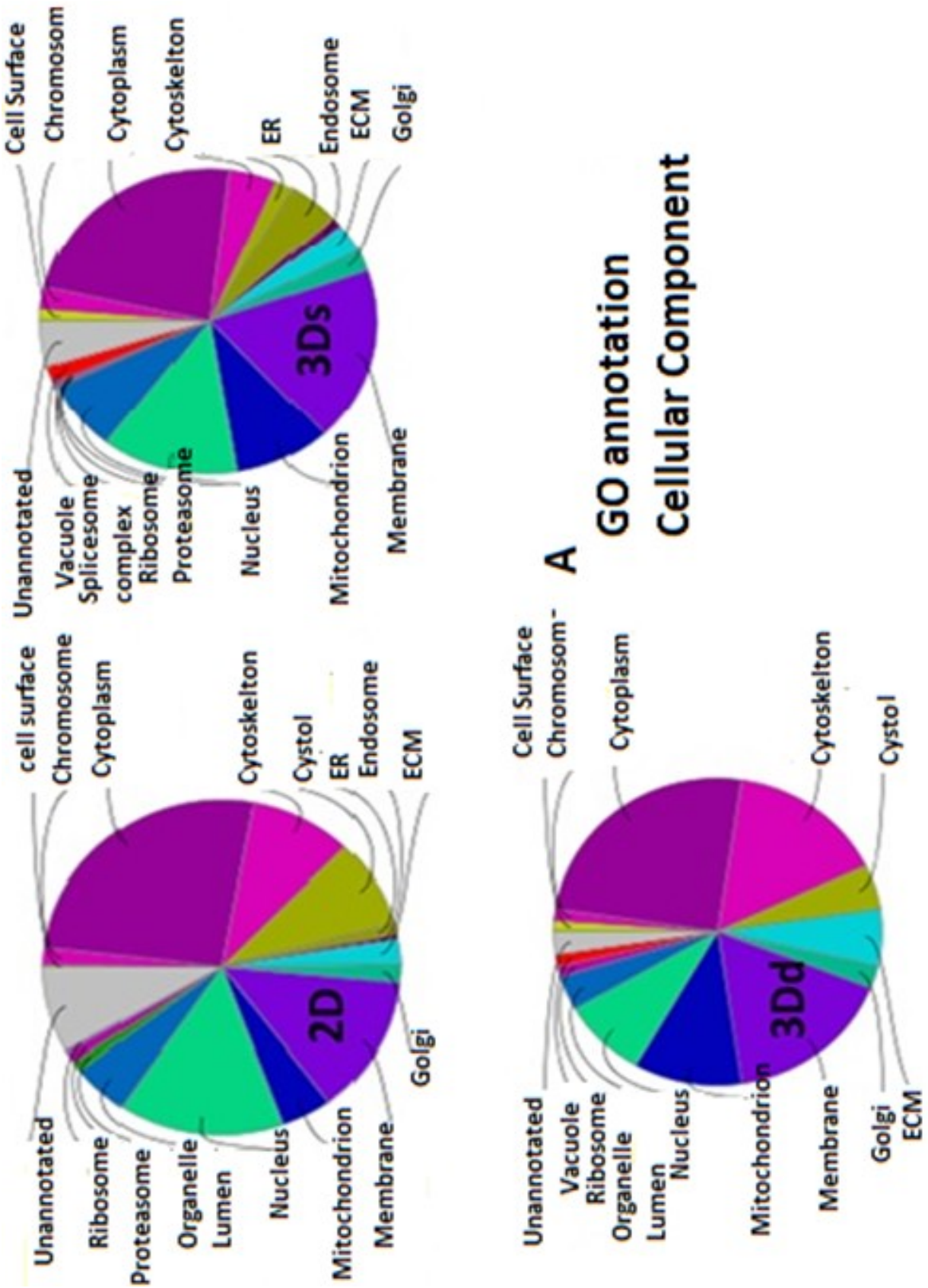

Figure 31 GO Annotation of Cellular Components

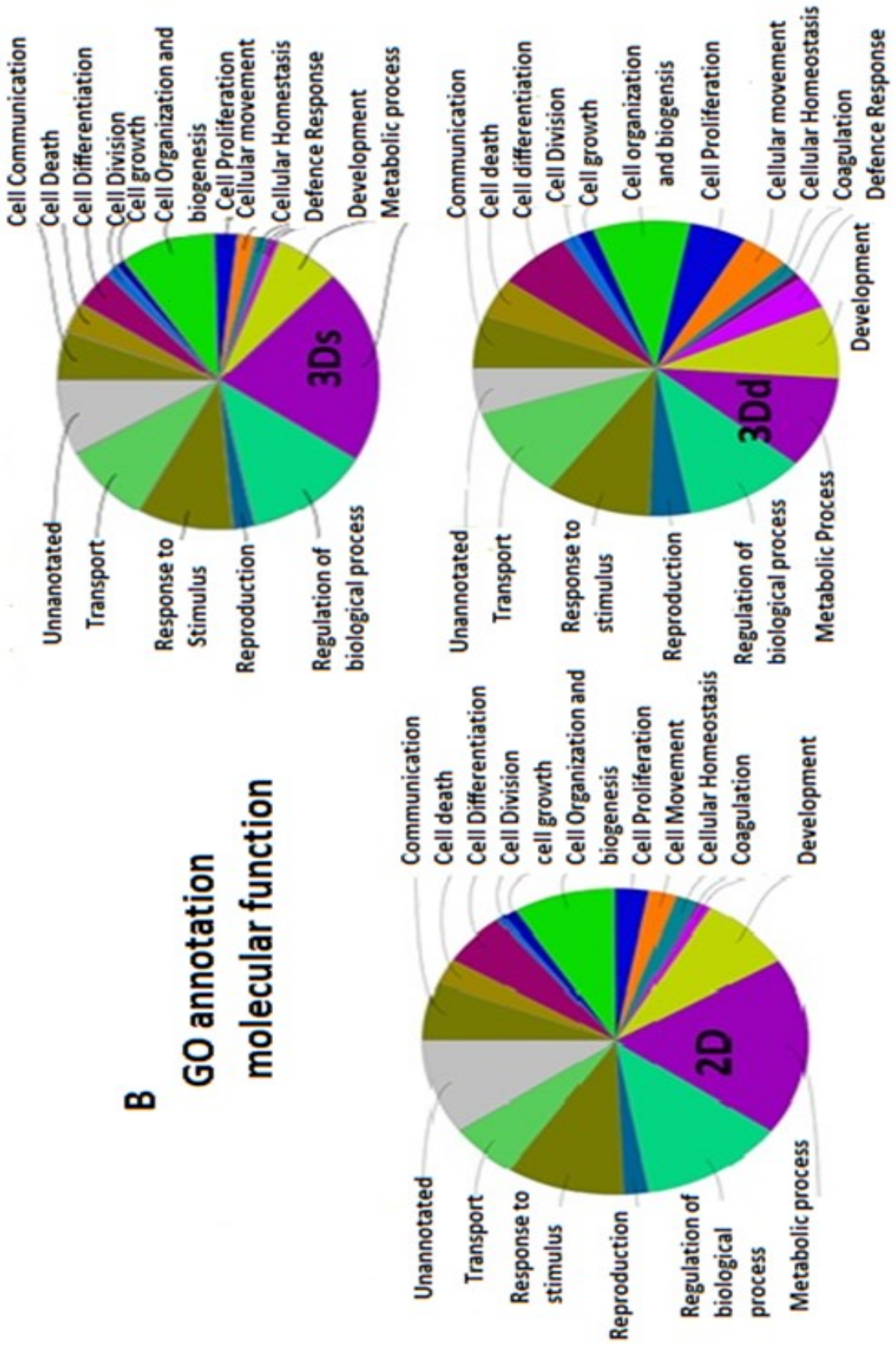

Figure 32 GO Annotation of Molecular Function

In accordance, molecular function (Fig. 32) annotation showed a rise in cell proliferation proteins (2%) in 3D dynamic culture. Proteins related to defence mechanisms (2%) showed an elevation in 3D dynamic compared to other cultures suggesting an increase in cellular stress response. Furthermore, proteins that participate in cellular motion increased in dynamic cultures suggesting a cellular response to HARV bioreactor. On the next results section we will discuss significant proteins changes on each groups based on their molecular function.

5.3.2. Proteins differentially expressed in 2D vs. 3D static culture

From 1968 proteins identified, less than 1% of proteins were up-regulated in 2D culture labelled with heavy SILAC compared to 13% of proteins that showed changes in 3D static cultures labelled with light isotopes. Of these proteins changed in 2D culture ~ 40% was responsible for self-renewal while the rest were involved in metabolism. For instance, a *Lin28a* was down-regulated in 3D statics compared with 2D culture. This suggests a decrease in pluripotency in static culture. Although *Lin28a* is not a transcriptional factor, it is involved in efficient re-programming of somatic cells to stem cells due to its role in "maternal-embryonic transition" and nucleolus maturation (Vogt et al., 2012).

In contrast, in static culture, 3% of the up-regulated proteins was apoptosis related (Table. 8). However, ~5% of these proteins were involved in differentiation, which is consistent with Lin28a down-regulation. Additionally, in 3D static culture 7% of the proteins were up-regulated and associated with the cytoskeleton and cell morphology (Appendix Table. 9). This may account for the differences in morphology seen in cell growing in 3D static cultures.

5.3.3. Proteins differentially expressed in 3D dynamic culture vs. 2D or 3D static culture

In cells maintained in 3D dynamic culture vs 2D cultures, 11% proteins were up-regulated and 3% proteins were down-regulated. Translation (31% of proteins), metabolism (25%), cytoskeleton (15%), and cell-survival (7%) were the major functional sub-categories with up-regulated proteins, whereas, down-regulated proteins belonged to glycolysis (30%) and apoptosis (13%). For example, in 3D dynamic culture, the expression of *Aldow, Eno1, Pkm,* was down regulated vs 2D, and 6-phosphfructokinase l (*Pfkl*), lactate dehydrogenase A (*Ldha*), phosphoglycerate kinase1 (*Pgk1*) and triosephosphate isomerarise (*Tpi*) expression was down-regulated in comparison with both 2D and 3D static cultures (Appendix Table. 10 appendix). However, proteins associated with electron transfer chain (ETC) complex III, IV and V were up-regulated on 3D dynamic culture along with multiple mitochondrial respiration associated proteins, such as complex II (*Ndufc2, Ndufb4*), complex III (*Cyb5b, Uqcrh, Uqcrq, Uqcrfs1*), complex VI (*Cox4i, Cox7c*), and complex V (*Atp5j2, Atp5l, Atp5i*) respectively (Appendix Table. 11). These observations indicate a decrease in glycolytic flux (Fig. 50 appendix) in 3D dynamic cultures and a simultaneous increase in mitochondrial respiration (Fig. 51 appendix) likely due to the dynamic bioreactor improving oxygen delivery and nutrition availability to the cells.

Apparently, up-regulation of mitochondrial proteins suggested non-glucose carbon source feed to ETC. In 3D dynamic culture compared with 2D 3 of 4 known glycine cleavage enzymes were up-regulated. These involved glycine dehydrogenases (decarboxylation) (*Gldc*), dihydrolipoyl dehydrogenase (*Dld*) and glycine cleavage system H (*Gcsh*) (Appendix Table. 12). This system breaks down glycine to a final product that either enters purine biosynthesis or produce acetyl CoA that feeds the TCA cycle. In addition, glutamate dehydrogenase (*Glud1*), glutamate mitochondrial carrier protein (*Slc25a13*), and Idh3β enzyme were also up-regulated on 3D dynamic culture compared with 2D condition. These observations suggest a reduced external glucose uptake and the cells might rely on another carbon source such as

amino acids (glutamine and glycine). This is due to increase energy demand beyond glycolysis that leads to down-regulation of glycolytic flux in order to balance ATP synthesis via oxidative phosphorylation.

Altered mitochondrial metabolism is intimately connected to stem cells' fate. Metabolic status and oxygen tension determine whether cells differentiate, proliferate or activate pro-death signalling. Thus, we analysed expression of differentiation related proteins to address how metabolic change in dynamic culture affects self-renewal of mESCs. *Crabp1* (protein epithelial inducer) *Hectd1* (required for mesenchyme and neural crest development), and *Nedd4* (responsible for neural development) were down-regulated in 3D dynamic culture compared to either 2D or 3D static culture. This protein enhances cell response to retinoic acid signalling and therefore cause mESCs differentiation (Uhrig et al., 2008). Moreover, *Dpsyl2, Hectd1, Pafah1b3* and *Gmpr2*, a set of proteins involved in mESCs differentiation toward the neuroectoderm were down-regulated in 3D dynamic culture (summarised on Table. 13 appendix). These observations indicated blocking of the neuroectoderm differentiation in 3D dynamic culture that spontaneously induced in mESCs LIF/serum maintenance condition. Thus, change on metabolic proteins had adverse effect on self-renewal by down-regulating the expression of differentiation associated proteins.

5.3.4. Proteins differentially expressed in 3D static vs. 3D dynamic culture

Overall, 5% of proteins were down-regulated in dynamic culture. The down-regulated proteins involved 27% related to protein synthesis (Table. 14 appendix), 12% related to cell cycle (Table. 15 appendix), 12% related to DNA damage (Table. 18 appendix), 12% related to epigenetic modification (Table. 16 appendix), and 7% of proteins were up-regulated in static vs. dynamic condition responsible for cell differentiation to primordial germ cell (Table. 17

appendix). The expression of majority DNA damage proteins was altered in static condition. For instance, DNA damage sensors *ATR* and *ATM* and the *Cdk2ap1* protein were u-regulated in 3D static vs 3D dynamic culture. The downstream target proteins of ATR/ATM such as *Tp53bp1, Rad50,* cell cycle kinases (*Cdk4, Cdk7, Cdk2ap1*) and Cyclin-A2, that mediate cell cycle inhibition (Nagaria et al., 2013) were up-regulated in 3D static culture. Consequently, the transducer proteins *Msh3*, *ATRX*, *Top2b*, *Asfia* and *Kntc1* were also u-regulated (summarised on Table. 18 appendix), suggesting an increase in DNA-repair mechanism in 3D static condition. These proteins also aid chromatin segregation, DNA repair and re-joining. Furthermore, they act as a checkpoint before cells proceed to mitosis (Koledova et al., 2010). The down-regulation of DNA damage related proteins on 3D dynamic vs static condition may be attributed to the presence of alginate scaffold in the latter sitting but in a poor diffusion environment. Cells at the centre position of 3D static scaffolds tend to prolong mitosis from 24 to 48 hours that will result in DNA damage due to nutrient and oxygen depletion (Laurent et al., 2013).

5.3.5. Proteins differentially expressed in both 3D static and 3D dynamic versus 2D culture

Notably, 91 proteins were up-regulated in both 3D cultures vs 2D (Table. 19 appendix), of which 12 were components of ECM (Table. 20 appendix , Fig. 34); such as Fibronectin 1 (*Fn1*; up-regulated 23-fold in 3D dynamic and 100-fold in 3D static culture), Laminin subunit alpha-5 (*LAMA5*, 100-fold up-regulated in 3D dynamic and 29-fold in static cultures vs 2D), Collagen type XVIII (*Col18a1*; up-regulated in encapsulated cells 10-fold in static and 27-fold in dynamic versus 2D culture), Agrin (*Agr* up-regulated 25- and 53 fold in 3D static and dynamic respectively vs 2D culture), Entactin or Nidogen *Nid-2* (BM glycoprotein family member, contains three global domains, up-regulated in both 3D cultures), and, Hepran sulphate

proteoglycan (*Hspg2*; 11-fold and 16-fold changes in 3D static and dynamic cell cultures). This increase in ECM components in both 3D cultures may help anchoring and adhering cells to secreted ECM proteins, replacing inherited poorly adhesive alginate nature. The different classes of up-regulated ECM proteins in 3D cultures play different roles e.g. trimers a mixture of lamnin and collagen strengthen the cells, whilst cell-binding domains like fibronectin helps cell anchoring and negatively charged GAGs (*Hspg2*, *Agrin*, and *Nid2*) provide a hydrated structure. Thus, the presence of these proteins may provide further protection for the cells in alginate from external hydrodynamic stress.

Other proteins up-regulated in both 3D cultures compared with their counterparts in 2D culture were linked to cell cycle arrest (Table. 21 appendix), as for instance, Gtse1 (53 fold), Cdc23 (6 fold) and Ckap2 (3.5 fold) proteins involved in G2/M cell cycle arrest. These proteins play crucial roles in chromosome segregation ensuring the copying of high fidelity DNA from parent to newly synthesized cells. However, high expression of these proteins may contribute to G2/M phase delay. Human ESCs grown in 3D possess longer G2/M phase compared with 2D culture (Azarin et al., 2012a).

Slc25a20 Carrier protein was also up-regulated in both 3D cultures compared with 2D culture. This protein facilitates translocation of acylcarnitine through the mitochondrial inner membrane to be later transfer to acyl-CoA thioesters to undergo beta oxidation in the mitochondrial matrix. Consistent with that, fatty acid oxidation (FAO) proteins *Acad9* and *Acaa2* were up regulated in both 3D static and dynamic culture compared with 2D. However, both *Etfα* and *Etfβ* enzymes showed no difference between three different cultures condition suggesting that basal expression of these 2 proteins is sufficient to cope with the extra FADH2 generated by up-regulation of Acad9 (Fig. 33). Activation of FAO in both 3D cultures can be also associated with higher energy demands as FAO yields twice the ATP as glycolysis (Carracedo et al., 2013).

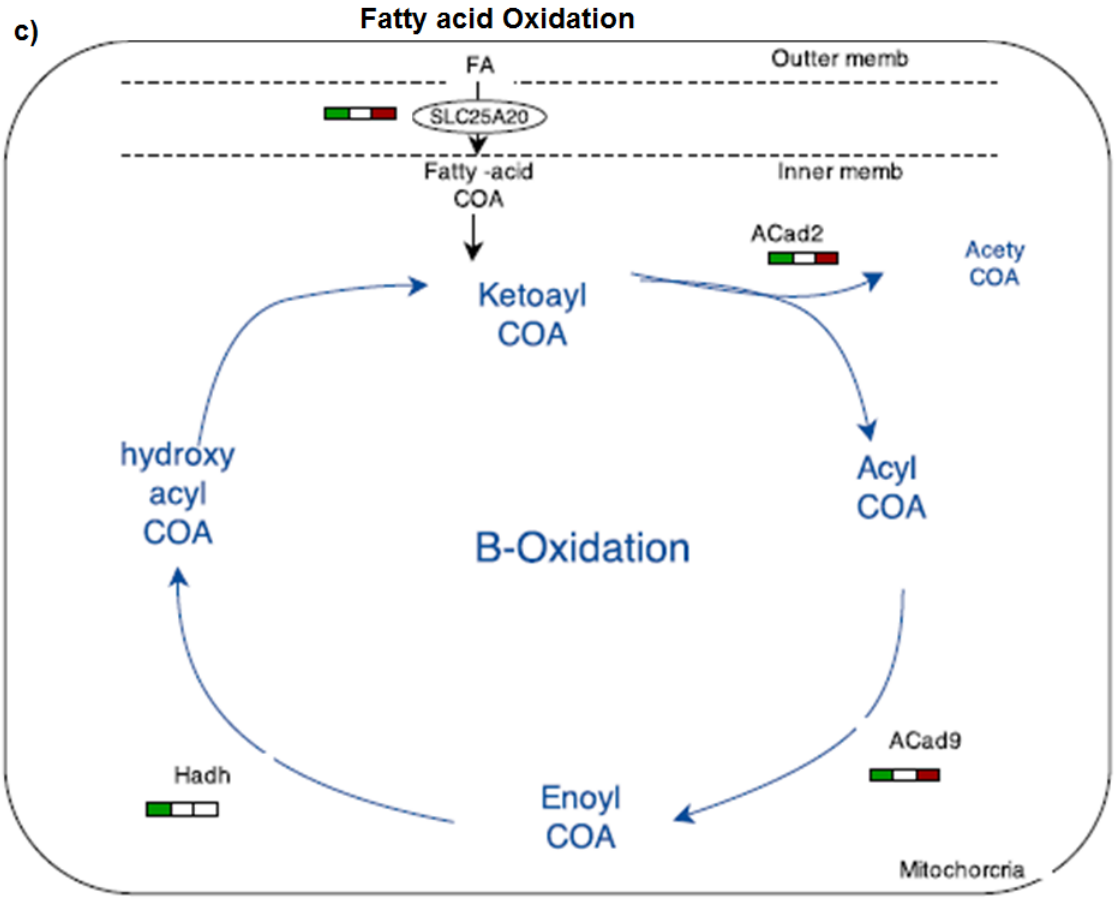

Figure 33 Schematic Up-regulation of Fatty Oxidation in Both 3D Cultures versus 2D Culture

a) Up-regulation of Slc25A20 carrier protein facilitates translocation of acylcarnitine through the mitochondrial inner membrane. Red square indicate up > 2.00-fold, the green for down < 0.5, and white no change 0.5 <Ratio> 2.00 for 2D/3D static, 3D static/3D dynamic, and 3D dynamic/2D SILAC ratio.

5.3.5.1. Validation of ECM results using qPCR

To validate proteomic changes in ECM components, relative mRNA expression levels of *Fn1* and *Hspg2* was measured. Both genes showed significant differences in expression in 2D *vs*. 3D cultures and 3D static *vs*. dynamic culture. For instance, *Hspg2* expression increased 2-fold in 3D dynamic compared to 3D static culture (Fig. 34) confirming SILAC data. Both *Fn1* and *Hspg2* are mechano-sensors. Thus, the fluid motion of dynamic bioreactor may enhance their expression compared to static condition and mediate the production of extracellular matrix to provide physical and chemical barriers for cell protection.

The poor alginate adhesion environment may be responsible for increases in the above combination of ECM proteins in both 3D dynamic and static cultures despite the presence of 1.1% gelatin (attachment enhancer) in our alginate mixture. Conversely, the presence of similar concentration of 1.1% gelatin use to coat 2D culture plates did not result in ECM secretion. It may be either the mechanical properties of the beads surfaces, the change in cell morphology or the cell-cell contacts that are responsible for differences in ECM production between 2D and 3D cultures.

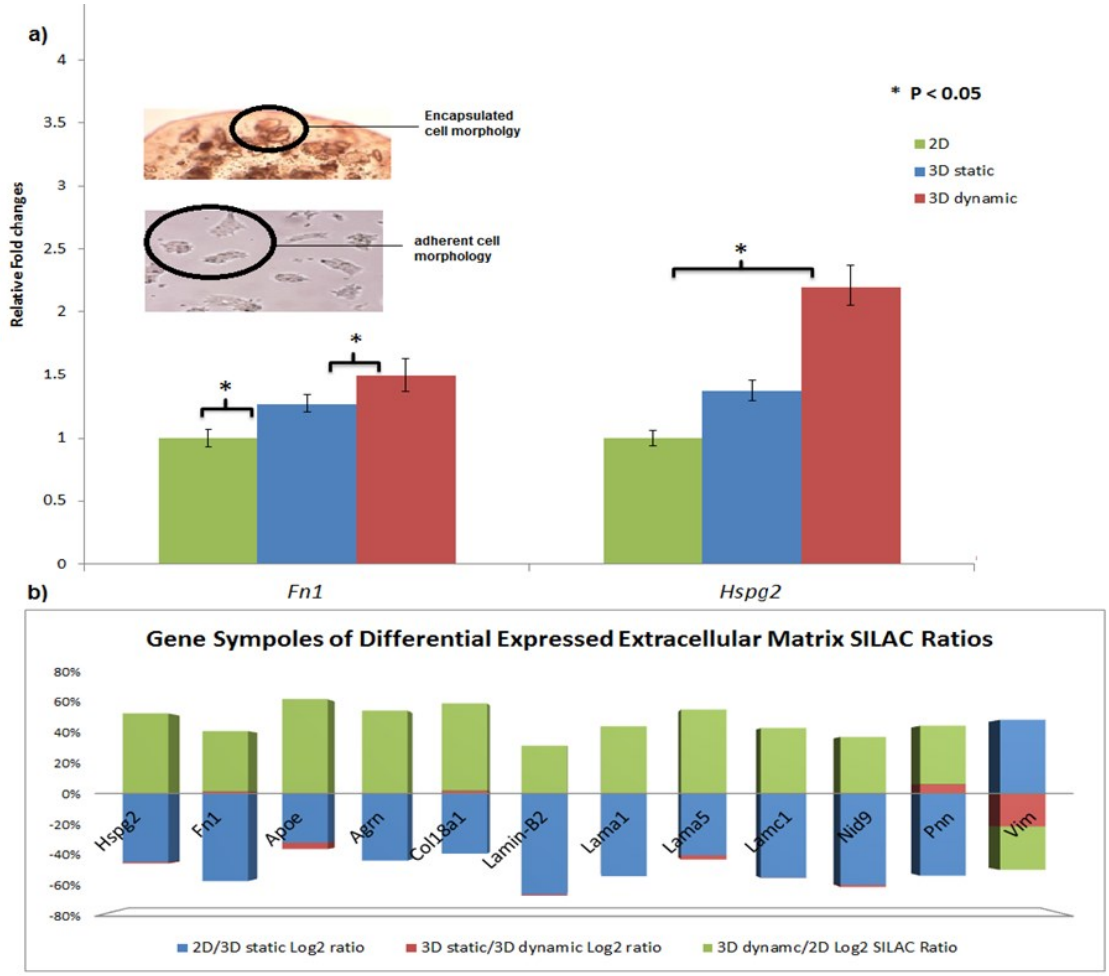

Figure 34 Up-regulation Of Extracellular Matrix Proteins

a) *Panel* a shows relative gene expression of fibronectin (Fn1) and heparan sulphate proteoglycan 2(Hspg2) of 3D static and 3D dynamic cultures normalised against 2D culture and β-actin. Values are means ± SD, N=3 (*: $p<0.05$).

b) Panel b shows Log2 ratio of ECM identified by MS showed no difference in expression between 3D static/dynamic ratio (red) compared with other two groups were significant difference toward 2D cultures compared to any 3D groups. For gene symbol full names please refer to Table 20 (appendix).

5.3.6. Change in mitochondrial proteins

From the SILAC results, it was shown that both 3D static and dynamic culture had up regulated March5 when compared to 2D culture. March5 is involved in controlling mitochondrial morphology. Similarly, Letm1, required for maintenance of mitochondrial tubular networks, crista organization and assembly of ETC, was up regulated in both 3D cultures versus 2D condition. 3D cultures also up-regulated VDAC (VDAC1, VDAC2 and VDAC3) proteins compared to 2D culture, which act as channels that transfer metabolites from the cytoplasm to the mitochondrial matrix and vice versa. In addition, other membrane carrier proteins such as OGC (malate/αKG) and AGC1 (Glutamate/ Aspartate) were also up-regulated on 3D condition (Fig. 35). These results demonstrate changes in the permeability of the mitochondrial membrane, possibly suggesting a change in mitochondrial structure. The nuclear/mitochondrial contact, cytosol/mitochondrial transport, and mitochondrial permeability were found to affect mitochondrial biogenesis (Folmes et al., 2012c). This change in mitochondrial structure in 3D culture may contribute in the change in metabolic status.

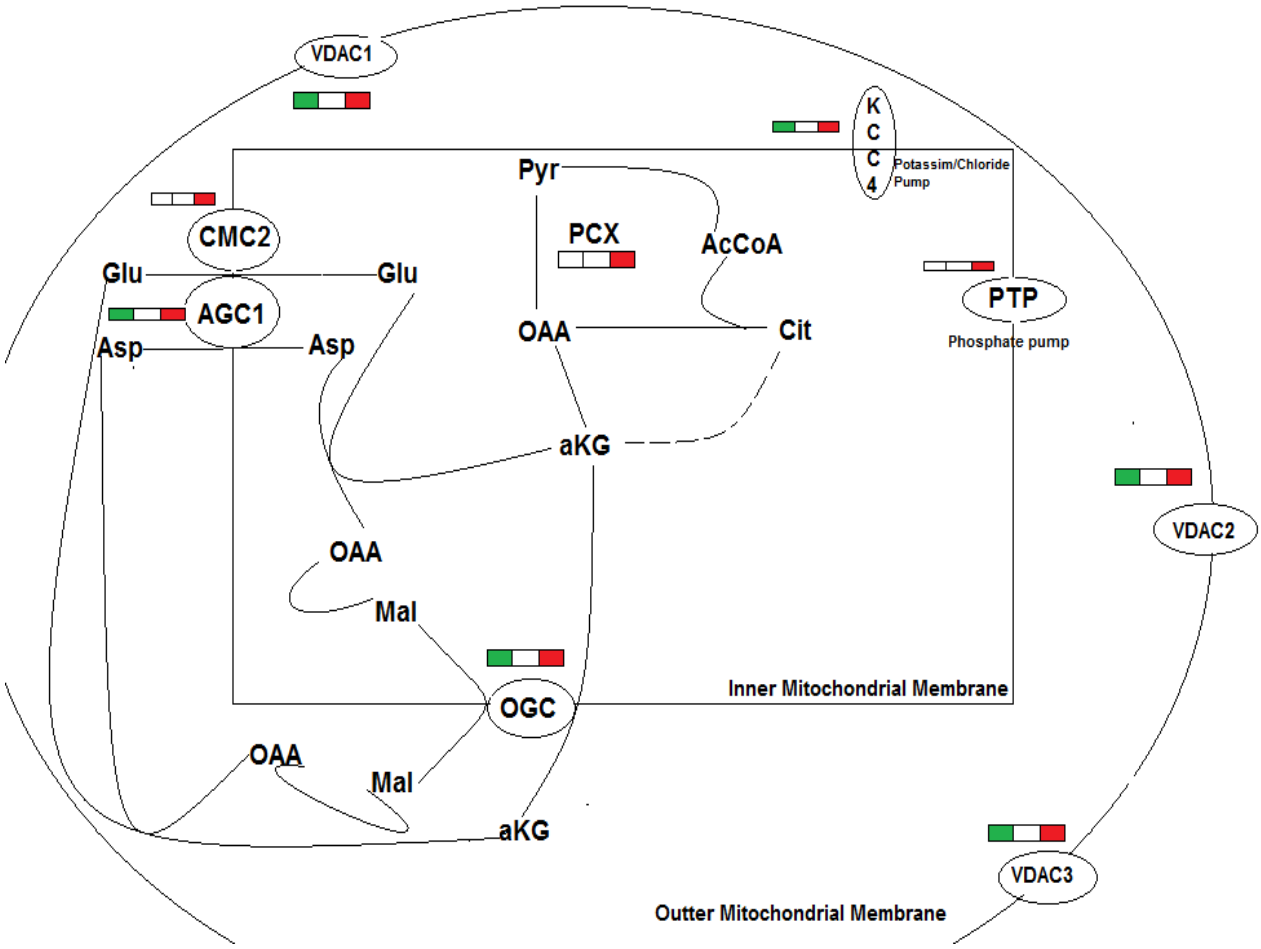

Figure 35 Up-regulation of Mitochondrial Carrie Protein

There were significant increase in voltage dependent anion channel (VDAC1, 2, and 3) locate in outer mitochondrial membrane. The rectangle resemble from left to right first square 2D/3D static SILAC ratio, the middle one (white) is 3D static/ 3D dynamic, and the last is 3D dynamic/ 2D culture. The red colour indicate up-regulation and green down-regulation. aKG; ketoglutarate, Glu; glutamate, Cit; citrate, OAA; oxaloacetate, Mal; malate, Asp; aspartate, Pyr; pyruvate, PCX; pyruvate carboxylase, AcCoA; acetyl-CoA.

5.4. Discussion

We used SILAC-based proteomics as an approach to understand differential protein expression in 2D culture, 3D static, and 3D dynamic cultures. Analysing the results by gene ontology illustrated that membrane and extracellular proteins (ECM) comprised 3% of the expression changes; whereas, 30% of proteins altered were related to metabolism. This is consistent with other comparative proteome analyses of monolayer with 3D culture that showed altered metabolic pathways (Bhattacharya et al., 2004, Pruksakorn et al., 2010, Gaedtke et al., 2007). For instance, glycolysis and stress related proteins were up-regulated in spheroids *vs.* flat cells (Bhattacharya et al., 2004).

Up-regulation of 12 secreted ECM proteins in both types of 3D culture compared to 2D indicates that absence of adhesive in alginate beads increases their production. For instance, Lama5 showed almost 100 fold increases in 3D dynamic condition compared with monolayer gelatin coated cultures. An enriched matrix containing both Lama5 and E-cadherin has recently been used to maintain and prolong self-renewing hESCs without feeder cells in serum-free environment (Rodin et al., 2014). Interestingly, single or multiple ECM proteins successfully control stem cells fate, as for example, fibronectin and Laminin direct neural cell lineage commitment, and collagen promotes osteogenic differentiation (Hosseinkhani et al., 2008, Goetz et al., 2006). Their approach however, using single or combination of two ECM underestimates the complexity of the *in-vivo* stem cell niche, which is dynamic and constantly interacts with external and internal environments during maturation and transition. Using decellularized 3D scaffolds of mESCs encapsulated for three days was sufficient to successfully reprogramming of MEFs to express pluripotency markers (Han et al., 2013). The up-regulation of these groups of ECM on our 3D condition may contribute to sustain mESCs self-renewal on alginate beads.

In addition to ECM components, expression of proteins associated with metabolic status was significantly enriched in 3D cultures vs 2D culture. The down-regulation of glycolytic enzymes in a 3D rotary wall dynamic bioreactor may link to decreased external glucose uptake or reliance on a different carbon source. Thus, there were up-regulation of FAO and amino-acid metabolism related proteins. The 3D dynamic cultures showed possible shift to amino-acid consumption such as glutamate and glycine. Recent findings demonstrate that highly proliferated cells are not necessarily relied on glucose conversion to lactate, alternatively, artificial expression of GLDC (which was up-regulated as well in our 3D dynamic culture) was sufficient to trigger self-renewal genes (Locasale, 2013). Thus, reliance on amino acids in 3D dynamic culture may contribute to self-renewal enhancement. However, comprehensive inhibition of glycolysis in mESCs can lead to differentiation (Pereira et al., 2013) while blocking of the respiratory chain reinforces pluripotent stem cells' ability to commit to any cell lineage. Therefore the mESCs mitochondrion is 'bivalent' and enables a metabolic switch based on cellular energy demand, whereas preferential use of glucose as the sole carbon source is essential for hESCs and adult stem cells' self-renewal but not mESCs,(Zhang et al., 2011). Murine ESCs found to be threonine reliant where threonine withdrawal induces cell death (Wang et al., 2009d). Interestingly, glycine cleavage system enzymes up-regulated in 3D dynamic is also a substrate of threonine metabolic pathway. Therefore, switch in metabolism toward amino-acid instead of glucose could help mESCs pluripotency.

There were also up-regulation of FAO enzymes in 3D both static and dynamic cultures. Silencing of FAO enzymes in mESCs results in ATP exhaustion and loss of resistance to nutrient depletion identifying the role of lipid as a primary energy source in stem cells (Zhang et al., 2012). In addition, FAO inhibition in HSCs induces differentiation (Ito et al., 2012). Our proteomics data suggests a tight regulation of FAO and anaerobic glycolysis to sustain self-renewal on 3D dynamic environment. However, the exact mechanism of how glycolysis-FAO

metabolic switch has not been elucidated (Ito et al., 2012). The switch toward fatty acid or amino-acids as sources of nutrients on 3D dynamic cultures sustains mESCs self-renewal. More precisely, the improvement of various nutrient delivery to cells on the 3D dynamic culture reduce the demands on glucose alone. Thus, TCA cycle and ETC proteins may be up-regulated by nonglucose carbon flux such as glutamate, glycine or FAO metabolism.

Finally, both 3D cultures showed 50 fold up-regulation of Gtse1. This protein is involved in p53 signalling that mediate M phase cell cycle-arrest. This is consistent with a number of 3D culture studies that demonstrated lengthening of the M phase or activating cycle-arrest when transferring cells from 2D to 3D culture. Likewise, hESCs grown in static 3D constructs show a relatively longer G1 phase compared to the 2D cultures (Azarin et al., 2012, Calder et al., 2013). This suggests the possibility of cytoskeleton disorganisation in 3D cultures owing to absence of spindle assemble and centromere positioning especially early on the culture. These factors are essential for chromosome segregation and their absence contribute to cell cycle delay at G2/M phase resulting in transit mitosis-arrest in mESCs (Wang et al., 2011). Embryonic development in simulated zero gravity (which is comparable to our HARV sitting) showed a disorganised cytoskeleton owing to gravity-dependent cytoskeleton anchor to assemble microtubule and localize centromere (Wakayama et al., 2009, Crawford-Young, 2006, Wang et al., 2011). In addition, the presence of free-fall environment may affect microtubule spindle assembly during M phase given to gravity dependence of anchorage and cytoskeleton assembly (Wang et al., 2011).

In conclusion, quantitative global proteomics comparison of monolayer vs alginate encapsulated mESCs using SILAC labelling demonstrated that the cells in 3D culture interact with environment by up-regulating cell cycle arrest and switching the metabolism to alternate ATP sources such as amino acids and fatty acids and express ECM proteins. However, these

changes have no consequence on self-renewal as proteins associated with pluripotency showed no difference on their SILAC ratios.

In conclusion, the results described in this chapter showed the capability of SILAC based proteomics to measure alterations in protein expression for thousands proteins primarily involved ECM and membrane related proteins. This confirms, the advantage of SILAC-based proteomics used in this study over conventional 2-DE gel approach. Usage of SILAC showed no effect on self-renewal phenotypes. In addition, protocol were developed and optimised for protein extractions show efficiency and reproducibility among comparison groups given to similarities of over 3290 proteins in different mass spectrometry files. The next chapter will discuss the functional validation of metabolic profiles change in response to switch from monolayer culture to 3D construct both dynamic and static.

CHAPTER 6: Effect of 3D Culture on mESCs Metabolic Profiles at Prolonged Adaption

6. Introduction

Metabolic status and oxygen tension determine cell-fate decisions such as differentiation, proliferation and apoptosis. The *in vitro* culture environment commonly uses a 16% oxygen atmosphere that subjects cells to high oxygen tension. This is in sharp contrast to *in vivo* conditions where the oxygen tension can be as low as 2% in stem cell niches such as the bone marrow (BM) (Folmes et al., 2012a, Mohyeldin et al., 2010). Oxygen measurements in the embryo have shown that development occurs under conditions of low oxygen (3-5%), leading to a reconsideration of the importance of oxygen for embryonic stem cells (ESCs) *in vitro.*

Low oxygen availability recognises by oxygen sensors known as hypoxia inducible factors (HIFs). The oxygen-regulator family consists of HIF-1α, HIF-2α and HIF-3α (Mathieu et al., 2014). HIF1α regulates cell signalling under low oxygen tension and plays a significant role in anaerobic glycolysis control. HIF transcriptionally activates pyruvate dehydrogenase 1 (PDK1), and inactivates PDH, thus preventing pyruvate fuelling to TCA cycle, and hence reduces mitochondrial oxygen consumption. Furthermore, HIF mediates pyruvate to lactate conversion (Lu et al., 2014). The HIF-2α heterodimer has been found to translocate from cytoplasm to nucleus under extended hypoxic exposure leading to activation of Oct4, Sox2, and Nanog thus enhancing self-renewal (Forristal et al., 2013). Similarly, HIF-2α binds the Oct4 promoter in mESCs under hypoxic conditions leading to its activation (Covello et al., 2006).

Stimulation of glycolysis in pluripotent stem cells, through hypoxia promotes stemness while inhibition of glycolysis halts proliferation and precipitates cell death (Folmes et al.,

2012a). Although anaerobic glycolysis only yields 2 ATP/mole of glucose compared with oxidative phosphorylation that produces 36-38 molecules of ATP, the high proliferation rate of stem cells is glycolysis-dependent as it yields a faster rate of ATP production. Thus, hypoxic conditions enable stem cells to reproduce 100-fold faster than in high oxygen environments. Therefore, there is a strong correlation between anaerobic metabolism and self-renewal (Fig. 36A). Conversely, up-regulation of TCA cycle proteins, down-regulation of glycolytic enzymes and increases in mitochondrial DNA (mtDNA) are associated with ES cells differentiation (Fig. 36 B) (Shyh-Chang et al., 2013). Murine ESCs show no difference in self-renewal under hypoxic (5% O_2) or normoxic conditions (20% O_2), but there was significant clonogenic improvement in 5% O_2 hypoxic conditions (Fernandes et al., 2010). On the other hand, higher oxygen 38% or lower as 0.9% has been shown to lead to stem cell differentiation (Powers et al., 2008). In addition, the transition of naïve mESCs (LIF/STAT3 dependent) to prime-like EpiSCs was primarily mediated by low oxygen exposure suggesting the role of hypoxia in LIF/STAT3 inhibition (Takehara et al., 2012).

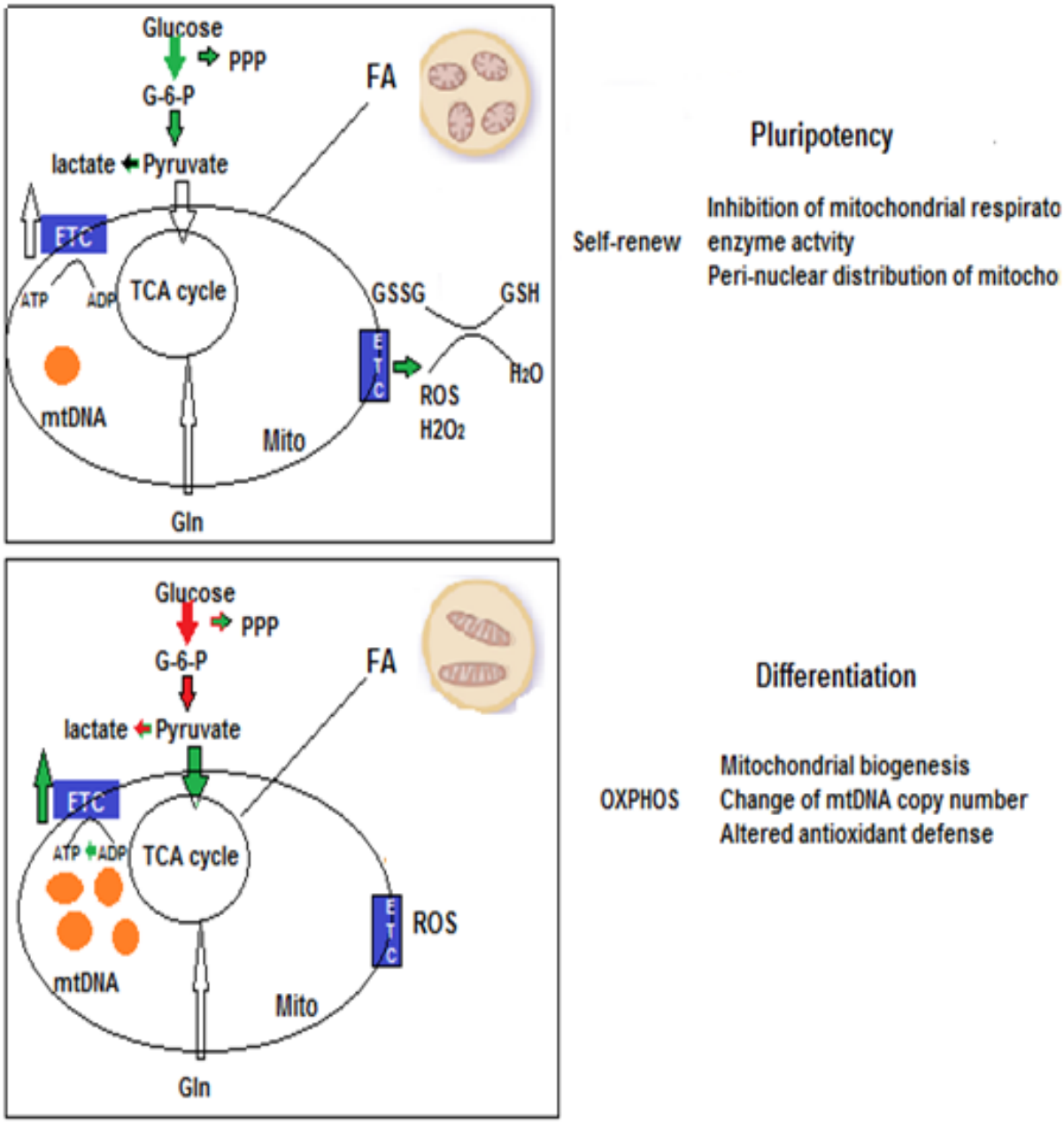

Figure 36 Metabolic Switch from Glycolysis to Oxidative Phosphorylation during ESC Differentiation

The above schematic illustrates the importance of metabolic balance in determining murine stem cell fate. Pluripotency is associated with a high glucose flux to lactate, and low mitochondrial DNA (mtDNA). Switch to differentiation is associated with increase in pyruvate oxidation, mitochondrial respiration and higher mtDNA.

However, cell proliferation is not only ATP dependent; also requiring fatty acids, amino acids, and nucleotides. Glucose metabolites from glycolysis enter a number of biosynthetic pathways. For instance, glucose-6-phosphate, fructose-6-phosphate, and glyceraldehyde-3-phosphate are shunted to the nucleotide synthesis pathway, whereas pyruvate generates nonessential amino acids via the pentose phosphate pathway (PPP) and importantly NADPH for lipid and other biosynthetic pathways. Therefore, avoiding mitochondrial respiration and elevation of glycolysis in stem cells offers sufficient precursor metabolites to support a higher proliferation rate and reduce ROS production (Kamarajugadda et al., 2012).

Based on the previous chapter, the significant enriched categorise included mitochondrial proteins. Owing to tight correlation between self-renewal and metabolism, we thought to examine the metabolic cell profiles between different culture conditions during short and long adaptation. 3D dynamic culture mRNA expression demonstrated up-regulation of Oct4, Rex1, Nanog, Cdh1 (all self-renewal markers), on the other hand, proteomics profiling showed up-regulation of mitochondrial respiration in 3D dynamic compared to 3D static and 2D culture. To further understand the link between culture conditions, metabolic profile and self-renewal, we measured oxygen consumption rate (OCR), HIF1α, HIF2α, and HKII gene expression.

6.1. Overall Aim

Based on the SILAC results (chapter 5), basic metabolic profiles enzymes were different between 3D culture static, or dynamic, compared to 2D cultures. The aim of this chapter is to validate SILAC data via functional metabolic assays. In addition, to find the link between the different metabolic profiles and pluripotency gene expression (chapter 3, section 3.2.3).

6.2. Results:

6.2.1 Comparison of proteomics data with oxygen consumption and gene expression measurement

To validate the SILAC results discussed in the previous chapter that shown increase in mitochondrial and TCA cycle proteins on 3D cultures compared to 2D, we measured OCR of mESCs mitochondria at same time point. The OCR was significantly increased in both 3D compared to 2D culture. We measured oxygen consumption rates (OCR) at different time points using a XP Seahorse instrument. Three mitochondrial inhibitors: oligomycin, FCCP and rotenone were used sequentially. For 2D-cultures the cells adhered to the wells, while for the 3D cultures the cells were decapsulated and allowed to adhere for 4 hours, prior to the measurement. This procedure was followed as the beads with encapsulated cells were too large for the instrument. Cells grown in dynamic culture showed the highest OCR whereas those from static cultures were lowers (Fig. 37, iv). In comparison, 2D cells showed the lowest rate. The increase in OCR on both 3D static and dynamic culture was consistent with SILAC data that showed up-regulation of TCA and mitochondrial respiration proteins (discussed on section 5.3.3. Chapter 5).

To further investigate the differences in OCR, both oxygen sensors HIF1α and HIF2α relative gene expression was checked at same time point as the SILAC experiment (day 3). Only HIF1α gene expression was significantly higher in 2D culture compared to 3D (both static and dynamic) (Fig. 37, i). This results agreed with the increase of oxygen availability role (as suggested by OCR results) to supress HIF. To validate more, Hexokinase isoform-2 (HKII) mRNA level, the first enzyme in glycolysis pathway, was measured to investigate further if switch to anaerobic glycolysis was occurred on 3D cultures (Fig. 37, ii). The HKII is abundant

in rapidly proliferating cells given to its ability to bind newly synthesized ATP via the ATP synthase complex (Amoedo et al., 2013). HKII had no significant change between the three modes of cultures. The mRNA data of both HIF and HKII showed consistency with OCR data by suggesting an increase in mitochondrial respiration in both 3D culture.

Finally, using western blots, UCP2 protein expression was assessed. UCP2 was expressed in both 3D static and 2D culture whereas it disappeared in 3D dynamic condition at day 3 of the culture (Fig. 37, iii). These results confirmed both SILAC and OCR measurements at that time points, suggesting a higher mitochondrial respiration rate only in dynamic culture given to the role of UCP2 to shunt pyruvate away from TCA cycle. However, the UCP2 expression on static culture was varying from both high OCR, up-regulation of TCA proteins and its role on regulating anaerobic glycolysis, by uncoupling pyruvate from mitochondrial oxidation. This dispute may relate to different role of UCP2 on 3D culture compare to data obtained from monolayer condition on the literatures.

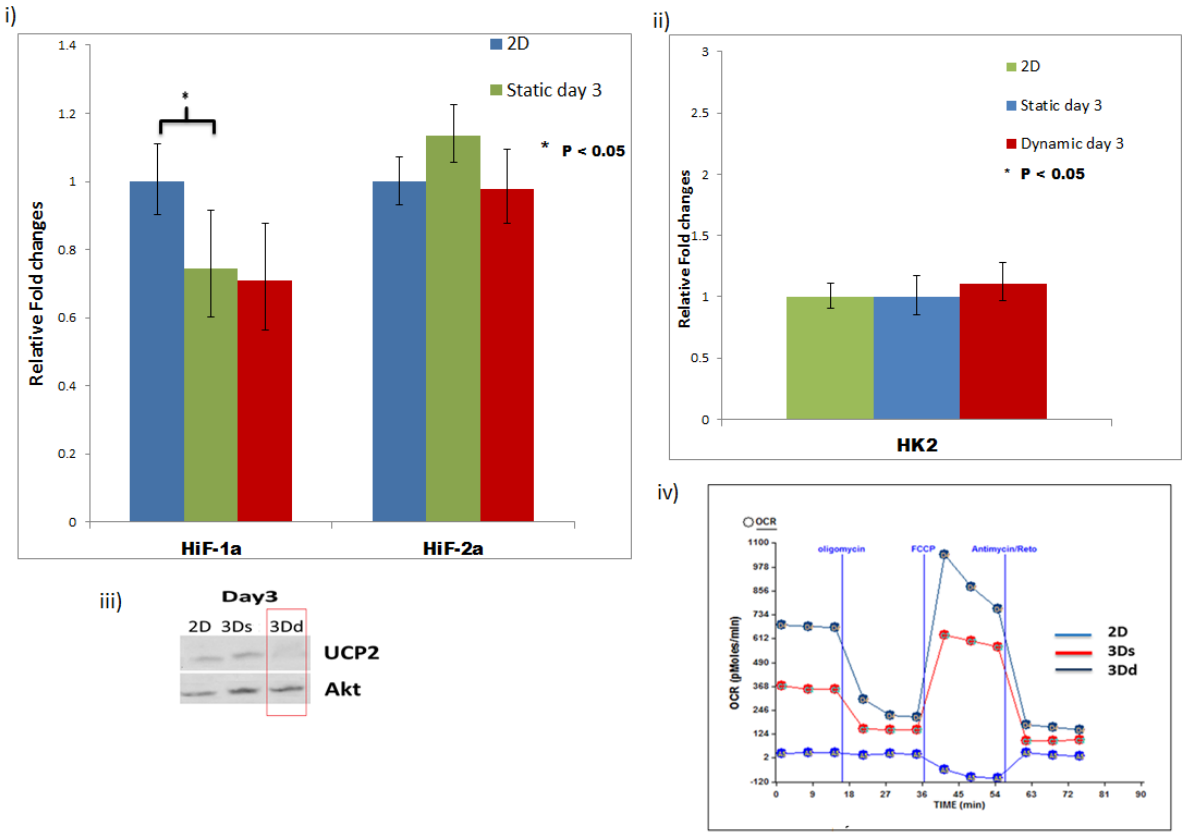

Figure 37 Correlation of UCP2 and Mitochondrial Oxygen Consumption Rate

i) Relative gene expression of HIF1α and HIF2α at day3 of both 3D static and dynamic normalised to 2D culture and β-actin expression. Only HIF1α gene expression was significantly higher in 2D culture compared to 3D (both static and dynamic); Values are means ± SD, N=3 (*: $p<0.05$).

ii) Relative gene expression of HKII.

iii) UCP2 day 3 and Akt loading control. UCP2 was expressed in both 3D static culture and 2D culture whereas it disappeared in 3D dynamic culture,

iv) Day 3 OCR measured using Seahorse XF24 analyser. Three mitochondrial inhibitors: oligomycin, FCCP and rotenone were used sequentially. Cells grown in dynamic culture showed the highest OCR whereas those from static cultures were lower. In comparison, 2D cells showed the lowest rate.

6.2.2. Prolonged adaption effect in encapsulated mESCs metabolism

After 9 days of adaptation in alginate beads, the protein expression of UCP2 was restored in both 3D dynamic and static culture (Fig. 38, iii). The role of UCP2 in anaerobic glycolysis regulation was consistent with increase of HIF2α and HIF1α expression (Fig. 38, i). HIF1α binds to a number of glycolytic enzymes and promotes their expression. Thus, HKII was highly expressed at day 9 for both 3D static and dynamic cultures (Fig. 38, i). In agreement with the increase in HIF1α, HIF2α and HKII, OCR for both 3D static and dynamic cells at day 9 were lower than 2D cells (Fig. 38, ii). This suggested switch of cells on alginate beads to hypoxic condition. Furthermore, lactate concentration was high at 8 mM as shown in chapter 3 section 3.2.2, suggesting increased flux of glucose to lactate. It has been suggested that increases in cell density are associated with decreases in oxygen diffusion and cells preferably consume glucose anaerobically (Volkmer et al., 2012). Similarly, the DNA quantification results shown in chapter 3 section 3.2.2, showed improvement on cells proliferation.

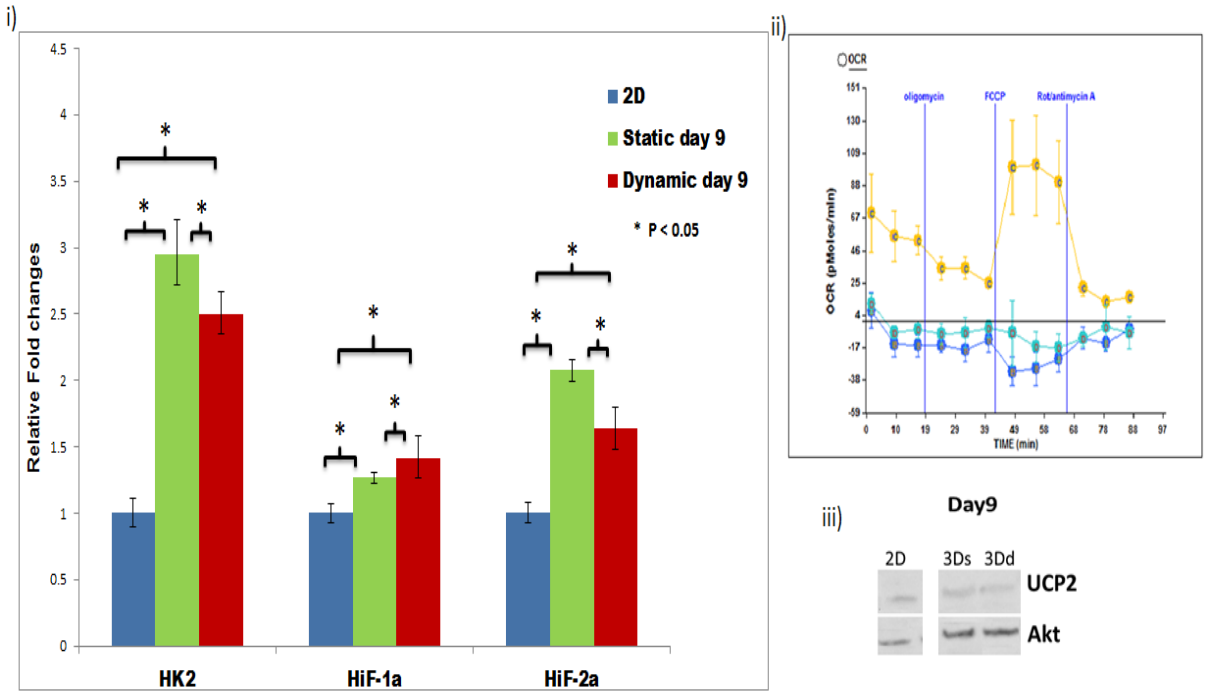

Figure 38 Glycolytic Up-regulation during Long Adaptation

i) Relative mRNA expression of HKII, HIF1α, and HIF2α at 3D culture at day 9, for 3D static and 3D dynamic culture. Results suggest a significant increase in glycolytic reliance later than day 9 of culture; Values are means ± SD, N=3 (*: $p<0.05$).

ii) Day 9 OCR showed a reduction in both 3D (light blue (static) dark blue (dynamic)) compared to 2D (yellow).

iii) Western blot of UCP2 day 9 and Akt loading control. UCP2 were expressed in both 3D static and 3D dynamic culture.

At day 18, cells in both 3D static and dynamic cultures was still retained a higher level of HIF2α and HIF1α mRNA expression (Fig. 39, i). This was consistent with the decrease in OCR (Fig. 39, ii) and continued UCP2 protein expression (Fig. 39, iii) in 3D static culture. However, this had no adverse effect on OCR which was increased in dynamic culture with no detectable UCP2 (Fig. 39, ii & iii). This suggested a metabolic switch to mitochondrial respiration in 3D dynamic culture. The detected mRNA level of HIF2α with a 2-fold increase compared with day 9 and HIF1α with not significantly changed in dynamic condition did not conflict with OCR result. As the mRNA level of HIF α subunits does not always correlate with protein amount due to post-translational modifications. The degradation of HIF1α and HIF2α in the presence of oxygen occurs via hydroxylation of proline residues by prolyl hydroxylases (Fig. 44 in next chapter) (PHDs) (Zhou et al., 2012a). Therefore, change in OCR measurement and UCP2 might suggest an increase of O_2 availability in 3D dynamic culture as TCA cycle regulation is subject to availability of oxidation factor.

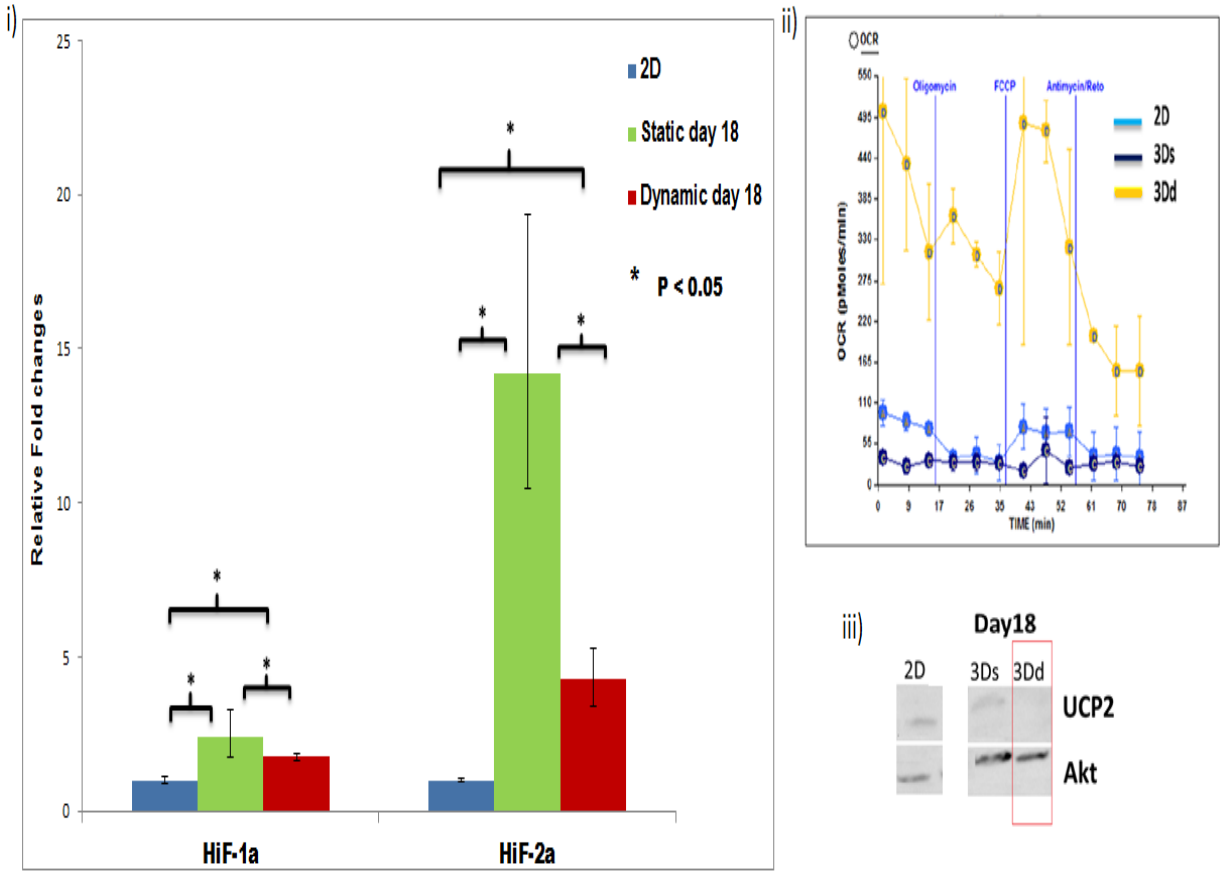

Figure 39 Switch in Metabolism n Dynamic Culture toward Oxidative Phosphorylation

i) Relative mRNA expression of HIF1α and HIF2α at 3D culture at day 18, for 3D static and 3D dynamic culture. Results suggest a significant increase in glycolytic reliance later than day 9 of culture; Values are means ± SD, N=3 (*: $p<0.05$).

ii) Day 18 OCR showed an increase in 3D dynamic (yellow) decrease in 3D static (light blue) compared to 2D (dark blue).

iii) Western blot of UCP2 day 18 and Akt loading control. UCP2 were disappeared gain in dynamic while retained expressed on 3D culture.

6.2.3. Metabolic switch enhances cell survival

The cell viability enhancement after prolonged adaptation of encapsulated cells could be related to switch to hypoxic conditions in our 3D culture (inferred from up-regulation of HIF expression). Both c-Myc and Snail, widely regarded as survival genes, were increased in 3D vs. 2D cultures (Fig. 40). HIF acts with c-Myc (proliferation gene) in metabolic regulation and cell survival.

The c-Myc mRNA showed up-regulation in both 3D cultures at day 9 with more than a 3 fold increase when DNA quantification results showed improvement of cell proliferation. However, by day 18 its expression dropped significantly in 3D static culture in accordance with DNA quantification (which shows decrease as well) whereas in 3D dynamic culture there was no significant difference (Fig. 40). This may correlate with a decrease in cell viability in 3D static culture (please refer to section 3.2.2). The c-Myc overexpression in both 3D cultures, besides its role in cell survival, may link to activation of genes that encode a number of glycolytic enzymes. Addition of c-Myc to the reprogramming cocktail of somatic cells was found to enhance self-renewal by inducing a metabolic switch to glycolysis (Zhang et al., 2012).

Further support to this hypothesis can be obtained from Snail expression at day 9 (survival enhancement gene), which was higher in both 3D cultures. Interestingly, this increase in expression is sustained up to day 18 with a 12-fold difference in 3D static culture compared with day 9, and 5-fold higher in dynamic culture (Fig. 40). The overexpression of Snail was irrelevant to its central role in the EMT, as discussed in chapter 3 section 3.2.4, but instead it may work together with HIF to inhibit mitochondrial respiration. Snail1 is regulated by HIF2α via its promoter; two hypoxia response elements (HREs). It was found as well that Snail helps

detached cells to migrate towards new targets and enable apoptosis resistance (Barrallo-Gimeno and Nieto, 2005).

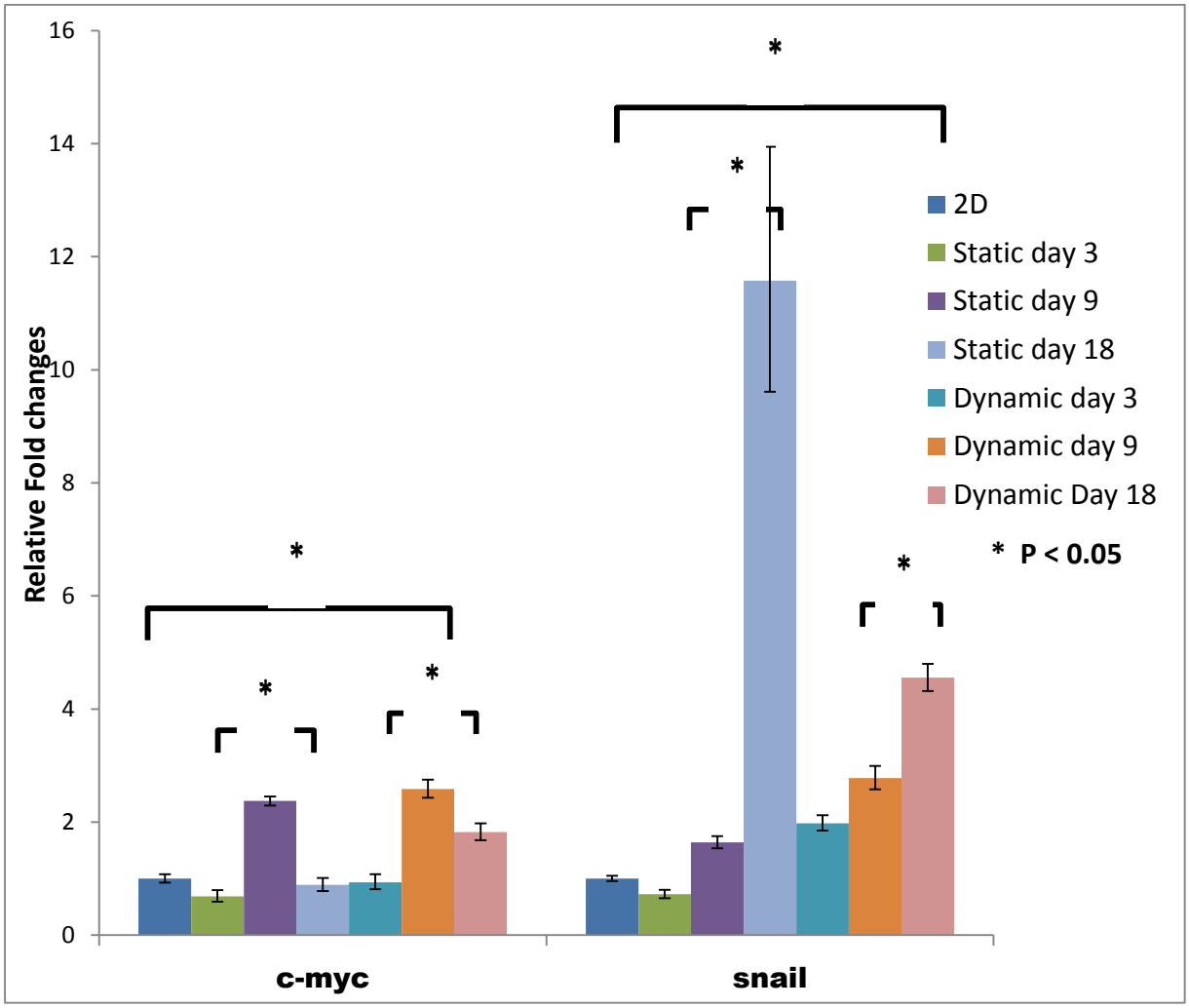

Figure 40: Schematic Illustration of HIF1α on Cell-Survival Regulator

Relative cell-survival gene expression of-Myc and Snail day3, day 9, and day 18 of both 3D static and dynamic normalised to 2D culture and β-actin expression. Values are means ± SD, N=3 (*: $p<0.05$). The C-Myc expression was up-regulated at day 9 and down-regulated at day 18. This suggests HIF1α protein degradation despite high gene expression.

6.2.4. Prolonged adaptation effects on self-renewal of encapsulated cells

Despite cell survival, high expression of HIF1α in cells in both 3D static and dynamic culture can suggest mESCs differentiation as it has been reported that increase in HIF1α induces transition of naïve mESCs to primed ESCs (Zhou et al., 2012c). Monitoring pluripotency marker Rex1, mRNA expression showed up-regulation up to day 18 in 3D dynamic cultures, and from day 3 onwards in 3D static cultures (Fig. 41, ii). Despite the switch in metabolism in encapsulated cells Rex1 expression was 8-fold higher at day 18 than day 3 of culture suggesting that self-renewal capacity is retained. Rex1 is recognised as a highly specific inner cell mass marker both at the mRNA and protein level (Climent et al., 2013). Consistent with that, Oct4 showed increase on expression through the culture as discussed on chapter 3 (Fig. 41, i).

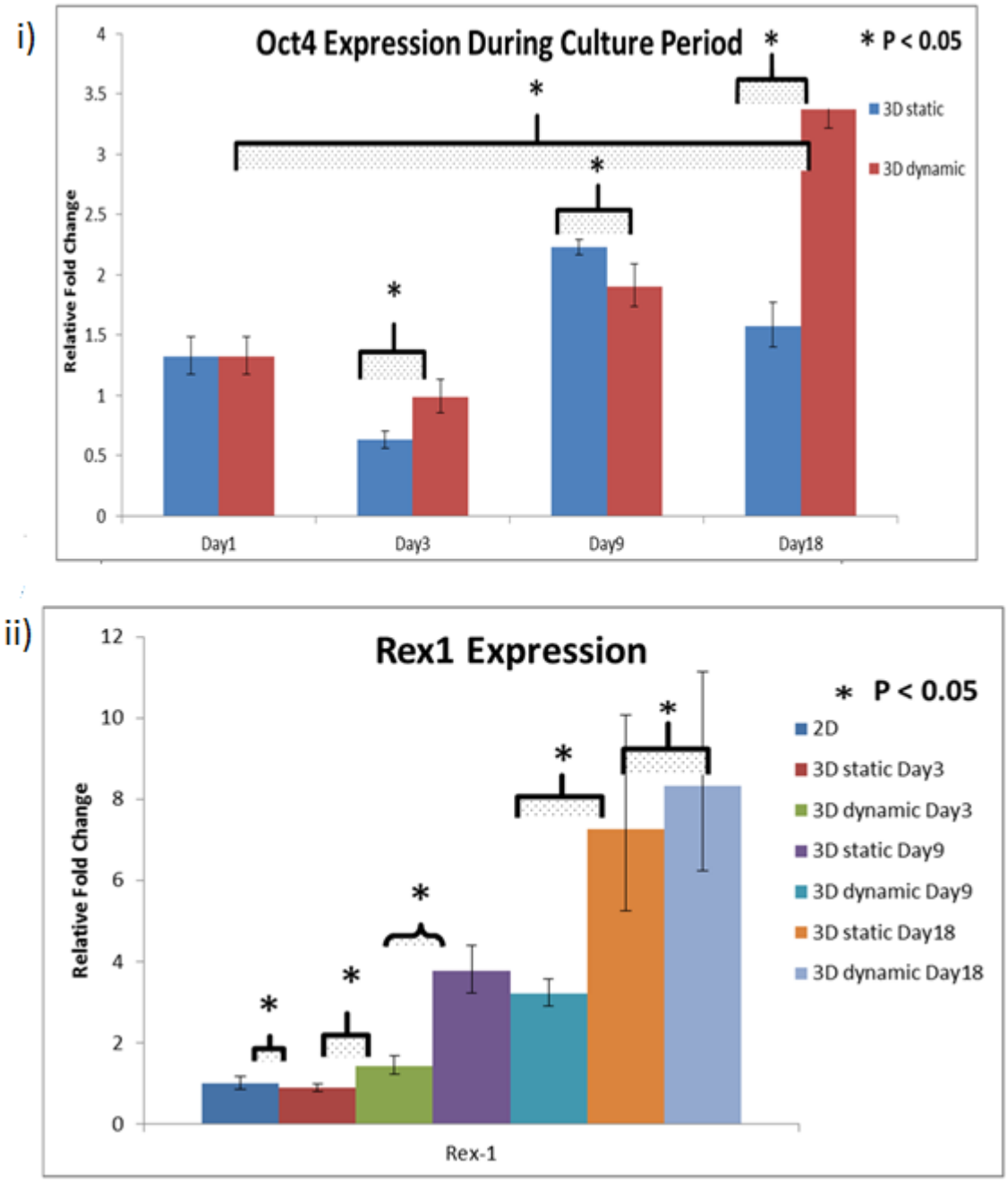

Figure 41: 3D Prolonged Adaption Effect on Self-Renewal

i) Relative gene expression of Oct4 at Day 1, Day 3, Day 9, and Day18.

ii) Relative gene expression of Rex1 day 1, day3, day 9, and day 18 of both 3D static and dynamic normalised to 2D culture and β-actin expression. Values are means ± SD, N=3 (*: $p<0.05$). There is steady increase in its expression.

6.2.5. Change in mitochondrion morphology in 3D dynamic

Transmission electron microscopy was used to examine morphological changes in 3D dynamic culture at day 9 where the switch to glycolytic metabolism occurred. The image showed rounded, damaged crista due to hyperoxia (high oxygenation) in dynamic culture. This can lead to cell toxicity, and increased mitochondrial permeability (Fig. 42, a-d). This switch may also be due to mtDNA mutation (mtDNA encode for 13 proteins, 22 tRNAs and 2 rRNA). ESC mitochondria are characterised by a punctate, perinuclear arrangement and immature cristae. Morphological modifications towards an electron-dense matrix and developed cristae occur during ESC differentiation and are accompanied by a shift from a glycolytic-based metabolism towards oxidative phosphorylation. Although ESCs favour glycolysis over oxidative phosphorylation, mitochondria in ESCs possess functional respiratory complexes. Conversely, an opposite change for most of these features is observed during the reprogramming of somatic cells. However, regulation of the metabolism in self-renewal is still unclear despite the clear UCP2 role (Zhang et al., 2011) in shunting pyruvate away from mitochondria leading to high HKII and low PDH expression (Varum et al., 2011).

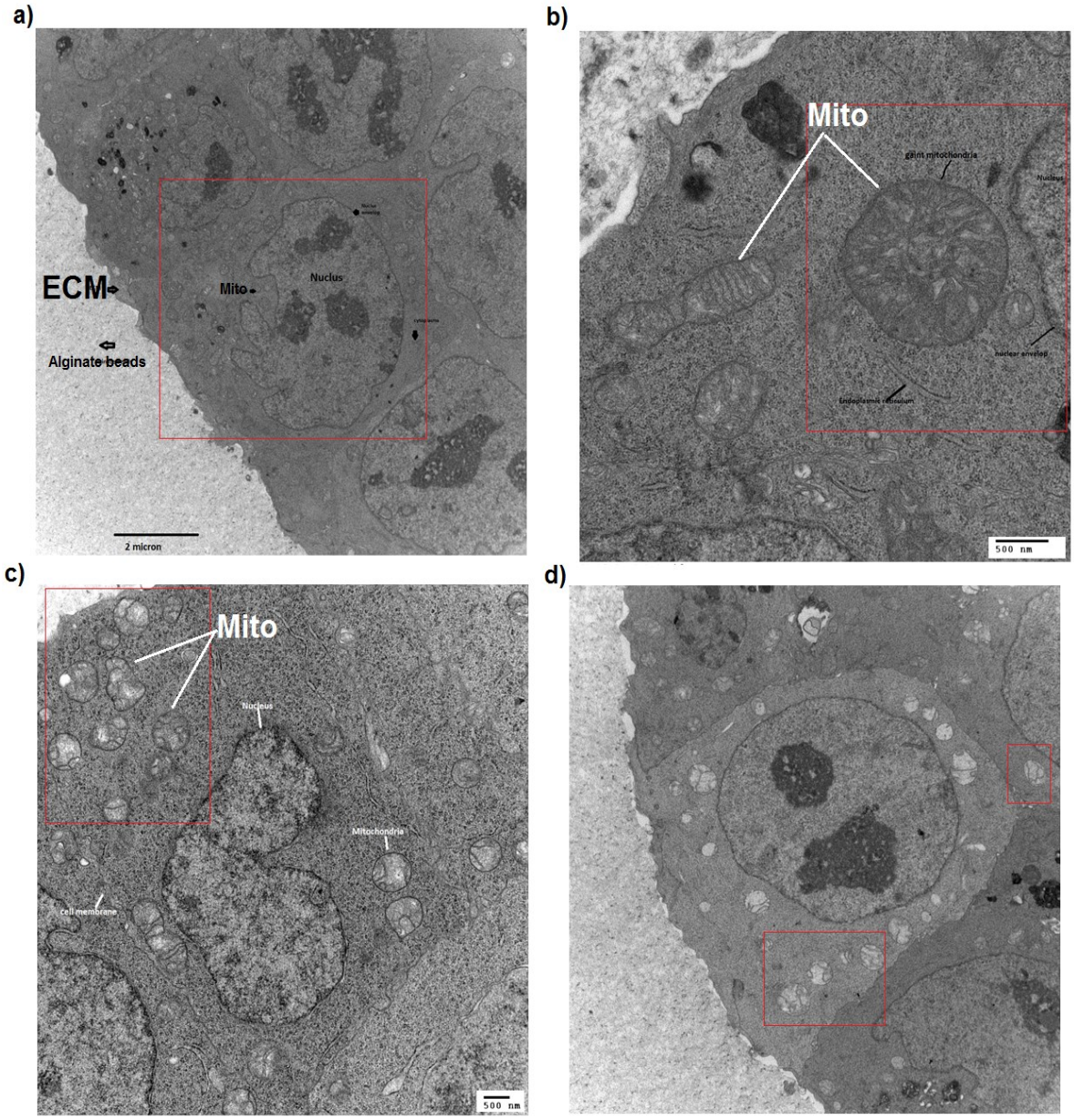

Figure 42: Mitochondrial Morphology Change and Effect on Metabolic Function

Electron micrograph of 3D dynamic culture at day 9. a) Peri-nuclear mitochondrial distribution with relatively large nucleus: cytoplasm ratio. b) Mitochondrial fusion mechanism suggesting cellular activity. c, d) mitochondrial crista degradation

6.3. Discussion

Our data suggested higher mitochondrial respiration in both 3D conditions at day 3 inferred by SILAC data, and OCR. However, UCP2 protein uncoupled mitochondrial activity was expressed on static and not in dynamic culture at day 3. The abundance of uncoupling protein-2 (UCP2) in the cytoplasm serves to shunt pyruvate away from mitochondrial respiration (Ito and Suda, 2014). Absence of UCP2 protein in dynamic culture was tightly a correlate with it is role in mitochondrial regulation, since metabolic profile showed a switch to oxidative phosphorylation. However, expression of UCP2 protein in 3D static culture had no effect in decrease mitochondrial activity (as it up-regulated). These results can be also contradicted to the literature that suggesting UCP2 role in slef-renewal control. The 3D dynamic culture showed significant high expression of Rex1, self-renewal marker wheile presence of UCP2 protein in static condition unable promoting the pluripotency. Rupprecht et al modulated mESC neuronal differentiation and comprehensively checked the UCP subfamily expression. Only UCP2 protein was expressed at early stages prior to loss of OCT4 expression. Their results confirm tight connection between UCP2 and self-renewal (Rupprecht et al., 2014). Down-regulation of UCP2 occur during mESCs differentiation to cardiomyocyte. Additionally, ectopic expression of UCP2 was found to impair ESC differentiation. Therefore, UCP2 has been regarded as an ESC self-renewal marker, the loss of expression indicates loss of self-renewal (Zhang et al., 2011). However Our results may suggest a distinct role of UCP2 in metabolic regulation not previously examined. As, the precise UCP2 mechanism that prevents pyruvate oxidation via mitochondrial respiration is still undetermined (for our hypothesis and further discussion please refer to section 7.3 in next chapter).

At day 9, 3D dynamic culture restore UCP2 protein expression, while 3D static UCP2 protein band remain expressed. There were switch occurred in both 3D cultures to hypoxic condition inferred by low OCR. Despite this switch, cells remained pluripotent inferred with

both Oct4 and Rex1 mRNA expression in dynamic, and likewise 3D static culture also retrieved pluripotent genes expression. In addition both, HIF1α and HIF2α expression increased on both 3D conditions. Ectopic expression of HIF1α has been shown to promote the transition of naive ESC to primed EpiSCs (Zhou et al., 2012c). Consistent with Zhou, Jeong et al revealed an association of HIF1α with LIF receptor (LIFR) protein inhibition at 5% O_2 leading to a decrease in LIF/STAT3 signalling and therefore differentiation of mESCs (Jeong et al., 2007). However, association of HIF and mESCs differentiation is controversial. For instance, Ying et al support our findings of pluripotency by showing that hypoxia and HIF promote mESCs self-renewal. In addition, exposure of non-stem cell populations (such as glioblastoma cells) to hypoxic conditions could activate the stem cell genotype such as Oct4, Nanog, and c-Myc (Varum et al., 2011). Under severe hypoxic condition, HIF1α in the cytoplasm translocate to the nucleus, and stabilises the expression of self-renewal proteins (Oct4, Nanog, and Sox2), while HIF2α binds to the Oct4 promoter and enhances its expression. Switching from oxidative phosphorylation to glycolysis and pluripotency activation is associated with successful somatic cell reprogramming to iPSC (Zhou et al., 2012a). Based on these studies, we could say that increase in hypoxic condition and HIF1α promote self-renewal on 3D cultures.

In addition, higher mRNA level of HIF1α can be linked as well to the increase on Snail and c-Myc expression during day 9 as their regulation is under its immediate control. Both act as well with HIF in metabolic regulation (Zhang et al., 2012). For instance Snail1 mediates a shift in metabolism toward anaerobic glycolysis. Three subunits of cytochrome C oxidase (COX), a part of complex IV of the ETC complex, such as COX7a, have been identified as direct target of Snai1. Cox7a inhibition is leading to repression of mitochondrial respiration. Furthermore, Snail1 was found to bind fructose-1, 6-biphosphatase1 (FBP1) and represses its expression. FBP1 is the rate-limiting enzyme that regulates glucose uptake and oxygen consumption. It is suppressed by Snail to shunt glucose from mitochondrial oxidation (Lu et al., 2014).

In addition to self-renewal enhancement and switch to anaerobic glycolysis at day 9, hypoxic conditions introduced later in the culture were responsible for cell viability and proliferation enhancement. As HIF is directly link to cell-survival genes such as C-Myc and Snail which both up-regulated on 3D condition. For instance, extreme reductions of O_2 (to 0.5%) in mESCs for 48 hours is found to enhance secretion of vascular endothelial growth factor (VEGF) that mediates cell-survival pathways (Brusselmans et al., 2005). Consistent with that, at low O_2 (1.5%) viability was shown to improve by 50% in comparison to ambient oxygen tension via Wnt/β-catenin signalling (Mazumdar et al., 2010).

On day 18 OCR was increased in 3D dynamic culture, UCP2 disappeared and Rex1 was 6 fold up-regulated, whereas in static condition OCR was very low, UCP2 and Rex1 sustained their expression. Positively expressed Rex1 is highly associated with mESCs self-renewal and Rex1 knockouts result in loss of pluripotency (Masui et al., 2008). The ability to sustain pluripotency throughout the culture period time was irrespective to the metabolic switch and temporal fluctuations in the expression of UCP2. So that, the low correlation between mitochondrial respiration and self-renewal in our results early or later on the culture, suggesting importance of functional mitochondria in stem cells at least on 3D dynamic sitting. Uses of carbonyl cyanide m-chlorophenylhydrazone (CCCP, a protonophore depolarising the inner mitochondrial membrane, resulting in uncoupled oxidative phosphorylation) in uncoupling oxidative phosphorylation result in a reduced mESCs proliferation rate suggesting a role of mitochondria in ESC energy production (Mandal et al., 2011). Further supporting to our results, when ESCs were treated with antimycin A (i.e. molecule blocking the electron flow in the complex III) there was an increased expression of NANOG not OCT4 with mRNA levels remaining unchanged. The ESCs under these conditions were able to form teratomas and repress differentiation genes. This work suggested that ROS production from complex III as a result of antimycin a treatment was responsible for the up-regulation of NANOG expression.

This result implies the role of mitochondrial respiration products in controlling pluripotency and differentiation (Varum et al., 2009).

Our result might suggest different metabolic regulator on 3D culture compared to exist data in literature obtained from monolayer culture. For instance, *in-vivo* energy production in early embryo development is reliant on glucose oxidation and acceleration of metabolic activity occurs after the 4- or 8-cell stage. This is associated with segregation of TE and ICM stage results in up-regulation of Glut1, HK, and PFK1 (Ito and Suda, 2014). This switch to anaerobic glycolysis is aimed at avoiding ROS release in order to protect the genome of primordial germ cells (PGCs) developed at this critical stage (Zhang et al., 2015). Thus, our 3D sitting is more relevant to embryo metabolic development compare to *in-vitro* culture. For instance, lower OCR was suggested for hepatocyte cells grown in hollow fibre bioreactors and this was explained by the fact that cell density in 3D constructs mimics intracellular organisation leading cells to be less stressed and show a basal oxygen demand (Patzer, 2004). In addition, mESCs mitochondria is ''bivalent'' having the ability to switch from glycolysis to oxidative phosphorylation based on energy demands (Zhang et al., 2011). In conclusion, flexibility of mitochondrial in dynamic culture suggest different energetic behaviour of mESCs from what known on the literature which need further investigation.

CHAPTER 7: General Conclusion and Further Work Suggestion

7.1. Summary and major finding of the thesis

For therapeutic transplant and tissue engineering, an appropriate cell number, xeno-free culture environment, and single cell population are required; however it remains inefficient to obtain good quality scale-up cells from current culture methods. Therefore, integration of tissue engineering and stem cells can successfully and efficiently induced appropriate SC population without propagate extrinsic factors (as discussed in literature review). Such a source of cells might be advantageous, because chemical inhibitors (inhibitors 2i, and 3i), gene mutation (due to frequent cell passaging,) and exogenous undefined growth factor treatment (FBS, MEF's feeder) are not required to achieve naïve state with also sufficient cell number.

A major new finding of the present study is that 3D with or without bioreactor can regulate murine ESCs' self-renewal. This can be due to deposition of ECM, and change in cell morphology. However, using dynamic culture can be more beneficial for prolong adaption and to obtain higher cell number. This may be associated with improvement of mass transfer and reduced metabolites waste accumulation.

The ability of 3D cultures to sustain cell viability, proliferation, and expression of self-renewal markers makes them an interesting model for *in vitro* processing as well important in large scale production of stem cells for therapeutic application. In working towards the objectives described in chapter 1 of this thesis, we first developed a protocol for the efficient extraction of mESCs from alginate beads that was able to overcome loss of cells (during the dissociation process). Application of these extraction methods facilitated the subsequent proteomic experimentation of the encapsulated mESCs. This thesis demonstrates that mESCs can be maintained in medium containing isotopically labelled arginine and lysine in conditions

compatible with SILAC protocol for the characterisation of mESC protein expression changes in 2D, 3D culture (both static and dynamic) settings (Chapter 5). From the SILAC proteomics screen, 1967 proteins were expressed in the three different culture modes of these proteins, 527 exhibited differentially expressed. Functional validation of metabolic differences identified on the basis of the SILAC experiments, was used to determine their effect on pluripotency in prolonged adaption of mESCs. Measuring oxygen consumption rates at different time points showed fluctuations from high values (at day 3) to lower ones (at day 9) on 3D conditions. Analysis of the expression of hypoxia-related gene 1 & 2 α subunits was carried out and additionally a combination of approaches includes measurement of glucose/lactate concentrations, and UCP2 protein expression elucidated the behaviour of mESCs in prolonged 3D culture affect (both static & dynamic). Our data suggest low correlation between metabolism and self-renewal on 3D culture unlike what is suggested on the literatures. Taken together, the 3D culture analysis (including gene expression), and detailed proteins profiling of mESCs' behaviour in 3D culture provide an effective toolbox for obtaining a more comprehensive understanding of how encapsulated mESCs are regulated *in vitro*.

7.2. General conclusions and thoughts

It was initially observed using DNA quantification that a decrease in cell viability occurred (almost 50%) from initial seeding and retrieves after 4 days in both 3D static and dynamic culture. The use of SILAC combined with mass spectrometry showed up-regulation of ECM, TCA cycle enzymes, cell cycle arrest and apoptosis proteins in both 3D cultures compared with 2D culture. The surviving cells escaped the stress of environmental change by firstly inducing cell-cycle arrest in order to reduce the energy demands required for metabolite precursor synthesis. Secondly, encapsulated cells activate fatty acid oxidation to cope with ATP demand

to enable ECM synthesis and their deposition to occur. Therefore, the number of ECM proteins was up-regulated. However, hyperoxia (high oxygenation) in dynamic culture can lead to cell toxicity, and increased mitochondrial permeability. Our SILAC data showed up-regulation of mitochondrial carrier proteins. Therefore, cells in dynamic culture reduce glucose flux through TCA via down-regulation of glycolytic enzymes to minimise the load on mitochondria. Thus, cells switch to glycine catabolism that occurs in cytosol. In contrast 3D static conditions, which broadly have lower mass transfer rates, showed up-regulation of pyruvate dehydrogenase suggesting an increase in pyruvate flux through the TCA cycle.

DNA damage as inferred from up-regulation of ATR and ATM proteins in 3D static culture. Activation of DNA single strand damage repair system (as inferred from up-regulation of ATR and ATM proteins) in 3D static culture, suggests cell differentiation due to the absence of this mechanism in ESCs. The absence of this mechanism is to prevent inheritance of mutation to daughter cells. Therefore, pluripotency gene profile showed variation with high Rex1, Nanog, and Oct4 expression in dynamic over static culture at day3 of encapsulation in spite of similarities shown between cells in the profile of pluripotency proteins. This is associated with either the low correlation between gene transcript level and protein concentration due to effect of post-translation regulation, or transitory differentiation stage. However, our SILAC combined with MS was not able to detect this low abundance proteins contribute to self-renewal transcription factors regulation.

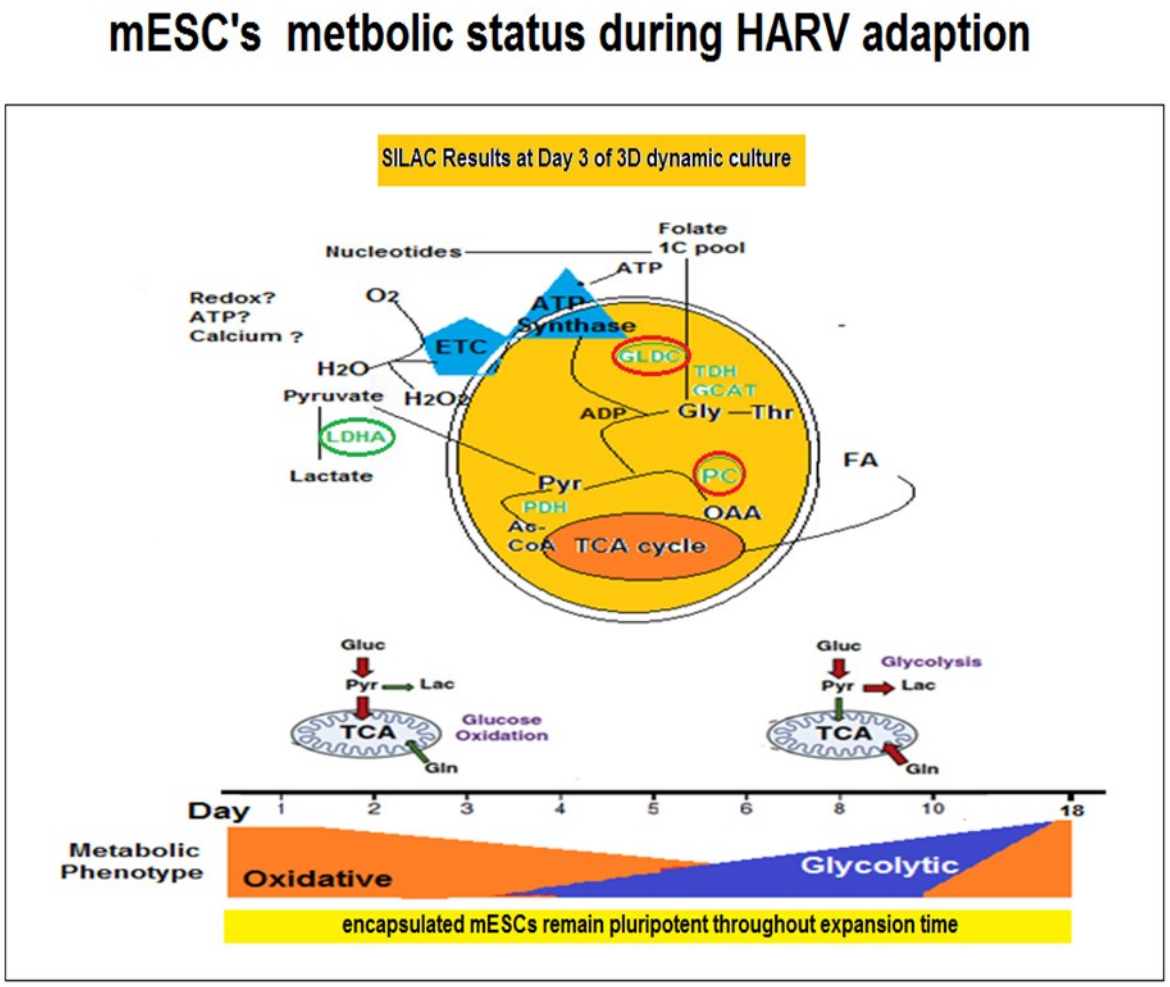

Figure 43 3D Dynamic Culture Metabolic Switch Effect on Self-Renewal

High mitochondrial activity was associated with down-regulation of glycolytic enzymes, up-regulation of GLDC and pyruvate carboxylase at day 3. Then at day 9 metabolic switch occur to anaerobic glycolysis with increase of pyruvate flux to lactate. However, at day 18 cells retain to OXPHO as suggested by increase on oxygen consumption rate.

The switch towards hypoxic conditions later in the prolonged adaption (day 9) was irrespective of unchanged atmospheric (20%) oxygen. It is known that in static culture conditions, there are low external and internal mass transfer rates. However switch to hypoxic in present of dynamic condition, which supposed to enhance diffusion, may be further attenuated by increases of cell density or ECM deposition. However after prolonged culture

(day 18), dynamic cultures switch to higher oxygen consumption, this may a sequence of an increase in breakdown of alginate beads (Fig. 43). This does not dispute with HIF1α mRNA expression at day 18 due to sensitivity of the protein to oxygen availability. Checking HIF1α protein stability at day 18 will illustrate the efficiency of its mRNA expression (Fig. 44).

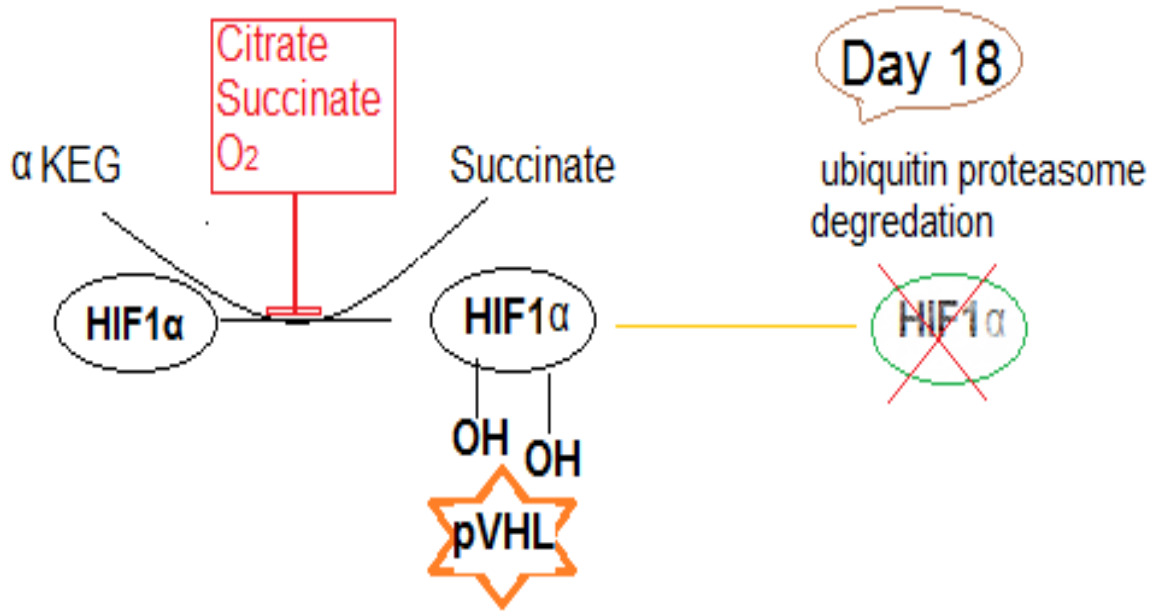

Figure 44: HIF1α Degradation Process in Presence of Oxygen

HIF1α protein has low stability and it regulate via oxygen, citrate and succinate concentration.

Previous work in our group (unpublished) showed that reducing ambient O2 to 5% decrease cell proliferation and coincides with a negative effect on pluripotency gene profile. In contrast, hypoxic condition acquired in our culture by up-regulation of an inducible hypoxia genes along with low oxygen consumption rates, contrariwise enhance cell proliferation and yet pluripotency. Similar finding of lower OCR were previously suggested for hepatocyte cells grown in hollow fibre bioreactors and it was argued the cells' density in 3D constructs mimics intracellular organisation, leading cells to be less stressed and so reduce demand for the basal

oxygen (Patzer, 2004). This result suggests a possible role of the ECM niche, formed during prolonged adaption, in controlling nutrient and oxygen diffusion to the cells rather than ambient oxygen tension.

7.3. UCP2 distinct role in 3D culture from 2D culture

UCP2 protein expression is detected at the pluripotency stage while it disappears upon embryoid body differentiation. In addition, UCP2 ectopic overexpression reduces the ability of cells to commit to any cell lineages (Zhang et al., 2011). This suggests that UCP2 plays a central role in the regulation of self-renewal genes. However, the exact mechanism of how UCP2 regulates self-renewal not identified yet (Hsu and Qu, 2013). Our results obtained from 3D cultures suggest distinct role from those already established in 2D culture. These differences come from the expression of UCP2 in differentiated 3D static culture with active mitochondrial at day 3. On the other hand, UCP2 disappear in pluripotent 3D dynamic cultures.

UCP2 decreases glycolytic flux to the TCA cycle (Zhang et al., 2011). We hypothesised that TCA intermediates flux from nonglucose carbon impose the need for UCP2 expression. Convection of dynamic bioreactor enhances internal and external diffusion. Therefore, uncoupled mitochondrial from glucose oxidation by UCP2 was not necessary. Availability of different carbon source glutamine or fatty acids in 3D dynamic replenishing critical intermediates to TCA cycle. Thus, UCP2 is highly conserved to pyruvate oxidation uncoupling from mitochondria. Increased UCP2 expression in 3D static condition was to shift from the pyruvate oxidation due to reduced metabolites availability. The presence of cells either on 3D or 2D in static condition increase the demand for UCP2 as differentiation resistance. It is role

in static to control diffusion of bulk glucose from surface to intracellular in order to decrease oxidative stress (Fig. 45).

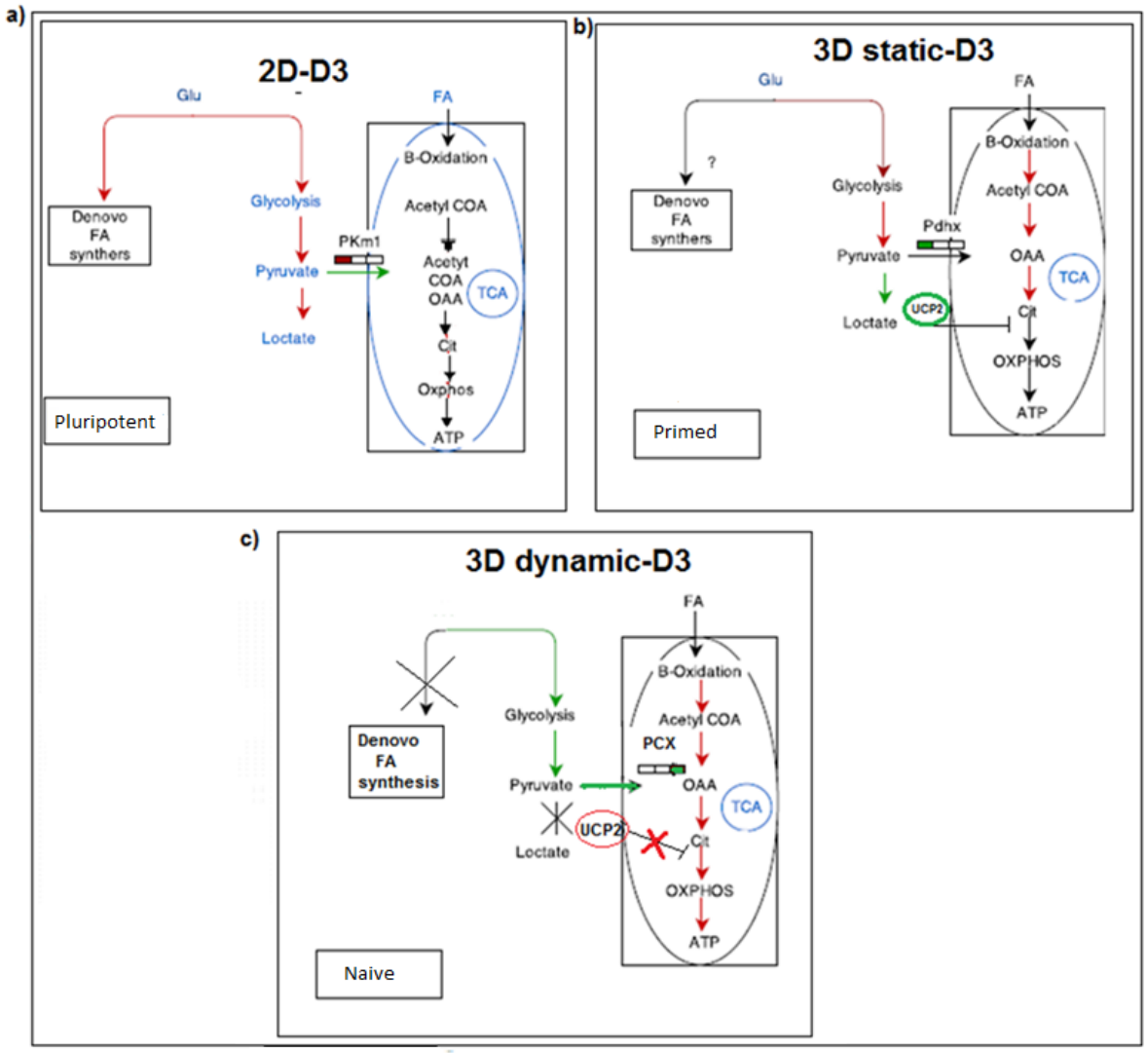

Figure 45 Effect of Metabolic Profile in Cell Pluripotency

a) The increase in glycolytic flux and de novo synthesis in 2D culture may suggest cell pluripotency.

b) There was increased in both glycolytic enzymes and fatty acid oxidation associated proteins in 3D static culture. Down-regulation of oxidative phosphorylation is inferred by up-regulation of UCP2. It may associate with priming ESCs.

c) There was no UCP2 expression, low de novo fatty synthesis and glycolytic enzymes and increase in fatty acid oxidation. This may contribute on naïve mESCs in 3D dynamic culture. The green arrows suggest low flux whereas red one propose high flux.

Our diagram at Fig. 45 explain suggestive possible role of UCP2 at day 3 of mESCs pluripotency expansion culture. The necessity of UCP2 to mESCs phenotype suggested in the literature (based on 2D culture model) is a defence mechanism and self-renewal exit control. This is because low diffusion rate for other metabolites, reliance on glucose as solely carbon source, and accumulation of metabolic by-product. In our 3D static culture, cells experience nutrient depletion as suggested by Glut1 up-regulation, thus UCP2 expression act to increase ATP production rate via avoiding mitochondrial respiration. This is to overcome the glucose oxidant stress that will leads to cell differentiation (Fig. 46). Furthermore, low correlation between self-renewal gene expression profiles and UCP2 expression may be associated with a decrease in mitochondria-nuclear crosstalk in encapsulated cells or suggest further regulation mechanism.

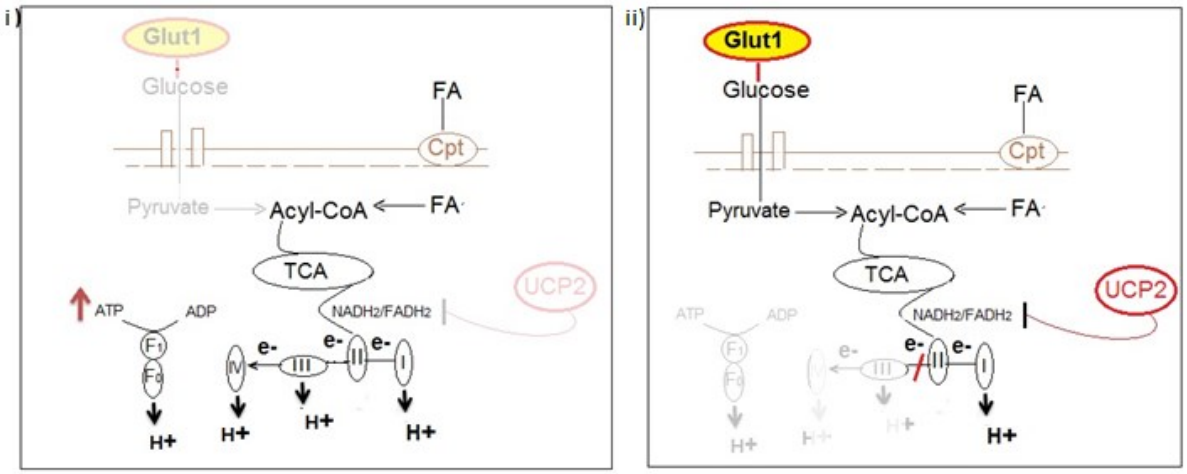

Figure 46: Model of UCP2 Role in Regulation of Electron Transport Chain

i) Electron carbon source of 3D dynamic culture in absence of UCP2 protein expression was from FA. This switch has no effect on cell pluripotency due to improve of diffusion rate.

ii) Blocked of $NADH_2/FADH_2$ electron transport via UCP2 action induces mESCs differentiation due to low mass transfer on static condition.

Finally our SILAC results suggest down-regulation of glycolysis and switch to FAO in 3D dynamic culture, this data suggest a tight regulation of these two metabolism for pluripotency. We are suggesting possible role of this switch to regulate pluripotency on 3D dynamic. As SILAC results, showed increase on FAO enzymes and down-regulation of glycolytic proteins. However, the mechanism of how fatty acid regulates self-renewal is remain to be study. To conclude, improvement of diffusion rate in dynamic culture provides variety of competed carbon source to encapsulated cells. In comparison, accumulation of bulk glucose in static in 2D or 3D leads to glucose-related oxidant stress.

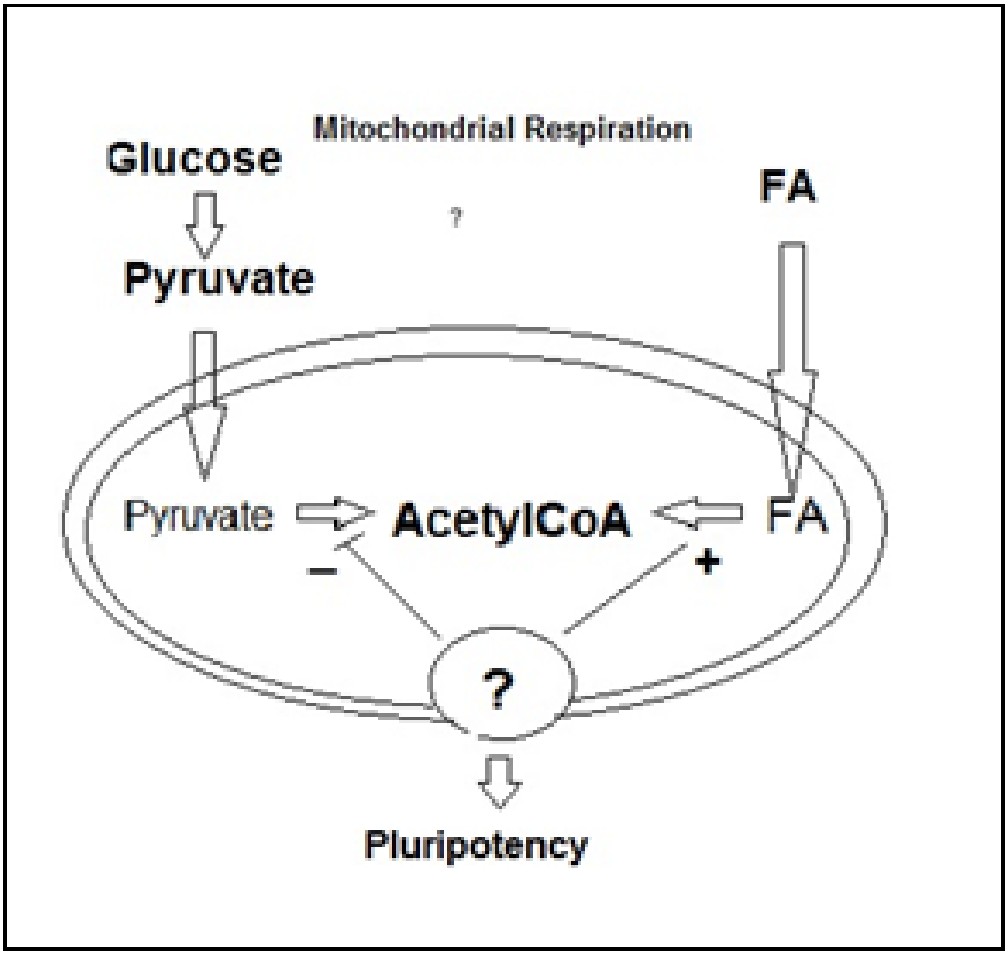

Figure 47 illustration of carbon metabolism regulate cell pluripotency.

Model of pluripotency regulation in 3D dynamic culture at day 3 via switch in carbon source from glucose to fatty acid (FA).

7.4. Suggestion for further work

Our assumption of naïve pluripotency in dynamic culture was made by the observation of high expression levels of the Rex1 and Oct4 genes and simultaneous low expression of the differentiation marker FGF5. Alternatively, stem cells functional assays such as chimera generation *in vivo* or embryoid body formation *in vitro* can establish the certainty of self-renewal.

One of the limitations of the work described in this thesis is that the population-average gene expression levels can mask intra-population heterogeneities. In relation to alginate entrapped mESCs, it is uncertain whether the gene expression levels are uniform throughout the entire population of the cells. Characterizing individual cells using FACS will sort into sub-populations and define the homogeneity of the sample.

Differential protein expression highlighted the role of oxidative stress and further work could be carried out by measuring ROS, glutathione and ATP at day three of the experiment to illustrate the effect of hyperoxia on cell self-renewal in dynamic conditions. This can be done in presence or absence of 2-Deoxy-D-glucose that will inhibit glucose uptake and reduce the flux through glycolysis and so investigate significance of 3D dynamic culture based on cell viability assays. If cells survive with high ATP production (measured by firefly luciferase), this will confirm using alternative carbon source such as glycine or fatty acids as suggested by the SILAC results. This switch toward amino acid or fatty acid catabolism will be an escape mechanism from oxidative stress, which could be confirmed using ROS assays. This finding will be consistent with the recent assumption of the importance of glycine and fatty acid catabolism in cancer proliferation and metastasis (Locasale, 2013). Further the result will shed light on presence of these alternative survival pathways in ESCs to avoid oxidative stress and sustain self-renewal with ability to adapt traumatic environment.

Down-regulation of cellular retinoic acid-binding protein 1 (Crabp1) in 3D dynamic culture (day3) compared with both 2D and 3D static suggest inhibition epidermal differentiation. This protein is regulated by RA treatment or Notch activation and negatively regulated by Wnt/β-catenin signalling. In addition to number of proteins discussed in chapter 5, section 5.6.7 and low expression of Nestin genes. Blocking spontaneous differentiation to ectoderm in ESCs culture is beneficial and promotes naïve cell population. The possible recognisable of neuroectodermal proteins down-regulation in 3D dynamic culture is oxidative stress. This link can be obtained from sensitivity of neural progenitor stem cells to oxidative stress which cause their damage and leads to a numerous of neurodegenerative disease. The Crabp1 proteins role in blocking ectoderm lineage and promote naïve ESCs is not clear yet. Identifying the pathway and functionality using both knockout and overexpression study may suggest new pluripotency master regulator.

Finally, this work can be beneficial for stem cell bioprocessing system enhancement. For instance, reducing oxidative stress at initial days will improve cell viability. This can be done for example using mitochondrial respiration inhibitors or decrease fluid motion rate. Another root direction is finding the link between hypo-methylation proteins and stress response signalling. In conclusion, this thesis can show in-depth effect of environment change in stem cells behaviour *in vitro* and display different corner view of stem cell characteristic.

Appendices

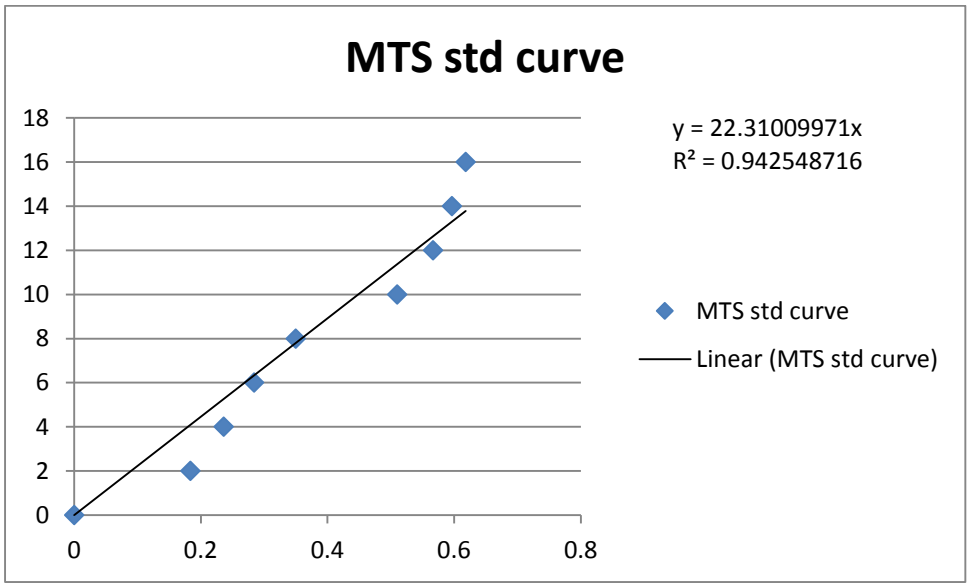

Figure 48 MTS standard Curve

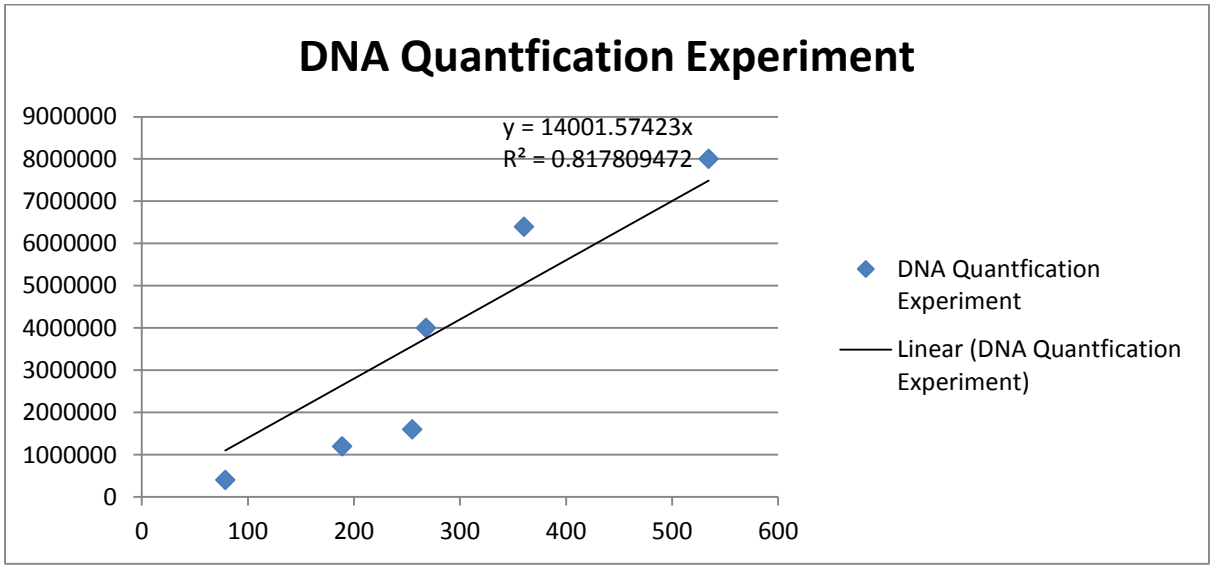

Figure 49 DNA quantification standard curve

Table 7: Self-renewal proteins

Description	Gene	Σ# Unique peptide	2D/3S	3S/3D	3D/2D
Telomere-associated protein RIF1	Rif1	44	0.7	1.2	1.4
Catenin alpha-1	Ctnna1	27	1.1	0.9	1.0
Alkaline phosphatase, tissue-nonspecific isozymes	Alpl	18	0.2	1.3	1.4
Undifferentiated embryonic cell transcription factor 1	Utf1	17	0.8	1.1	2.0
Cbx3 protein	Cbx3	14	0.9	1.1	1.1
Developmental pluripotency-associated protein 5A s	Dpaga	11	0.9	0.8	1.0
Cadherin-1	Cdh1	9	1.0	0.9	1.7
Basal cell adhesion molecule	Bcam	8	2.0	0.7	1.0
Beta-catenin-like protein 1	Ctnnbl1	6	0.9	1.0	1.4
POU domain, class 5, transcription factor 1	Pouf5f1	6	1.0	1.4	0.6
Transcription factor SOX-2	Sox2	5	1.2	1.5	0.8
GTPase Eras	Eras	5	2.0	1.3	0.5
CD9 antigen	Cd9	4	0.7	0.8	1.7
E3 ubiquitin-protein ligase RING2	Rnf2	4	1.3	1.2	0.6
Isoform Stat3B of Signal transducer and activator of transcription 3	Stat3	4	1.1	1.0	1.0
Isoform 2 of Glycerol-3-phosphate dehydrogenase 1	Gpdl1	2	1.0	1.1	0.6

Table 8: Apoptosis

Description	Gene	Σ# Uniq pept	3S/2D	3S/3D	3D/2D
Cytochrome c oxidase subunit 7A2, mitochondrial	Cox7a2	2	1.85	**7.11**	1.10
DNA mismatch repair protein Msh3	Msh3	3	**100.00**	**100.00**	0.51
DNA repair protein RAD50	Rad50	10	**100.00**	0.94	1.11
Heat shock 70 kDa protein 1A	Hspa1a	10	**2.58**	**0.30**	**3.91**
Histone chaperone ASF1A	Asf1a	4	**3.58**	**7.03**	0.68
Isoform Mt-VDAC1 of Voltage-dependent anion-selective channel protein 1	Vdac1	16	**2.06**	0.84	**3.07**
Kinetochore-associated protein 1	Kntc1	7	**4.19**	**6.44**	0.59
Membrane-associated progesterone receptor component 2	Pgrmc2	5	**15.36**	1.15	**2.21**

Programmed cell death protein 5	Pdcd5	9	0.61	0.89	**0.43**
Thioredoxin-related transmembrane protein 1	Tmx1	6	**3.86**	1.17	**10.83**
Thioredoxin-related transmembrane protein 2	Tmx2	6	1.85	**5.94**	**2.55**
Tumor suppressor p53-binding protein 1	Tp53bp1	6	1.20	**20.33**	1.05
DNA mismatch repair protein Msh3	Msh3	3	**100.00**	**100.00**	0.51
DNA topoisomerase 2-beta	Top2b	6	**100.00**	**2.66**	0.56
Histone chaperone ASF1A	Asf1a	4	**3.58**	**7.03**	0.68
Kinetochore-associated protein 1	Kntc1	7	**4.19**	**6.44**	0.59
Protein FAM162A	32.26	5	**2.07**	**7.40**	1.66
Lysine-specific demethylase 3A	9.30	9	**5.06**	1.27	0.87
Presenilins-associated rhomboid-like protein, mitochondrial	parl	3	**21.80**	1.68	1.67
Vesicle transport through interaction with t-SNAREs homolog 1B	vit1b	4	**5.23**	0.86	1.15

Table 9: Cell Cytoskeleton

Description	*Gene*	*Σ# Unique peptide*	*3S/2D*	*3S/3D*	*3D/2D*
Protein Fat1	*fat1*	*28*	*18.87*	*1.04*	*1.95*
Moesin	*Msn*	*25*	*0.60*	*0.73*	*0.49*
A-kinase anchor protein 12	*Akap12*	*24*	*0.77*	*1.17*	*0.48*
Protein Kif13b	*kif13b*	*16*	*10.64*	*1.08*	*0.92*
Rho GDP-dissociation inhibitor 1	*Arhgdia*	*16*	*0.63*	*0.94*	*0.48*
LIM domain and actin-binding protein 1	*lima1*	*13*	*100.00*	*0.92*	*1.12*
LIM and SH3 domain protein 1	*lasp1*	*12*	*100.00*	*0.73*	*0.83*
Laminin subunit gamma-1	*lamc1*	*11*	*2.05*	*1.00*	*1.75*
Serine/threonine-protein phosphatase 2A catalytic subunit alpha isoform	*ppp2ca*	*9*	*15.38*	*1.02*	*0.66*
Capping protein (Actin filament), gelsolin-like	*Capg*	*7*	*100.00*	*0.79*	*1.70*
Isoform 2 of Twinfilin-2	*twf2*	*7*	*4.31*	*1.49*	*0.51*
Cofilin-2	*Cfl2*	*7*	*0.77*	*1.07*	*0.05*
Nucleoporin NDC1	*Tmem48*	*6*	*100.00*	*1.26*	*1.97*
Protein Gm2904	*Esd*	*6*	*6.49*	*0.84*	*1.34*
Actin, alpha cardiac muscle 1	*Actc1*	*6*	*0.82*	*6.37*	*0.87*
Transgelin	*Tagln*	*6*	*0.59*	*1.06*	*0.48*
Isoform 2 of Transmembrane emp24 domain-containing protein 1	*tmed1*	*4*	*5.62*	*0.99*	*1.59*
Rho-related GTP-binding protein RhoC	*Rhoc*	*4*	*0.84*	*1.54*	*0.34*
Phosphoserine phosphatase	*Psph*	*3*	*0.84*	*0.96*	*0.47*

Table 10: Glycolysis Enzyme Down-Regulated In both 2D and 3D static vs.3D dynamic

Description	*Gene*	*Σ# Unique peptide*	*2D/3S*	*3D/3S*	*3D/2D*
Phosphoglycerate kinase 1	*Pgk1*	*32*	*1.4*	*0.5*	*0.5*
L-lactate dehydrogenase A chain	*Ldha*	*20*	*1.8*	*0.4*	*0.3*
Triosephosphate isomerase	*Tpi1*	*14*	*0.8*	*0.4*	*0.3*
6-phosphofructokinase, liver type	*Pfkl*	*26*	*1.3*	*0.4*	*0.5*

Table 11: Oxidative Phosphorylation

Description	*Gene*	*Σ# Uniq pept*	*3S/2D*	*3S/3D*	*3D/2D*
Cytochrome c oxidase subunit 7C, mitochondrial	*Cox7c*	*3*	*1.452*	*1.227*	***41.760***
NADH dehydrogenase [ubiquinone] 1 subunit C2	*Ndufc2*	*8*	*1.757*	*0.848*	***9.587***
Dehydrogenase/reductase SDR family member 1	*Dhrs1*	*4*	*0.739*	*0.891*	***8.791***
ATP synthase subunit g, mitochondrial	*Atp5l*	*10*	*1.276*	*0.912*	***7.910***
CDGSH iron-sulfur domain-containing protein 1	*Cisd1*	*7*	*1.667*	*0.985*	***6.583***
Cytochrome b-c1 complex subunit 6, mitochondrial	*Uqcrh*	*7*	*1.185*	*1.038*	***6.014***
cAMP-dependent protein kinase type I-alpha regulatory subunit	*Prkar1a*	*5*	*0.756*	*0.816*	***5.686***
Isocitrate dehydrogenase 3 (NAD+) beta	*Idh3b*	*6*	*1.101*	*0.962*	***5.516***
Isoform 2 of Estradiol 17-beta-dehydrogenase 11	*Hsd17b11*	*6*	*1.285*	*1.173*	***5.179***
Reactive oxygen species modulator 1	*Romo1*	*4*	*1.182*	*0.945*	***4.734***
Amine oxidase [flavin-containing] A OS=Mus musculus GN=Maoa PE=1 SV=3 - [AOFA_MOUSE]	*Maoa*	*9*	*1.002*	*1.253*	***2.758***
Mitochondrial import inner membrane translocase subunit Tim10	*Tim10*	*5*	*1.117*	*0.832*	***2.251***
ATP synthase subunit e, mitochondrial	*Atp5i*	*13*	*1.278*	*0.903*	***2.234***
Cytochrome b5 type B	*Cyb5b*	*6*	*1.146*	*1.005*	***2.209***
ATP synthase subunit f, mitochondrial	*Atp5j2*	*8*	*1.361*	*0.900*	***2.192***
Cytochrome c oxidase subunit 4 isoform 1, mitochondrial	*Cox4i*	*21*	*1.493*	*1.143*	***2.179***
Cytochrome b-c1 complex subunit Rieske, mitochondrial	*Uqcrfs1*	*11*	*1.367*	*1.351*	***2.142***
Cytochrome b-c1 complex subunit 8	*Uqcrq*	*9*	*1.278*	*0.866*	***2.129***
Aspartate--tRNA ligase, mitochondrial	*Dars2*	*5*	*1.026*	*1.203*	***2.122***
Isoform 2 of Cytochrome c1, heme protein, mitochondrial	*Cyc1*	*11*	*1.389*	*0.812*	***2.116***
Mitochondrial Rho GTPase 1	*Rhot1*	*4*	*1.433*	*0.933*	***2.114***
NADH dehydrogenase [ubiquinone] 1 beta subcomplex subunit 4	*Ndufb4*	*6*	*1.466*	*1.165*	***2.077***
Pyruvate carboxylase	*Pcx*	*25*	*1.672*	*1.161*	***2.012***

Table 12: Glycine Cleavage System

Description	Gene	Σ# Uniq pept	3S/2D	3S/3D	3D/2D
Dihydrolipoyl dehydrogenase, mitochondrial	Dld	18	1.265	0.865	**2.002**
Glycine cleavage system H protein, mitochondrial	Gcsh	3	1.106	0.990	**2.092**
Glycine dehydrogenase [decarboxylating], mitochondrial	Gldc	20	1.677	0.752	**2.323**

Table 13: Differentiation protein on 3D static condition

Description	Gene	Σ# Uniq pept	3S/2D	3S/3D	3D/2D
E3 ubiquitin-protein ligase HECTD1	Hectd1	16	0.904	1.201	**0.019**
E3 ubiquitin-protein ligase NEDD4	Nedd4	26	**0.495**	1.193	**0.488**
Protein Zfml	Zfml	8	**5.983**	1.285	1.084
Targeting protein for Xklp2	Tpx2	10	**100.000**	1.119	1.672
AFG3-like protein 2	Afg3l2	6	**6.624**	1.111	1.379
Dihydropyrimidinase-related protein 2	Dpsyl2	6	0.623	0.845	**0.258**
GMP reductase 2	Gmpr2	3	0.747	0.600	**0.452**
H1 histone family, member X	H1fx	6	**0.241**	1.925	0.913
Lysine-specific demethylase 3A	kdm3a	9	**5.064**	1.268	0.875

Table 14: Protein Synthesis

Description	*Gene*	*Σ# Uniq pept*	*3S/2D*	*3S/3D*	*3D/2D*
Thiosulfate sulfurtransferase	*Tst*	*8*	***5.13***	***2.28***	*1.21*
Ubiquitin-conjugating enzyme E2 O	*Ube2o*	*7*	*0.71*	***100.00***	*0.75*
Isoform 4 of Coatomer subunit gamma-2	*Copg2*	*6*	***5.96***	***8.01***	*0.93*
28S ribosomal protein S26, mitochondrial	*Mrps26*	*5*	*0.87*	***6.13***	***48.41***
Cathepsin B	*Ctsb*	*4*	***100.00***	***100.00***	***9.36***
Protein RER1	*Rer1*	*4*	***100.00***	***100.00***	*12.44*
39S ribosomal protein L28, mitochondrial	*Mrpl28*	*4*	*0.95*	***6.63***	*0.98*
60S ribosomal export protein NMD3	*Nmd3*	*4*	*0.90*	***5.06***	*0.82*
Golgi reassembly stacking protein 2	*Gorasp2*	*4*	***100.00***	***2.20***	*0.97*
Interferon-induced transmembrane protein 2	*Ifitm2*	*3*	*0.77*	***100.00***	*1.80*
39S ribosomal protein L41, mitochondrial	*Mrpl41*	*3*	*0.74*	***6.65***	*1.00*
DnaJ homolog subfamily C member 3	*Dnajc3*	*3*	***100.00***	***5.74***	*0.73*
Interferon-stimulated 20 kDa exonuclease-like 2	*Isg2012*	*2*	***5.07***	***7.99***	*1.81*

Table 15: Cell Cycle

Description	Gene	Σ# Uniq pept	3S/2D	3S/3D	3D/2D
Cytoskeleton-associated protein 4	Ckap4	25	2.82	1.04	2.57
Ataxia telangiectasia mutated homolog	Atm	22	0.72	8.25	0.72
G2 and S phase-expressed protein 1	Gtse1	14	3.85	0.77	53.91
Bromodomain adjacent to zinc finger domain protein 2A	Baz2a	13	9.43	1.57	7.38
Histone deacetylase 6 (Fragment)	Hdac6	10	100.00	1.04	1.01
Centromere protein V	cenpv	10	5.71	1.68	1.34
Cytoskeleton-associated protein 2	Cap2	9	100.00	0.76	3.59
Isoform 1 of Core histone macro-H2A.1	H2afy	9	2.17	1.29	1.60
Isoform 2 of Cell division cycle protein 23 homolog	Cdc23	8	100.00	0.77	6.00
Cullin-1 (Fragment)	Cul1	8	0.64	6.78	0.87
Sister chromatid cohesion protein PDS5 homolog A	Pds5a	7	5.35	1.32	1.24
Mitotic spindle assembly checkpoint protein MAD1	Mad1	7	5.05	1.60	2.30
Kinetochore-associated protein 1	Kntc1	7	4.18	6.44	0.59
Isoform 3 of Histone acetyltransferase KAT7	Kat	7	1.38	1.33	2.44

Cell division cycle protein 20 homolog	Cdc20	6	100.00	1.00	1.26
DNA topoisomerase 2-beta	Top2b	6	100.00	2.66	0.56
Isoform 2 of Basigin	Bsg	6	0.97	100.00	1.03
Dynactin subunit 2	Dctn2	6	0.85	1.63	0.07
Dynactin subunit 3	Dctn3	6	0.34	1.42	0.62
Isoform 2 of Inner centromere protein	Incenp	5	100.00	100.00	2.69
Cyclin-dependent kinase 7	Cdk7	5	1.03	2.08	1.07
Cyclin-dependent kinase 4 (Fragment)	Cdk4	5	0.51	6.51	0.53
Histone chaperone ASF1A	Asf1a	4	3.58	7.03	0.69
Cyclin-dependent kinase 2-associated protein 1	Cdk2ap1	4	0.82	5.79	0.94
Cyclin-A2	Ccna2	3	100.00	1.11	0.86
Histone H2A	H2afy2	3	5.92	1.36	1.82
Histone H1.0	H1f0	2	1.57	2.32	1.62

Table 16: Histone and DNA Modification Proteins (Epigenetic Related Proteins)

Description	Gene	Σ# Uniq pept	3S/2D	3S/3D	3D/2D
Protein Bptf	Bbtf	22	1.53	**32.02**	1.24
Lamin-B2	lmnb2	20	**4.03**	0.98	1.94
Paraspeckle component 1	pspc1	13	**2.27**	1.17	1.14
Structural maintenance of chromosomes flexible hinge domain-containing protein 1	Smchd1	12	0.91	**3.23**	0.97
Isoform 2 of Methyl-CpG-binding domain protein 3	mbd3	12	**18.11**	1.08	1.34
Isoform 2 of DNA (cytosine-5)-methyltransferase 3A	Dnmt3a	12	**0.49**	**2.05**	0.77
Histone deacetylase 6 (Fragment)	Hdac6	10	**100.00**	1.04	1.01
Methionine aminopeptidase 2	merap2	10	**100.00**	1.06	0.60
SWI/SNF-related matrix-associated actin-dependent regulator of chromatin subfamily E member 1	Smarce1	10	**7.37**	1.14	1.21
Elongator complex protein 3	Elp3	9	1.13	**6.51**	0.66
Isoform 1 of Core histone macro-H2A.1	H2afy	9	**2.17**	1.29	1.60
Lysine-specific demethylase 3A	kdm3a	9	**5.06**	1.27	0.87
Bifunctional protein NCOAT	Mgea5	8	0.96	**100.00**	0.66
Parafibromin	cdc73	8	**21.48**	1.02	1.00
Transcriptional regulator ATRX	Atrx	7	**20.50**	**6.27**	0.82

Protein dpy-30 homolog	Dpy30	5	0.88	**4.17**	0.99
MCG11326, isoform CRA_b	Hnrnph3	5	**2.35**	1.01	1.25
Heterogeneous nuclear ribonucleoprotein H2	Hnrnph2	4	**3.47**	1.49	1.08
Isoform 2 of Mortality factor 4-like protein 1	morf4l1	4	**5.11**	1.07	1.54
Histone chaperone ASF1A	Asf1a	4	**3.58**	**7.03**	0.68
Isoform 2 of Methionine adenosyltransferase 2 subunit beta	mat2b	4	**6.14**	0.91	0.81
RNA polymerase II-associated protein 1	rpap1	3	**7.81**	1.04	1.06

Table 17: Spermatogenesis

Description	*Gene*	*# Unique peptide*	*3S/2D*	*3S/3D*	*3D/2D*
NADPH:adrenodoxin oxidoreductase	*Fdxr*	*7*	*100.0*	*0.9*	*1.8*
V-type proton ATPase subunit C 1	*atp6v1c1*	*3*	*6.9*	*1.0*	*1.0*
60S ribosomal protein L10-like	*Rpl10l*	*4*	*6.6*	*1.0*	*0.6*
RIKEN cDNA 1110033J19	*Rps4y2*	*7*	*5.5*	*2.5*	*1.2*
Lysine-specific demethylase 3A	*kdm3a*	*9*	*5.1*	*1.3*	*0.9*
Paraspeckle component 1	*pspc1*	*13*	*2.3*	*1.2*	*1.1*
Hematological and neurological expressed 1-like protein	*Hn1l*	*3*	*1.5*	*5.7*	*0.6*
Cellular retinoic acid-binding protein 1	*Crabp1*	*6*	*1.4*	*10.6*	*0.3*
Isoform 2 of Basigin	*Bsg*	*6*	*1.0*	*100.0*	*1.0*

Table 18: DNA Repair Mechanism Proteins on 3D static

Description	Gene	Σ# Unique peptide	3S/2D	3S/3D	3D/2D
DNA repair protein RAD50	Rad50	10	100.0	0.9	1.1
Histone deacetylase 6 (Fragment)	Hdac6	10	100.0	1.0	1.0
DNA topoisomerase 2-beta	Top2b	6	100.0	2.7	0.6
Isoform 2 of Inner centromere protein	Incenp	5	100.0	100.0	2.7
DNA mismatch repair protein Msh3	Msh3	3	100.0	100.0	0.5
DNA repair protein RAD50	Rad50	10	100.0	0.9	1.1
Procollagen-lysine,2-oxoglutarate 5-dioxygenase 3	plod3	5	6.1	0.8	1.8
Histone H2A	H2afy2	3	5.9	1.4	1.8
TIP41-like protein	tiprl	3	5.0	1.0	0.9

DNA-directed RNA polymerase II subunit RPB7	Porl2g	4	4.2	0.9	1.0
Target of EGR1 protein 1	toe1	3	3.8	0.9	0.8
Histone chaperone ASF1A	Asf1a	4	3.6	7.0	0.7
Heterogeneous nuclear ribonucleoprotein H2	Hnrnph2	4	3.5	1.5	1.1
Isoform 1 of Core histone macro-H2A.1	H2afy	9	2.2	1.3	1.6
Serine/threonine-protein kinase ATR	Atr	14	1.9	39.5	0.6
Isoform 2 of Uncharacterized protein C9orf114 homolog]	D2wsu81e	6	1.7	6.6	1.7
DNA ligase	Lig3	6	1.4	2.5	10.1
H/ACA ribonucleoprotein complex subunit 4	Dkc1	20	1.2	1.0	2.2
Tumor suppressor p53-binding protein 1	TP53b	6	1.2	20.3	1.0
H/ACA ribonucleoprotein complex subunit 1	Gar1	4	1.1	1.1	2.5
COP9 signalosome complex subunit 7b	Cops7b	3	1.1	7.3	0.6
Structural maintenance of chromosomes flexible hinge domain-containing protein 1	Smchd1	12	0.9	3.2	1.0
E3 ubiquitin-protein ligase RBX1	Rbx1	3	0.7	100.0	0.9
Ataxia telangiectasia mutated homolog (Human)	Atm	22	0.7	8.3	0.7
DNA polymerase delta subunit 2	Pold2	5	0.7	2.2	0.5
Isoform 2 of DNA (cytosine-5)-methyltransferase 3A	Dnmt3a	12	0.5	2.0	0.8
H1 histone family, member X	H1Fx	6	0.2	1.9	0.9

Table 19: Proteins differentially expressed in both 3D cultures compared to 2D

Description	*Gene*	*# Unique peptide*	*3S/2D*	*3S/3D*	*3D/2D*
ATP-binding cassette sub-family B member 7, mitochondrial	*Abcb7*	*3*	***100.00***	*0.93*	***2.15***
3-ketoacyl-CoA thiolase, mitochondrial	*Acaa2*	*10*	***3.83***	*0.75*	***3.71***
Acyl-CoA dehydrogenase family member 9, mitochondrial	*Acad9*	*13*	***100.00***	*0.95*	***2.20***
Isoform 3 of ADP-dependent glucokinase	*Adpgk*	*8*	***11.24***	*1.18*	***2.18***
Adenylate kinase isoenzyme 4, mitochondrial	*Ak4*	*7*	***10.11***	*1.05*	***4.49***
V-type proton ATPase subunit d 1	*Atp6v0d1*	*7*	***2.00***	*0.97*	***2.73***
Bromodomain adjacent to zinc finger domain protein 2A	*Baz2a*	*13*	***9.41***	*1.57*	***7.38***
CD 81 antigen, isoform CRA_c	*Cd81*	*3*	***2.02***	*1.19*	***100.00***
Isoform 2 of Cell division cycle protein 23 homolog	*Cdc23*	*8*	***100.00***	*0.77*	***6.00***
CDP-diacylglycerol--inositol 3-phosphatidyltransferase	*Cdipt*	*4*	***2.01***	*0.83*	***3.07***
Cytoskeleton-associated protein 2	*Ckap2*	*9*	***100.00***	*0.76*	***3.59***
Cytoskeleton-associated protein 4	*Ckap4*	*25*	***2.81***	*1.04*	***2.57***
Catechol O-methyltransferase domain-containing protein 1	*Comtd1*	*3*	***3.27***	*0.61*	***2.59***
Cathepsin D	*Ctsd*	*8*	***2.02***	*0.80*	***3.36***
Dolichol-phosphate (Beta-D) mannosyltransferase 1	*Dpm1*	*4*	***100.00***	*1.12*	***2.67***
Dipeptidyl peptidase 2	*Dpp7*	*4*	***100.00***	*0.92*	***14.61***
Isoform 2 of Protein ECT2	*Ect2*	*5*	***5.83***	*1.12*	***100.00***
Isoform 2 of ER membrane protein complex subunit 1	*Emc1*	*8*	***4.40***	*0.99*	***2.29***
Erlin-2	*Erlin2*	*15*	***19.97***	*1.06*	***2.86***
ERO1-like protein alpha	*Ero1l*	*7*	***100.00***	*1.70*	***2.85***
Endoplasmic reticulum resident protein 44	*Erp44*	*4*	***2.09***	*1.19*	***2.37***
Protein Fam38a	*Fam38a*	*15*	***6.75***	*1.33*	***2.15***
Lysosomal alpha-glucosidase	*Gaa*	*11*	***20.25***	*0.88*	***2.28***
Golgi apparatus protein 1 (Fragment)	*Glg1*	*22*	***2.07***	*1.19*	***2.19***
Uncharacterized protein	*Gm17386*	*7*	***100.00***	*0.63*	***2.52***
Glutathione S-transferase omega-1	*Gsto1*	*3*	***5.22***	*0.63*	***8.74***
G2 and S phase-expressed protein 1	*Gtse1*	*14*	***3.84***	*0.77*	***53.91***
3-hydroxyisobutyrate dehydrogenase, mitochondrial	*Hibadh*	*6*	***3.48***	*1.19*	***2.18***
Isoform 2 of Intercellular adhesion molecule 1	*Icam1*	*5*	***100.00***	*0.90*	***100.00***
Isochorismatase domain-containing protein 2A, mitochondrial	*Isoc2a*	*7*	***3.17***	*0.74*	***2.69***
Kinesin-like protein KIF22	*Kif22*	*11*	***3.60***	*1.45*	***8.91***
Protein Kifc5b	*Kifc5b*	*11*	***4.44***	*0.86*	***2.63***
Ragulator complex protein LAMTOR2	*Lamator2*	*5*	***100.00***	*1.38*	***59.07***

Lysosome-associated membrane glycoprotein 1	*Lamp1*	*3*	***100.00***	*1.13*	***2.19***
LETM1 and EF-hand domain-containing protein 1, mitochondrial	*Letm1*	*6*	***5.49***	*0.86*	***11.98***
Alpha-2-macroglobulin receptor-associated protein	*Lrpap1*	*22*	***100.00***	*0.74*	***2.87***
Mitotic spindle assembly checkpoint protein MAD1	*Mad1l*	*7*	***5.05***	*1.60*	***2.30***
E3 ubiquitin-protein ligase MARCH5	*March.5*	*9*	***100.00***	*1.16*	***16.44***
LDLR chaperone MESD	*Mesdc2*	*5*	***2.23***	*1.14*	***2.34***
Melanoregulin	*Mreg*	*4*	***7.12***	*0.93*	***100.00***
Isoform 2 of Metastasis-associated protein MTA3	*Mta3*	*6*	***9.13***	*1.10*	***100.00***
Isoform 2 of Mitochondrial carrier homolog 1	*Mtch1*	*5*	***100.00***	*0.87*	***4.31***
Protein LYRIC	*Mtdh*	*6*	***17.98***	*1.50*	***24.85***
Myeloid-associated differentiation marker	*Myadm*	*4*	***100.00***	*1.06*	***2.32***
Myoferlin	*Myof*	*32*	***28.55***	*0.89*	***100.00***
NADH dehydrogenase [ubiquinone] 1 beta subcomplex subunit 8, mitochondria	*Ndufb8*	*5*	***5.87***	*1.07*	***2.28***
NADH dehydrogenase [ubiquinone] iron-sulfur protein 6, mitochondrial	*Ndufs6*	*5*	***22.23***	*1.13*	***9.16***
NADH dehydrogenase [ubiquinone] flavoprotein 1, mitochondrial	*Ndufv1*	*9*	***100.00***	*1.51*	***2.17***
E3 ubiquitin-protein ligase NEDD4	*Nedd4*	*26*	***0.49***	*1.19*	***0.49***
Nipsnap homolog 3A (C. elegans)	*Nipsnap3b*	*6*	***2.10***	*1.03*	***2.85***
Nodal modulator 1	*Nomo1*	*13*	***21.42***	*1.00*	***2.45***
Protein Nup153	*Nup153*	*14*	***5.75***	*0.89*	***2.16***
Prenylcysteine oxidase-like	*Pcyox1l*	*6*	***10.73***	*1.02*	***4.56***
Membrane-associated progesterone receptor component 2	*Pgrmc2*	*5*	***15.36***	*1.15*	***2.21***
Inorganic pyrophosphatase 2, mitochondrial	*Ppa2*	*5*	***5.40***	*1.19*	***9.28***
DNA-directed RNA polymerase I subunit RPA49 (Fragment)	*Pplr1e*	*3*	***100.00***	*1.86*	***7.12***
Phosphoribosyl pyrophosphate synthase-associated protein 2	*Prpsap2*	*6*	***22.29***	*0.91*	***7.13***
Sulfated glycoprotein 1	*Psap*	*9*	***2.25***	*0.88*	***100.00***
Ras-related protein Rap-2b	*Rap2b*	*3*	***2.11***	*0.87*	***100.00***
mRNA cap guanine-N7 methyltransferase	*Rnmt*	*11*	***2.13***	*1.39*	***9.78***
Dolichyl-diphosphooligosaccharide--protein glycosyltransferase subunit 2	*Rpn2*	*14*	***2.19***	*1.10*	***2.50***
Protein S100-A6	*S100a6*	*5*	***2.05***	*0.60*	***2.64***
U4/U6.U5 tri-snRNP-associated protein 1	*Sart1*	*6*	***6.26***	*1.17*	***8.04***
Signal peptidase complex catalytic subunit SEC11A	*Sec11a*	*8*	***2.50***	*0.96*	***2.69***
Sphingosine-1-phosphate lyase 1	*Sgpl1*	*12*	***100.00***	*1.06*	***3.35***
Solute carrier family 12 member 7	*Slc12a7*	*5*	***100.00***	*1.12*	***100.00***

Mitochondrial 2-oxoglutarate/malate carrier protein	*Slc25a11*	*9*	***100.00***	*0.98*	***2.26***
Calcium-binding mitochondrial carrier protein Aralar1	*Slc25a12*	*3*	***5.06***	*1.91*	***3.55***
Mitochondrial carnitine/acylcarnitine carrier protein	*Slc25a20*	*9*	***4.31***	*0.72*	***10.18***
Beta-2-syntrophin	*Sntb*	*8*	***100.00***	*1.42*	***2.05***
Serum response factor-binding protein 1	*Srfbp*	*5*	***100.00***	*0.90*	***2.21***
Serine/arginine repetitive matrix 1	*Srrm1*	*7*	***6.98***	*1.04*	***100.00***
Dolichyl-diphosphooligosaccharide--protein glycosyltransferase subunit STT3A	*Stt3a*	*17*	***2.03***	*1.04*	***2.07***
ATP-dependent RNA helicase SUPV3L1, mitochondrial	*Supv3l1*	*5*	***2.23***	*0.74*	***9.60***
Transmembrane and coiled-coil domain-containing protein 1	*Tmco1*	*6*	***6.88***	*1.02*	***3.13***
Transmembrane protein 43	*Tmm43*	*5*	***100.00***	*1.27*	***100.00***
Thioredoxin-related transmembrane protein 1	*Tmx1*	*6*	***3.86***	*1.17*	***10.83***
UDP-glucose:glycoprotein glucosyltransferase 1	*Uggt1*	*21*	***2.05***	*0.99*	***2.53***
Isoform Mt-VDAC1 of Voltage-dependent anion-selective channel protein 1	*Vdac1*	*16*	***2.06***	*0.84*	***3.07***
Voltage-dependent anion-selective channel protein 2 (Fragment)	*Vdac1*	*12*	***2.10***	*0.88*	***2.62***
Voltage-dependent anion-selective channel protein 3	*Vdac3*	*10*	***2.54***	*1.00*	***2.07***

Table 20: ECM proteins

Description	*Gene*	*Σ# Unique peptides*	*3S/2D*	*3S/3D*	*3D/2D*
Anastellin	*Fn1*	*38*	*100.0*	*1.1*	*24.0*
Nidogen-2	*Nid2*	*6*	*100.0*	*0.9*	*17.4*
Laminin subunit alpha-5	*Lama5*	*18*	*29.4*	*0.8*	*100.0*
Myoferlin	*Myof*	*32*	*28.6*	*0.9*	*100.0*
Isoform 3 of Agrin	*Agr*	*10*	*25.6*	*1.0*	*53.2*
Basement membrane-specific heparan sulfate proteoglycan	*Hspg2*	*54*	*11.0*	*1.0*	*16.6*
Isoform 3 of Collagen alpha-1(XVIII) chain	*col18a1*	*6*	*9.8*	*1.1*	*27.9*
Lamin-B2	*Lmnb2*	*20*	*4.0*	*1.0*	*1.9*
Pinin	*Pin*	*11*	*3.4*	*1.1*	*2.4*
Apolipoprotein E	*Apoe*	*18*	*2.4*	*0.9*	*5.4*
Sulfated glycoprotein 1	*Psap*	*9*	*2.3*	*0.9*	*100.0*
Laminin subunit gamma-1	*Lamc1*	*11*	*2.1*	*1.0*	*1.8*

Table 21: Cell Cycle Arrest Proteins on both 3D Cultures

Description	Gene	Σ# Uniq pept	2D/3Ds: H/L	3Ds/3Dd: H/L	3Dd/2D:H/L
G2 and S phase-expressed protein 1	Gtse1	14	3.846154	0.771	53.907
Bromodomain adjacent to zinc finger domain protein 2A	Baz2a	13	9.433962	1.57	7.376
Isoform 2 of Cell division cycle protein 23 homolog	Cdc23	8	100	0.768	6.002
Cytoskeleton-associated protein 2	Cap2	9	100	0.759	3.588
Isoform 2 of Inner centromere protein	Incenp	5	100	100	2.689
Cytoskeleton-associated protein 4	Ckap4	25	2.816901	1.04	2.573

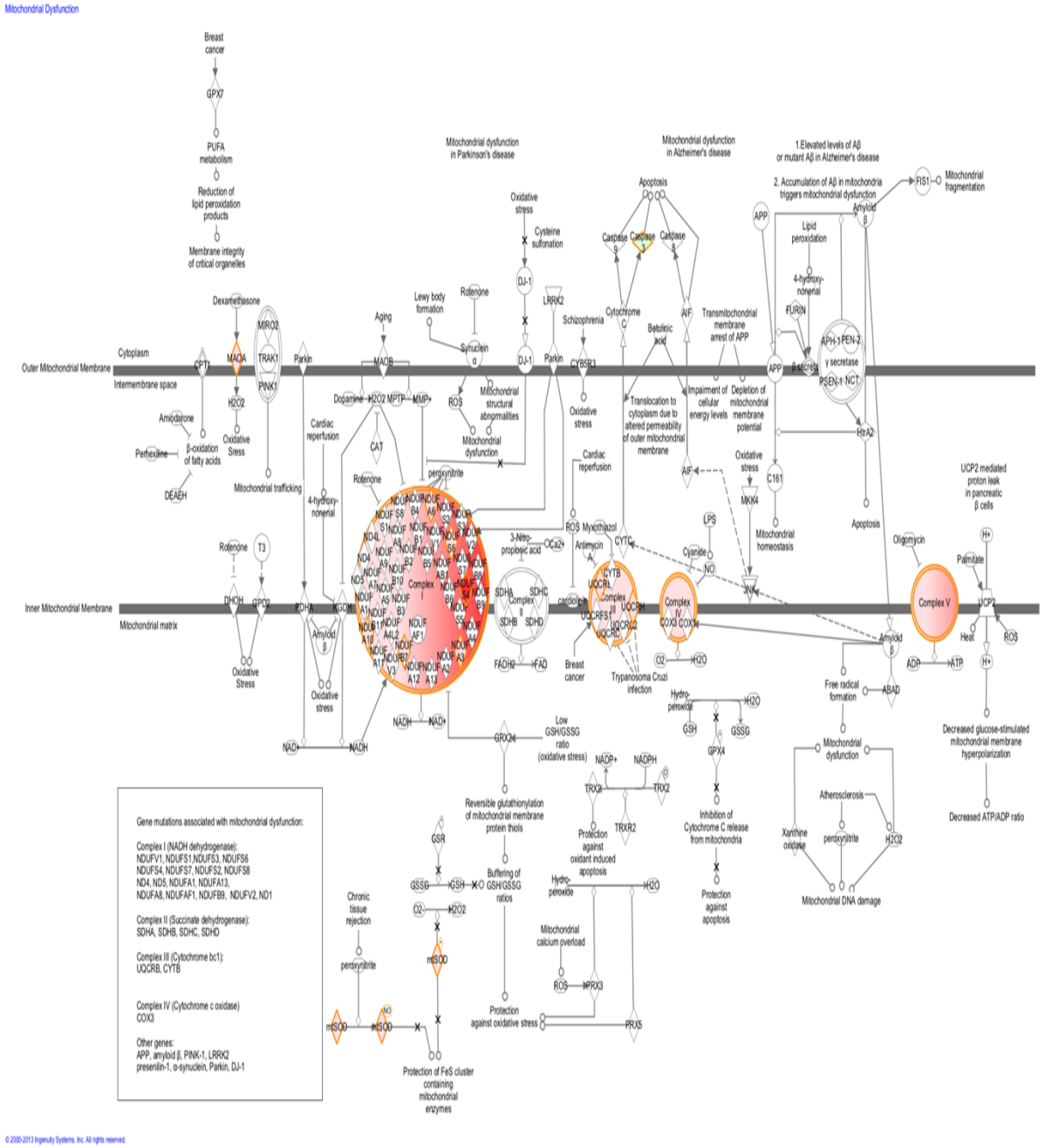

Figure 50: Oxidative Phosphorylation Up-regulation in 3D dynamic vs. 2D culture

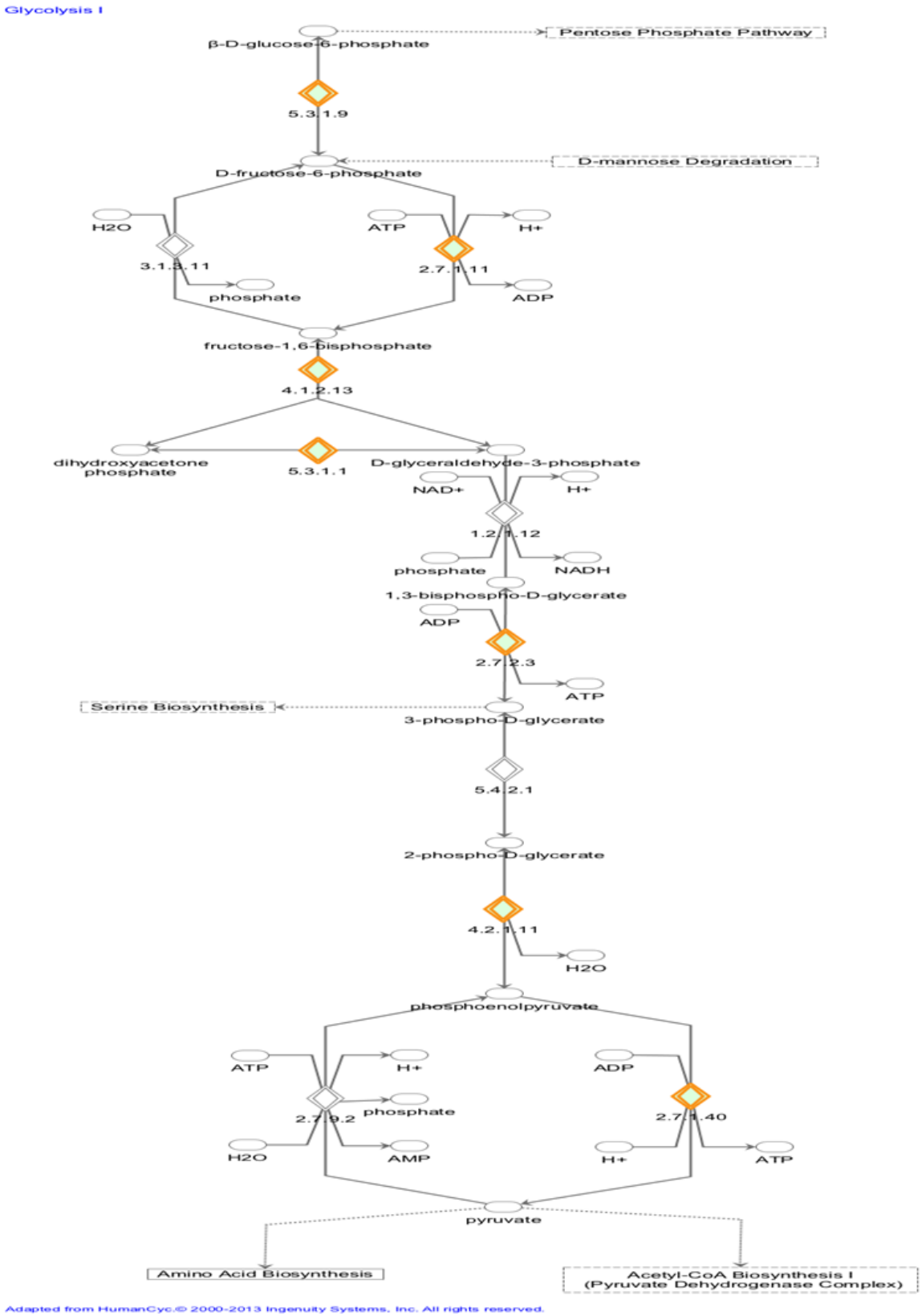

Figure 51: Glycolysis Down-regulation in 2D vs. 3D dynamic

Table 22: List of Abberviation

Abbreviation	Definition
EB	Embryoid Bodies
EC	Embryonic Carcinoma
µL	Micro letter
1D gel	1-dimensional gel electrophoresis
2D	Monolayer Plastic Culture Flask
2-DE	Two-dimensional gel electrophoresis
3D	Alginate encapsulated 3D culture
Acca2	Thiolase
ASC	Adult Stem Cells
ATCC	American Type Culture Collection
ATP	Adenosine triphosphate
Ba2+	Barium
BAC	Benzyldimethyl-n-hexadacylammonium chloride
BM	Basement membrane
BMP	Bone Morphogenic Protein
BSA	Bovine serum albumin
Ca+2	Calcium Ion
CaCl2	Calcium chloride
CDK2	Cyclin-dependent kinase 2
CDK4	Cyclin-dependent kinase 4
CHAPS	Zwitterionic detergent
CID	Collision induced dissociation
CSCs	Cancer stem cell
Ctnnb1	Catenin (cadherin-associated protein), beta 1
Cyb5b	Cytochrome b5 type B
DIGE	Difference gel electrophoresis
DIGE	2-D Fluorescence Difference Gel Electrophoresis
DMEM	Dulbecco's Modified Eagles Media
DNA	Deoxyribonucleic acid
DNMTs	DNA methyltransferase
DRB	Damage repair break
DSB	Double strand break
DTT	Dithiothreitol
ECAR	Extracellular acidifications rates
ECD	Electron capture detection
ECL	Electro chemi luminescence
ECM	Extracellular Matrix
ECM	Extracellular cellular matrix
ECM	Extracellular matrix
ECM	Extracellular matrix
EDTA	Ethylene diamine tetra acetic
Eif5b	Translation initiation proteins
ELISA	Enzyme-linked immunosorbent assay

EMT	Epithelial mesenchymal transition
EpiSCs	Epiblast Stem Cells
ER	Endoplasmic Reticulum
ERAD	Endoplasmic-reticulum-associated protein degradation
ERK	Extracellular-signal-regulated kinase
ERK1/2	mitogen-activated protein kinase
ESCs	Embryonic stem cells
ESI	Electrospray ionization
ESN2	DMEM/F12 supplemented with N2 (transferrin, insulin, progesterone, putrecine and selenite 9), LIF and basic FGF
ETC	Electron transport chain
ETD	Electron transfer dissociation
EthD-1	Ethidium homodimer-1
FASP	filter-aided sample preparation
FBS	Fetal bovine serum
FBS	Foetal bovine serum
FCCP	p-triflouromethoxyphenylhydrazone
FGF	Fibroblast Growth Factor
FGF4	fibroblast growth factor-4
FITC	Fluorescein isothiocyanate
FN	Fibronectin
FSCs	Foetal Stem Cells
FT-ICR	Fourier transform ion cyclotron resonance
GAGs	Glycosaminoglycans ECM protein
GO	Gene ontology
GOI	Gene of interest
GP	Grade plastic
GSK3	Glycogen synthase kinase 3
H2O2	Hydrogen peroxide
H4, H3, H2A and H2b	Major families of histones
HARV	high aspect ratio vessel
HCD	Higher-energy C-trap dissociation
HECTD1	HECT domain containing E3 ubiquitin protein ligase 1
hESC's	Human embryonic stem cells
hiPSCs	Human Induced Pluripotent stem cells
HO	Hydroxyl radicals
HRP	Horseradish peroxidase
HSC	Haematopoietic Stem Cell
HSP	Heat shock proteins
HSPG2	Heparan sulphate proteoglycan core protein
Hsps	Heat shocks proteins
ICC	Immunocytochemistry
ICM	Inner Cell MAss
IgG	Immunoglobulin G
ISD	In-solution digested
KORS	Knockout replacement serum

KSR	Knockout serum replacement
kPa	kilopascal
LC	Liquid chromatography
LC/MSMS	Liquid chromatography–mass spectrometry
LIF	Leukemic Inhibitor Factor
LIT	Ion trap
LN	Laminin
MALDI	Matrix-assisted laser desorption ionization
MAPK	Mitogen-activated protein kinase
MDCK	Madin-Darby canine kidney
MEFs	Mouse embryonic fibroblast cells
mEpiSCs	Mouse epiblast stem cells
MESC's	Mouse embryonic stem cells
MET	Mesenchymal–epithelial transition
MF	Mouse Feeder
MGF2	Fibroblast Growth Factor 2
mRNA	Messenger RNA
MS	Mass Spectrometry
MS	Mass spectrometry
MSC	Mesnchymal stem cells
MSCs	Mesenchymal stem cell
MTS	[3-(4,5-dimethylthiazol-2-yl)-5-(3-carboxymethoxyphenyl)-2-(4-sulfophenyl)-2H-tetraz
Myh9	Cytoskeleton myosin 9
NAD+	nicotinamide adenine dinucleotide
O2. -	Superoxide anion
OCR	Oxygen consumption rates
OMM	Outer membrane
PBS	Phosphate buffered saline
PCR	Polymerase chain reaction
Pcyox1l	Cysteine oxidase
PDMS	Polydimethylsiloxane
PE	Primitive endoderm
PGCs	Primordial germ cell
PPP	Pentose phosphate pathway
Prdx2	Peroxiredoxin-2
PSCs	Pluripotent Stem Cells
Psmb1 and Psmb3	Psmb1 and Psmb3
Psmg1, Psmg3	Proteasomes
PTM	Post-translational modifications
PVDF	Polyvinylidene difluoride
rBM	Reconstituted basement membrane
RIPA	Radio-Immunoprecipitation Assay
RLT	Lysis of cells and tissues before RNA isolation
ROS	Reactive oxygen species
RP	Reversed phase
RPM	revolutions per minute

RT-PCR	Reverse transcription-polymerase chain reaction
RWV	Rotating wall vessel
SC	Stem Cells
Sca-1+	Cell surface antigen used in the isolation of hematopoietic stem cells
SCX	Strong cation exchange
SDS	Sodium dodecyl sulfate polyacrylamide gel electrophoresis
SILAC	Stable isotope labelling of amino acids in cell culture
SSEA	Specific surface antigens embryonic antigens
STLV	Slow turning lateral vessel
Tcf3	Transcription factor 3
TE	Trophectoderm
TEM	Transmission electron microscopy
TMT	Tandem mass tags
TOF	Time of flight
UPR	Unfolded-protein repair mechanism
VDAC	Voltage-dependent anion channel
XF	Extracellular Flux Analyzers
qPCR	Quantitative PCR
RT-PCR	Real-time polymerase chain reaction

Table 23: List of Protein Abberviation

Abbreviation	Definition
NADH	Nicotinamide adenine dinucleotide
OCt4/POU5F1	octamer-binding transcription factor 4
Aldoa	Fructose-bisphosphate aldolase A
Asf1a	Histone chaperone
ATF6	Activating transcription factor 6
Atp5i	ATP synthase subunit e
Atp5j2	ATP synthase subunit f
Atp5l	ATP synthase subunit g
ATRX	Transcriptional regulator ATRX
Bcl2	B-cell lymphoma 2
CD9	Surface antigen marker
Cdc23	Isoform 2 of Cell division cycle protein 23 homolog
Cdk2ap1	Cyclin-dependent kinase 2-associated protein 1
Cdk4	Cyclin-dependent kinase 4
Cdk7	Cyclin-dependent kinase 7
Ckap2	Cytoskeleton-associated protein 2
Cox4i	Cytochrome c oxidase subunit 4 isoform 1
Cox7c	Cytochrome c oxidase subunit 7C
Cyb5b	Cytochrome b5 type B
Dnaj	groups of chaperone DnaJ
DNMT1	DNA (cytosine-5)-methyltransferase 1
DNMT3A	Isoform 2 of DNA (cytosine-5)-methyltransferase 3A
DNMT3b	Isoform 3 of DNA (cytosine-5)-methyltransferase 3B
Dppa5a	Developmental pluripotency-associated protein 5A
Dpsyl2	Dihydropyrimidinase-related protein 2
DSB	Double Strnad Break
ECM	Extracellular Matrix Protein
Eif	Eukaryotic initiation facto
Eif2b5	Translation initiation factor eIF-2B subunit epsilon
Eif4a2	Eukaryotic initiation factor 4A-II
Eif5b	Eukaryotic translation initiation factor 5B
Eif2a	Eukaryotic translation initiation factor 2A
EMT	Epithelial-Mesencymal transition
Eno1	Alpha-enolase
ER	Endoplasmic Reticulum
ERAD	ER-associated degradation
ERK1/2	extracellular-signal-regulated kinases
Ero1a	ERO1-like protein alpha
ETC	Elctron Transfer Chain
FGF2	Fibroblast Growth Factor 2
FGF4	Fibroblast Growth Factor 4
FGF5	Fibroblast Growth Factor 5
FN	Fibronectin

G1 phase	Growth1 or Gap 1 Phasae
Gmpr2	GMP reductase 2
Gsto1	Glutathione S-transferase omega-1
HECTD1	E3 ubiquitin-protein ligase HECTD1
Hsp70	Heat shock Protein 70
HSPG2	Basement membrane-specific heparan sulfate proteoglycan core protein
IP3Rs	1,4,5-trisphosphate receptors
iPSC	Induced Pluripotent Stem Cells
IRE1	ser/thr protein kinase
kdm3a	Lysine-specific demethylase 3A
Kif11	Kinesin-like protein
Kifc1	Kinesin-like protein
Kntc1	Kinetochore-associated protein 1
LDA	L-lactate dehydrogenase A
LIN28a	Protein lin-28 homolog A
LN	Laminin
Lys9	Lysine 9
MET	Mesnchymal-Epithelial transition
Morc3	MORC family CW-type zinc finger protein 3
Msh3	DNA mismatch repair protein
Mta3	Isoform 2 of Metastasis-associated protein
Myh9	Myosin-9
NAD +	NADH dehydrogenase
Nanog	Homeobox transcription factor protein
NCPI	National Center for Biotechnology Information
Ndufb4	NADH dehydrogenase [ubiquinone] 1 beta subcomplex subunit 4
Ndufc2	NADH dehydrogenase [ubiquinone] 1 subunit C2
Nup214	Nuclear pore complex protein
OMM	outer mitochondrial membrane
Orc1	Origin recognition complex subunit 1
P21	cyclin-dependent kinase inhibitor 1
Pafah1b3	Platelet-activating factor acetylhydrolase IB subunit gamma
Pcyox1l	Prenylcysteine oxidase-like
Pdcd5	Programmed cell death protein 5
PERK	protein kinase RNA-like endoplasmic reticulum kinase
Pfkl	6-phosphofructokinase, liver type
Pgk1	Phosphoglycerate kinase 1
Pkm	Isoform M1 of Pyruvate kinase isozymes M1/M2
Pnn	Pinin
PPP	phosphoprotein phosphatase
PQC	Protein Quality Control
Prdx2	Peroxiredoxin-2
PRM1	protamine 1
Psma2	Proteasome subunit alpha type-2
Psmb1	Proteasome subunit beta type-1
Psmb3	Proteasome subunit beta type-3

Psmg1	Proteasome assembly chaperone 1
Psmg3	Proteasome assembly chaperone 3
Rbx1	E3 ubiquitin-protein ligase
Rnmt	mRNA cap guanine-N7 methyltransferase
Romo1	Reactive oxygen species modulator 1
Rps4y2	Ribosomal protein S4, Y-linked 2
Rtn3	Isoform 3 of Reticulon-3
Rtn4	Reticulon-4
Slc25a3	Phosphate carrier protein
Smchd1	Structural maintenance of chromosomes flexible hinge domain-containing protein 1
Snai1	Zinc finger protein
Sod2	Superoxide dismutase
Ssr4	Translocon-associated protein subunit delta
SSEA1	stage-specific embryonic antigen-1
Ssr3	Isoform 2 of Translocon-associated protein subunit gamma
Thrap3	Thyroid hormone receptor-associated protein 3
Tmx1	Thioredoxin-related transmembrane protein 1
Tmx2	Thioredoxin-related transmembrane protein 2
Tpr	Nuclear pore complex-associated intranuclear coiled-coil protein
Ube2k	Ubiquitin-conjugating enzyme E2 K
Ube4b	Ubiquitin conjugation factor E4 B
Uhrf1	E3 ubiquitin-protein ligase
UPR	Unfolded protein response
Uqcrfs1	Cytochrome b-c1 complex subunit Rieske
Uqcrh	Cytochrome b-c1 complex subunit 6
Uqcrq	Cytochrome b-c1 complex subunit 8
VDAC	Voltage-dependent anion-selective channel protein
Vdac1	Voltage-dependent anion-selective channel protein 1
Vdac2	Voltage-dependent anion-selective channel protein 2
Vdac3	Voltage-dependent anion-selective channel protein 3
XBP1	X-box binding protein 1
X-linked	located in X chromosome
Y-linked region	located in Y chromosome

References

AHN, S. M., SIMPSON, R. & LEE, B. 2010. Genomics and proteomics in stem cell research: the road ahead. *Anat Cell Biol,* 43**,** 1-14.

AMOEDO, N. D., VALENCIA, J. P., RODRIGUES, M. F., GALINA, A. & RUMJANEK, F. D. 2013. How does the metabolism of tumour cells differ from that of normal cells. *Biosci Rep,* 33.

ANDERSON, L. & SEILHAMER, J. 1997. A comparison of selected mRNA and protein abundances in human liver. *Electrophoresis,* 18**,** 533-7.

ANDREWS, P. W., BENVENISTY, N., MCKAY, R., PERA, M. F., ROSSANT, J., SEMB, H. & STACEY, G. N. 2005. The International Stem Cell Initiative: toward benchmarks for human embryonic stem cell research. *Nat Biotechnol,* 23**,** 795-7.

APPELLA, E. & ANDERSON, C. W. 2007. New prospects for proteomics--electron-capture (ECD) and electron-transfer dissociation (ETD) fragmentation techniques and combined fractional diagonal chromatography (COFRADIC). *Febs j,* 274**,** 6255.

AZARIN, S. M., LARSON, E. A., ALMODOVAR-CRUZ, J. M., DE PABLO, J. J. & PALECEK, S. P. 2012a. Effects of 3D microwell culture on growth kinetics and metabolism of human embryonic stem cells. *Biotechnol Appl Biochem,* 59**,** 88-96.

AZARIN, S. M., LARSON, E. A., ALMODÓVAR-CRUZ, J. M., DE PABLO, J. J. & PALECEK, S. P. 2012b. Effects of 3-D microwell culture on growth kinetics and metabolism of human embryonic stem cells. *Biotechnology and applied biochemistry,* 59**,** 88-96.

AZARIN, S. M. & PALECEK, S. P. 2010. Development of Scalable Culture Systems for Human Embryonic Stem Cells. *Biochem Eng J,* 48**,** 378.

BAHARVAND, H., FATHI, A., GOURABI, H., MOLLAMOHAMMADI, S. & SALEKDEH, G. H. 2008. Identification of mouse embryonic stem cell-associated proteins. *J Proteome Res,* 7**,** 412-23.

BAHARVAND, H., FATHI, A., VAN HOOF, D. & SALEKDEH, G. H. 2007a. Concise Review: Trends in Stem Cell Proteomics. *STEM CELLS,* 25**,** 1888-1903.

BAHARVAND, H., FATHI, A., VAN HOOF, D. & SALEKDEH, G. H. 2007b. Concise review: trends in stem cell proteomics. *Stem Cells,* 25**,** 1888-903.

BAKER, B. M. & CHEN, C. S. 2012. Deconstructing the third dimension – how 3D culture microenvironments alter cellular cues. *Journal of Cell Science,* 125**,** 3015-3024.

BARRALLO-GIMENO, A. & NIETO, M. A. 2005. The Snail genes as inducers of cell movement and survival: implications in development and cancer. *Development,* 132**,** 3151-61.

BENDALL, S. C., HUGHES, C., CAMPBELL, J. L., STEWART, M. H., PITTOCK, P., LIU, S., BONNEIL, E., THIBAULT, P., BHATIA, M. & LAJOIE, G. A. 2009. An enhanced mass spectrometry approach reveals human embryonic stem cell growth factors in culture. *Mol Cell Proteomics,* 8**,** 421-32.

BENDALL, S. C., HUGHES, C., STEWART, M. H., DOBLE, B., BHATIA, M. & LAJOIE, G. A. 2008. Prevention of amino acid conversion in SILAC experiments with embryonic stem cells. *Mol Cell Proteomics,* 7**,** 1587-97.

BENOIT, D. S., SCHWARTZ, M. P., DURNEY, A. R. & ANSETH, K. S. 2008. Small functional groups for controlled differentiation of hydrogel-encapsulated human mesenchymal stem cells. *Nat Mater,* 7**,** 816-23.

BERNEMANN, C., GREBER, B., KO, K., STERNECKERT, J., HAN, D. W., ARAUZO-BRAVO, M. J. & SCHOLER, H. R. 2011. Distinct developmental ground states of epiblast stem cell lines determine different pluripotency features. *Stem Cells,* 29**,** 1496-503.

BERNFIELD, M., GOTTE, M., PARK, P. W., REIZES, O., FITZGERALD, M. L., LINCECUM, J. & ZAKO, M. 1999. Functions of cell surface heparan sulfate proteoglycans. *Annu Rev Biochem,* 68**,** 729-77.

BERTOLOTTI, A., BORGOGNA, M., FACOETTI, A., MARSICH, E. & NANO, R. 2009. The effects of alginate encapsulation on NIT-1 insulinoma cells: viability, growth and insulin secretion. *In Vivo,* 23**,** 929-35.

BHATTACHARYA, B., MIURA, T., BRANDENBERGER, R., MEJIDO, J., LUO, Y., YANG, A. X., JOSHI, B. H., GINIS, I., THIES, R. S., AMIT, M., LYONS, I., CONDIE, B. G., ITSKOVITZ-ELDOR, J., RAO, M. S. & PURI, R. K. 2004. Gene expression in human embryonic stem cell lines: unique molecular signature. *Blood,* 103**,** 2956-64.

BOUTILIER, K., ROSS, M., PODTELEJNIKOV, A. V., ORSI, C., TAYLOR, R., TAYLOR, P. & FIGEYS, D. 2005. Comparison of different search engines using validated MS/MS test datasets. *Analytica Chimica Acta,* 534**,** 11-20.

BOYER, L. A., LEE, T. I., COLE, M. F., JOHNSTONE, S. E., LEVINE, S. S., ZUCKER, J. P., GUENTHER, M. G., KUMAR, R. M., MURRAY, H. L., JENNER, R. G., GIFFORD, D. K., MELTON, D. A., JAENISCH, R. & YOUNG, R. A. 2005. Core transcriptional regulatory circuitry in human embryonic stem cells. *Cell,* 122**,** 947-56.

BRADLEY, A., EVANS, M., KAUFMAN, M. H. & ROBERTSON, E. 1984. Formation of germ-line chimaeras from embryo-derived teratocarcinoma cell lines. *Nature,* 309**,** 255-6.

BREWIS, I. A. & BRENNAN, P. 2010. Proteomics technologies for the global identification and quantification of proteins. *Adv Protein Chem Struct Biol,* 80**,** 1-44.

BRILL, L. M., XIONG, W., LEE, K.-B., FICARRO, S. B., CRAIN, A., XU, Y., TERSKIKH, A., SNYDER, E. Y. & DING, S. 2009. Phosphoproteomic Analysis of Human Embryonic Stem Cells. *Cell Stem Cell,* 5**,** 204-213.

BRONS, I. G., SMITHERS, L. E., TROTTER, M. W., RUGG-GUNN, P., SUN, B., CHUVA DE SOUSA LOPES, S. M., HOWLETT, S. K., CLARKSON, A., AHRLUND-RICHTER, L., PEDERSEN, R. A. & VALLIER, L. 2007. Derivation of pluripotent epiblast stem cells from mammalian embryos. *Nature,* 448**,** 191-5.

CARRACEDO, A., CANTLEY, L. C. & PANDOLFI, P. P. 2013. Cancer metabolism: fatty acid oxidation in the limelight. *Nat Rev Cancer,* 13**,** 227-32.

CARSON, D. D., TANG, J. P. & JULIAN, J. 1993. Heparan sulfate proteoglycan (perlecan) expression by mouse embryos during acquisition of attachment competence. *Dev Biol,* 155**,** 97-106.

CHAMBERS, I., SILVA, J., COLBY, D., NICHOLS, J., NIJMEIJER, B., ROBERTSON, M., VRANA, J., JONES, K., GROTEWOLD, L. & SMITH, A. 2007. Nanog safeguards pluripotency and mediates germline development. *Nature,* 450**,** 1230-4.

CHANG, T.-C., CHEN, Y.-C., YANG, M.-H., CHEN, C.-H., HSING, E.-W., KO, B.-S., LIOU, J.-Y. & WU, K. K. 2010a. Rho Kinases Regulate the Renewal and Neural Differentiation of Embryonic Stem Cells in a Cell Plating Density–Dependent Manner. *PLoS ONE,* 5**,** e9187.

CHANG, T. C., CHEN, Y. C., YANG, M. H., CHEN, C. H., HSING, E. W., KO, B. S., LIOU, J. Y. & WU, K. K. 2010b. Rho kinases regulate the renewal and neural differentiation of embryonic stem cells in a cell plating density-dependent manner. *PLoS One,* 5**,** e9187.

CHAUDHRY, M. A., BOWEN, B. D. & PIRET, J. M. 2009. Culture pH and osmolality influence proliferation and embryoid body yields of murine embryonic stem cells. *Biochemical Engineering Journal,* 45**,** 126-135.

CHAYOSUMRIT, M., TUCH, B. & SIDHU, K. 2010. Alginate microcapsule for propagation and directed differentiation of hESCs to definitive endoderm. *Biomaterials,* 31**,** 505-14.

CHEN, X., CHEN, A., WOO, T. L., CHOO, A. B., REUVENY, S. & OH, S. K. 2010. Investigations into the metabolism of two-dimensional colony and suspended microcarrier cultures of human embryonic stem cells in serum-free media. *Stem Cells Dev,* 19**,** 1781-92.

CHERNUSHEVICH, I. V., LOBODA, A. V. & THOMSON, B. A. 2001. An introduction to quadrupole–time-of-flight mass spectrometry. *Journal of Mass Spectrometry,* 36**,** 849-865.

CHOWDHURY, F., LI, Y., POH, Y. C., YOKOHAMA-TAMAKI, T., WANG, N. & TANAKA, T. S. 2010a. Soft substrates promote homogeneous self-renewal of embryonic stem cells via downregulating cell-matrix tractions. *PLoS One,* 5**,** e15655.

CHOWDHURY, F., NA, S., LI, D., POH, Y. C., TANAKA, T. S., WANG, F. & WANG, N. 2010f. Material properties of the cell dictate stress-induced spreading and differentiation in embryonic stem cells. *Nat Mater,* 9**,** 82-8.

CHU, J. H., YU, S., HAYWARD, S. W. & CHAN, F. L. 2009. Development of a three-dimensional culture model of prostatic epithelial cells and its use for the study of epithelial-mesenchymal transition and inhibition of PI3K pathway in prostate cancer. *Prostate,* 69**,** 428-42.

CLAPHAM, D. E. 2007. Calcium signaling. *Cell,* 131**,** 1047-58.

CLIMENT, M., ALONSO-MARTIN, S., PEREZ-PALACIOS, R., GUALLAR, D., BENITO, A. A., LARRAGA, A., FERNANDEZ-JUAN, M., SANZ, M., DE DIEGO, A., SEISDEDOS, M. T., MUNIESA, P. & SCHOORLEMMER, J. 2013. Functional analysis of Rex1 during preimplantation development. *Stem Cells Dev,* 22**,** 459-72.

CLOONAN, N., FORREST, A. R., KOLLE, G., GARDINER, B. B., FAULKNER, G. J., BROWN, M. K., TAYLOR, D. F., STEPTOE, A. L., WANI, S., BETHEL, G., ROBERTSON, A. J., PERKINS, A. C., BRUCE, S. J., LEE, C. C., RANADE, S. S., PECKHAM, H. E., MANNING, J. M., MCKERNAN, K. J. & GRIMMOND, S. M. 2008. Stem cell transcriptome profiling via massive-scale mRNA sequencing. *Nat Methods,* 5**,** 613-9.

COSTELL, M., GUSTAFSSON, E., ASZODI, A., MORGELIN, M., BLOCH, W., HUNZIKER, E., ADDICKS, K., TIMPL, R. & FASSLER, R. 1999. Perlecan maintains the integrity of cartilage and some basement membranes. *J Cell Biol,* 147**,** 1109-22.

COVELLO, K. L., KEHLER, J., YU, H., GORDAN, J. D., ARSHAM, A. M., HU, C. J., LABOSKY, P. A., SIMON, M. C. & KEITH, B. 2006. HIF-2alpha regulates Oct-4: effects of hypoxia on stem cell function, embryonic development, and tumor growth. *Genes Dev,* 20**,** 557-70.

CRAWFORD-YOUNG, S. J. 2006. Effects of microgravity on cell cytoskeleton and embryogenesis. *Int J Dev Biol,* 50**,** 183-91.

DAHERON, L., OPITZ, S. L., ZAEHRES, H., LENSCH, M. W., ANDREWS, P. W., ITSKOVITZ-ELDOR, J. & DALEY, G. Q. 2004. LIF/STAT3 signaling fails to maintain self-renewal of human embryonic stem cells. *Stem Cells,* 22**,** 770-8.

DANCIK, V., ADDONA, T. A., CLAUSER, K. R., VATH, J. E. & PEVZNER, P. A. 1999. De novo peptide sequencing via tandem mass spectrometry. *J Comput Biol,* 6**,** 327-42.

DOMON, B. & AEBERSOLD, R. 2006. Mass spectrometry and protein analysis. *Science,* 312**,** 212-7.

DOMON, B. & AEBERSOLD, R. 2010. Options and considerations when selecting a quantitative proteomics strategy. *Nat Biotechnol,* 28**,** 710-21.

ENGLER, A. J., SEN, S., SWEENEY, H. L. & DISCHER, D. E. 2006. Matrix elasticity directs stem cell lineage specification. *Cell,* 126**,** 677-89.

EVANS, M. J. & KAUFMAN, M. H. 1981. Establishment in culture of pluripotential cells from mouse embryos. *Nature,* 292**,** 154-6.

EVANS, N., MINELLI, C., GENTLEMAN, E., LAPOINTE, V., PATANKAR, S., KALLIVRETAKI, M., CHEN, X., ROBERTS, C. & STEVENS, M. 2009. Substrate stiffness affects early differentiation events in embryonic stem cells. *European Cells and Materials,* 18**,** 1-14.

FANG, Y., ROBINSON, D. P. & FOSTER, L. J. 2010. Quantitative analysis of proteome coverage and recovery rates for upstream fractionation methods in proteomics. *J Proteome Res,* 9**,** 1902-12.

FEI, T., XIA, K., LI, Z., ZHOU, B., ZHU, S., CHEN, H., ZHANG, J., CHEN, Z., XIAO, H., HAN, J. D. & CHEN, Y. G. 2010. Genome-wide mapping of SMAD target genes reveals the role of BMP signaling in embryonic stem cell fate determination. *Genome Res,* 20**,** 36-44.

FENN, J. B., MANN, M., MENG, C. K., WONG, S. F. & WHITEHOUSE, C. M. 1989. Electrospray ionization for mass spectrometry of large biomolecules. *Science,* 246**,** 64-71.

FERNANDES, T. G., DIOGO, M. M., FERNANDES-PLATZGUMMER, A., DA SILVA, C. L. & CABRAL, J. M. 2010. Different stages of pluripotency determine distinct patterns of proliferation, metabolism, and lineage commitment of embryonic stem cells under hypoxia. *Stem Cell Res,* 5**,** 76-89.

FINCH, B. W. & EPHRUSSI, B. 1967. RETENTION OF MULTIPLE DEVELOPMENTAL POTENTIALITIES BY CELLS OF A MOUSE TESTICULAR TERATOCARCINOMA DURING PROLONGED CULTURE in vitro AND THEIR EXTINCTION UPON HYBRIDIZATION WITH CELLS OF PERMANENT LINES. *Proc Natl Acad Sci U S A,* 57**,** 615-21.

FISHER, O. Z., KHADEMHOSSEINI, A., LANGER, R. & PEPPAS, N. A. 2009. Bioinspired Materials for Controlling Stem Cell Fate. *Accounts of Chemical Research,* 43**,** 419-428.

FOLMES, C. D., DZEJA, P. P., NELSON, T. J. & TERZIC, A. 2012a. Metabolic plasticity in stem cell homeostasis and differentiation. *Cell Stem Cell,* 11**,** 596-606.

FOLMES, C. D., DZEJA, P. P., NELSON, T. J. & TERZIC, A. 2012c. Mitochondria in control of cell fate. *Circ Res,* 110**,** 526-9.

FORNER, F., FOSTER, L. J. & TOPPO, S. 2007. Mass Spectrometry Data Analysis in the Proteomics Era. *Current Bioinformatics,* 2**,** 63-93.

FORRISTAL, C. E., CHRISTENSEN, D. R., CHINNERY, F. E., PETRUZZELLI, R., PARRY, K. L., SANCHEZ-ELSNER, T. & HOUGHTON, F. D. 2013. Environmental oxygen tension regulates the energy metabolism and self-renewal of human embryonic stem cells. *PLoS One,* 8**,** e62507.

FORSBERG, E., PEJLER, G., RINGVALL, M., LUNDERIUS, C., TOMASINI-JOHANSSON, B., KUSCHE-GULLBERG, M., ERIKSSON, I., LEDIN, J., HELLMAN, L. & KJELLEN, L. 1999. Abnormal mast cells in mice deficient in a heparin-synthesizing enzyme. *Nature,* 400**,** 773-776.

FRENCH, M. M., SMITH, S. E., AKANBI, K., SANFORD, T., HECHT, J., FARACH-CARSON, M. C. & CARSON, D. D. 1999. Expression of the heparan sulfate proteoglycan, perlecan, during mouse embryogenesis and perlecan chondrogenic activity in vitro. *J Cell Biol,* 145**,** 1103-15.

FRIDLEY, K. M., FERNANDEZ, I., LI, M. T., KETTLEWELL, R. B. & ROY, K. 2010. Unique differentiation profile of mouse embryonic stem cells in rotary and stirred tank bioreactors. *Tissue Eng Part A,* 16**,** 3285-98.

GAEDTKE, L., THOENES, L., CULMSEE, C., MAYER, B. & WAGNER, E. 2007. Proteomic analysis reveals differences in protein expression in spheroid versus monolayer cultures of low-passage colon carcinoma cells. *J Proteome Res,* 6**,** 4111-8.

GALVIN, K. E., TRAVIS, E. D., YEE, D., MAGNUSON, T. & VIVIAN, J. L. 2010. Nodal signaling regulates the bone morphogenic protein pluripotency pathway in mouse embryonic stem cells. *J Biol Chem,* 285**,** 19747-56.

GEORGE, E. L., GEORGES-LABOUESSE, E. N., PATEL-KING, R. S., RAYBURN, H. & HYNES, R. O. 1993. Defects in mesoderm, neural tube and vascular development in mouse embryos lacking fibronectin. *Development,* 119**,** 1079-91.

GERSDORFF, N., MULLER, M., OTTO, S., POSCHADEL, R., HUBNER, S. & MIOSGE, N. 2005. Basement membrane composition in the early mouse embryo day 7. *Dev Dyn,* 233**,** 1140-8.

GIZZI, G., HOOGENBOOM, L. A., VON HOLST, C., ROSE, M. & ANKLAM, E. 2005. Determination of dioxins (PCDDs/PCDFs) and PCBs in food and feed using the DR CALUX bioassay: results of an international validation study. *Food Addit Contam,* 22**,** 472-81.

GOETZ, A. K., SCHEFFLER, B., CHEN, H. X., WANG, S., SUSLOV, O., XIANG, H., BRUSTLE, O., ROPER, S. N. & STEINDLER, D. A. 2006. Temporally restricted substrate interactions direct fate and specification of neural precursors derived from embryonic stem cells. *Proc Natl Acad Sci U S A,* 103**,** 11063-8.

GRAUMANN, J., HUBNER, N. C., KIM, J. B., KO, K., MOSER, M., KUMAR, C., COX, J., SCHOLER, H. & MANN, M. 2008a. Stable isotope labeling by amino acids in cell culture (SILAC) and proteome quantitation of mouse embryonic stem cells to a depth of 5,111 proteins. *Mol Cell Proteomics,* 7**,** 672-83.

GRAUMANN, J., HUBNER, N. C., KIM, J. B., KO, K., MOSER, M., KUMAR, C., COX, J., SCHÖLER, H. & MANN, M. 2008c. Stable Isotope Labeling by Amino Acids in Cell Culture (SILAC) and Proteome Quantitation of Mouse Embryonic Stem Cells to a Depth of 5,111 Proteins. *Molecular & Cellular Proteomics,* 7**,** 672-683.

GREBER, B., WU, G., BERNEMANN, C., JOO, J. Y., HAN, D. W., KO, K., TAPIA, N., SABOUR, D., STERNECKERT, J., TESAR, P. & SCHOLER, H. R. 2010. Conserved and divergent roles of FGF signaling in mouse epiblast stem cells and human embryonic stem cells. *Cell Stem Cell,* 6**,** 215-26.

GUNDRY, R. L., TCHERNYSHYOV, I., SHENG, S., TARASOVA, Y., RAGINSKI, K., BOHELER, K. R. & VAN EYK, J. E. 2010. Expanding the mouse embryonic stem cell proteome: combining three proteomic approaches. *Proteomics,* 10**,** 2728-32.

GUNDRY, R. L., WHITE, M. Y., MURRAY, C. I., KANE, L. A., FU, Q., STANLEY, B. A. & VAN EYK, J. E. 2009. Preparation of proteins and peptides for mass spectrometry analysis in a bottom-up proteomics workflow. *Curr Protoc Mol Biol,* Chapter 10**,** Unit10 25.

GUNWAR, S., BALLESTER, F., NOELKEN, M. E., SADO, Y., NINOMIYA, Y. & HUDSON, B. G. 1998. Glomerular basement membrane. Identification of a novel disulfide-cross-linked network of alpha3, alpha4, and alpha5 chains of type IV collagen and its implications for the pathogenesis of Alport syndrome. *J Biol Chem,* 273**,** 8767-75.

GUO, G., YANG, J., NICHOLS, J., HALL, J. S., EYRES, I., MANSFIELD, W. & SMITH, A. 2009. Klf4 reverts developmentally programmed restriction of ground state pluripotency. *Development,* 136**,** 1063-9.

GUO, Z., KANJANAPANGKA, J., LIU, N., LIU, S., LIU, C., WU, Z., WANG, Y., LOH, T., KOWOLIK, C., JAMSEN, J., ZHOU, M., TRUONG, K., CHEN, Y., ZHENG, L. & SHEN, B. 2012. Sequential Posttranslational Modifications Program FEN1 Degradation during Cell-Cycle Progression. *Mol Cell,* 47**,** 444-456.

GUOFENG HAN, HONGTAO WANG & JIJUN HAO 2013. *Molecular Mechanisms of Embryonic Stem Cell Pluripotency, Pluripotent Stem Cells,* .

HAN, J., CHEN, L., LUO, G., DAI, B., WANG, X. & DAI, J. 2013. Three-dimensional culture may promote cell reprogramming. *Organogenesis,* 9**,** 118-20.

HARTINGER, J., STENIUS, K., HOGEMANN, D. & JAHN, R. 1996. 16-BAC/SDS-PAGE: a two-dimensional gel electrophoresis system suitable for the separation of integral membrane proteins. *Anal Biochem,* 240**,** 126-33.

HAUSMANN, N., FENGLER, S., HENNIG, A., FRANZ-WACHTEL, M., HAMPP, R. & NEEF, M. 2013. Cytosolic calcium, hydrogen peroxide and related gene expression and protein modulation in Arabidopsis thaliana cell cultures respond immediately to altered gravitation: parabolic flight data. *Plant Biol (Stuttg)*.

HAYASHI, Y., FURUE, M. K., OKAMOTO, T., OHNUMA, K., MYOISHI, Y., FUKUHARA, Y., ABE, T., SATO, J. D., HATA, R. & ASASHIMA, M. 2007. Integrins regulate mouse embryonic stem cell self-renewal. *Stem Cells,* 25**,** 3005-15.

HAYES, R. N. & GROSS, M. L. 1990. Collision-induced dissociation. *Methods Enzymol,* 193**,** 237-63.

HOSSEINKHANI, H., HOSSEINKHANI, M., GABRIELSON, N. P., PACK, D. W., KHADEMHOSSEINI, A. & KOBAYASHI, H. 2008. DNA nanoparticles encapsulated in 3D tissue-engineered scaffolds enhance osteogenic differentiation of mesenchymal stem cells. *J Biomed Mater Res A,* 85**,** 47-60.

HSU, P. & QU, C.-K. 2013. Metabolic Plasticity and Hematopoietic Stem Cell Biology. *Current opinion in hematology,* 20**,** 289-294.

HUNT, G. C., SINGH, P. & SCHWARZBAUER, J. E. 2012. Endogenous production of fibronectin is required for self-renewal of cultured mouse embryonic stem cells. *Exp Cell Res,* 318**,** 1820-31.

HWANG, Y. S., CHO, J., TAY, F., HENG, J. Y., HO, R., KAZARIAN, S. G., WILLIAMS, D. R., BOCCACCINI, A. R., POLAK, J. M. & MANTALARIS, A. 2009. The use of murine embryonic stem cells, alginate encapsulation, and rotary microgravity bioreactor in bone tissue engineering. *Biomaterials,* 30**,** 499-507.

ITO, K., CARRACEDO, A., WEISS, D., ARAI, F., ALA, U., AVIGAN, D. E., SCHAFER, Z. T., EVANS, R. M., SUDA, T., LEE, C. H. & PANDOLFI, P. P. 2012. A PML-PPAR-delta pathway for fatty acid oxidation regulates hematopoietic stem cell maintenance. *Nat Med,* 18**,** 1350-8.

ITO, K. & SUDA, T. 2014. Metabolic requirements for the maintenance of self-renewing stem cells. *Nat Rev Mol Cell Biol,* 15**,** 243-256.

JEONG, C. H., LEE, H. J., CHA, J. H., KIM, J. H., KIM, K. R., KIM, J. H., YOON, D. K. & KIM, K. W. 2007. Hypoxia-inducible factor-1 alpha inhibits self-renewal of mouse embryonic stem cells in Vitro via negative regulation of the leukemia inhibitory factor-STAT3 pathway. *J Biol Chem,* 282**,** 13672-9.

JODDAR, B. & ITO, Y. 2013. Artificial niche substrates for embryonic and induced pluripotent stem cell cultures. *J Biotechnol,* 168**,** 218-28.

JOGI, A., ORA, I., NILSSON, H., LINDEHEIM, A., MAKINO, Y., POELLINGER, L., AXELSON, H. & PAHLMAN, S. 2002. Hypoxia alters gene expression in human neuroblastoma cells toward an immature and neural crest-like phenotype. *Proc Natl Acad Sci U S A,* 99**,** 7021-6.

JOHNSON, R. S., DAVIS, M. T., TAYLOR, J. A. & PATTERSON, S. D. 2005. Informatics for protein identification by mass spectrometry. *Methods,* 35**,** 223-36.

JONES, A. R., SIEPEN, J. A., HUBBARD, S. J. & PATON, N. W. 2009. Improving sensitivity in proteome studies by analysis of false discovery rates for multiple search engines. *Proteomics,* 9**,** 1220-9.

KAMARAJUGADDA, S., STEMBOROSKI, L., CAI, Q., SIMPSON, N. E., NAYAK, S., TAN, M. & LU, J. 2012. Glucose oxidation modulates anoikis and tumor metastasis. *Mol Cell Biol,* 32**,** 1893-907.

KAWAHARA, Y., MANABE, T., MATSUMOTO, M., KAJIUME, T., MATSUMOTO, M. & YUGE, L. 2009. LIF-Free Embryonic Stem Cell Culture in Simulated Microgravity. *PLoS ONE,* 4**,** e6343.

KEUNG, A. J., DE JUAN-PARDO, E. M., SCHAFFER, D. V. & KUMAR, S. 2011a. Rho GTPases Mediate the Mechanosensitive Lineage Commitment of Neural Stem Cells. *Stem Cells,* 29**,** 1886-1897.

KEUNG, A. J., DE JUAN-PARDO, E. M., SCHAFFER, D. V. & KUMAR, S. 2011b. Rho GTPases mediate the mechanosensitive lineage commitment of neural stem cells. *Stem Cells,* 29**,** 1886-97.

KINNEY, M. A., SARGENT, C. Y. & MCDEVITT, T. C. 2011. The multiparametric effects of hydrodynamic environments on stem cell culture. *Tissue Eng Part B Rev,* 17**,** 249-62.

KLIMANSKAYA, I., CHUNG, Y., BECKER, S., LU, S. J. & LANZA, R. 2006. Human embryonic stem cell lines derived from single blastomeres. *Nature,* 444**,** 481-5.

KLIMANSKAYA, I., CHUNG, Y., BECKER, S., LU, S. J. & LANZA, R. 2007. Derivation of human embryonic stem cells from single blastomeres. *Nat Protoc,* 2**,** 1963-72.

KOHFELDT, E., SASAKI, T., GOHRING, W. & TIMPL, R. 1998. Nidogen-2: a new basement membrane protein with diverse binding properties. *J Mol Biol,* 282**,** 99-109.

KOLEDOVA, Z., KAFKOVA, L. R., CALABKOVA, L., KRYSTOF, V., DOLEZEL, P. & DIVOKY, V. 2010. Cdk2 inhibition prolongs G1 phase progression in mouse embryonic stem cells. *Stem Cells Dev,* 19**,** 181-94.

KOLIND, K., LEONG, K. W., BESENBACHER, F. & FOSS, M. 2012. Guidance of stem cell fate on 2D patterned surfaces. *Biomaterials,* 33**,** 6626-6633.

KONZE, S. A., VAN DIEPEN, L., SCHRODER, A., OLMER, R., MOLLER, H., PICH, A., WEISSMANN, R., KUSS, A. W., ZWEIGERDT, R. & BUETTNER, F. F. 2014. Cleavage of E-cadherin and beta-catenin by calpain affects Wnt signaling and spheroid formation in suspension cultures of human pluripotent stem cells. *Mol Cell Proteomics*.

KRAEHENBUEHL, T. P., LANGER, R. & FERREIRA, L. S. 2011. Three-dimensional biomaterials for the study of human pluripotent stem cells. *Nat Meth,* 8**,** 731-736.

KRAUSHAAR, D. C., YAMAGUCHI, Y. & WANG, L. 2010. Heparan sulfate is required for embryonic stem cells to exit from self-renewal. *J Biol Chem,* 285**,** 5907-16.

KRIJGSVELD, J., KETTING, R. F., MAHMOUDI, T., JOHANSEN, J., ARTAL-SANZ, M., VERRIJZER, C. P., PLASTERK, R. H. & HECK, A. J. 2003. Metabolic labeling of C. elegans and D. melanogaster for quantitative proteomics. *Nat Biotechnol,* 21**,** 927-31.

KUO, C.-T., CHIANG, C.-L., YUN-JU HUANG, R., LEE, H. & WO, A. M. 2012. Configurable 2D and 3D spheroid tissue cultures on bioengineered surfaces with acquisition of epithelial-mesenchymal transition characteristics. *NPG Asia Mater,* 4**,** e27.

LAM, H., DEUTSCH, E. W., EDDES, J. S., ENG, J. K., STEIN, S. E. & AEBERSOLD, R. 2008. Building consensus spectral libraries for peptide identification in proteomics. *Nat Methods,* 5**,** 873-5.

LANNER, F., LEE, K. L., SOHL, M., HOLMBORN, K., YANG, H., WILBERTZ, J., POELLINGER, L., ROSSANT, J. & FARNEBO, F. 2010. Heparan sulfation-dependent fibroblast growth factor signaling maintains embryonic stem cells primed for differentiation in a heterogeneous state. *Stem Cells,* 28**,** 191-200.

LARANCE, M., BAILLY, A. P., POURKARIMI, E., HAY, R. T., BUCHANAN, G., COULTHURST, S., XIRODIMAS, D. P., GARTNER, A. & LAMOND, A. I. 2011. Stable-isotope labeling with amino acids in nematodes. *Nat Methods,* 8**,** 849-51.

LAURENT, J., FRONGIA, C., CAZALES, M., MONDESERT, O., DUCOMMUN, B. & LOBJOIS, V. 2013. Multicellular tumor spheroid models to explore cell cycle checkpoints in 3D. *BMC Cancer,* 13**,** 73.

LEE, S. W., JEONG, H. K., LEE, J. Y., YANG, J., LEE, E. J., KIM, S. Y., YOUN, S. W., LEE, J., KIM, W. J., KIM, K. W., LIM, J. M., PARK, J. W., PARK, Y. B. & KIM, H. S. 2012. Hypoxic priming of mESCs accelerates vascular-lineage differentiation through HIF1-mediated inverse regulation of Oct4 and VEGF. *EMBO Mol Med,* 4**,** 924-38.

LEUNG, H. W., CHEN, A., CHOO, A. B., REUVENY, S. & OH, S. K. 2011. Agitation can induce differentiation of human pluripotent stem cells in microcarrier cultures. *Tissue Eng Part C Methods,* 17**,** 165-72.

LI, L., ARMAN, E., EKBLOM, P., EDGAR, D., MURRAY, P. & LONAI, P. 2004. Distinct GATA6- and laminin-dependent mechanisms regulate endodermal and ectodermal embryonic stem cell fates. *Development,* 131**,** 5277-86.

LI, Q. R., XING, X. B., CHEN, T. T., LI, R. X., DAI, J., SHENG, Q. H., XIN, S. M., ZHU, L. L., JIN, Y., PEI, G., KANG, J. H., LI, Y. X. & ZENG, R. 2011. Large scale phosphoproteome profiles comprehensive features of mouse embryonic stem cells. *Mol Cell Proteomics,* 10**,** M110 001750.

LI, S., EDGAR, D., FASSLER, R., WADSWORTH, W. & YURCHENCO, P. D. 2003. The role of laminin in embryonic cell polarization and tissue organization. *Dev Cell,* 4**,** 613-24.

LI, S., HARRISON, D., CARBONETTO, S., FASSLER, R., SMYTH, N., EDGAR, D. & YURCHENCO, P. D. 2002. Matrix assembly, regulation, and survival functions of laminin and its receptors in embryonic stem cell differentiation. *J Cell Biol,* 157**,** 1279-90.

LIU, H., LIN, J. & ROY, K. 2006. Effect of 3D scaffold and dynamic culture condition on the global gene expression profile of mouse embryonic stem cells. *Biomaterials,* 27**,** 5978-89.

LIU, X., REN, X., DENG, X., HUO, Y., XIE, J., HUANG, H., JIAO, Z., WU, M., LIU, Y. & WEN, T. 2010. A protein interaction network for the analysis of the neuronal differentiation of neural stem cells in response to titanium dioxide nanoparticles. *Biomaterials,* 31**,** 3063-70.

LOCASALE, J. W. 2013. Serine, glycine and one-carbon units: cancer metabolism in full circle. *Nat Rev Cancer,* 13**,** 572-583.

LOH, Y. H., WU, Q., CHEW, J. L., VEGA, V. B., ZHANG, W., CHEN, X., BOURQUE, G., GEORGE, J., LEONG, B., LIU, J., WONG, K. Y., SUNG, K. W., LEE, C. W., ZHAO, X. D., CHIU, K. P., LIPOVICH, L., KUZNETSOV, V. A., ROBSON, P., STANTON, L. W., WEI, C. L., RUAN, Y., LIM, B. & NG, H. H. 2006. The Oct4 and Nanog transcription network regulates pluripotency in mouse embryonic stem cells. *Nat Genet,* 38**,** 431-40.

LOSSNER, C., WARNKEN, U., PSCHERER, A. & SCHNOLZER, M. 2011. Preventing arginine-to-proline conversion in a cell-line-independent manner during cell cultivation under stable isotope labeling by amino acids in cell culture (SILAC) conditions. *Anal Biochem,* 412**,** 123-5.

LU, J., TAN, M. & CAI, Q. 2014. The Warburg effect in tumor progression: Mitochondrial oxidative metabolism as an anti-metastasis mechanism. *Cancer Lett*.

LUND, A. W., YENER, B., STEGEMANN, J. P. & PLOPPER, G. E. 2009. The natural and engineered 3D microenvironment as a regulatory cue during stem cell fate determination. *Tissue Eng Part B Rev,* 15**,** 371-80.

LUTOLF, M. P., GILBERT, P. M. & BLAU, H. M. 2009. Designing materials to direct stem-cell fate. *Nature,* 462**,** 433-441.

MANDAL, S., LINDGREN, A. G., SRIVASTAVA, A. S., CLARK, A. T. & BANERJEE, U. 2011. Mitochondrial Function Controls Proliferation and Early Differentiation Potential of Embryonic Stem Cells. *STEM CELLS,* 29**,** 486-495.

MANN, M. 2006. Functional and quantitative proteomics using SILAC. *Nature reviews Molecular cell biology,* 7**,** 952-958.

MARÍA CHÁVARRI, I. M. O. N. A. M. A. C. V. N. 2012. Encapsulation Technology to Protect Probiotic Bacteria. *InTech*.

MARTIN, G. R. 1981. Isolation of a pluripotent cell line from early mouse embryos cultured in medium conditioned by teratocarcinoma stem cells. *Proc Natl Acad Sci U S A,* 78**,** 7634-8.

MARTIN, G. R. & EVANS, M. J. 1975. Differentiation of clonal lines of teratocarcinoma cells: formation of embryoid bodies in vitro. *Proc Natl Acad Sci U S A,* 72**,** 1441-5.

MASUI, S., NAKATAKE, Y., TOYOOKA, Y., SHIMOSATO, D., YAGI, R., TAKAHASHI, K., OKOCHI, H., OKUDA, A., MATOBA, R., SHAROV, A. A., KO, M. S. & NIWA, H. 2007. Pluripotency governed by Sox2 via regulation of Oct3/4 expression in mouse embryonic stem cells. *Nat Cell Biol,* 9**,** 625-35.

MASUI, S., OHTSUKA, S., YAGI, R., TAKAHASHI, K., KO, M. S. H. & NIWA, H. 2008. Rex1/Zfp42 is dispensable for pluripotency in mouse ES cells. *BMC Developmental Biology,* 8**,** 45-45.

MATHIEU, J., ZHOU, W., XING, Y., SPERBER, H., FERRECCIO, A., AGOSTON, Z., KUPPUSAMY, KAVITHA T., MOON, RANDALL T. & RUOHOLA-BAKER, H. 2014. Hypoxia-Inducible Factors Have Distinct and Stage-Specific Roles during Reprogramming of Human Cells to Pluripotency. *Cell Stem Cell,* 14**,** 592-605.

MIKKELSEN, T. S., KU, M., JAFFE, D. B., ISSAC, B., LIEBERMAN, E., GIANNOUKOS, G., ALVAREZ, P., BROCKMAN, W., KIM, T.-K., KOCHE, R. P., LEE, W., MENDENHALL, E., O'DONOVAN, A., PRESSER, A., RUSS, C., XIE, X., MEISSNER, A., WERNIG, M., JAENISCH, R., NUSBAUM, C., LANDER, E. S. & BERNSTEIN, B. E. 2007. Genome-wide maps of chromatin state in pluripotent and lineage-committed cells. *Nature,* 448**,** 553-560.

MINTZ, B. & ILLMENSEE, K. 1975. Normal genetically mosaic mice produced from malignant teratocarcinoma cells. *Proc Natl Acad Sci U S A,* 72**,** 3585-9.

MITSUI, K., TOKUZAWA, Y., ITOH, H., SEGAWA, K., MURAKAMI, M., TAKAHASHI, K., MARUYAMA, M., MAEDA, M. & YAMANAKA, S. 2003. The homeoprotein Nanog is required for maintenance of pluripotency in mouse epiblast and ES cells. *Cell,* 113**,** 631-42.

MOHYELDIN, A., GARZÓN-MUVDI, T. & QUIÑONES-HINOJOSA, A. 2010. Oxygen in Stem Cell Biology: A Critical Component of the Stem Cell Niche. *Cell stem cell,* 7**,** 150-161.

MOLEDINA, F., CLARKE, G., OSKOOEI, A., ONISHI, K., GUNTHER, A. & ZANDSTRA, P. W. 2012a. Predictive microfluidic control of regulatory ligand trajectories in individual pluripotent cells. *Proc Natl Acad Sci U S A,* 109**,** 3264-9.

MOLEDINA, F., CLARKE, G., OSKOOEI, A., ONISHI, K., GÜNTHER, A. & ZANDSTRA, P. W. 2012b. Predictive microfluidic control of regulatory ligand trajectories in individual pluripotent cells. *Proceedings of the National Academy of Sciences*.

MORRIS, H. R., PAXTON, T., DELL, A., LANGHORNE, J., BERG, M., BORDOLI, R. S., HOYES, J. & BATEMAN, R. H. 1996. High sensitivity collisionally-activated decomposition tandem mass spectrometry on a novel quadrupole/orthogonal-acceleration time-of-flight mass spectrometer. *Rapid Commun Mass Spectrom,* 10**,** 889-96.

MUELLER, L. N., BRUSNIAK, M. Y., MANI, D. R. & AEBERSOLD, R. 2008. An assessment of software solutions for the analysis of mass spectrometry based quantitative proteomics data. *J Proteome Res,* 7**,** 51-61.

NAGARIA, P., ROBERT, C. & RASSOOL, F. V. 2013. DNA double-strand break response in stem cells: mechanisms to maintain genomic integrity. *Biochim Biophys Acta,* 1830**,** 2345-53.

NAGY, A., ROSSANT, J., NAGY, R., ABRAMOW-NEWERLY, W. & RODER, J. C. 1993. Derivation of completely cell culture-derived mice from early-passage embryonic stem cells. *Proc Natl Acad Sci U S A,* 90**,** 8424-8.

NG, K. W., LEONG, D. T. & HUTMACHER, D. W. 2005. The challenge to measure cell proliferation in two and three dimensions. *Tissue Eng,* 11**,** 182-91.

NICHOLS, J., SILVA, J., ROODE, M. & SMITH, A. 2009. Suppression of Erk signalling promotes ground state pluripotency in the mouse embryo. *Development,* 136**,** 3215-22.

NICHOLS, J. & SMITH, A. 2009. Naive and primed pluripotent states. *Cell Stem Cell,* 4**,** 487-92.

NICHOLS, J., ZEVNIK, B., ANASTASSIADIS, K., NIWA, H., KLEWE-NEBENIUS, D., CHAMBERS, I., SCHOLER, H. & SMITH, A. 1998. Formation of pluripotent stem cells in the mammalian embryo depends on the POU transcription factor Oct4. *Cell,* 95**,** 379-91.

NIWA, H., MIYAZAKI, J. & SMITH, A. G. 2000. Quantitative expression of Oct-3/4 defines differentiation, dedifferentiation or self-renewal of ES cells. *Nat Genet,* 24**,** 372-6.

NOONAN, D. M. & HASSELL, J. R. 1993. Perlecan, the large low-density proteoglycan of basement membranes: Structure and variant forms. *Kidney Int,* 43**,** 53-60.

O'BRIEN, R. N., SHEN, Z., TACHIKAWA, K., LEE, P. A. & BRIGGS, S. P. 2010. Quantitative proteome analysis of pluripotent cells by iTRAQ mass tagging reveals post-transcriptional regulation of proteins required for ES cell self-renewal. *Mol Cell Proteomics,* 9**,** 2238-51.

ONG, S. E., BLAGOEV, B., KRATCHMAROVA, I., KRISTENSEN, D. B., STEEN, H., PANDEY, A. & MANN, M. 2002. Stable isotope labeling by amino acids in cell culture, SILAC, as a simple and accurate approach to expression proteomics. *Mol Cell Proteomics,* 1**,** 376-86.

ORFORD, K. W. & SCADDEN, D. T. 2008. Deconstructing stem cell self-renewal: genetic insights into cell-cycle regulation. *Nat Rev Genet,* 9**,** 115-28.

OUYANG, A., NG, R. & YANG, S. T. 2007. Long-term culturing of undifferentiated embryonic stem cells in conditioned media and three-dimensional fibrous matrices without extracellular matrix coating. *Stem Cells,* 25**,** 447-54.

PAMPALONI, F., STELZER, E. H., LEICHT, S. & MARCELLO, M. 2010. Madin-Darby canine kidney cells are increased in aerobic glycolysis when cultured on flat and stiff collagen-coated surfaces rather than in physiological 3-D cultures. *Proteomics,* 10**,** 3394-413.

PARK, J. H., RYU, J. M. & HAN, H. J. 2011. Involvement of caveolin-1 in fibronectin-induced mouse embryonic stem cell proliferation: Role of FAK, RhoA, PI3K/Akt, and ERK 1/2 pathways. *J Cell Physiol,* 226**,** 267-275.

PARK, S. S., WU, W. W., ZHOU, Y., SHEN, R. F., MARTIN, B. & MAUDSLEY, S. 2012. Effective correction of experimental errors in quantitative proteomics using stable isotope labeling by amino acids in cell culture (SILAC). *J Proteomics,* 75**,** 3720-32.

PATTERSON, S. D. & AEBERSOLD, R. H. 2003. Proteomics: the first decade and beyond. *Nat Genet,* 33 Suppl**,** 311-23.

PATZER, J. F. 2004. Oxygen Consumption in a Hollow Fiber Bioartificial Liver—Revisited. *Artificial Organs,* 28**,** 83-98.

PENOLAZZI, L., TAVANTI, E., VECCHIATINI, R., LAMBERTINI, E., VESCE, F., GAMBARI, R., MAZZITELLI, S., MANCUSO, F., LUCA, G., NASTRUZZI, C. & PIVA, R. 2010. Encapsulation of mesenchymal stem cells from Wharton's jelly in alginate microbeads. *Tissue Eng Part C Methods,* 16**,** 141-55.

PERA, M. F., REUBINOFF, B. & TROUNSON, A. 2000. Human embryonic stem cells. *J Cell Sci,* 113 (Pt 1)**,** 5-10.

PEREIRA, S. L., GRÃOS, M., RODRIGUES, A. S., ANJO, S. I., CARVALHO, R. A., OLIVEIRA, P. J., ARENAS, E. & RAMALHO-SANTOS, J. 2013. Inhibition of Mitochondrial Complex III Blocks Neuronal Differentiation and Maintains Embryonic Stem Cell Pluripotency. *PLoS ONE,* 8**,** e82095.

PETERMAN, S. M., DUFRESNE, C. P. & HORNING, S. 2005. The use of a hybrid linear trap/FT-ICR mass spectrometer for on-line high resolution/high mass accuracy bottom-up sequencing. *J Biomol Tech,* 16**,** 112-24.

PIMTON, P., SARKAR, S., SHETH, N., PERETS, A., MARCINKIEWICZ, C., LAZAROVICI, P. & LELKES, P. I. 2011. Fibronectin-mediated upregulation of alpha5beta1 integrin and cell adhesion during differentiation of mouse embryonic stem cells. *Cell Adh Migr,* 5**,** 73-82.

PLACZEK, M. R., CHUNG, I. M., MACEDO, H. M., ISMAIL, S., MORTERA BLANCO, T., LIM, M., CHA, J. M., FAUZI, I., KANG, Y., YEO, D. C., MA, C. Y., POLAK, J. M., PANOSKALTSIS, N. & MANTALARIS, A. 2009. Stem cell bioprocessing: fundamentals and principles. *J R Soc Interface,* 6**,** 209-32.

POWERS, D. E., MILLMAN, J. R., HUANG, R. B. & COLTON, C. K. 2008. Effects of oxygen on mouse embryonic stem cell growth, phenotype retention, and cellular energetics. *Biotechnol Bioeng,* 101**,** 241-54.

PRIES, A. R., SECOMB, T. W. & GAEHTGENS, P. 2000. The endothelial surface layer. *Pflugers Arch,* 440**,** 653-66.

PRUKSAKORN, D., LIRDPRAPAMONGKOL, K., CHOKCHAICHAMNANKIT, D., SUBHASITANONT, P., CHIABLAEM, K., SVASTI, J. & SRISOMSAP, C. 2010. Metabolic alteration of HepG2 in scaffold-based 3-D culture: proteomic approach. *Proteomics,* 10**,** 3896-904.

RALF J. BRAUN, N. K., HANS ZISCHKA, AND MARIUS UEFFIN 2009. 16-BAC/SDS-PAGE Analysis of Membrane Proteins of Yeast Mitochondria Purified by Free Flow Electrophoresis. *Membrane Proteomics,* 528**,** 83-107.

RANDERS-EICHHORN, L., BARTLETT, R. A., FREY, D. D. & RAO, G. 1996. Noninvasive oxygen measurements and mass transfer considerations in tissue culture flasks. *Biotechnol Bioeng,* 51**,** 466-78.

RANDLE, W. L., CHA, J. M., HWANG, Y. S., CHAN, K. L., KAZARIAN, S. G., POLAK, J. M. & MANTALARIS, A. 2007. Integrated 3-dimensional expansion and osteogenic differentiation of murine embryonic stem cells. *Tissue Eng,* 13**,** 2957-70.

RATCLIFFE, E., THOMAS, R. J. & WILLIAMS, D. J. 2011. Current understanding and challenges in bioprocessing of stem cell-based therapies for regenerative medicine. *Br Med Bull,* 100**,** 137-55.

RICHARDS, M., TAN, S. P., TAN, J. H., CHAN, W. K. & BONGSO, A. 2004. The transcriptome profile of human embryonic stem cells as defined by SAGE. *Stem Cells,* 22**,** 51-64.

RIPPON, H. J. & BISHOP, A. E. 2004. Embryonic stem cells. *Cell Prolif,* 37**,** 23-34.

RODIN, S., ANTONSSON, L., NIAUDET, C., SIMONSON, O. E., SALMELA, E., HANSSON, E. M., DOMOGATSKAYA, A., XIAO, Z., DAMDIMOPOULOU, P., SHEIKHI, M., INZUNZA, J., NILSSON, A.-S., BAKER, D., KUIPER, R., SUN, Y., BLENNOW, E., NORDENSKJÖLD, M., GRINNEMO, K.-H., KERE, J., BETSHOLTZ, C., HOVATTA, O. & TRYGGVASON, K. 2014. Clonal culturing of human embryonic stem cells on laminin-521/E-cadherin matrix in defined and xeno-free environment. *Nat Commun,* 5.

RODRIGUES, C. A., FERNANDES, T. G., DIOGO, M. M., DA SILVA, C. L. & CABRAL, J. M. 2011. Stem cell cultivation in bioreactors. *Biotechnol Adv,* 29**,** 815-29.

ROEPSTORFF, P. 2000. MALDI-TOF mass spectrometry in protein chemistry. *Exs,* 88**,** 81-97.

RONAGHI, M., ERCEG, S., MORENO-MANZANO, V. & STOJKOVIC, M. 2010. Challenges of stem cell therapy for spinal cord injury: human embryonic stem cells, endogenous neural stem cells, or induced pluripotent stem cells? *Stem Cells,* 28**,** 93-9.

ROSS, P. L., HUANG, Y. N., MARCHESE, J. N., WILLIAMSON, B., PARKER, K., HATTAN, S., KHAINOVSKI, N., PILLAI, S., DEY, S., DANIELS, S., PURKAYASTHA, S., JUHASZ, P., MARTIN, S., BARTLET-JONES, M., HE, F., JACOBSON, A. & PAPPIN, D. J. 2004. Multiplexed protein quantitation in Saccharomyces cerevisiae using amine-reactive isobaric tagging reagents. *Mol Cell Proteomics,* 3**,** 1154-69.

RUPPRECHT, A., SITTNER, D., SMORODCHENKO, A., HILSE, K. E., GOYN, J., MOLDZIO, R., SEILER, A. E. M., BRÄUER, A. U. & POHL, E. E. 2014. Uncoupling Protein 2 and 4 Expression Pattern during Stem Cell Differentiation Provides New Insight into Their Putative Function. *PLoS ONE,* 9**,** e88474.

SASAKI, N., OKISHIO, K., UI-TEI, K., SAIGO, K., KINOSHITA-TOYODA, A., TOYODA, H., NISHIMURA, T., SUDA, Y., HAYASAKA, M., HANAOKA, K., HITOSHI, S., IKENAKA, K. & NISHIHARA, S. 2008. Heparan sulfate regulates self-renewal and pluripotency of embryonic stem cells. *J Biol Chem,* 283**,** 3594-606.

SHAIN, K. H., YARDE, D. N., MEADS, M. B., HUANG, M., JOVE, R., HAZLEHURST, L. A. & DALTON, W. S. 2009. Beta1 integrin adhesion enhances IL-6-mediated STAT3 signaling in myeloma cells: implications for microenvironment influence on tumor survival and proliferation. *Cancer Res,* 69**,** 1009-15.

SHARMA, A. D., GILL, P. K. & SINGH, P. 2003. RNA isolation from plant tissues rich in polysaccharides. *Analytical Biochemistry,* 314**,** 319-321.

SHOSHAN-BARMATZ, V., ISRAELSON, A., BRDICZKA, D. & SHEU, S. S. 2006. The voltage-dependent anion channel (VDAC): function in intracellular signalling, cell life and cell death. *Curr Pharm Des,* 12**,** 2249-70.

SHYH-CHANG, N., DALEY, G. Q. & CANTLEY, L. C. 2013. Stem cell metabolism in tissue development and aging. *Development,* 140**,** 2535-47.

SINGH, P. & SCHWARZBAUER, J. E. 2012. Fibronectin and stem cell differentiation - lessons from chondrogenesis. *J Cell Sci,* 125**,** 3703-12.

SITI-ISMAIL, N., BISHOP, A. E., POLAK, J. M. & MANTALARIS, A. 2008. The benefit of human embryonic stem cell encapsulation for prolonged feeder-free maintenance. *Biomaterials,* 29**,** 3946-52.

SMITH, A. G. 2001. Embryo-derived stem cells: of mice and men. *Annu Rev Cell Dev Biol,* 17**,** 435-62.

SMITH, A. G., HEATH, J. K., DONALDSON, D. D., WONG, G. G., MOREAU, J., STAHL, M. & ROGERS, D. 1988. Inhibition of pluripotential embryonic stem cell differentiation by purified polypeptides. *Nature,* 336**,** 688-90.

SMITH, K. T. & WORKMAN, J. L. 2009. Introducing the acetylome. *Nat Biotech,* 27**,** 917-919.

SMYTH, N., VATANSEVER, H. S., MURRAY, P., MEYER, M., FRIE, C., PAULSSON, M. & EDGAR, D. 1999. Absence of basement membranes after targeting the LAMC1 gene results in embryonic lethality due to failure of endoderm differentiation. *J Cell Biol,* 144**,** 151-60.

SON, M. Y., CHOI, H., HAN, Y. M. & CHO, Y. S. 2013. Unveiling the critical role of REX1 in the regulation of human stem cell pluripotency. *Stem Cells*.

STANTON, L. W. & BAKRE, M. M. 2007. Genomic and proteomic characterization of embryonic stem cells. *Curr Opin Chem Biol,* 11**,** 399-404.

SWANEY, D. L., MCALISTER, G. C. & COON, J. J. 2008. Decision tree-driven tandem mass spectrometry for shotgun proteomics. *Nat Methods,* 5**,** 959-64.

TAKAHASHI, K. & YAMANAKA, S. 2006. Induction of pluripotent stem cells from mouse embryonic and adult fibroblast cultures by defined factors. *Cell,* 126**,** 663-76.

TAKEHARA, T., TERAMURA, T., ONODERA, Y., HAMANISHI, C. & FUKUDA, K. 2012. Reduced oxygen concentration enhances conversion of embryonic stem cells to epiblast stem cells. *Stem Cells Dev,* 21**,** 1239-49.

TAMM, C., KJELLEN, L. & LI, J. P. 2012. Heparan sulfate biosynthesis enzymes in embryonic stem cell biology. *J Histochem Cytochem,* 60**,** 943-9.

TESAR, P., CHENOWETH, J., BROOK, F., DAVIES, T., EVANS, E., MACK, D., GARDNER, R. & MCKAY, R. 2007. New cell lines from mouse epiblast share defining features with human embryonic stem cells. *Nature,* 448**,** 196-9.

THERESE ANDERSEN, B. L. S., KJETII FORMO, EBEN ALSBERG & CHRISTENSEN, A. B. E. 2012. Alginates as biomaterials in tissue

engineering. *Carbohydrate chemistry,* 37**,** 227—258.

THOMSON, J. A. 1998. Embryonic Stem Cell Lines Derived from Human Blastocysts. *Science,* 282**,** 1145-1147.

TOH, Y. C. & VOLDMAN, J. 2011. Fluid shear stress primes mouse embryonic stem cells for differentiation in a self-renewing environment via heparan sulfate proteoglycans transduction. *Faseb j,* 25**,** 1208-17.

TZUR, A., KAFRI, R., LEBLEU, V. S., LAHAV, G. & KIRSCHNER, M. W. 2009. Cell growth and size homeostasis in proliferating animal cells. *Science,* 325**,** 167-71.

UHRIG, M., BRECHLIN, P., JAHN, O., KNYAZEV, Y., WENINGER, A., BUSIA, L., HONARNEJAD, K., OTTO, M. & HARTMANN, T. 2008. Upregulation of CRABP1 in human neuroblastoma cells overproducing the Alzheimer-typical Aβ42 reduces their differentiation potential. *BMC Medicine,* 6**,** 1-12.

UNWIN, R. D. & WHETTON, A. D. 2006. Systematic proteome and transcriptome analysis of stem cell populations. *Cell Cycle,* 5**,** 1587-91.

UNWIN, R. D. & WHETTON, A. D. 2007. How Will Haematologists Use Proteomics? *Blood Reviews,* 21**,** 315-326.

VALLIER, L., TOUBOUL, T., CHNG, Z., BRIMPARI, M., HANNAN, N., MILLAN, E., SMITHERS, L. E., TROTTER, M., RUGG-GUNN, P., WEBER, A. & PEDERSEN, R. A. 2009. Early cell fate decisions of human embryonic stem cells and mouse epiblast stem cells are controlled by the same signalling pathways. *PLoS One,* 4**,** e6082.

VAN HOOF, D., MUMMERY, C. L., HECK, A. J. & KRIJGSVELD, J. 2006. Embryonic stem cell proteomics. *Expert Rev Proteomics,* 3**,** 427-37.

VARUM, S., MOMCILOVIC, O., CASTRO, C., BEN-YEHUDAH, A., RAMALHO-SANTOS, J. & NAVARA, C. S. 2009. Enhancement of human embryonic stem cell pluripotency through inhibition of the mitochondrial respiratory chain. *Stem Cell Res,* 3**,** 142-56.

VARUM, S., RODRIGUES, A. S., MOURA, M. B., MOMCILOVIC, O., EASLEY, C. A. I. V., RAMALHO-SANTOS, J., VAN HOUTEN, B. & SCHATTEN, G. 2011. Energy Metabolism in Human Pluripotent Stem Cells and Their Differentiated Counterparts. *PLoS ONE,* 6**,** e20914.

VOLKMER, E., OTTO, S., POLZER, H., SALLER, M., TRAPPENDREHER, D., ZAGAR, D., HAMISCH, S., ZIEGLER, G., WILHELMI, A., MUTSCHLER, W. & SCHIEKER, M. 2012. Overcoming hypoxia in 3D culture systems for tissue engineering of bone in vitro using an automated, oxygen-triggered feedback loop. *J Mater Sci Mater Med,* 23**,** 2793-801.

WAKAYAMA, S., KAWAHARA, Y., LI, C., YAMAGATA, K., YUGE, L. & WAKAYAMA, T. 2009. Detrimental Effects of Microgravity on Mouse Preimplantation Development In Vitro. *PLoS ONE,* 4**,** e6753.

WANG, C., HAO, J., ZHANG, F., SU, K. & WANG, D. A. 2008. RNA extraction from polysaccharide-based cell-laden hydrogel scaffolds. *Anal Biochem,* 380**,** 333-4.

WANG, C., LI, X., YAO, Y. & WANG, D. A. 2009a. Concurrent extraction of proteins and RNA from cell-laden hydrogel scaffold free of polysaccharide interference. *J Chromatogr B Analyt Technol Biomed Life Sci,* 877**,** 3762-6.

WANG, N., ADAMS, G., BUTTERY, L., FALCONE, F. H. & STOLNIK, S. 2009d. Alginate encapsulation technology supports embryonic stem cells differentiation into insulin-producing cells. *J Biotechnol,* 144**,** 304-12.

WANG, Y., AN, L., JIANG, Y. & HANG, H. 2011. Effects of Simulated Microgravity on Embryonic Stem Cells. *PLoS ONE,* 6**,** e29214.

WEI, C. L., MIURA, T., ROBSON, P., LIM, S. K., XU, X. Q., LEE, M. Y., GUPTA, S., STANTON, L., LUO, Y., SCHMITT, J., THIES, S., WANG, W., KHREBTUKOVA, I., ZHOU, D., LIU, E. T., RUAN, Y. J., RAO, M. & LIM, B. 2005. Transcriptome profiling of human and murine ESCs identifies divergent paths required to maintain the stem cell state. *Stem Cells,* 23**,** 166-85.

WHITEHOUSE, C. M., DREYER, R. N., YAMASHITA, M. & FENN, J. B. 1985. Electrospray interface for liquid chromatographs and mass spectrometers. *Anal Chem,* 57**,** 675-9.

WIKSTRÖM, J. 2013. Alginate-based microencapsulation and lyophilization of human retinal pigment epithelial cell line (ARPE-19) for cell therapy.

WILLIAMS, R. L., HILTON, D. J., PEASE, S., WILLSON, T. A., STEWART, C. L., GEARING, D. P., WAGNER, E. F., METCALF, D., NICOLA, N. A. & GOUGH, N. M. 1988. Myeloid leukaemia inhibitory factor maintains the developmental potential of embryonic stem cells. *Nature,* 336**,** 684-7.

WILLIAMSON, A. J. K. & WHETTON, A. D. 2011. The requirement for proteomics to unravel stem cell regulatory mechanisms. *Journal of Cellular Physiology,* 226**,** 2478-2483.

WILSON, J. L., NAJIA, M. A., SAEED, R. & MCDEVITT, T. C. 2014. Alginate encapsulation parameters influence the differentiation of microencapsulated embryonic stem cell aggregates. *Biotechnol Bioeng,* 111**,** 618-31.

XU, C. & MA, B. 2006. Software for computational peptide identification from MS-MS data. *Drug Discov Today,* 11**,** 595-600.

XU, R. H., CHEN, X., LI, D. S., LI, R., ADDICKS, G. C., GLENNON, C., ZWAKA, T. P. & THOMSON, J. A. 2002. BMP4 initiates human embryonic stem cell differentiation to trophoblast. *Nat Biotechnol,* 20**,** 1261-4.

YANG, J. & WEINBERG, R. A. 2008. Epithelial-mesenchymal transition: at the crossroads of development and tumor metastasis. *Dev Cell,* 14**,** 818-29.

YEO, D., KIPARISSIDES, A., CHA, J. M., AGUILAR-GALLARDO, C., POLAK, J. M., TSIRIDIS, E., PISTIKOPOULOS, E. N. & MANTALARIS, A. 2013. Improving Embryonic Stem Cell Expansion through the Combination of Perfusion and Bioprocess Model Design. *PLoS ONE,* 8**,** e81728.

YOST, R. A. & BOYD, R. K. 1990. Tandem mass spectrometry: quadrupole and hybrid instruments. *Methods Enzymol,* 193**,** 154-200.

YU, C. B., PAN, X. P., YU, L., YU, X. P., DU, W. B., CAO, H. C., LI, J., CHEN, P. & LI, L. J. 2014. Evaluation of a novel choanoid fluidized bed bioreactor for future bioartificial livers. *World J Gastroenterol,* 20**,** 6869-77.

YU, J., VODYANIK, M. A., SMUGA-OTTO, K., ANTOSIEWICZ-BOURGET, J., FRANE, J. L., TIAN, S., NIE, J., JONSDOTTIR, G. A., RUOTTI, V., STEWART, R., SLUKVIN, II & THOMSON, J. A. 2007. Induced pluripotent stem cell lines derived from human somatic cells. *Science,* 318**,** 1917-20.

ZHANG, J., KHVOROSTOV, I., HONG, J. S., OKTAY, Y., VERGNES, L., NUEBEL, E., WAHJUDI, P. N., SETOGUCHI, K., WANG, G., DO, A., JUNG, H.-J., MCCAFFERY, J. M., KURLAND, I. J., REUE, K., LEE, W.-N. P., KOEHLER, C. M. & TEITELL, M. A. 2011. UCP2 regulates energy metabolism and differentiation potential of human pluripotent stem cells. *EMBO J,* 30**,** 4860-4873.

ZHANG, J., NUEBEL, E., DALEY, GEORGE Q., KOEHLER, CARLA M. & TEITELL, MICHAEL A. 2012. Metabolic Regulation in Pluripotent Stem Cells during Reprogramming and Self-Renewal. *Cell stem cell,* 11**,** 589-595.

ZHANG, K., LI, L., HUANG, C., SHEN, C., TAN, F., XIA, C., LIU, P., ROSSANT, J. & JING, N. 2010. Distinct functions of BMP4 during different stages of mouse ES cell neural commitment. *Development,* 137**,** 2095-105.

ZHANG, S., YANG, C., YANG, Z., ZHANG, D., MA, X., MILLS, G. & LIU, Z. 2015. Homeostasis of redox status derived from glucose metabolic pathway could be the key to understanding the Warburg effect. *American Journal of Cancer Research,* 5**,** 928-944.

ZHOU, W., CHOI, M., MARGINEANTU, D., MARGARETHA, L., HESSON, J., CAVANAUGH, C., BLAU, C. A., HORWITZ, M. S., HOCKENBERY, D., WARE, C. & RUOHOLA-BAKER, H. 2012a. HIF1[alpha] induced switch from bivalent to exclusively glycolytic metabolism during ESC-to-EpiSC/hESC transition. *EMBO J,* 31**,** 2103-2116.

ZHOU, W., CHOI, M., MARGINEANTU, D., MARGARETHA, L., HESSON, J., CAVANAUGH, C., BLAU, C. A., HORWITZ, M. S., HOCKENBERY, D., WARE, C. & RUOHOLA-BAKER, H. 2012c. HIF1alpha induced switch from bivalent to exclusively glycolytic metabolism during ESC-to-EpiSC/hESC transition. *Embo j,* 31**,** 2103-16.

ZHOU, W., LV, R., QI, W., WU, D., XU, Y., LIU, W., MOU, Y. & WANG, L. 2014. Snail contributes to the maintenance of stem cell-like phenotype cells in human pancreatic cancer. *PLoS One,* 9**,** e87409.

ZUBAREV, R. A., HORN, D. M., FRIDRIKSSON, E. K., KELLEHER, N. L., KRUGER, N. A., LEWIS, M. A., CARPENTER, B. K. & MCLAFFERTY, F. W. 2000. Electron capture dissociation for structural characterization of multiply charged protein cations. *Anal Chem,* 72**,** 563-73.